3.4.12.9 The Temporal Bone of Patient IP

Distances (Figure 3.30(n)):

Squamous Temporal Bone: The squamous temporal bone was not measurable in this child due to lack of visibility of the asterion (as), sphenion (spt) and the stylomastoid foramen (smf).

External Auditory Meatus: The configuration of the external auditory meatus was abnormal and asymmetrical, with increased distances recorded on both sides (eampl-pol, pol-eamal, eamir-eampr, eamar-eamir).

Zygomatic Process: The length of the zygomatic arch (ztl-aul, ztr-aur) was decreased bilaterally. The articular fossa height (afl-ael, afr-aer) was normal, however, posteriorly the left EAM-articular fossa length (eamal-afl) was increased.

Petrous Temporal Bone (Figure 3.30(o)): The prominence of the mastoid process (mal-jfll, mar-jflr) was increased bilaterally compared with the experimental standard. The distances of the temporal bone showed the right jugular foramen to be narrowed (jflr-jfmr) with an similar tendency on the left. The inferior petrous temporo-occipital suture (jfml-ptsl, jfmr-ptsr) was increased in length.

Dimensions (Figure 3.30(o)): The petrous temporal ridge distance (petal-petpl, petar-petpr) was increased bilaterally. The dimensions between the temporal bones was increased between the external auditory meatus (pol-por). The angles of the auditory canal (pol-iaml/iamr-por), the petrous temporal bone angles (petpl-petal/petar-petpr) and the zygoma projection (petal-aul-ztl, petar-aur-ztr) were not significantly different from the experimental standard.

Discussion: Bony distortion was found at the external auditory meatus and the zygomatic arch which was reduced in length. The jugular foramen was narrowed while the temporal occipital suture medially and the distance to the mastoid laterally were increased. The overall length of the petrous ridge was also increased. This was reflected in the significantly increased distances between the external auditory canals. The distances between the internal auditory meatus and jugular foramen were relatively normal. There appeared to be lengthening of the petrous temporal bone at the expense of narrowing of the jugular foramen and this would be consistent with sutural involvement and compensatory bone lengthening.

Figure 3.30(n) Z Scores of the Distances of the Temporal Bone for Patient IP compared with the 2 Year Old Experimental Standard

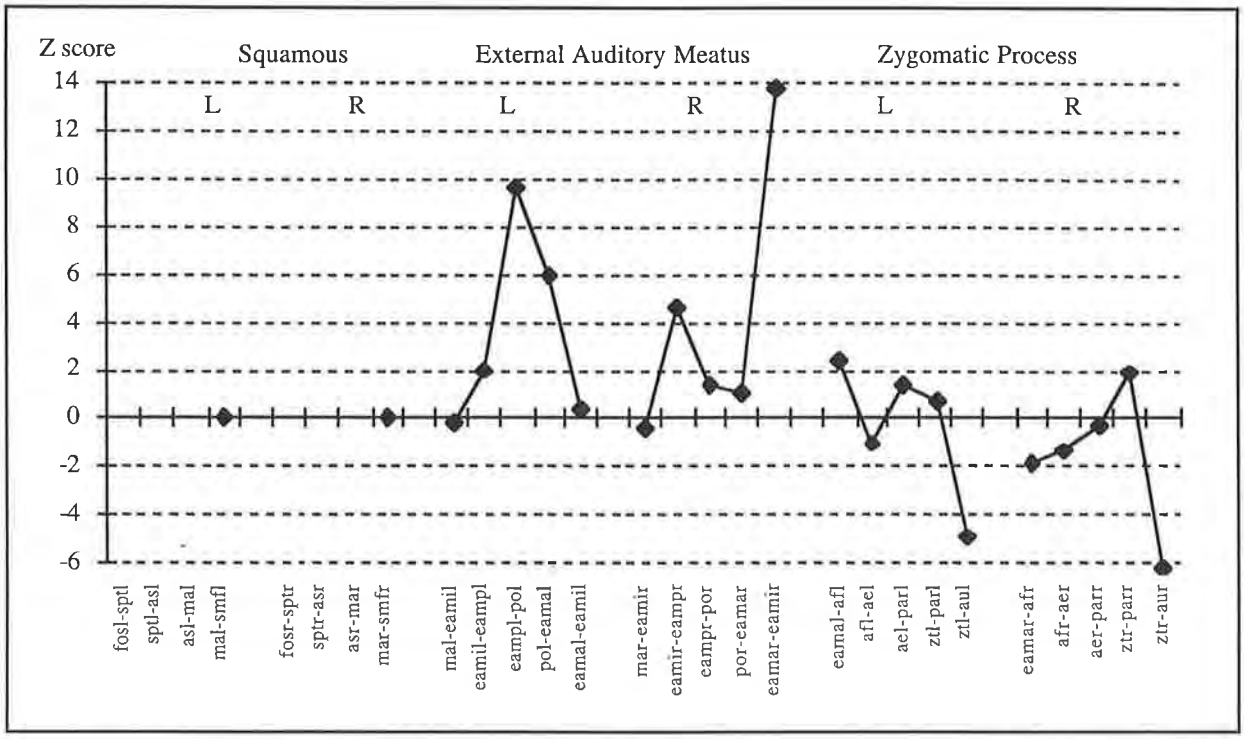

Figure 3.30(o) Z Scores of the Measurements of the Temporal Bone for Patient IP compared with the 2 Year Old Experimental Standard

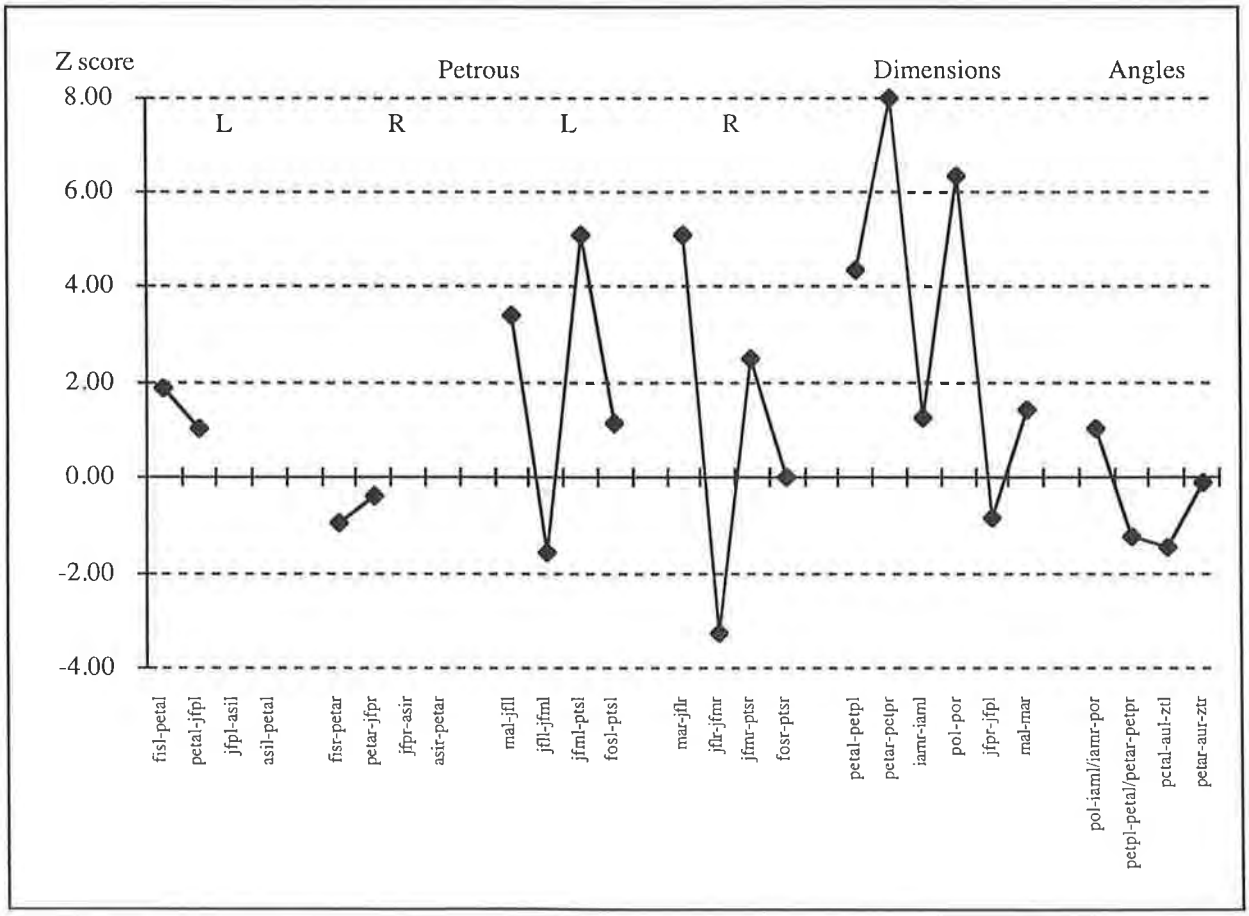

3.4.12.10 The Parietal Bone of Patient IP

Distances: The key landmarks for the parietal bone for Patient IP were not visible due to suture fusion and could not be reliably estimated. Therefore the parietal bone was not measured and a pattern profile of Z scores was not generated for the parietal bone. The measurement data for the experimental standard are reported in Appendix 2.

3.4.12.11 The Occipital Bone of Patient IP

Distances (Figure 3.30(p)): The medial temporo-occipital suture (inferior) (jfml-ptsl, jfmr-ptsr) was bilaterally significantly increased in length compared with the experimental standard. The left anterior foramen magnum distance (ba-fmll) and the right posterior foramen magnum distance (fmlr-o) were increased. The inferior spheno-occipital synchondrosis was normal (see sphenoid and cranial case sutures).

Dimensions (Figure 3.30(p)): The dimensions were not significantly different from the experimental standard.

Discussion: The occipital bone was involved medially along the sutures with the temporal bone and also laterally where the calvarial sutures were fused (see temporal bone).

Figure 3.30(p) Z Scores of the Measurements of the Occipital Bone for Patient IP compared with the 2 Year Old Experimental Standard

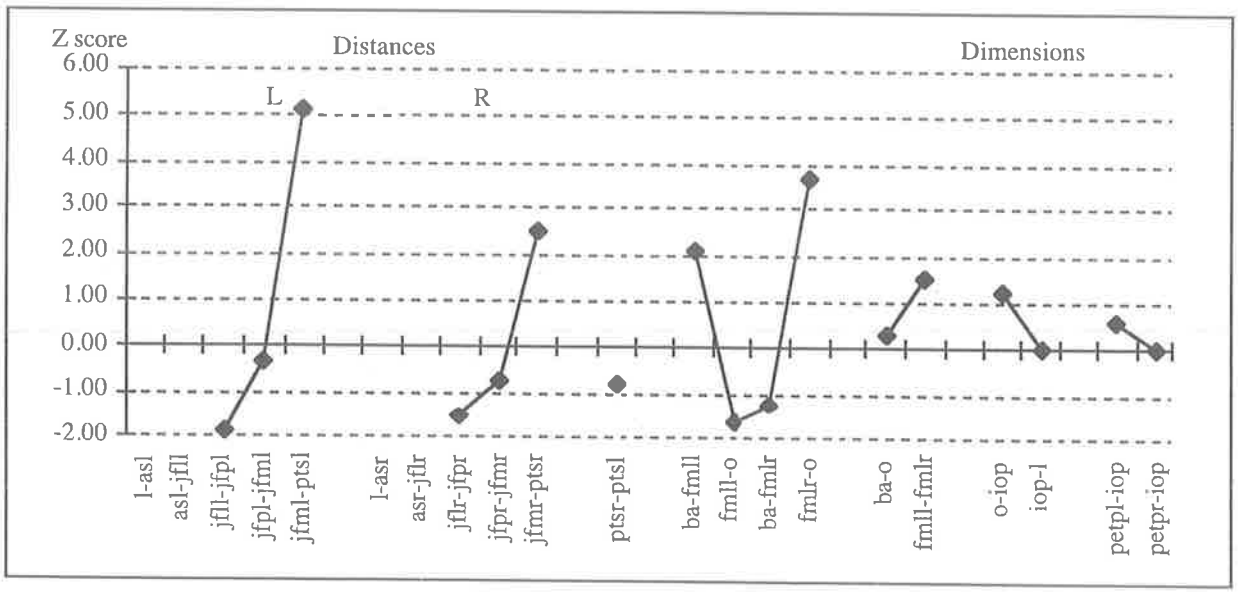

3.4.12.12 The Cranial Base Sutures of Patient IP

Anterior Cranial Fossa (Figure 3.30(q)): The majority of distances measured were abnormal. The spheno-ethmoid synchondrosis (es-cppl, es-cppr) was increased in length. The spheno-frontal suture in the anterior cranial fossa (cppl-spal, cppr-spar) was of normal length, while in the orbit, the suture (spal-zfsl, spar-zfsr) was reduced in length. The spheno-zygomatic suture (zfsl-gwll, zfsr-gwlr) length was increased.

Middle Cranial Fossa (Figure 3.30(q)): The lateral spheno-squamous temporal suture (gwll-fisl) was increased in length on the left side.

Posterior Cranial Fossa (Figure 3.30(q)): The medial temporo-occipital suture (inferior) (jfml-ptsl, jfmr-ptsr) and the occipital mastoid suture (superior) (jfll-petpl, jflr-petpr) were lengthened. The superior and inferior parts of the spheno-occipital synchondrosis (petal-petar, ptsl-ptsr) were normal, while the lateral part of the synchondrosis was increased in height (ptsl-petal, ptsr-petar).

Discussion: The cranial base sutures were abnormal anteriorly and laterally. Medially the spheno-occipital synchondrosis was deformed. The larger number of abnormal sutural findings in this patient are reflected by the more severe clinical deformity.

Figure 3.30(q) Z Scores of the Dimensions of the Cranial Base Sutures for Patient IP compared with the 2 Year Old Experimental Standard

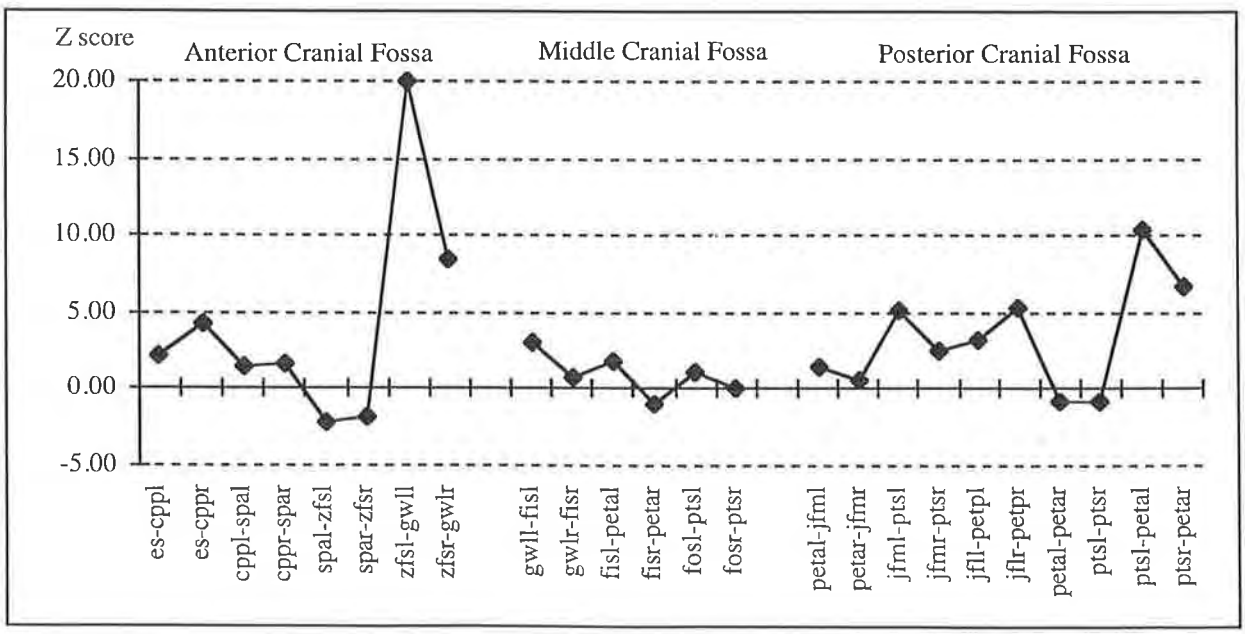

3.4.12.13 The Craniofacial Dimensions and Angles of Patient IP

Dimensions and Angles (Figure 3.30(r)): The facial heights were increased, however the patient's mouth was open, and the findings were not valid. The SNA angle was significantly reduced. (SNB was not valid for reasons stated previously). The cranial base angle (ba-s-n) was more obtuse. The cranial base dimensions were increased generally.

Discussion: This patient exhibits platybasia of the cranial base, and demonstrates the corresponding reduction in facial angle as a result of the distorted cranial base and the lack of forward projection of the maxilla (see maxilla).

Figure 3.30(r) Z Scores of the Craniofacial Dimensions and Angles for Patient IP compared with the 2 Year Old Experimental Standard

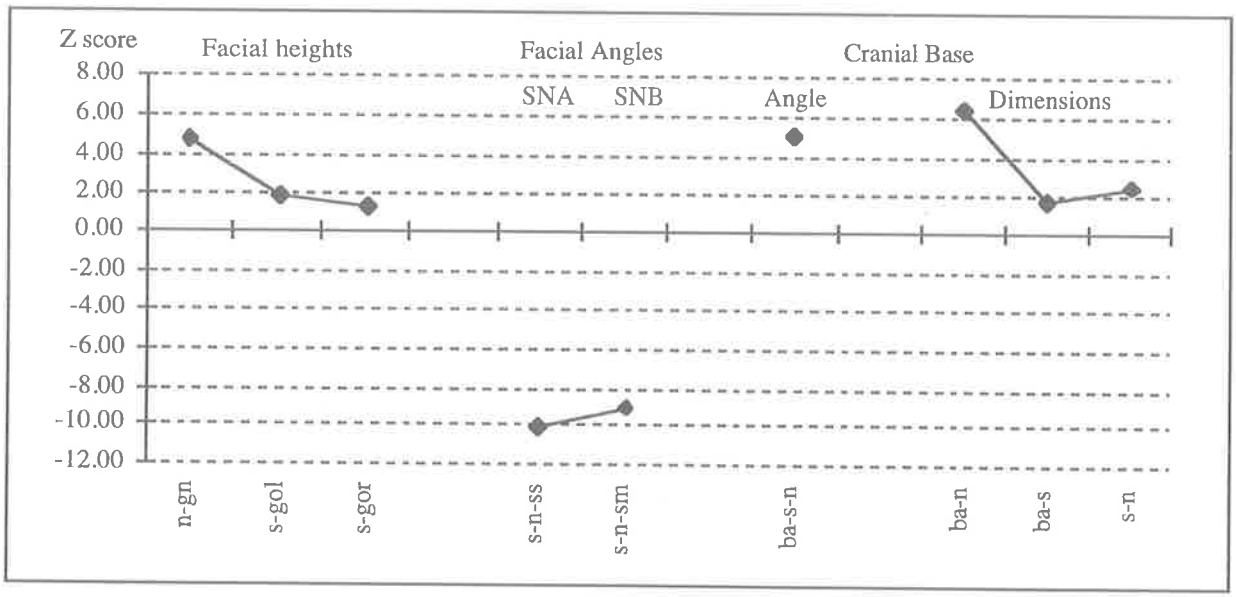

3.4.13 Clinical and Radiographic Findings for Patient LW

Clinical Features

This child presented aged 5 years and 6 months (Figure 3.5). There was no family history of Crouzon syndrome. A sagittal synostectomy had been performed elsewhere when he was 3 months of age. On examination, the calvarial shape was oxycephalic. He had proptosis and hypertelorism. Ptosis of the left eyelid, left amblyopia and astigmatism were also present. Mild bilateral papilloedema was found. He suffered chronic nasal obstruction and had bilateral middle ear effusions and hyponasal speech. Maxillary hypoplasia was evident and he had a class III occlusal relationship.

Lateral, Antero-Posterior and Basal Radiographs

Lateral, antero-posterior, and basal views showed fusion of all sutures with a copper-beaten appearance of the calvaria. The spheno-occipital synchondrosis was patent (best seen on the post-operative radiographs in Figure 3.5). The sella had an additional depression anteriorly in the region of the jugum sphenoidale. The lesser wings were swept up laterally producing the harlequin-mask appearance on the antero-posterior radiograph. The orbits were mildly dystopic with the left lower than the right. The second dentition was appearing in the hypoplastic maxilla.

3D CT Reconstruction

Calvarial bones: The head shape was mildly oxycephalic and scaphocephalic with complete calvarial suture fusion, including the zygomatico-spheno-temporal complex. A bilateral ridge along the sagittal suture was present, possibly a result of the previous craniectomy.

Cranial base: The cribriform plate was thin in the anterior cranial fossa. Small bony defects were seen above the orbits and in the region of the jugum sphenoidale and ethmoid spine. The lesser wings of the sphenoid were swept up and the greater wings were protruding into the orbits. Depression of the jugum sphenoidale anteriorly produced the appearance of double depression to the sella. The spheno-occipital synchondrosis was not visible as being patent on the 3D CT reconstruction. The jugular foramen was prominent on the left side and gave the

impression of a double system due to the notching in the foramen. The right hand jugular foramen was small in comparison.

Orbital: The orbital aperture was not greatly swept up laterally. The junction of the greater wing of the sphenoid with the zygomatic bone (at landmark greater wing laterale) produced a very deep notch. The medial wall and roof of the orbit showed evidence of bony thinning presumed due to endocranial resorption. The inferior orbital rim appeared to be hypoplastic and lower on the left side, compared with the right.

Maxilla: The second dentition was appearing. Hypoplasia of the zygomatic bone and maxilla were identified.

3.4.14 Features of the CT Scan and 3D Reconstruction of Patient LW that made Landmark Identification difficult

The calvarial landmarks (l, as, br, spt, spc) could not be identified nor reliably estimated. The peri-orbital sutures and cranial base landmarks were identified from the regional bony contours and junctions defined in the landmarks (Figures 3.15-3.26). The areas of bony absence in the region of the ethmoid and orbit did not interfere with the landmark identification.

3.4.15 Results and Discussion of the Quantitative Analysis of Patient LW compared with the 6 Year Old Experimental Standard

Figures 3.31(a)-(r)

3.4.15.1 The Mandible of Patient LW

Distances (Figure 3.31(a)): Several distances between the adjacent landmarks representing the outline of the bone were statistically significant compared with the experimental standard. The posterior superior body distance (em1il-cbl, em1ir-cbr) was increased bilaterally. The left posterior mandibular notch (mnl-cdl) was also increased.

Dimensions and Angles (Figure 3.31(b)): The only dimension outside the experimental standard limits was the anterior symphyseal height (gn-id). Similarly the angles were not involved except for the right mandibular notch angle (cdr-mnr-ctr) which was significantly smaller.

Discussion: In Patient LW only minor degrees of abnormality of the mandible were found. The increase in anterior symphyseal height may reflect a primary growth abnormality or a secondary growth change to compensate for the class III occlusion. In general the major dimensions and angles, affecting the shape and size of the whole mandible, were not different from the experimental standard and the anterior symphyseal height increase most likely represents a secondary change.

Figure 3.31(a) Z Scores of the Distances of the Mandible for Patient LW compared with the 6 Year Old Experimental Standard

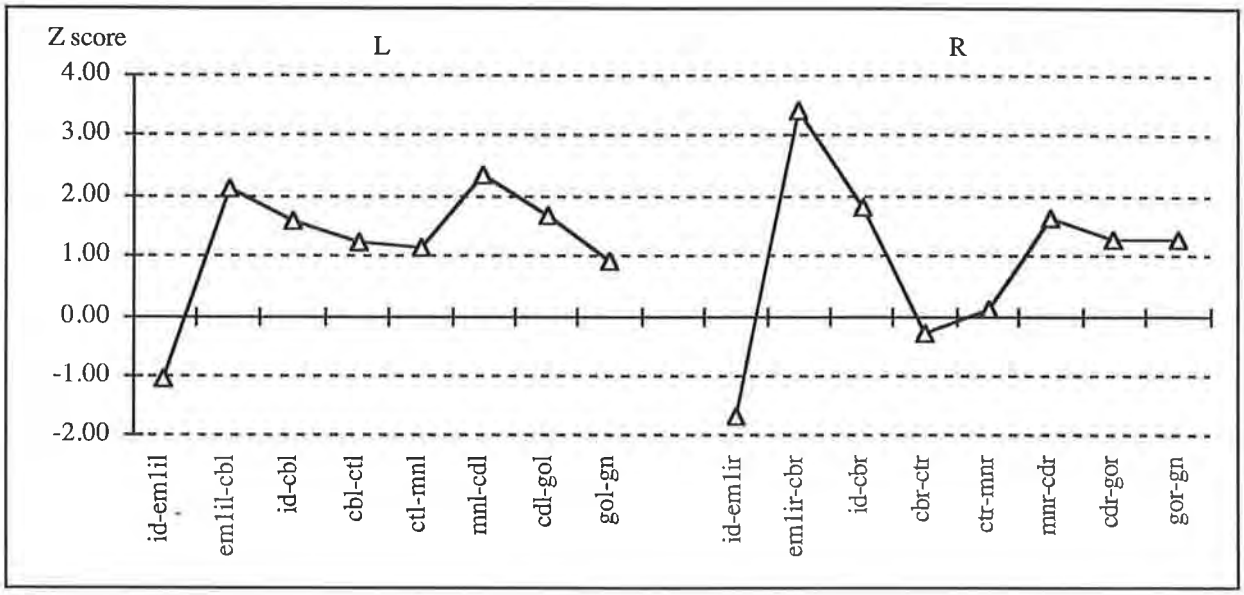

Figure 3.31(b) Z Scores of the Dimensions and Angles of the Mandible for Patient LW compared with the 6 Year Old Experimental Standard

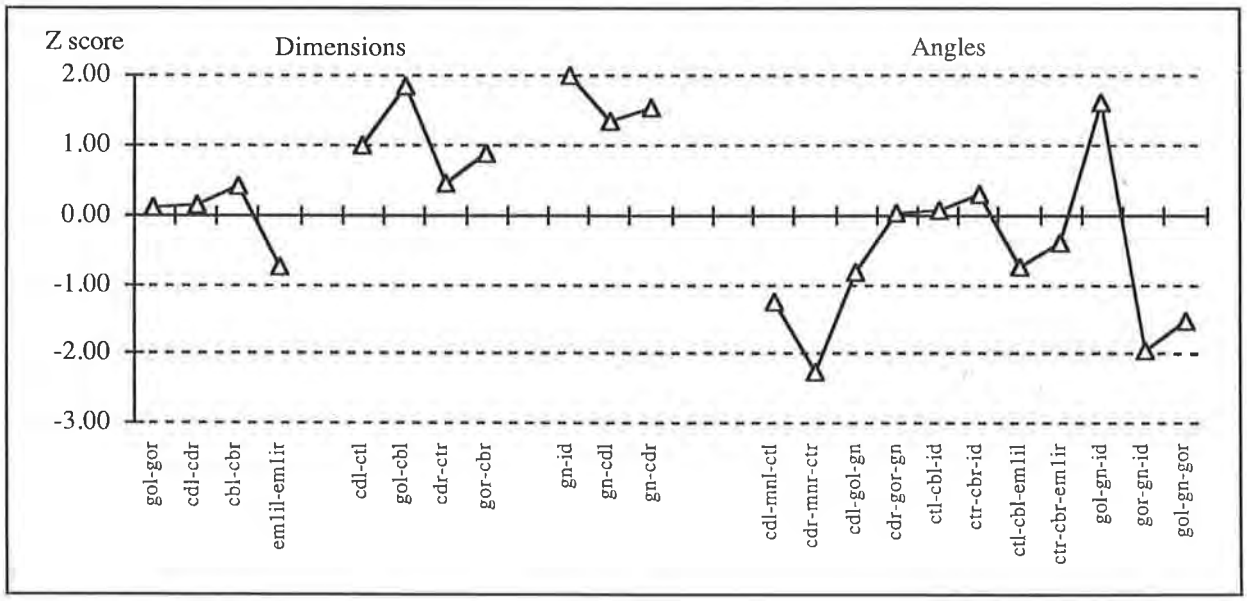

3.4.15.2 The Maxilla of Patient LW

Distances (Figure 3.31(c)): Multiple distances were significant in this patient. The fronto-maxillary suture (snml-morl, snmr-morr) was increased in length compared with the experimental standard. The frontal process of the orbital rim (nlil-morl, nlir-morr) was reduced in length while the medial infra-orbital rim (orl-nlil, orr-nlir) was increased in length. The anterior zygo-maxillary suture (zmil-orl) was shorter on the left with a tendency to be shorter on the right (zmir-orr). The lateral maxillary wall height (zmil-em1il, zmir-em1ir) was increased bilaterally. The lower pyriform margin (ans-all) was increased on the left side and the upper pyriform margin (all-inml, alr-inmr) was increased bilaterally. The right naso-maxillary suture (inmr-snmr) was reduced in length. Increased distances were recorded at the posterior alveolar margin (em1sl-mxtl, em1sr-mxtr), the posterior maxillary wall height (mxtr-msr) on the right, the posterior palatal height (em1sl-gpfl, em1sr-gpfr) and the superior palatal length (ans-pns).

Dimensions and Angles (Figure 3.31(d)): Most distances were within or close to the standard measurements. The anterior midline height of the maxilla (na-pr) was significantly increased. The superior length of the maxilla (msl-inml, msr-inmr) was increased bilaterally. The orbital floor angle (nlil-msl-iobfl) was increased on the left side. The posterior inferior angles of the maxilla (msl-gpfl-em1sl, msr-gpfr-em1sr) were increased. The palatal angle (gpfl-ans-gpfr) was reduced.

Discussion: The measurements in this patient reflect the reduced proportions of the maxilla on the left hand side. The left body and infra-orbital rim of the maxilla, in particular the attachment to the zygomatic bone was smaller than on the right. The alveolar height and postero-lateral wall of the maxilla were correspondingly increased. The midline structures, superiorly, were not significantly different from the experimental standard or were significantly increased. The measurements therefore reflect the clinical appearance of the hypoplastic inferior orbital rim especially on the left, and the relatively normal anterior position of the nasal complex.

Figure 3.31(c) Z Scores of the Distances of the Maxilla for Patient LW compared with the 6 Year Old Experimental Standard

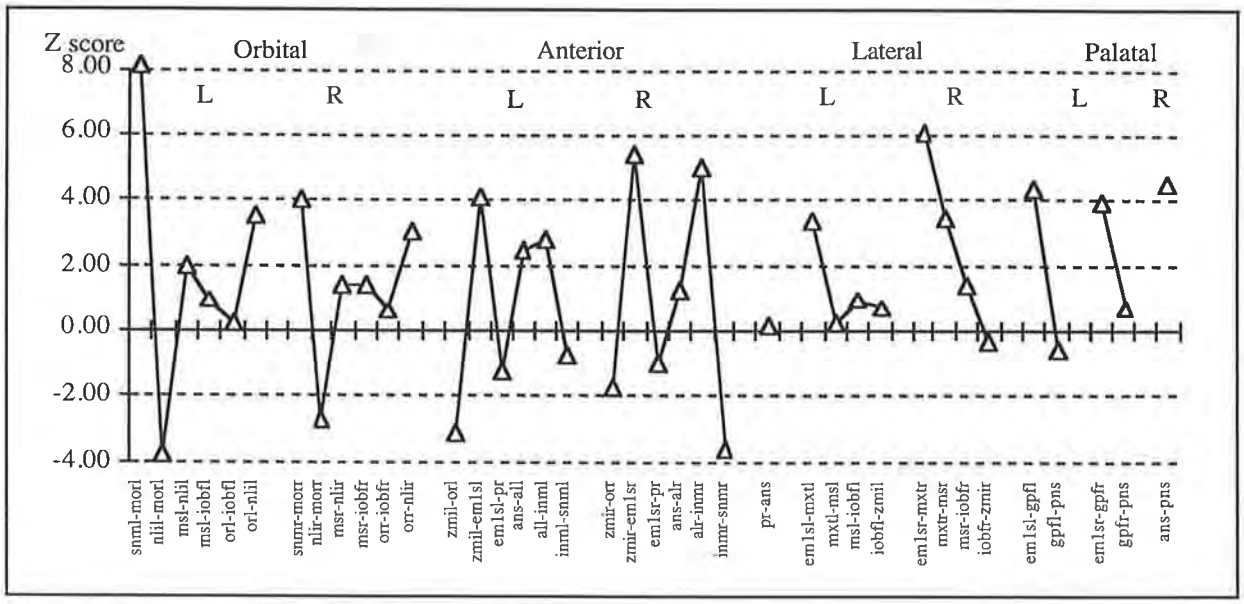

Figure 3.31(d) Z Scores of the Dimensions and Angles of the Maxilla for Patient LW compared with the 6 Year Old Experimental Standard

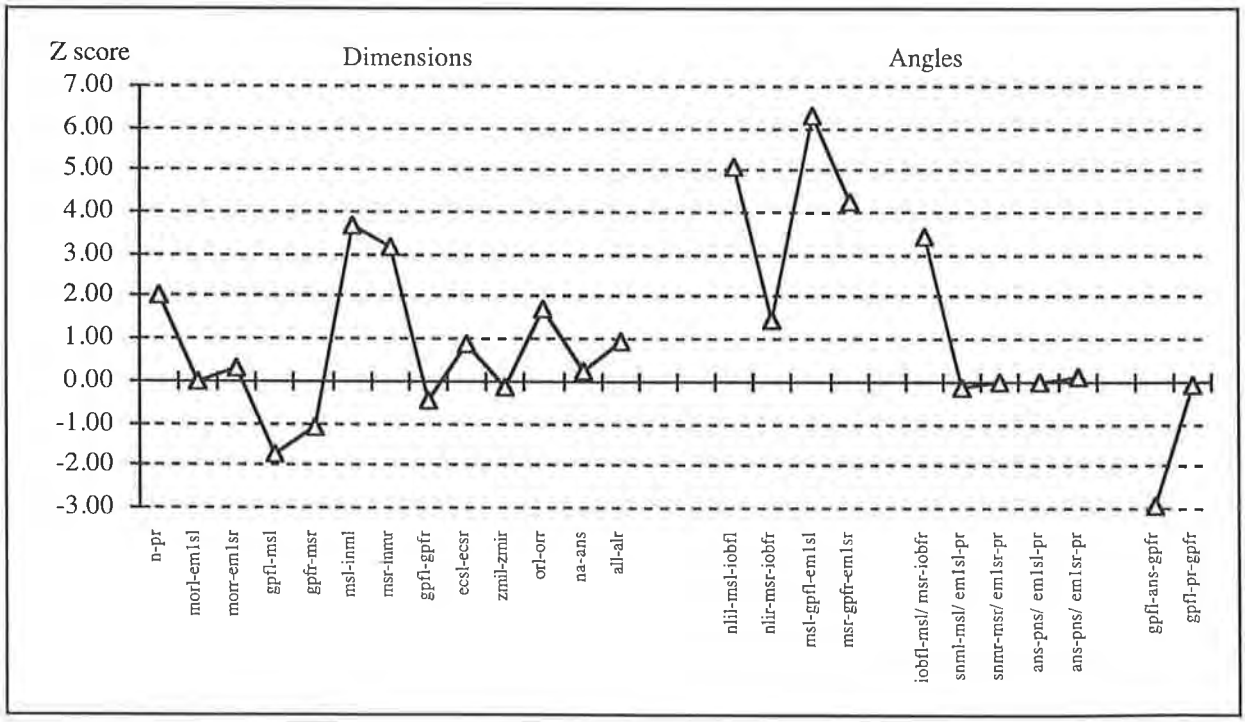

3.4.15.3 The Nasal Bones of Patient LW

Distances (Figure 3.31(e)): The length of the nasal bone (na-n) medially was at the upper limit of the experimental standard range. The length and width of the nasal bone was decreased on the right hand side (inmr-snmr, snmr-n).

Dimensions and Angles (Figure 3.31(e)): The superior width of the nasal complex (snml-snmr) was decreased. The angle of the nasal bones from the cranial base (s-n-na) was increased as was the splay of the nasal bones (inml-snml/snmr-inmr).

Discussion: The nasal bones were generally reduced in size. The deformity was more pronounced superiorly and laterally. The small bones were compensated for in size by the midline projection of the nasal complex. The nasal bones were anteriorly placed (see maxilla) and with an increased angle of projection.

Figure 3.31(e) Z Scores of the Measurements of the Nasal Bones for Patient LW compared with the 6 Year Old Experimental Standard

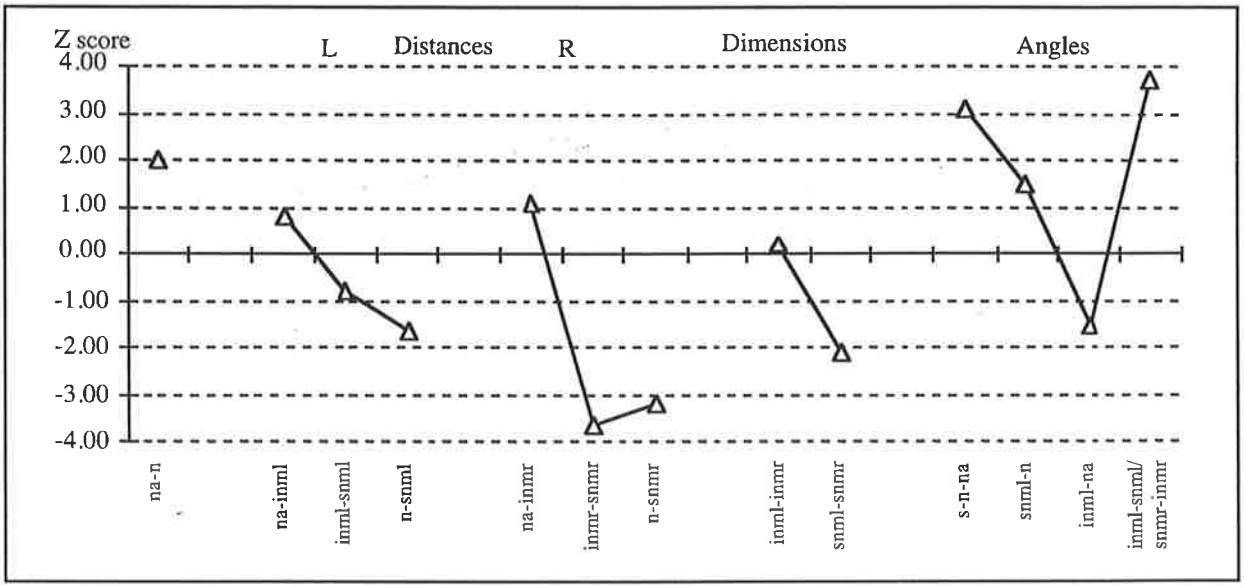

3.4.15.4 The Frontal Bone of Patient LW

Distances (Figure 3.31(f)):

Supra-orbital Region: Medially the fronto-nasal suture (n-snml, n-snmr) showed a trend to be reduced on the left and was significantly reduced on the right side. The fronto-maxillary sutures (snml-morl, snmr-morr) were significantly increased. Increased distances were also recorded at the superior medial orbital rim (sorl-slorl, sorr-slorr) and in the region of the anterior fronto-zygomatic suture (slorl-zfl, slorr-zfr). The right superior lateral orbital rim (sorr-slorr) was decreased.

Ethmoid Attachment: The projection of the nasal root from the foramen caecum (n-fc) was reduced. The frontal ethmoid attachment length (cpal-cppl, cpar-cppr) was increased at the level of the cribriform plate with decreased distances in the width of the attachment (cppl-ofaml, cppr-ofamr) and in its length in the orbital region (morl-ofaml, morr-ofamr) where it attaches to the lateral plate.

Sphenoid Attachment: The width or length of the superior orbital fissure (ofaml-sobfl, ofamr-sobfr) was decreased on the left with a similar trend seen on the right. The lesser wing length (spal-cppl, spar-cppr) was increased on the right with a similar trend found on the left side. The parietal attachment (spc-br) and sphenoid attachments (zfs-spc and spc-spa) were not recordable due to the fusion of sutures and hence poor visibility of landmarks in this region.

Dimensions (Figure 3.31(f)): The anterior prominence of the frontal bone was within the normal range (s-g) and the depth of the anterior cranial fossa (sorl-spal, sorr-spar) was not significantly different from the experimental standard. The anterior superior orbital width of the frontal bone (sorl-sorr), the antero-lateral superior orbital width (slorl-slorr), and the posterior width (spal-spar) were all significantly increased compared with the experimental standard.

Discussion: The fronto-maxillary sutures were increased in length and may contribute to displacing the orbits laterally. In addition the fronto-zygomatic suture was increased in length, and was related to the fusion of the of coronal sutures extending down into this region. A lesser severe abnormality was seen at the sphenoid lesser wing.

Figure 3.31(f) Z Scores of the Distances and Dimensions of the Frontal Bone for Patient LW compared with the 6 Year Old Experimental Standard

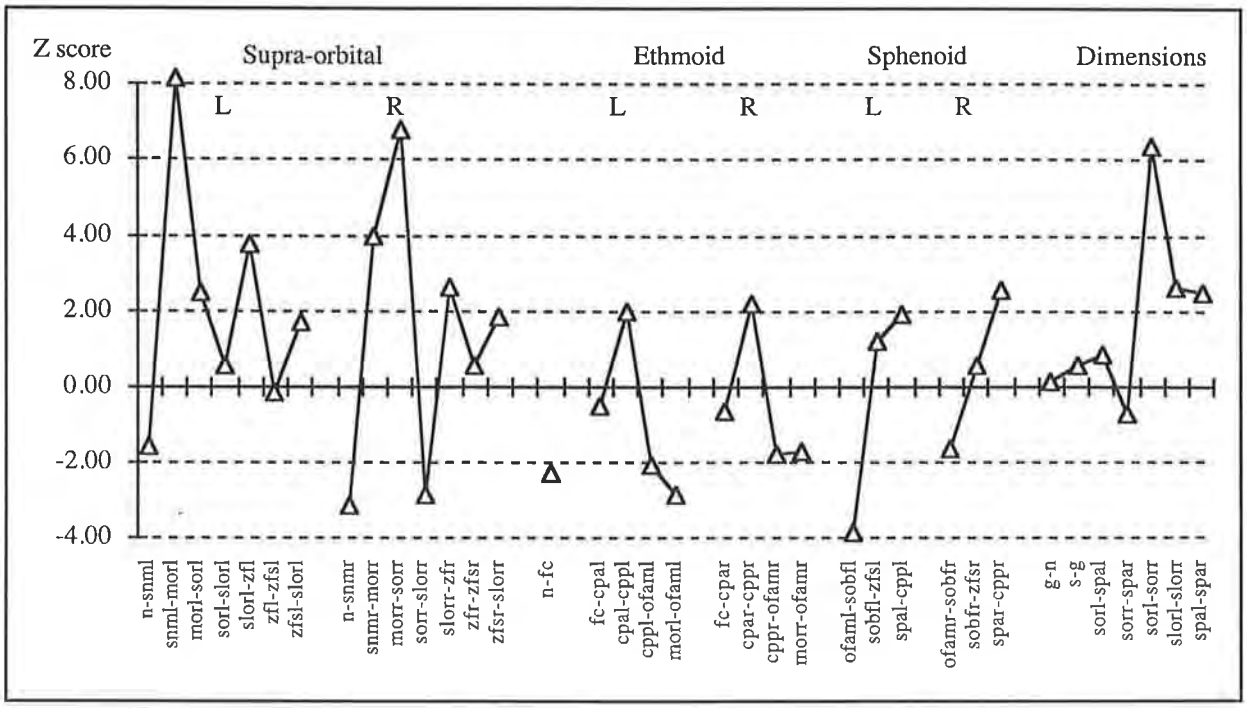

3.4.15.5 The Zygomatic Bone of Patient LW

Distances (Figure 3.31(g)): The spheno-zygomatic suture length (zfsl-gwll, zfsr-gwlr) was reduced on the left with a tendency to be reduced on the right. The anterior fronto-zygomatic suture (slorl-zfl, slorr-zfr) distance was increased bilaterally. The height of the lateral orbital wall (lorl-slorl, lorr-slorr) was increased, with a reduced height of the frontal process of the zygomatic bone (zfl-ztl) on the left. The zygo-maxillary suture (zmil-orl) was decreased on the left.

Dimensions (Figure 3.31(g)): No significantly different dimensions were measured.

Discussion: The length of the fronto-zygomatic suture was clearly abnormal. Fusion at this suture would be expected to reduce the vertical growth of the bone. The overall height of the zygomatic bone was within the limits of the experimental standard with the height of the lateral orbital rim being increased but the lateral frontal process reduced in height. A reduction in length of the zygo-maxillary suture was found and was related to the hypoplasia of the infra-orbital rim of the maxilla. Suture fusion, found qualitatively at the frontal, parietal and sphenoid junctions, also holds the zygomatic bone and lateral orbital wall posterior relative to the medial structures.

Figure 3.31(g) Z Scores of the Distances and Dimensions of the Zygomatic Bone for Patient LW compared with the 6 Year Old Experimental Standard

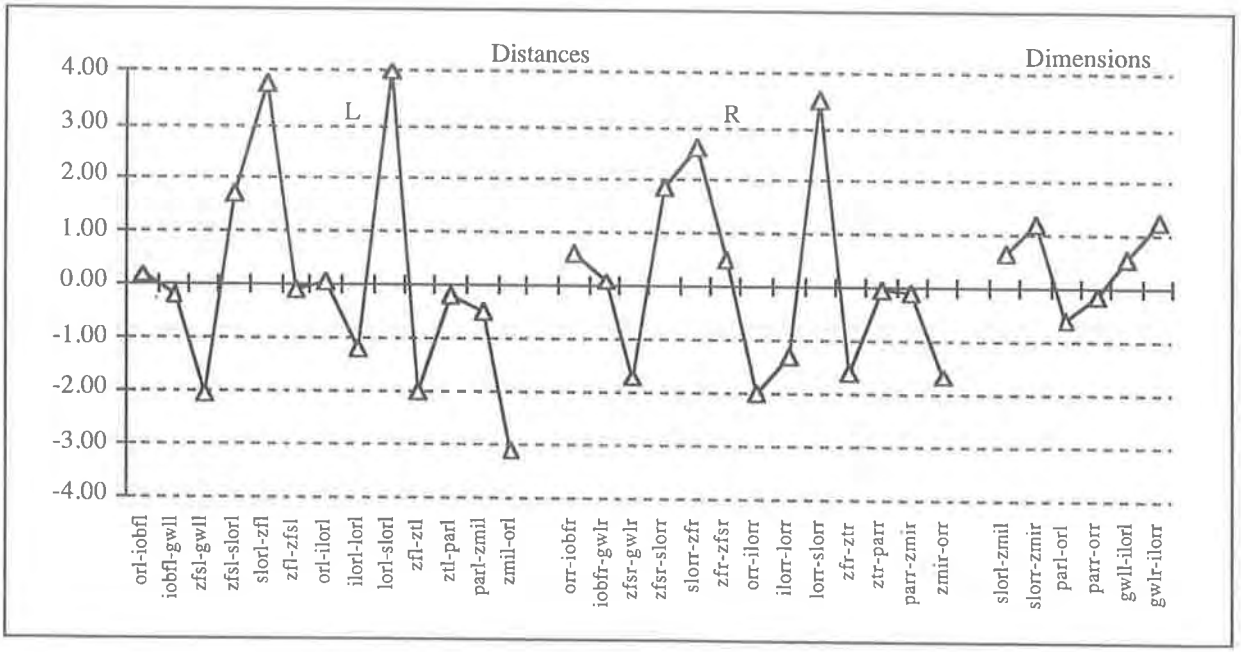

3.4.15.6 The Vomerine Bone of Patient LW

Distances, Dimensions and Angles (Figure 3.31(h)): The palatal distance (ans-pns) was increased compared with the experimental standard. The longitudinal dimension (h-ans) was not significantly different from the experimental standard. The angle of the vomer relative to the cranial base (s-n/h/ans) was significantly decreased.

Discussion: The vomer showed some variation in this patient but remained close to normal limits. The decreased angle of the vomer was related to the medial prominence of the naso-maxillary complex (see maxilla) and may have partly resulted from the cranial base deformity in this patient, where the cranial base angle was found to be reduced (see craniofacial dimensions and angles).

Figure 3.31(h) Z Scores of the Measurements of the Vomer for Patient LW compared with the 6 Year Old Experimental Standard

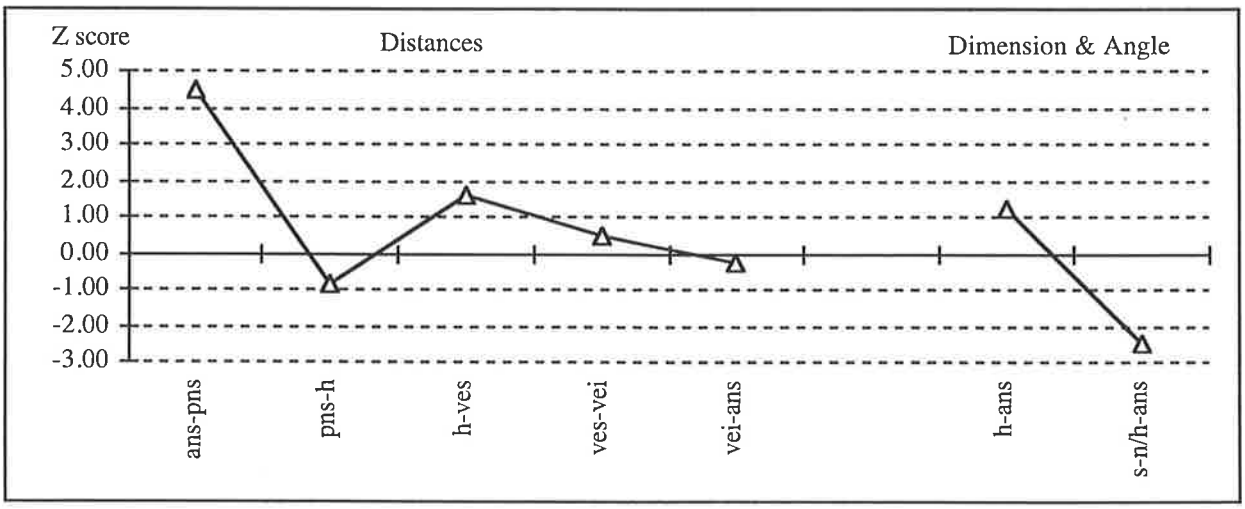

3.4.15.7 The Ethmoid Bone of Patient LW

Lateral Ethmoid Plate (Figure 3.31(i)):

Distances: The majority of lateral ethmoid plate distances forming the medial orbital wall, that were measured, were reduced. The anterior border of the lateral plate (nlil-morl, nlir-morr) was reduced in height and the orbital length of the frontal ethmoid attachment (morl-ofaml, morr-ofamr) was reduced bilaterally. The height of the posterior border of the lateral plate (ofamr-msr) was also reduced on the right. The exception was the junction with the maxilla at the inferior border of the lateral plate (msl-nlil, msr-nlir) which was increased on the left and showed a similar trend on the right. The posterior frontal ethmoid attachment (cppl-ofaml, cppr-ofamr) was reduced, with a tendency for an increased width anteriorly (morl-cpal, morr-cpar).

Dimensions and Angles: The inter-orbital dimension (morl-morr) and the dimension between the optic canals (ofaml-ofamr) were significantly increased. The splay of the lateral plates (msl-ofaml/ofamr-msr) was reduced posteriorly.

Figure 3.31(i) Z Scores of the Measurements of the Lateral Ethmoid Plate for Patient LW compared with the 6 Year Old Experimental Standard

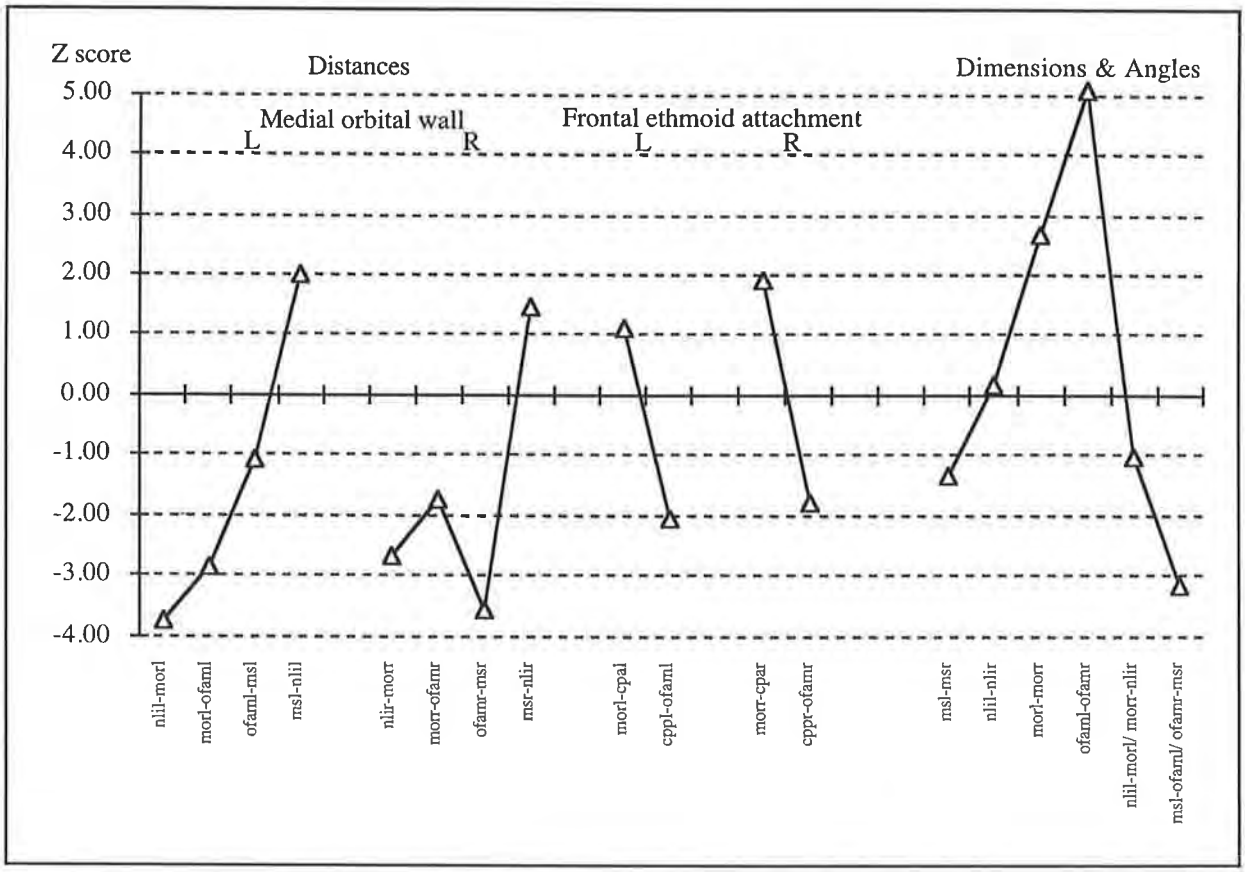

3.4.15.7 The Ethmoid Bone of Patient LW (continued)

Cribriform Plate (Figure 3.31(j)):

Distances: The spheno-ethmoid synchondrosis (es-cppl, es-cppr) was increased in width. The length of the plate was increased bilaterally (cpal-cppl, cpar-cppr).

Angles: The lateral angle of the cribriform plate compared with the nasion - sella line (s-n/cpar-cppr) was significantly increased on the right. The medial angle of the cribriform plate (n-s/es-fc) was reduced suggesting depression of the cribriform plate.

Medial Ethmoid Plate (Figure 3.31(j)):

Distances: The distance from the nasion to foramen caecum (n-fc) was decreased with the remainder of the measurements of the medial plate not significantly different from the experimental standard.

Dimensions: The dimensions were not significantly different from the experimental standard.

Discussion: The lateral plate was reduced in height and in superior length. The cribriform plate was increased in length but was depressed, while the medial plate was relatively normal. Anteriorly, the inter-orbital distance was increased and posteriorly the spheno-ethmoid synchondrosis was widened. The pattern of distortion of the ethmoid was of a reduced orbital component with a broadening and an increased length of the cribriform plate. This fits with the clinical appearance of a predominant orbital volume and rim deficit with hypertelorism, with a reasonable midline protrusion.

Figure 3.31(j) Z Scores of the Measurements of the Cribriform and Medial Ethmoid Plates for Patient LW compared with the 6 Year Old Experimental Standard

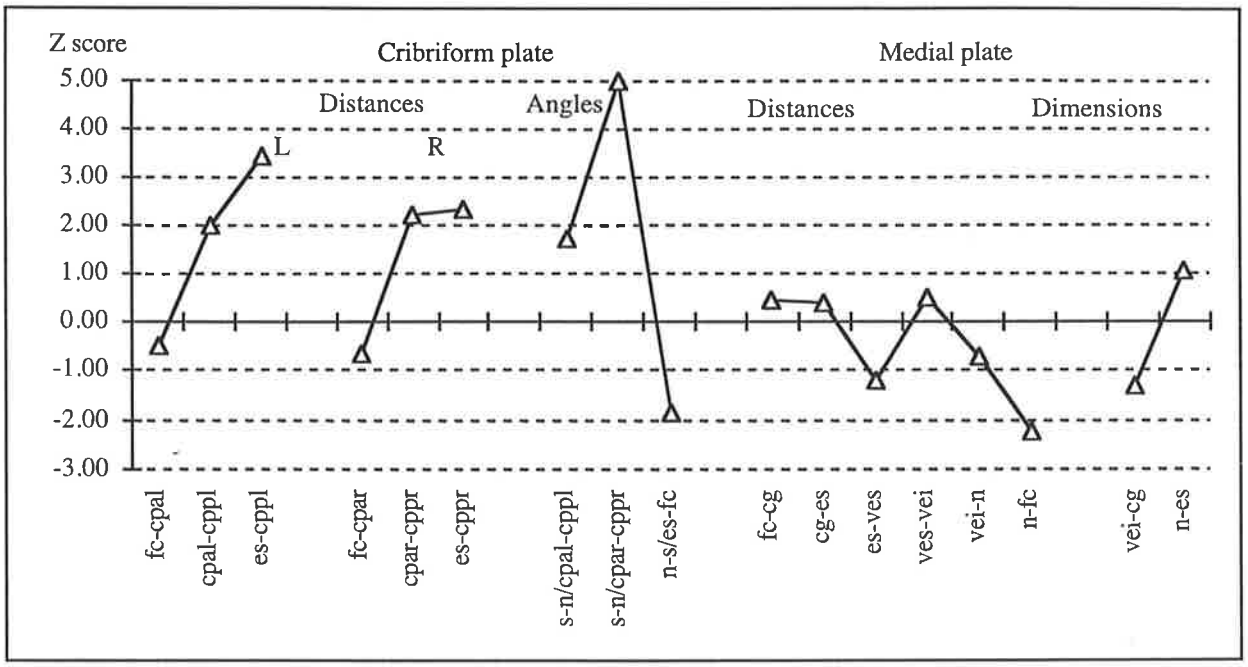

3.4.15.8 The Sphenoid Bone of Patient LW

Lesser Wing (Figure 3.31(k)):

Distances: All the distance measurements of the lesser wing (ofaml-acl, ofamr-acr, acl-spal, acr-spar, spal-es, spar-es) were increased bilaterally compared with the experimental standard.

Dimensions and Angles: The dimension between the tips of the wings (spal-spar) was increased. The angle of the lesser wings (spal-es-spar) was not significantly different from the experimental standard, while the splay of the lesser wings from the midline (n-s/acl-spal, n-s/acr-spar) was significantly increased bilaterally.

Pterygoid Plate (Figure 3.31(k)):

Distances and Angles: The distances of the pterygoid plate were not significantly different from the experimental standard. The axis of the pterygoid plates (n-s/ptsl-hpl, n-s/ptsr-hpr) was significantly decreased bilaterally, implying they were angled more medially and/or anteriorly from the midline than the controls when measured from the nasion-sella line.

Greater Wing (Figure 3.31(l)):

Distances: The spheno-zygomatic suture (gwll-zfsl) and the superior orbital fissure length (gwml-sobfl) were reduced on the left side compared with the experimental standard. A tendency for these distances to be reduced on the right side was also seen. Landmarks on the squamous sphenoid bone (spt and spc) could not be identified bilaterally, due to fusion of the calvarial bone in this region and hence the distances of the lateral part of the bone could not be measured. The posterior floor of the greater wing was increased in length (fosl-petal) adjacent the spheno-temporal suture on the left side.

Dimensions and Angles: While the angles of protrusion of the greater wing were increased (zfsl-gwml/gwmr-zfsr and gwll-gwml/gwmr-gwlr), the angle of splay of the greater wing relative to the floor (zfsl-gwml-ptsl, zfsr-gwmr-ptsr) was decreased. The posterior angle of the greater wing (fosl-petal/petar-fosr) was normal.

Figure 3.31(k) Z Scores of the Measurements of the Lesser Wing and Pterygoid Plate of the Sphenoid for Patient LW compared with the 6 Year Old Experimental Standard

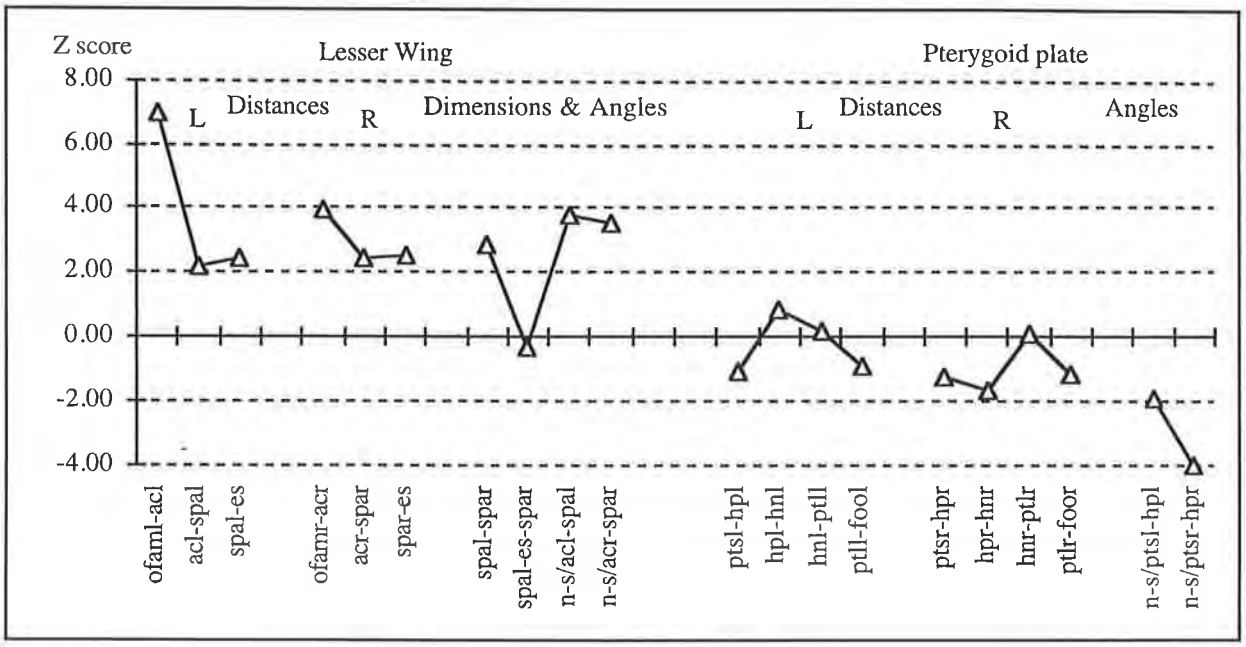

Figure 3.31(l) Z Scores of the Measurements of the Greater Wing of the Sphenoid for Patient LW compared with the 6 Year Old Experimental Standard

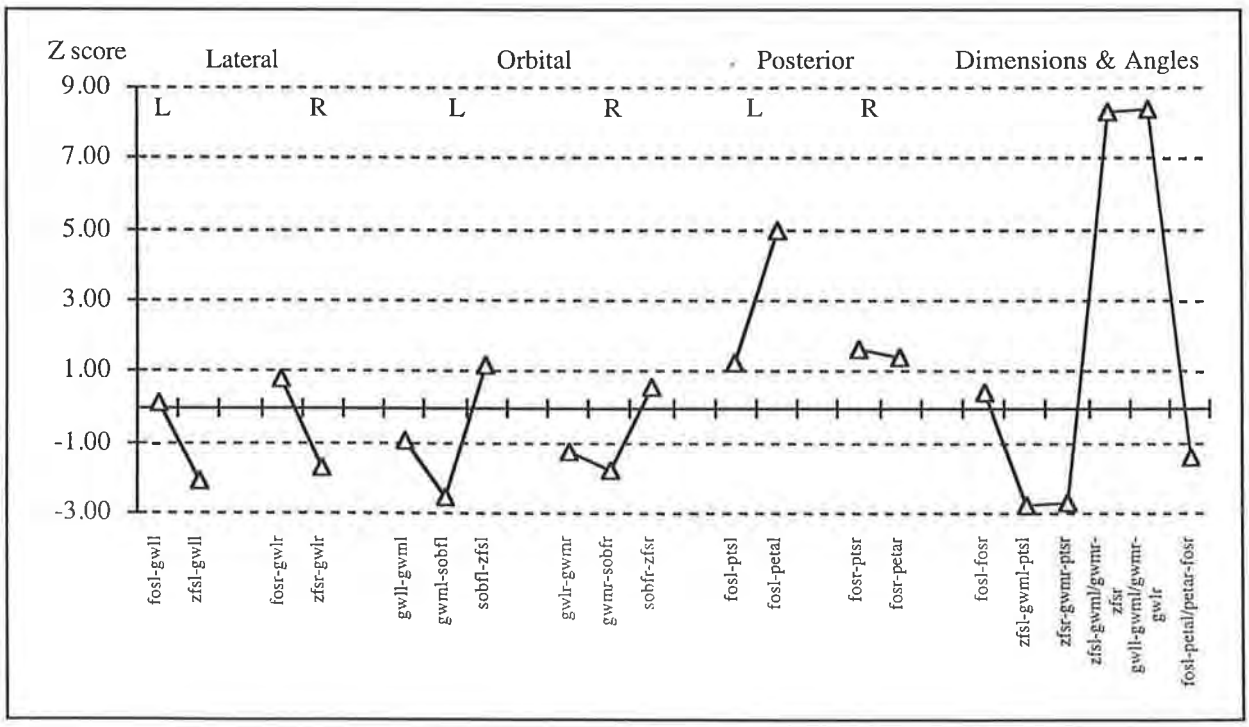

3.4.15.8 The Sphenoid Bone of Patient LW (continued)

Body of Sphenoid (Figure 3.31(m)):

Distances: The majority of the body distances were larger than the mean of the experimental standard. The inferior lateral length (gwml-ptsl, gwmr-ptsr) was increased along with the lateral height of the spheno-occipital synchondrosis (ptsl-petal, ptsr-petar) bilaterally. The anterior body had increased distances at the spheno-ethmoid synchondrosis (es-cppl, es-cppr). The posterior frontal ethmoid attachment (cppl-ofaml, cppr-ofamr) was reduced in length with a corresponding increase in distance to the greater wing mediale (ofaml-gwml). The measured distances of the floor and sella were not significantly different from the experimental standard.

Dimensions and Angles: While the anterior inferior width of the body (gwml-gwmr) was within the experimental standard, the measurement between the anterior optic foramina was increased (ofaml-ofamr). The superior spheno-occipital synchondrosis (petal-petar) was normal. The height of the posterior clinoid processes was increased on the left side (ptsl-pcl). The angles of the body from the midline were normal. The angle of the floor of the sphenoid body (es-ves-h) was more acute.

Discussion: This sphenoid bone in this patient was abnormal in most areas. The lesser wings were elongated with greater protrusion of the lesser and greater wings. Medially, the spheno-ethmoid synchondrosis was lengthened. The pterygoid plate was splayed anteriorly and medially. This position may account for the relatively prominent midline facial structures (see maxilla and nasal bones). The deformity was also present posteriorly, in particular, in the region around the spheno-occipital synchondrosis and the sphenoid body was enlarged. The findings were consistent with a mixed pattern of sutural involvement and the effects of raised intracranial pressure on the size of the sphenoid body.

Figure 3.31(m) Z Scores of the Measurements of the Body of the Sphenoid for Patient LW compared with the 6 Year Old Experimental Standard

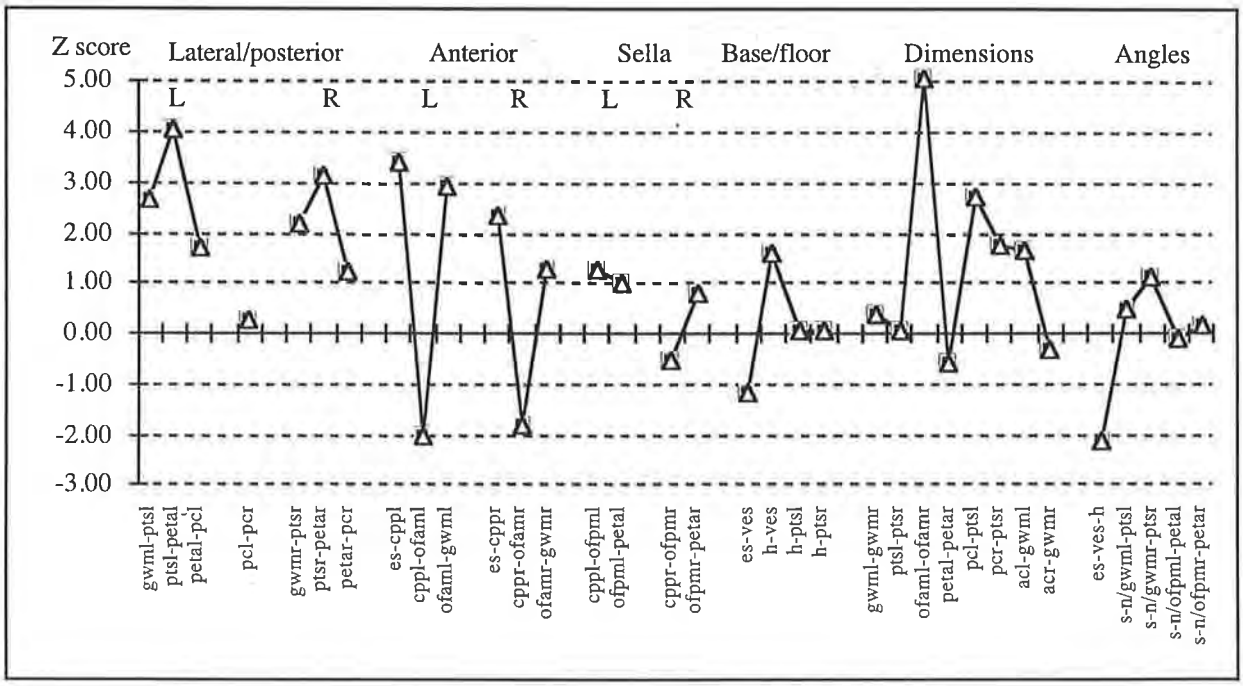

3.4.15.9 The Temporal Bone of Patient LW

Distances (Figure 3.31(n)):

Squamous Temporal Bone: The temporal squamous bone was not fully measurable in this child due to lack of visibility of the asterion (as) and sphenion (spt). The medial mastoid height (mal-smfl) was significantly increased on the left compared with the experimental standard.

External Auditory Meatus: The lateral mastoid prominence (mal-eamil, mar-eamir) was increased bilaterally. The configuration of the external auditory meatus was symmetrical with decreased distances of the superior anterior rim on the right (por-eamar) with a similar trend seen on the left.

Zygomatic Process: The zygomatic process had symmetrical pattern profiles, where the length of the zygomatic arch (ztl-aul) decreased on the left with a similar tendency on the right. The articular fossa height (afl-ael, afr-aer) was normal.

Petrous Temporal Bone (Figure 3.31(o)): The sphenoid-petrous temporal suture (fisr-petar) was increased in length on the right with a tendency to be increased on the left. The right jugular foramen width was narrowed (jflr-jfmr) with a similar pattern profile seen on the left. The inferior occipital mastoid suture distance (mal-jfll, mar-jflr) was increased bilaterally, along with the left medial temporo-occipital suture (inferior) (jfml-ptsl).

Dimensions and Angles (Figure 3.31(o)): The petrous temporal ridge dimension (petal-petpl, petar-petpr) was increased bilaterally. The dimensions between the temporal bone were normal. The angle of the zygoma projection (petal-aul-ztl, petar-aur-ztr) was normal, as were the angles of the auditory canal (pol-iaml/iamr-por) and the petrous temporal bone (petpl-petal/petar-petpr).

Discussion: The mastoid process was prominent with minimal symmetrical deformity of the external auditory meatus. The length of the zygomatic process was decreased and may be related to fusion of surrounding squamous sutures. Sutures around the petrous temporal bone were increased in length producing some lengthening of the petrous temporal bone with narrowing of the jugular foraminae. This was a common finding for this region in the patients studied.

Figure 3.31(n) Z Scores of the Distances of the Temporal Bone for Patient LW compared with the 6 Year Old Experimental Standard

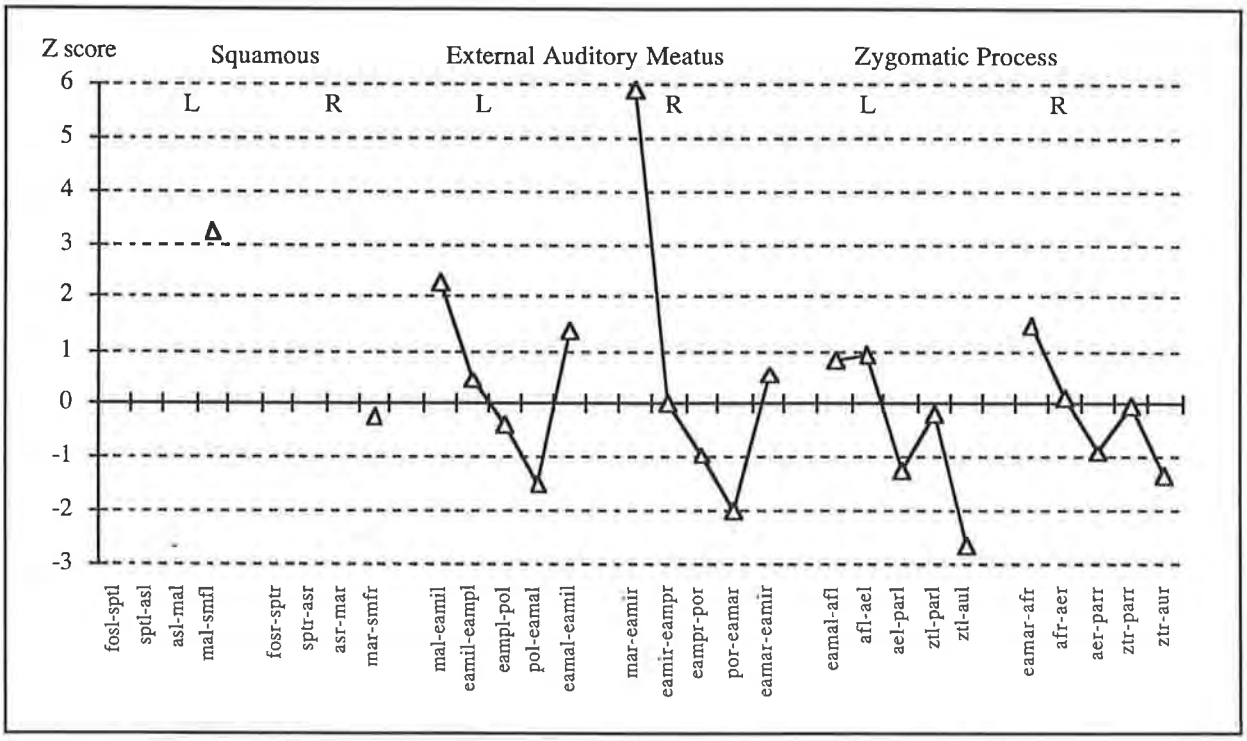

Figure 3.31(o) Z Scores of the Measurements of the Temporal Bone for Patient LW compared with the 6 Year Old Experimental Standard

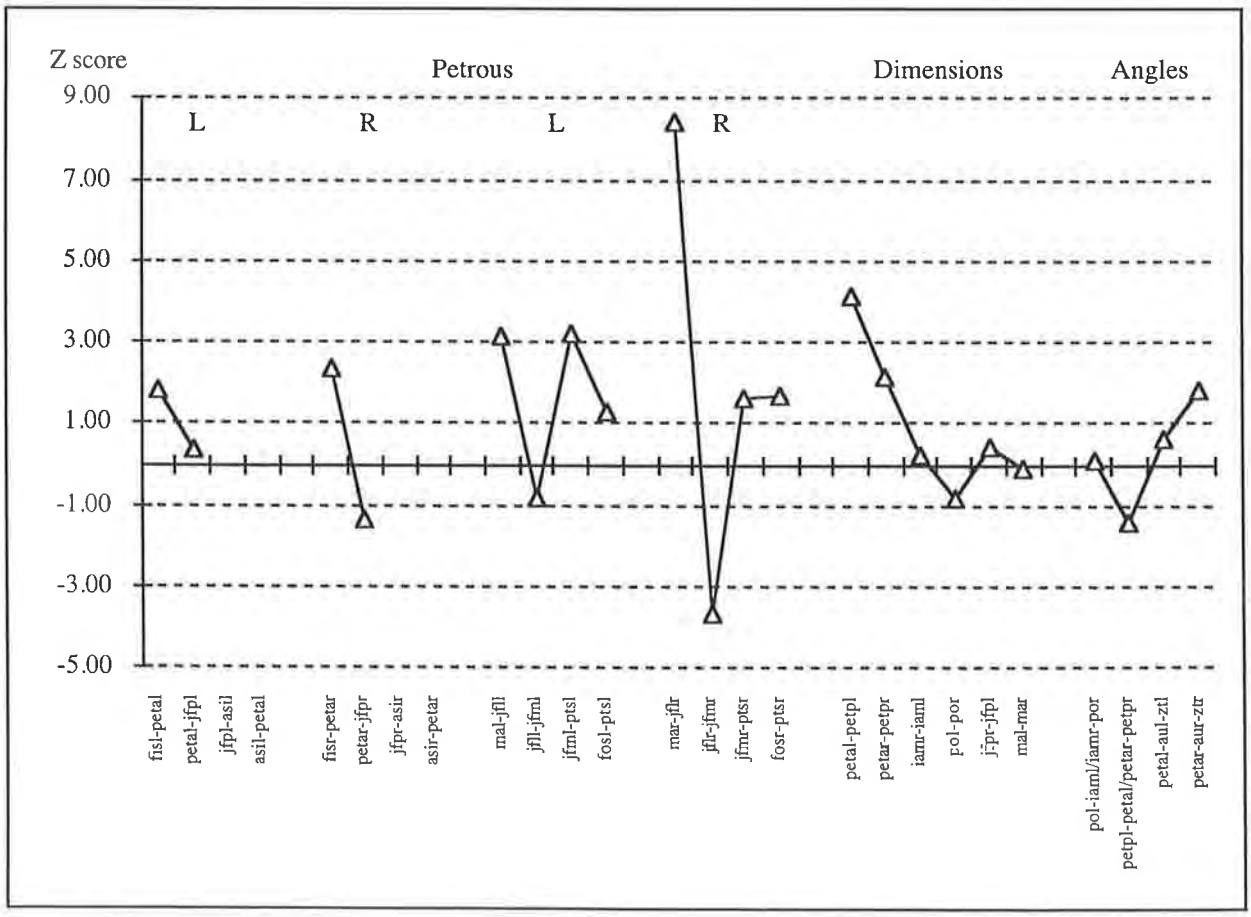

3.4.15.10 The Parietal Bone of Patient LW

Distances: The key landmarks for the parietal bone for Patient LW were not visible due to suture fusion and could not be reliably estimated. Therefore the parietal bone was not measured and a pattern profile of Z scores was not generated. The measurement data for the experimental standard are reported in Appendix 2.

3.4.15.11 The Occipital Bone of Patient LW

Distances (Figure 3.31(p)): The distances measured on the occipital bone and the foramen magnum were not significantly different from the experimental standard except for the medial temporo-occipital suture (inferior) (jfml-ptsl), which was increased in length on the left with a similar tendency on the right. The inferior spheno-occipital synchondrosis was not significantly different (see sphenoid and cranial base sutures for other distances.

Dimensions (Figure 3.31(p)): The dimensions were not significantly different from the experimental standard.

Discussion: The measurements of the occipital bone were abnormal along the suture with the temporal bone. Qualitatively, the lambdoid sutures were fused.

Figure 3.31(p) Z Scores of the Distances and Dimensions of the Occipital Bone for Patient LW compared with the 6 Year Old Experimental Standard

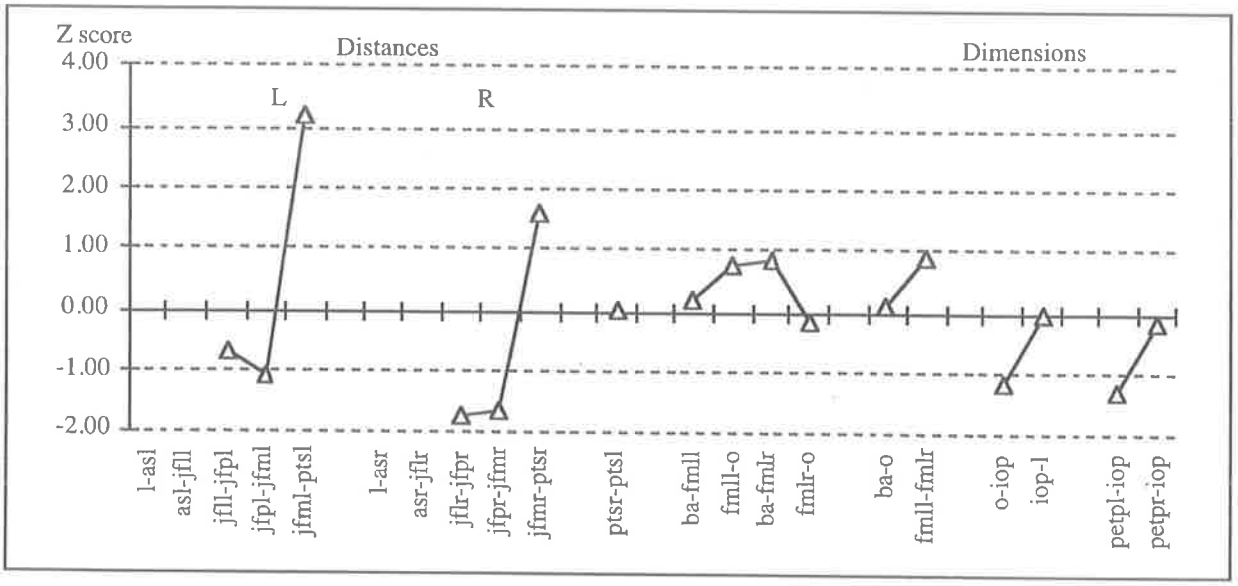

3.4.15.12 The Cranial Base Sutures of Patient LW

Anterior Cranial Fossa (Figure 3.31(q)): The spheno-ethmoid synchondrosis (es-cppl, es-cppr) was increased in length along with the spheno-frontal suture (cppl-spal, cppr-spar) in the anterior cranial fossa. In the orbit, the suture was normal and the spheno-zygomatic suture (zfsl-gwll, zfsr-gwlr) was reduced in length.

Middle Cranial Fossa (Figure 3.31(q)): The sutures were relatively normal with a posterior increase in length of the right spheno-petrous temporal suture (fisr-petar).

Posterior Cranial Fossa (Figure 3.31(q)): The left medial temporo-occipital suture (inferior) (jfml-ptsl) and the occipital mastoid sutures (superior) (jfll-petpl, jflr-petpr) were significantly increased. The superior and inferior parts of the spheno-occipital synchondrosis (petal-petar, ptsl-ptsr) were normal, while the lateral part of the synchondrosis (petal-ptsl, petar-ptsr) was increased in height.

Discussion: Many abnormal measurements were found in the cranial base in this patient. Anteriorly, significant involvement was seen medially while posteriorly the temporal bone was involved laterally and the spheno-occipital synchondrosis deformed medially.

Figure 3.31(q) Z Scores of the Dimensions of the Cranial Base Sutures for Patient LW compared with the 6 Year Old Experimental Standard

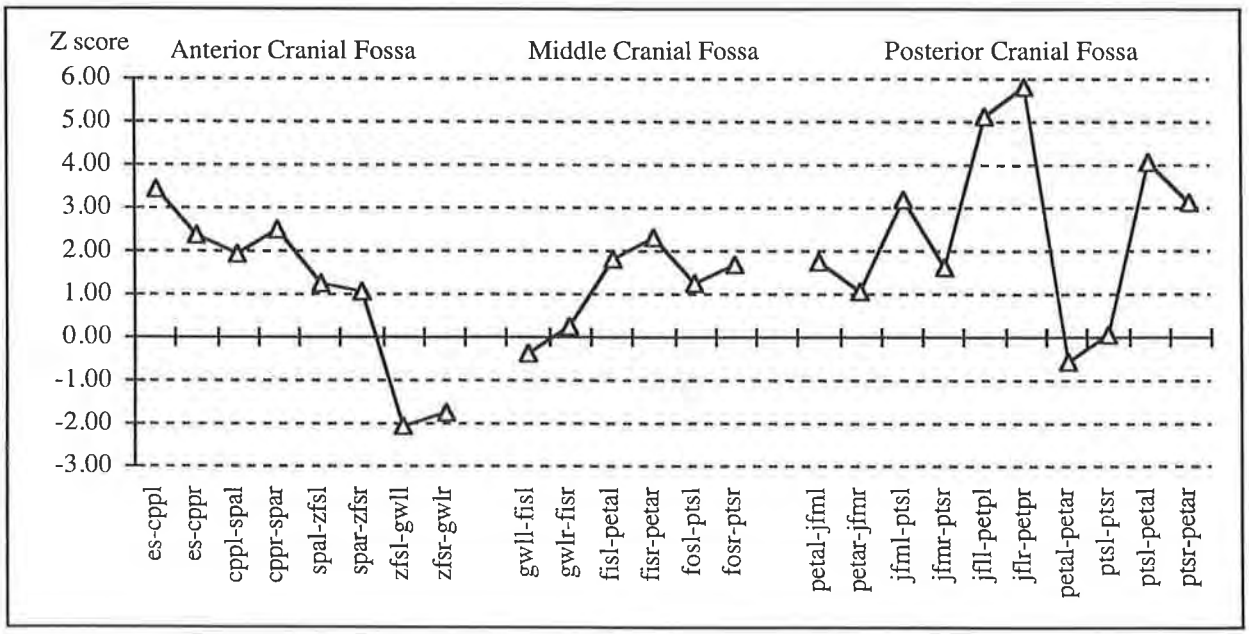

3.4.15.13 The Craniofacial Dimensions and Angles of Patient LW

Dimensions and Angles (Figure 3.31(r)): The facial heights were increased, however the patient's mouth was open during the CT scan and the measurements were not valid. The SNA angle (s-n-ss) was normal and the SNB angle (s-n-sm) was not valid. The cranial base angle (ba-s-n) was more acute in this patient. The cranial base dimensions were not significantly different from the experimental standard, with a tendency for the clivus to be lengthened (b-s).

Discussion: The cranial base angle was reduced in this patient. The SNA angle was normal and reflects the midline projection of the naso-maxillary complex. Therefore the medial orbital wall was prominent, however, the lateral orbital wall was deficient, influenced by the lateral calvarial suture fusion.

Figure 3.31(r) Z Scores of the Craniofacial Dimensions and Angles for Patient LW compared with the 6 Year Old Experimental Standard

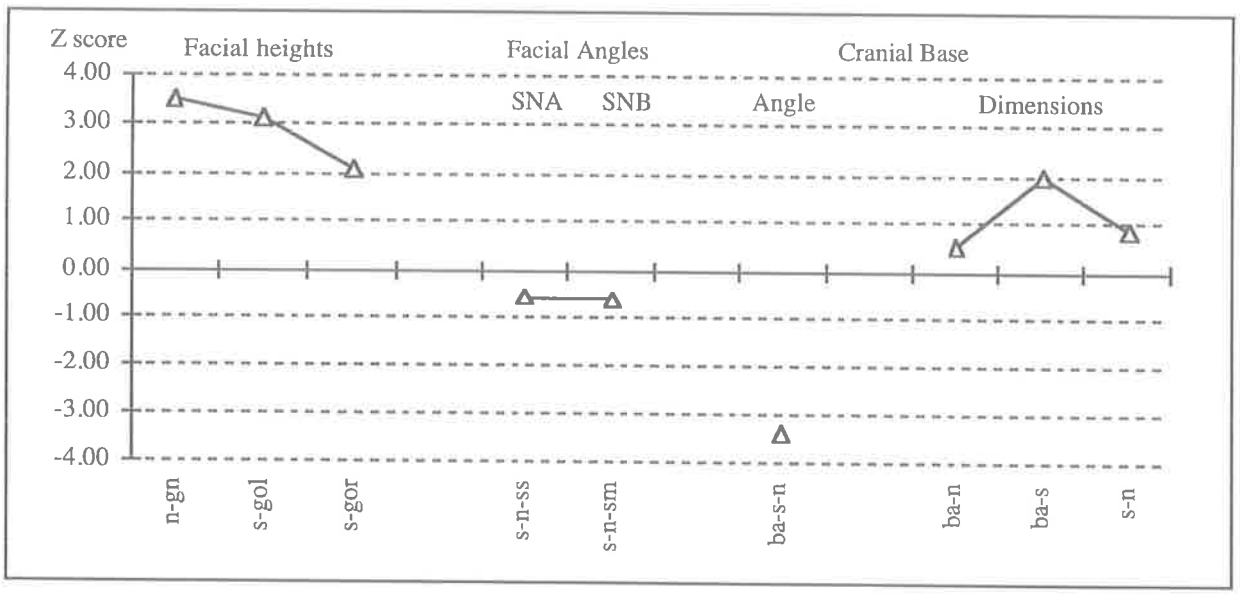

NB: Supramentale (sm) not accurate due to open mouth of patient.

3.4.16 Clinical and Radiographic Findings for Patient AY

Clinical Features

This patient first presented aged 5 years and 5 months with a mild form of Crouzon syndrome (Figure 3.6). There was no family history. A ventriculo-peritoneal shunt had been inserted elsewhere as an infant. The calvarial shape was turricephalic and he displayed mild proptosis, hypertelorism and had a divergent squint. The nasal septum was deviated and the maxilla was hypoplastic with a class 3 occlusal relationship. The palate was described as being high and arched. There was no evidence of upper airway obstruction however his speech was hypo- and hypernasal with articulation difficulties. There was no functional indication for surgical intervention and the patient was under annual review.

Lateral and Antero-Posterior Radiographs

The lateral and antero-posterior radiographs demonstrated the shunt in situ. A mild oxycephalic head shape was seen with a very mild copper-beaten appearance of the calvaria. The coronal sutures appeared to be faintly visible inferiorly. The other sutures were not seen. The spheno-occipital synchondrosis was patent. The lesser wings of the sphenoid were swept up laterally. Hypertelorism was associated with broad ethmoid and maxillary sinuses. The second dentition was emerging.

3D CT Reconstruction

Calvarial bones: A faint outline of the coronal sutures was present otherwise all sutures were fused.

Cranial base: The lesser wing of the sphenoid appeared to be short in its lateral projection. Protrusion of the greater wing of the sphenoid into the orbit was noted. The middle cranial fossa was unremarkable. The spheno-occipital synchondrosis was not visible. The foramen magnum was long and pointed posteriorly.

Orbital: The shape of the orbital aperture was somewhat ovoid in the horizontal axis. Mild medial and lateral wall bulging was noted. The zygomatic bone and orbital rim were underdeveloped. The left external auditory meatus was hidden by the zygomatic arch.

Maxilla: The maxilla was narrow and short.

3.4.17 Features of the CT Scan and 3D Reconstruction for Patient AY that made Landmark Identification difficult

The infra-orbital foramen could not be identified. The calvarial landmarks (l, as, br, spt, spc) could not be identified nor reliably estimated. The peri-orbital sutures and cranial base landmarks were identified from the regional bony contours and junctions defined in the landmarks (Figures 3.15-3.26).

3.4.18 Results and Discussion of the Quantitative Analysis of Patient AY compared with the 6 Year Old Experimental Standard

Figures 3.32(a)-(r)

3.4.18.1 The Mandible of Patient AY

Distances (Figure 3.32(a)): The anterior superior body length (id-em1il, id-em1ir) was significantly reduced compared with the experimental standard while the posterior superior body length (em1il-cbl, em1ir-cbr) was increased bilaterally. This may be accounted for by an anterior position of the first molar tooth. The left anterior ramal length (cbl-ctl) was reduced.

Dimensions and Angles (Figure 3.32(b)): The dimension of intermolar distance (em1il-em1ir) was significantly reduced consistent with the anterior placement of the first molar in this patient. The left inferior ramal distance (gol-cbl) was increased and the anterior symphyseal height (gn-id) was increased. The left and right gonial angles (cdl-gol-gn, cdr-gor-gn) were significantly increased.

Discussion: The first molar was anteriorly placed in the dental arch accounting for many of the significant findings. The anterior symphyseal height was increased and probably represented a compensatory growth change due to the occlusal relationship (see Patient LW). The pathogenesis of the increased gonial angles is unclear, however, disturbances in maxillary growth or muscle forces may be implicated.

Figure 3.32(a) Z Scores of the Distances of the Mandible for Patient AY compared with the 6 Year Old Experimental Standard

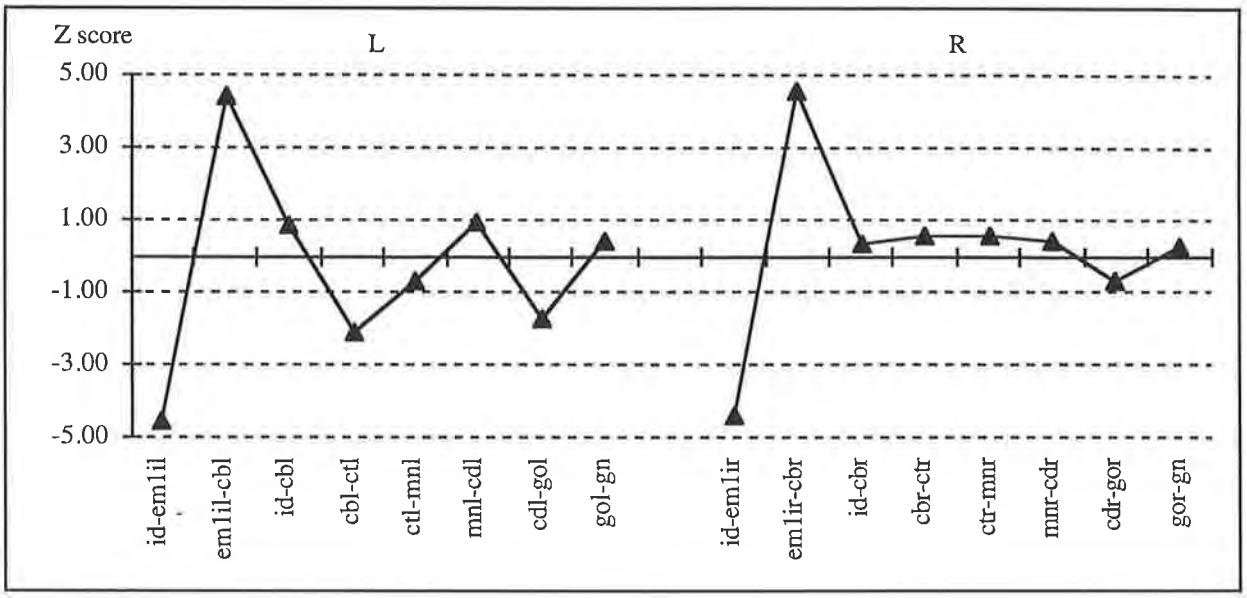

Figure 3.32(b) Z Scores of the Dimensions and Angles of the Mandible for Patient AY compared with the 6 Year Old Experimental Standard

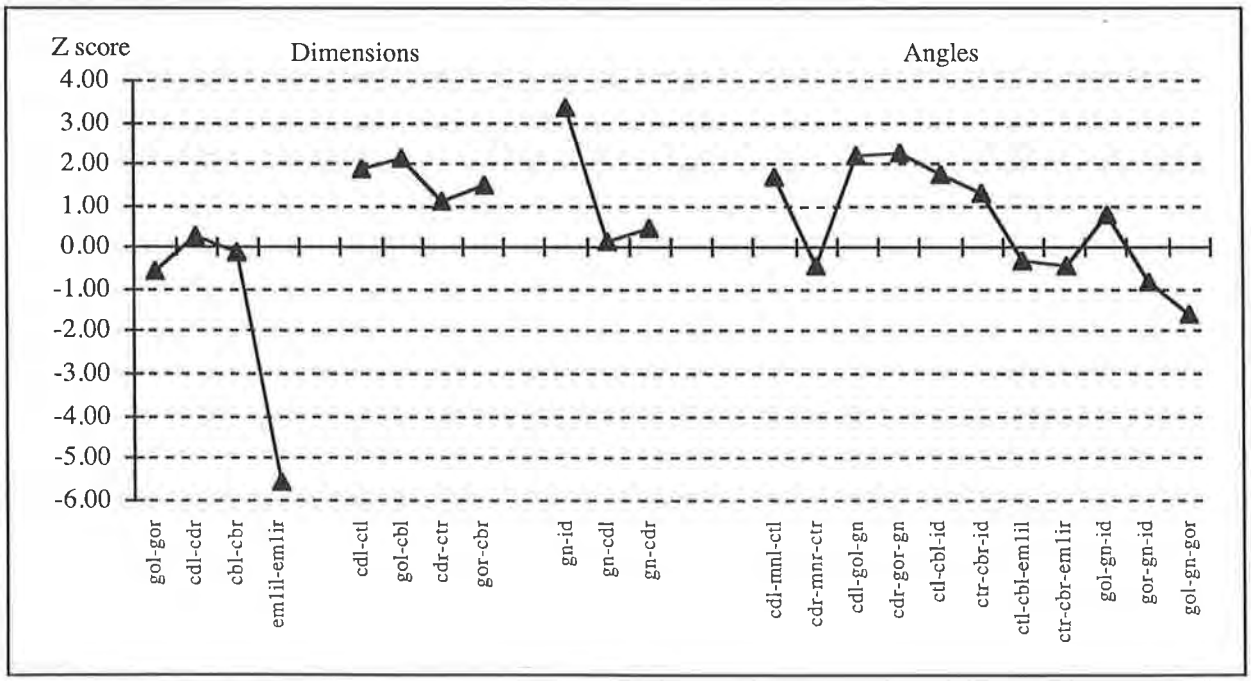

3.4.18.2 The Maxilla of Patient AY

Distances (Figure 3.32(c)): The left fronto-maxillary suture (snml-morl) was increased on the left and the medial orbital floor and the anterior border of the lateral ethmoid plate (nlil-morl, nlir-morr) was decreased bilaterally. The posterior lateral orbital floor distance (msl-iobfl, msr-iobfr) (bilateral) and the maxillary infra-orbital rim (orl-nlil, orr-nlir) were increased. Increased distances were recorded at the lateral maxillary wall (zmil-em1sl, zmir-em1sr) with decreased distances anteriorly along the anterior alveolar margin (em1sl-pr, em1sr-pr). The left upper pyriform margin (all-inml) was increased. The posterior alveolar margin (em1sl-mxtl, em1sr-mxtr) was increased bilaterally, the posterior maxillary wall (mxtr-msr) was increased on the right and the posterior lateral orbital wall (msl-iobfl, msr-iobfr) was increased bilaterally. The posterior palatal height (em1sl-gpfl, em1sr-gpfr) was also increased and the posterior palatal width (gpfr-pns) was also increased on the right.

Dimensions and Angles (Figure 3.32(d)): The posterior height of the right maxilla (gpfr-msr) was increased along with the superior length of the maxilla (msl-inml, msr-inmr). Other dimensions measured were normal. The orbital floor angle on the left (nlil-msl-iobfl) was increased. The left posterior inferior angle of the maxilla (msl-gpfl-em1sl) was also increased. The palatal angles were normal.

Discussion: This patient had similar features to Patient LW with slight asymmetry to the maxilla. The left maxilla was smaller than the right at the orbital level. The orbital distances reflected broader well-developed inferior and medial orbital rims and this correlated with the milder degree of clinical deformity. The first maxillary molar was situated anteriorly in the maxillary arch in a similar manner to the molar in the mandibular arch.

Figure 3.32(c) Z Scores of the Distances of the Maxilla for Patient AY compared with the 6 Year Old Experimental Standard

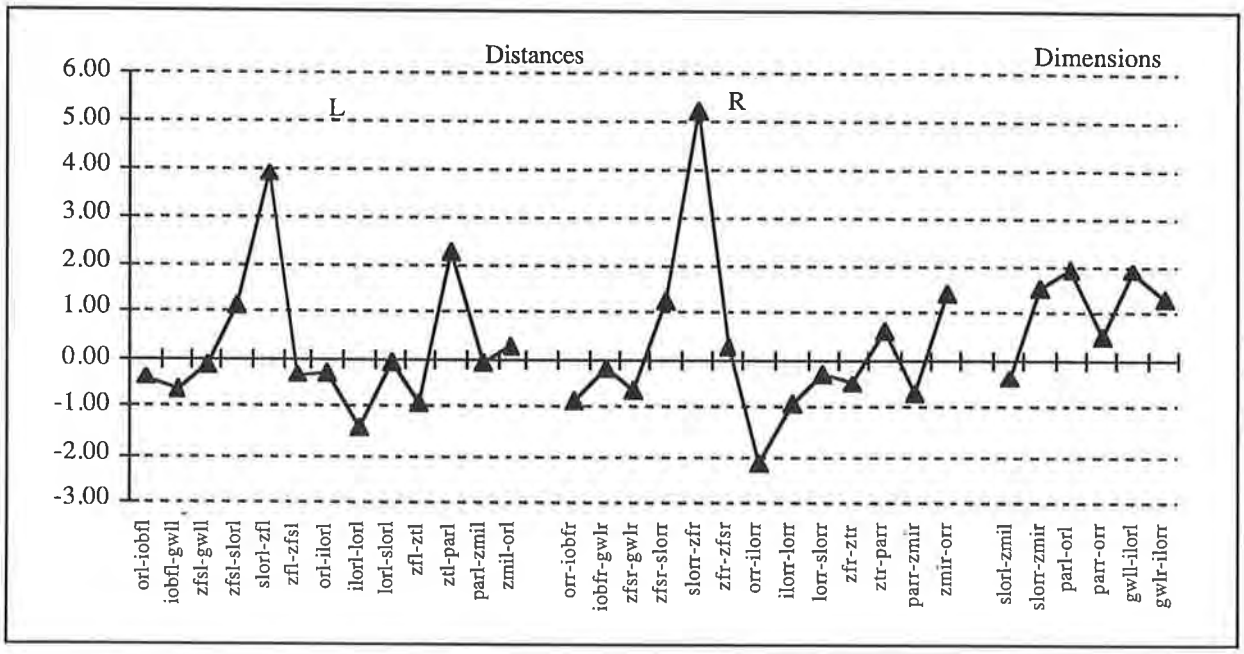

Figure 3.32(d) Z Scores of the Dimensions and Angles of the Maxilla for Patient AY compared with the 6 Year Old Experimental Standard

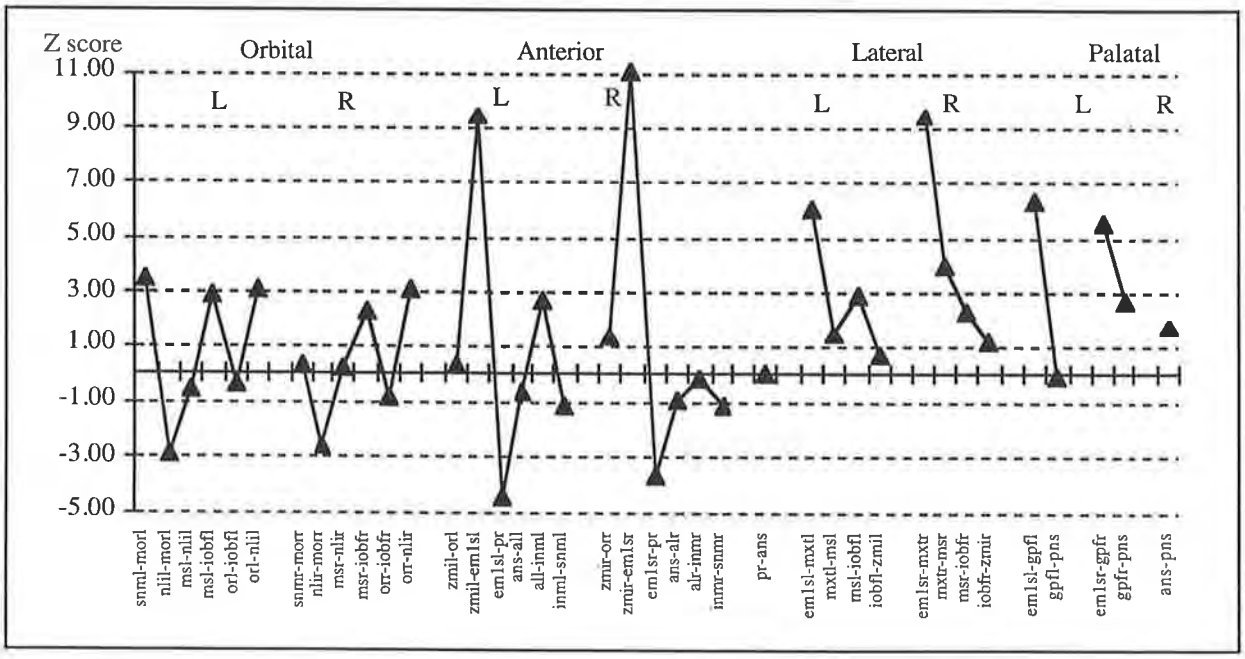

3.4.18.3 The Nasal Bones of Patient AY

Distances, Dimensions and Angles (Figure 3.32(e)): The nasal bones were not significantly different from the experimental standard with the exception of the right sided fronto-nasal suture (n-snmr) which was increased in length. The dimensions and angles measured were not significantly different from the experimental standard.

Discussion: There was minimal abnormality with regard to the distances and dimensions and angles of the nasal bones in this patient. This corresponded with the mild clinical deformity.

Figure 3.32(e) Z Scores of the Measurements of the Nasal Bones for Patient AY compared with the 6 Year Old Experimental Standard

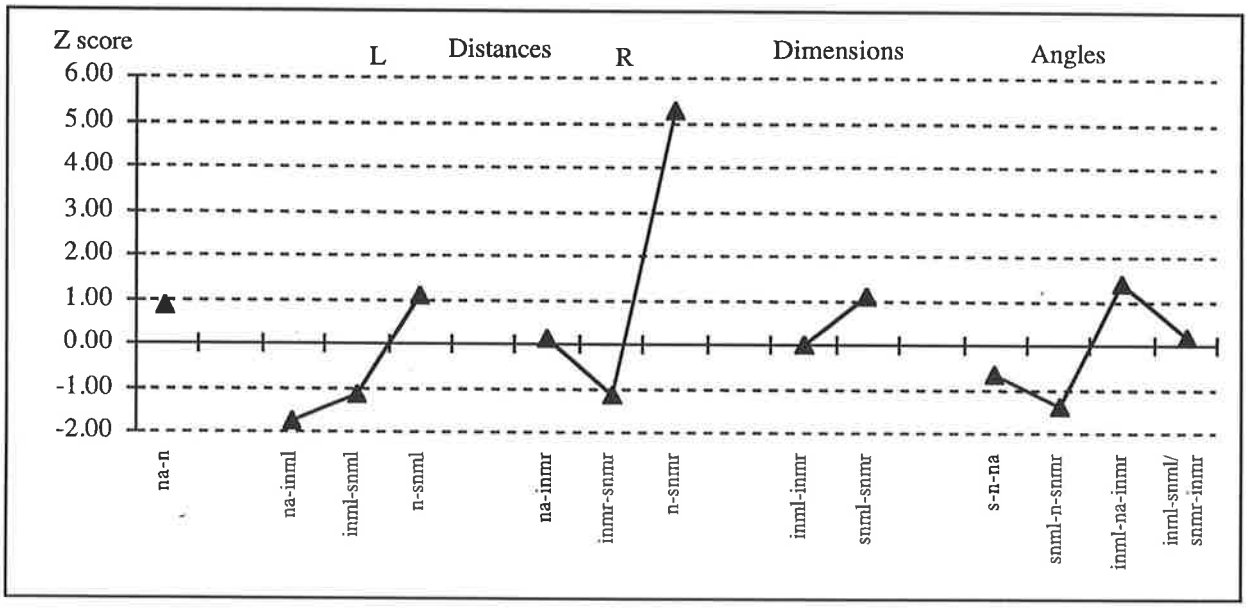

3.4.18.4 The Frontal Bone of Patient AY

Distances (Figure 3.32(f)):

Supra-orbital Region: The fronto-maxillary suture (snml-morl) was increased on the left. The anterior fronto-zygomatic suture (slorl-zfl, slorr-zfr) was increased bilaterally. The right fronto-nasal suture (n-snmr) was increased.

Ethmoid Attachment: The measurements of the ethmoid attachment were not significantly different from the experimental standard.

Sphenoid Attachment: The length of the superior orbital fissure (ofaml-sobfl) was reduced on the left side. This was not compensated for by an increased lateral distance of the fronto-sphenoid suture (sobfl-zfsl). The length of the lesser wing was reduced (spal-cppl, spar-cppr). The parietal attachment (spc-br) and sphenoid attachments (zfs-spc and spc-spa) were not recordable due to the fusion of sutures and hence poor visibility of landmarks in this region.

Dimensions (Figure 3.32(f)): The dimensions demonstrated reduction in the glabellar height (g-n), implying a closer relationship between the glabella and nasion in this patient. The anterior superior orbital widths of the frontal bone (sorl-sorr) and the superior lateral orbital widths (slorl-slorr) were increased.

Discussion: The predominant measured deformity of the frontal bone was along the region of the supra-orbital ridge at its junction with the nasal bones and the zygomatic bones. In the region of the ethmoid and sphenoid bones, the distances were normal or if anything, were reduced. These measurements reflect the clinical picture which shows some prominence of the supra-orbital ridge but a mild degree of proptosis.

Figure 3.32(f) Z Scores of the Distances and Dimensions of the Frontal Bone for Patient AY compared with the 6 Year Old Experimental Standard

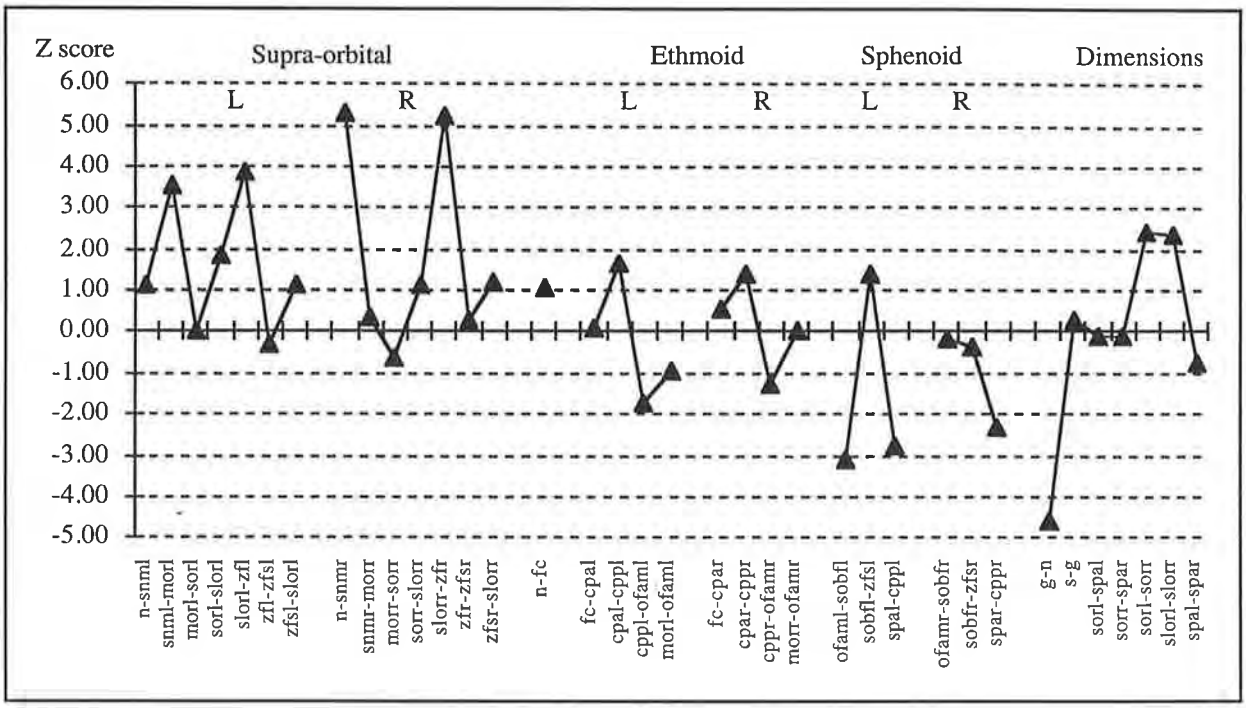

3.4.18.5 The Zygomatic Bone of Patient AY

Distances (Figure 3.32(g)): Similar pattern profiles were recorded bilaterally. The fronto-zygomatic suture distance was increased bilaterally (slorl-zfl, slorr-zfr). The zygomatico-temporal suture distance (ztr-parr) was increased on the right. The length of the lateral orbital rim (orr-ilorr) was decreased on the right.

Dimensions (Figure 3.32(g)): The dimensions were not significantly different from the experimental standard.

Discussion: The length of the fronto-zygomatic suture was increased. The abnormality was not as severe as in the patient of a similar age (Patient LW). The suture deformity did not have a significant impact on the measured dimensions of the zygomatic bone.

Figure 3.32(g) Z Scores of the Distances and Dimensions of the Zygomatic Bone for Patient AY compared with the 6 Year Old Experimental Standard

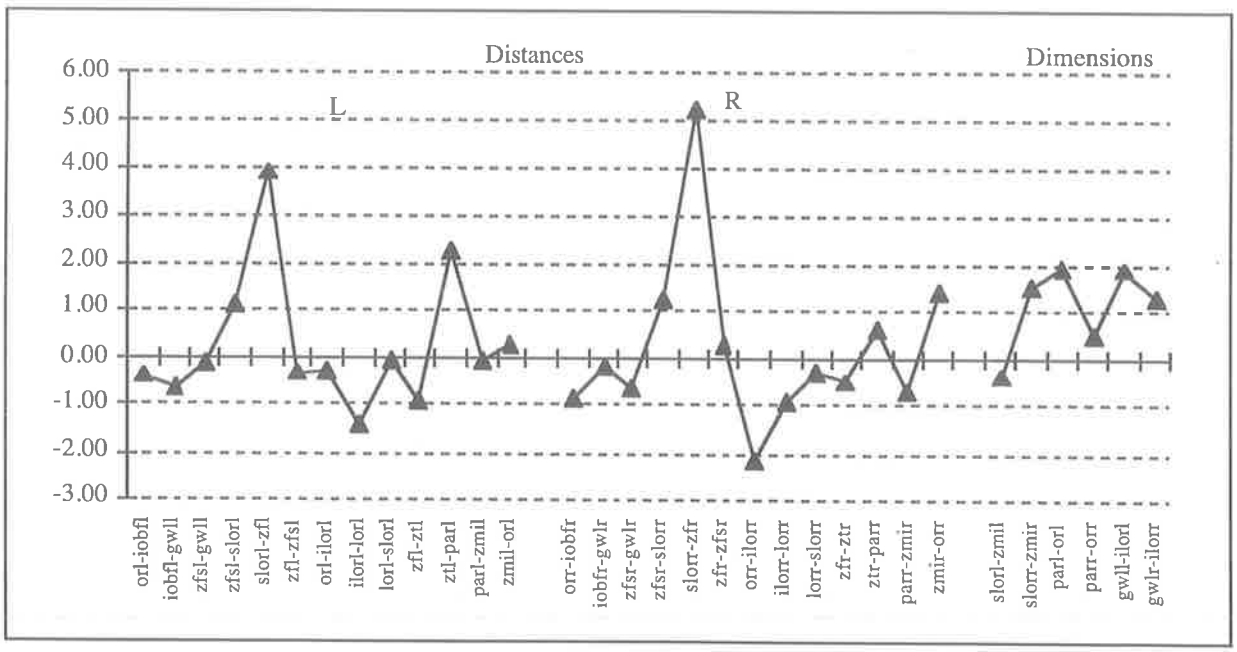

3.4.18.6 The Vomerine Bone of Patient AY

Distances, Dimensions and Angles: (Figure 3.32(h)): The distances measured were not significantly different from the experimental standard. The longitudinal dimension was not significantly different from the experimental standard. The angle of the vomer relative to the cranial base (s-n/h-ans) was significantly decreased.

Discussion: The vomer showed some variation in this patient but remained close to normal limits. The decreased angle of the vomer may partly result from the cranial base deformity in this patient, where the cranial base angle was found to be reduced (see craniofacial dimensions and angles).

Figure 3.32(h) Z Scores of the Measurements of the Vomer for Patient AY compared with the 6 Year Old Experimental Standard

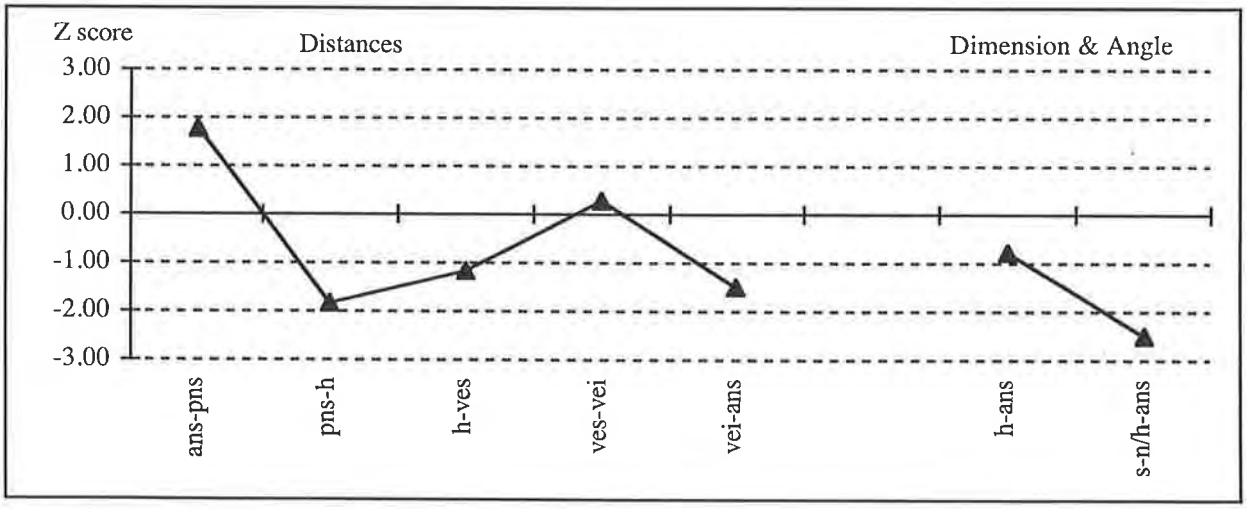

3.4.18.7 The Ethmoid of Patient AY

Lateral Ethmoid Plate (Figure 3.32(i)):

Distances: The lateral ethmoid plate distances, forming the medial orbital wall, were reduced in height anteriorly (nlil-morl, nlir-morr) and posteriorly (ofaml-msl, ofamr-msr), but not in length. The junction of the lateral plate with the cribriform plate (frontal ethmoid attachment) was not significantly different from the experimental standard.

Dimensions and Angles: The inter-orbital dimension (morl-morr) and the dimension between the optic canals (ofaml-ofamr) were significantly increased. The splay of the lateral plate msl-ofaml/ofamr-msr) was reduced posteriorly, with a tendency for an anterior (nlil-morl/morr-nlir) decrease also.

Cribriform Plate (Figure 3.32(j)):

Distances: The spheno-ethmoid synchondrosis on the left (es-cppl) was increased in length with a tendency for an increase on the right. The anterior widths of the cribriform plate were in the experimental range. The length of the cribriform plate was normal.

Angles: The cribriform plate was not depressed.

Medial Ethmoid Plate (Figure 3.32(j)):

Distances, Dimensions and Angles: The medial ethmoid plate measurements were within the normal limits of the experimental standard.

Discussion: The lateral ethmoid plate was reduced in height reducing orbital volume and contributing to the proptosis. The cribriform plate shows an increase in width posteriorly while the medial plate was normal. The spheno-ethmoid synchondrosis appears to direct the anterior growth laterally contributing to the increased inter-orbital distance. The splay of the lateral plates were decreased as a result of the posterior broadening. The pathology of the ethmoid bone was not as severe as the other patients and the resultant clinical deformity was less profound.

Figure 3.32(i) Z Scores of the Measurements of the Lateral Ethmoid Plate for Patient AY compared with the 6 Year Old Experimental Standard

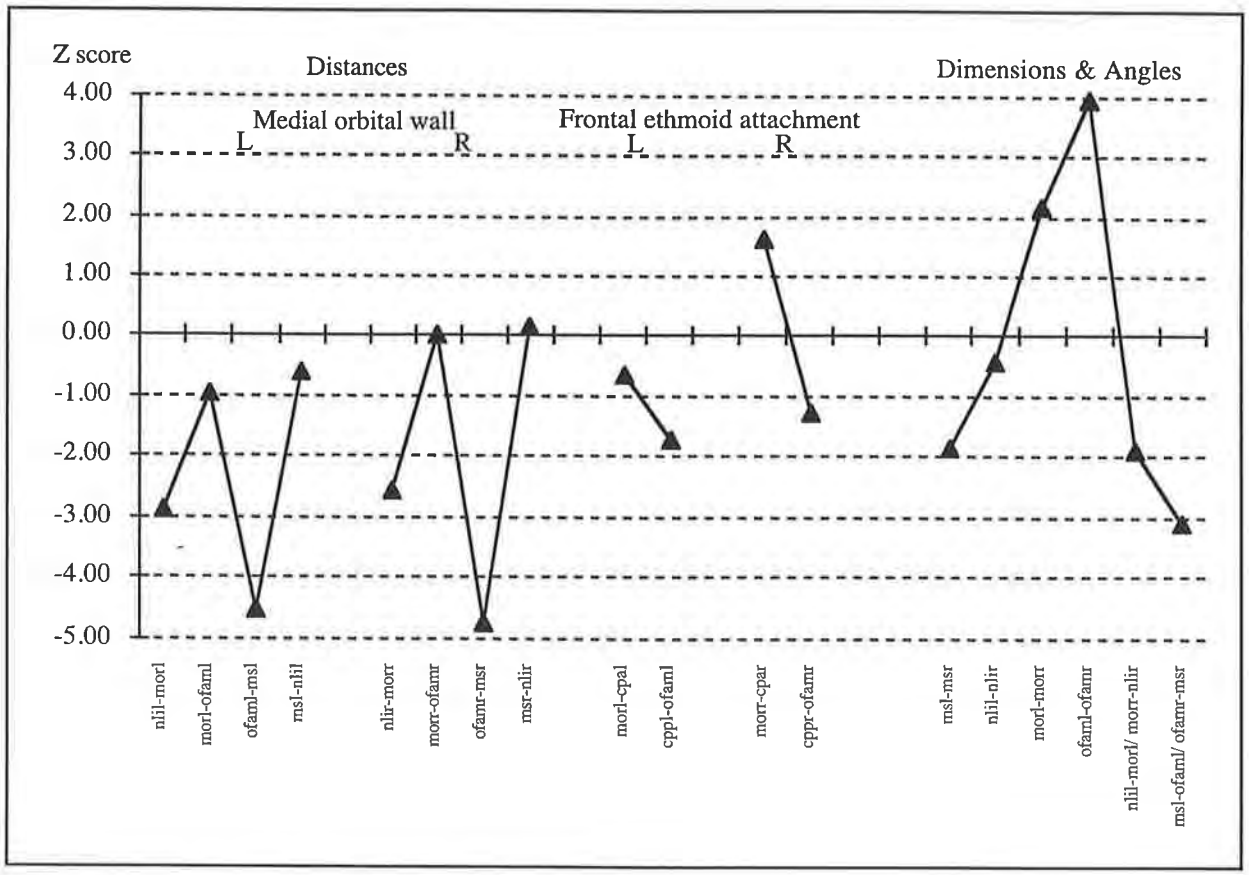

Figure 3.32(j) Z Scores of the Measurements of the Cribriform and Medial Ethmoid Plates for Patient AY compared with the 6 Year Old Experimental Standard

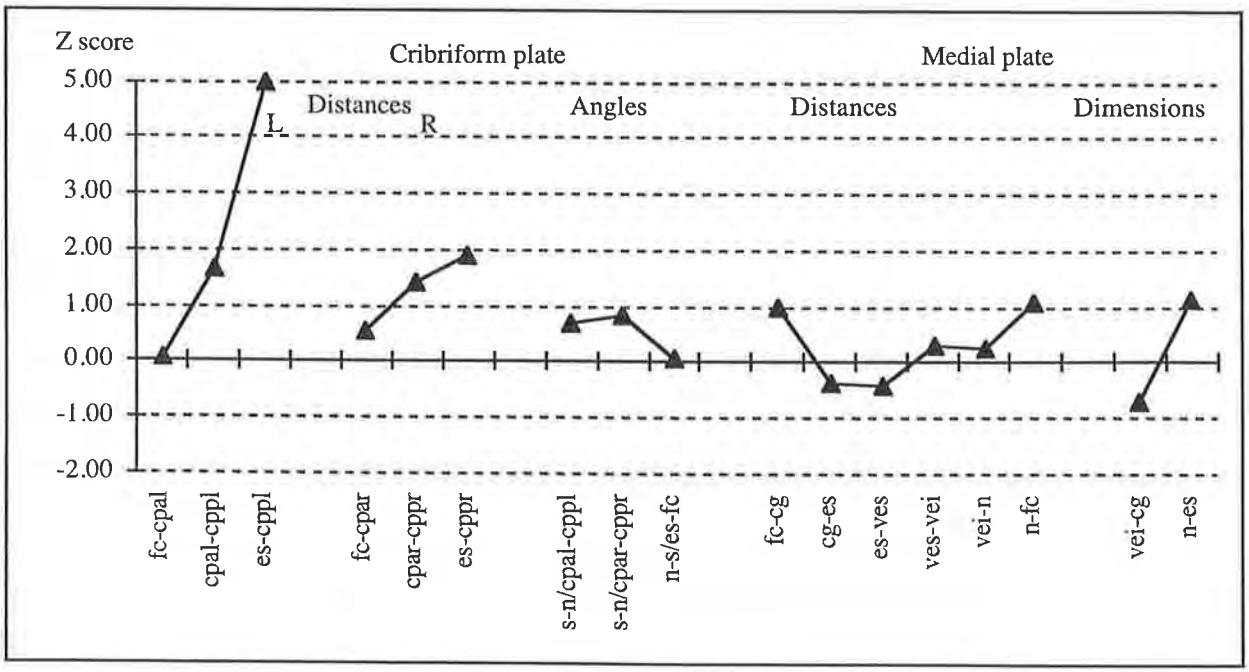

3.4.18.8 The Sphenoid of Patient AY

Lesser Wing (Figure 3.32(k)):

Distances: The length of the lesser wing was increased on the left medially (ofaml-acl) and decreased posteriorly (acl-spal) implying lateral prominence of the anterior clinoid process.

Dimensions and Angles: The dimensions and angles were not significantly different from the experimental standard.

Pterygoid Plate (Figure 3.32(k)):

Distances and Angles: The medial pterygoid plate height (ptsl-hpl) on the left was significantly increased. The remaining pterygoid plate distances and axes were not significantly different from the experimental standard.

Greater Wing (Figure 3.32(l)):

Distances: The measured lateral and orbital distances were not significantly different from the experimental standard. Landmarks on the squamous sphenoid bone (spt and spc) could not be identified bilaterally, due to fusion of the calvarial bone in this region and hence all the distances of the lateral part of the bone could not be measured. The posterior part of the greater wing was increased at the spheno-petrous temporal suture (inferior) (fosr-ptsr) on the right side, and at the posterior floor of the middle cranial fossa (fosl-petal) adjacent the superior spheno-temporal suture (superior) on the left side.

Dimensions and Angles: The angle of the floor of the greater wing (zfsl-gwml-ptsl, zfsr-gwmr-ptsr) was decreased. The angles of protrusion of the greater wing were increased (zfsl-gwml /gwmr-zfsr and gwll-gwml/gwmr-gwlr) indicating the broader position of the wings. Landmarks on the squamous sphenoid bone (spt and spc) could not be identified bilaterally, due to fusion of the calvarial bone in this region and hence the distances of the lateral part of the bone could not be measured. The posterior angle of the greater wing (fosl-petal/petar-fosr) was normal.

Figure 3.32(k) Z Scores of the Measurements of the Lesser Wing and Pterygoid Plate of the Sphenoid for Patient AY compared with the 6 Year Old Experimental Standard

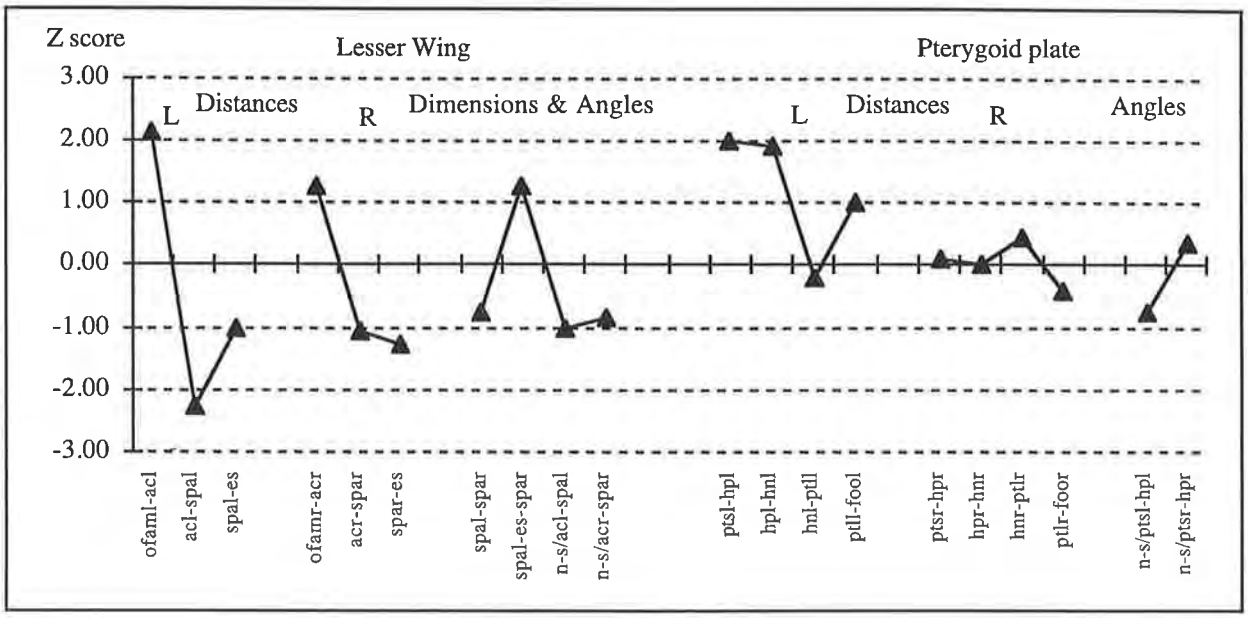

Figure 3.32(l) Z Scores of the Measurements of the Greater Wing of the Sphenoid for Patient AY compared with the 6 Year Old Experimental Standard

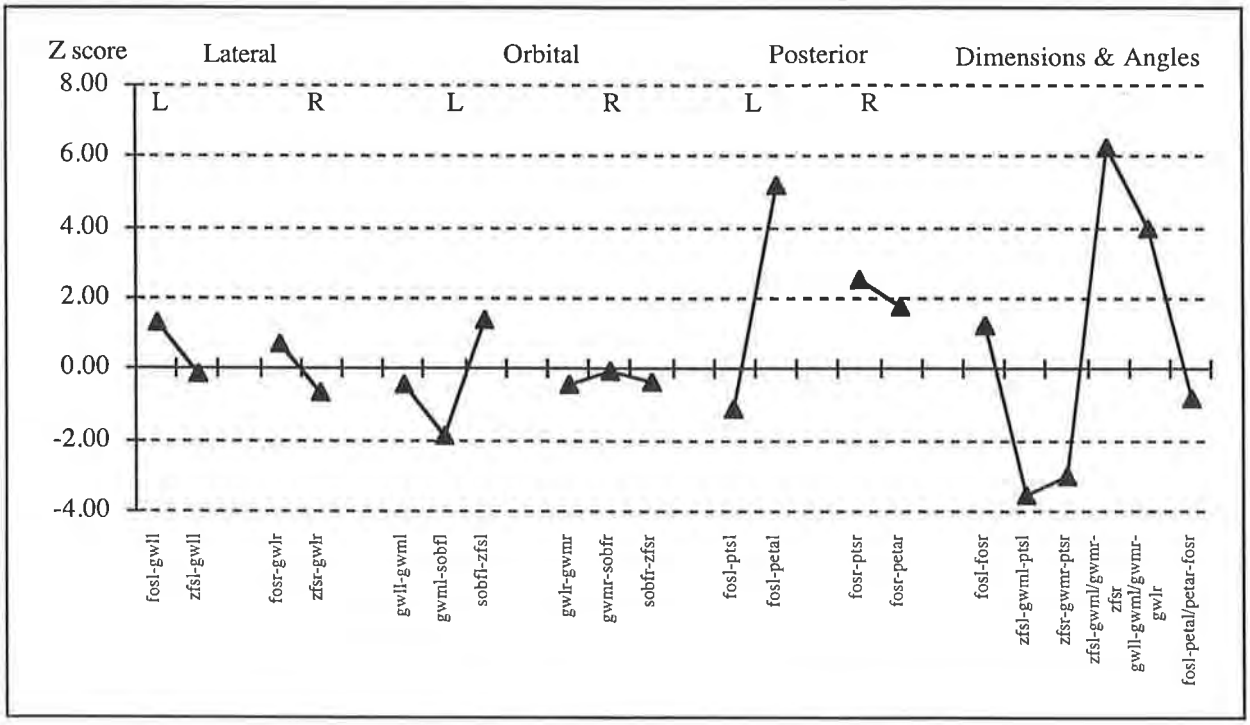

3.4.18.8 The Sphenoid of Patient AY (continued)

Body of Sphenoid (Figure 3.32(m)):

Distances: The left inferior lateral distance (gwml-ptsl) was increased along with the lateral height of the spheno-occipital synchondrosis bilaterally (ptsl-petal, ptsr-petar). The anterior body was increased in width at the spheno-ethmoid synchondrosis (es-cppl, es-cppr). The optic foramen was closer to the cribriform plate at the posterior frontal ethmoid attachment (cppl-ofpml, cppr-ofpmr) with a corresponding increase in the left lateral sella length (ofpml-petal) with a similar trend on the right. The distances of the floor were not significantly different from the experimental standard except the increased left posterior width (ptsl-h).

Dimensions and Angles: The dimensions revealed a normal distance between the greater wing medial points at the anterior inferior body width (gwml-gwmr). The distance between the anterior optic foramina (ofaml-ofamr) was increased. The inferior spheno-occipital synchondrosis (ptsl-ptsr) was increased while the superior spheno-occipital synchondrosis (petal-petar) was normal. The height of the posterior sphenoid was increased on the left (ptsl-pcl). The angles of the lateral protrusion of the body from the midline were increased superiorly (s-n/ofpml-petal, s-n/ofpmr-petar).

Discussion: This lesser wings of the sphenoid bone were relatively normal in this patient. The left anterior clinoid process was laterally displaced. The pterygoid plates were not greatly different from the experimental standard. The size of the greater wings was normal however the angle between the greater wings was increased due to less anterior protrusion of the greater wings with a greater degree of lateral splay. The spheno-temporal sutures were increased in length and pathology at this site influence the anterior or posterior position of the greater wing. The spheno-ethmoid synchondrosis was elongated, and the spheno-occipital synchondrosis was increased in height. The dimensions around the sella were increased implying the sella was enlarged and would be consistent endocranial resorption in this area.

Figure 3.32(m) Z Scores of the Measurements of the Body of the Sphenoid for Patient AY compared with the 6 Year Old Experimental Standard

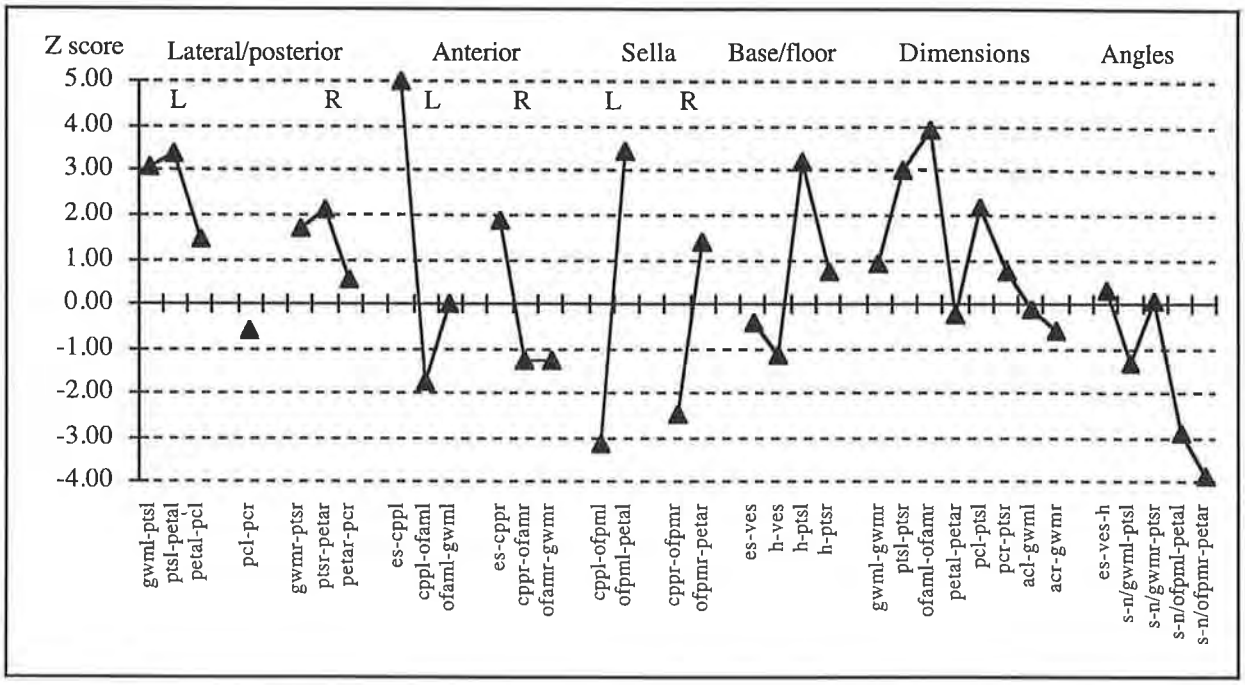

3.4.18.9 The Temporal Bone of Patient AY

Distances (Figure 3.32(n)):

Squamous Temporal Bone: The squamous temporal bone was not fully measurable in this child due to lack of visibility of the asterion (as) and sphenion (spt). The remaining distance, the medial mastoid height (mal-smfl) was not significantly different from the experimental standard on the right but increased on the left.

External Auditory Meatus: The left posterior superior rim of the external auditory meatus (eampl-pol) and the superior anterior rim (pol-eamal, por-eamar) bilaterally were increased. The lateral mastoid prominence (mar-eamir) was increased on the right.

Zygomatic Process: The zygomatic process showed some similarity in the pattern profiles between the left and right sides, but was generally within the normal range. The left zygomatico-temporal suture (parl-ztl) was increased.

Petrous Temporal Bone (Figure 3.32(o)): The sphenoid-petrous temporal suture (superior) (fisl-petal) was increased in length on the left with a tendency to be increased on the right. The occipital mastoid (inferior) suture (mal-jfll, mar-jflr) was increased in length. The petrous temporal-occipital suture (petal-jfpl, petar-jfpr) was increased bilaterally. The jugular foramen width (jfll-jfml, jflr-jfmr) was narrowed. The mastoid to jugular foramen distance was increased bilaterally, along with the left medial temporo-occipital suture (inferior) (jfml-ptsl). The spheno-petrous temporal suture (ptsr-fosr) was increased on the right.

Dimensions (Figure 3.32(o)): The petrous ridge distance (petal-petpl, petar-petpr) was increased bilaterally and the distance between the external auditory meati (pol-por). The angle of the zygoma projection (petal-aul-ztl, petar-aur-ztr) and the angles of the auditory canal (pol-iaml /iamr-por) and the petrous temporal bone (petpl-petal/petar-petpr) were normal.

Discussion: The predominant abnormalities were in the region of the external auditory meatus which was distorted with increased distances. The zygomatic process was essentially normal. Lengthening of medial and lateral temporal occipital sutures resulted in narrowing of the jugular foramen. The external auditory canals were displaced laterally however the angles of splay of the bones were not significantly different from the experimental standard.

Figure 3.32(n) Z Scores of the Distances of the Temporal Bone for Patient AY compared with the 6 Year Old Experimental Standard

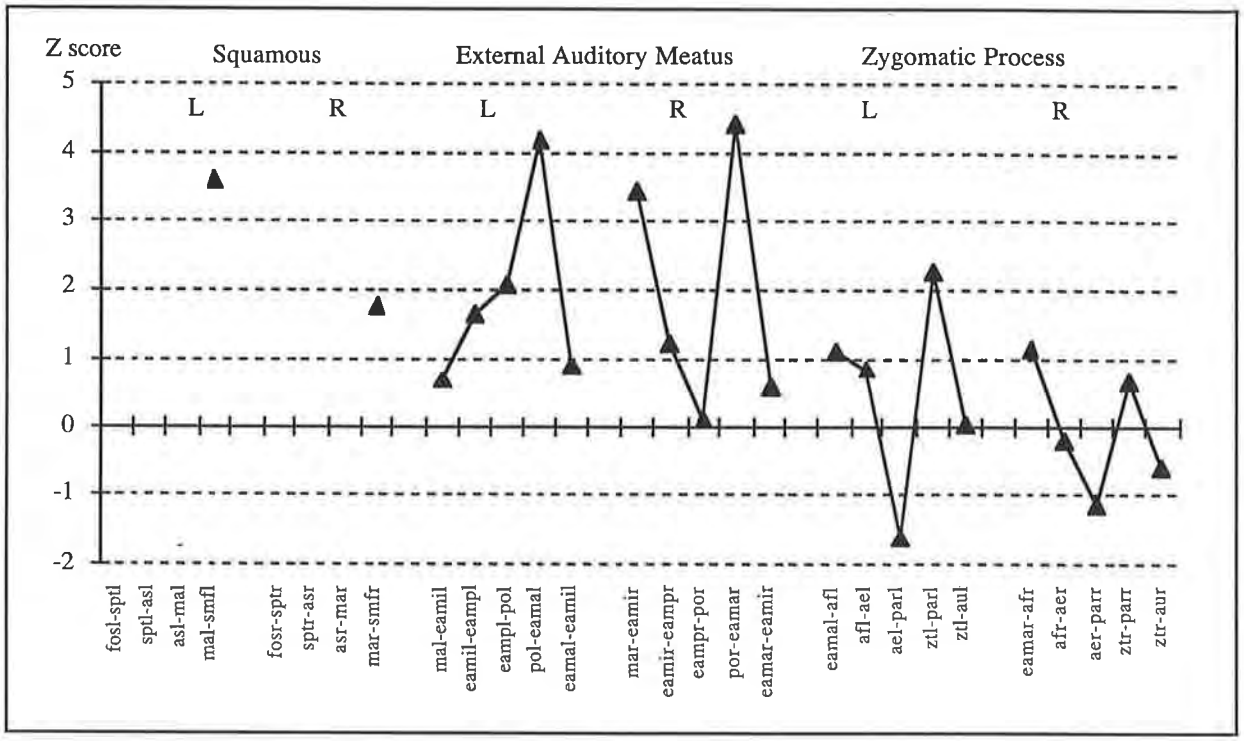

Figure 3.32(o) Z Scores of the Measurements of the Temporal Bone for Patient AY compared with the 6 Year Old Experimental Standard

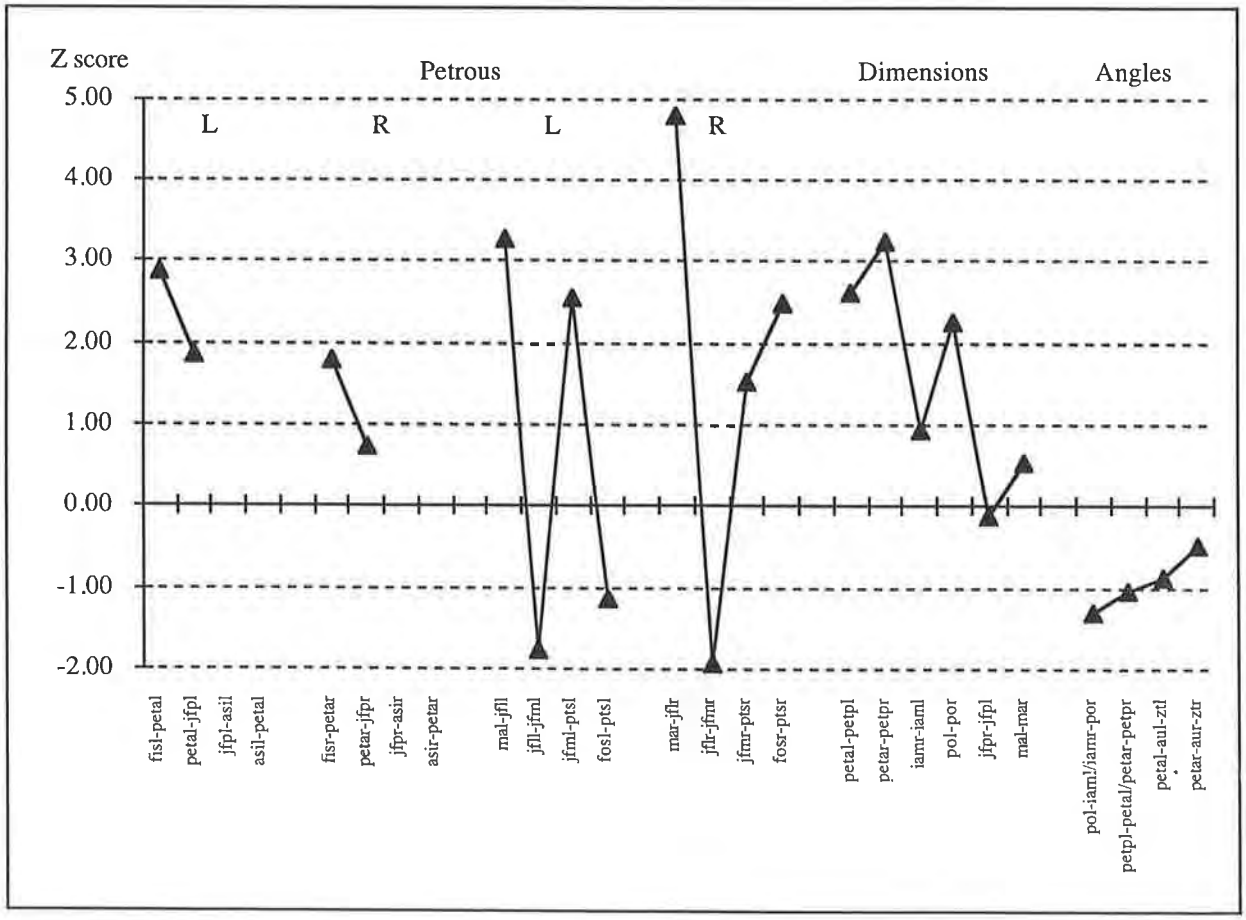

3.4.18.10 The Parietal Bone of Patient AY

Distances: The key landmarks for the parietal bone for Patient AY were not visible due to suture fusion and could not be reliably estimated. Therefore the parietal bone was not measured and a pattern profile of Z scores was not generated. The measurement data for the experimental standard are reported in Appendix 2.

3.4.18.11 The Occipital Bone of Patient AY

Distances (Figure 3.32(p)): The jugular foramen showed a trend for reduced distances with one distance (jfll-jfpl) significantly reduced. The left medial temporo-occipital suture (inferior) (jfml-ptsl) was increased in length with a tendency to be increased on the right. The inferior spheno-occipital synchondrosis (ptsl-ptsr) was increased in length (see sphenoid and cranial base sutures for other distances). The foramen magnum was not significantly different from the experimental standard.

Dimensions (Figure 3.32(p)): The dimensions were not significantly different from the experimental standard.

Discussion: The occipital bone showed some distortion along the sutures with the temporal bone, with narrowing of the jugular foramen.

Figure 3.32(p) Z Scores of the Distances and Dimensions of the Occipital Bone for Patient AY compared with the 6 Year Old Experimental Standard

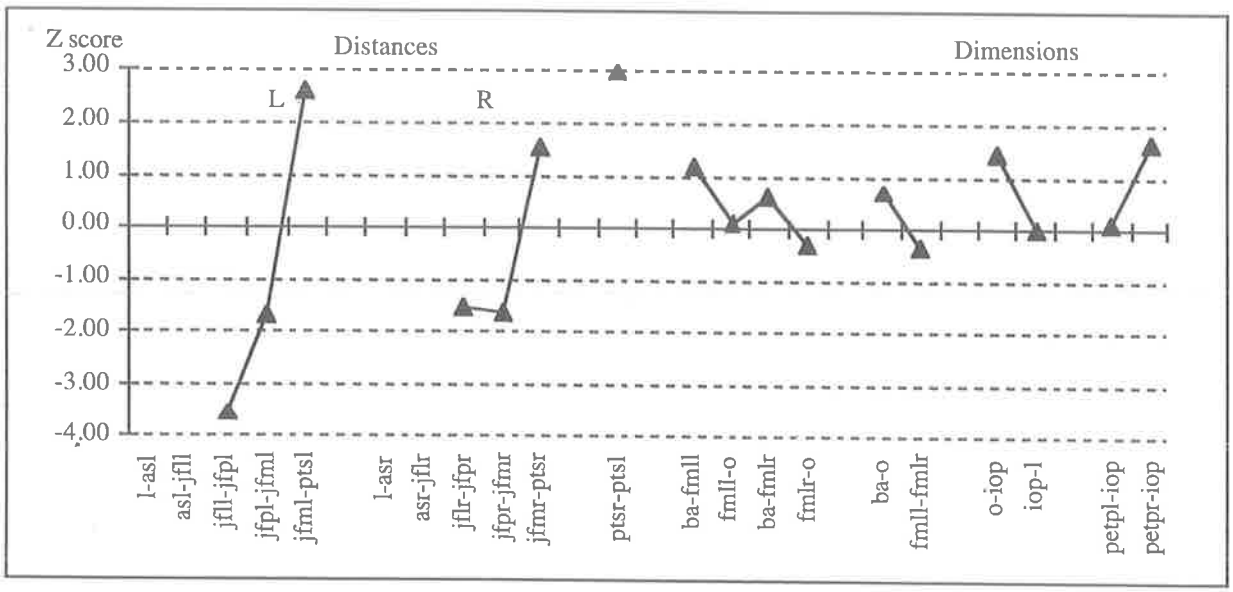

3.4.18.12 The Cranial Base Sutures of Patient AY

Anterior Cranial Fossa (Figure 3.32(q)): The spheno-ethmoid synchondrosis (es-cppl, es-cppr) was increased in length. The spheno-frontal suture (cppl-spal, cppr-spar) in the anterior cranial fossa was reduced in size. In the orbit, the spheno-frontal (spal-zfsl, spar-zfsr) and spheno-zygomatic (zfsl-gwll, zfsr-gwlr) sutures were normal.

Middle Cranial Fossa (Figure 3.32(q)): The spheno-petrous temporal sutures were increased in length superiorly (fisl-petal) on the left and inferiorly (fosr-ptsr) on the right.

Posterior Cranial Fossa (Figure 3.32(q)): The superior (petal-jfml, petar-jfmr) and left inferior (jfml-ptsl) medial temporo-occipital sutures were increased in length. The right occipital mastoid suture (jflr-petpr) was increased in length. The superior spheno-occipital synchondrosis (petal-petar) was normal, while inferiorly (ptsl-ptsr) and laterally (ptsl-petal, ptsr-petar) the lengths were increased.

Discussion: Significant suture abnormality was found in the cranial base anteriorly with no lateral involvement. Presumably the sutures at this site are less severely involved in the pathological process. Posteriorly, the temporal bone was involved laterally, while medially the spheno-occipital synchondrosis was deformed.

Figure 3.32(q) Z Scores of the Dimensions of the Cranial Base Sutures for Patient AY compared with the 6 Year Old Experimental Standard

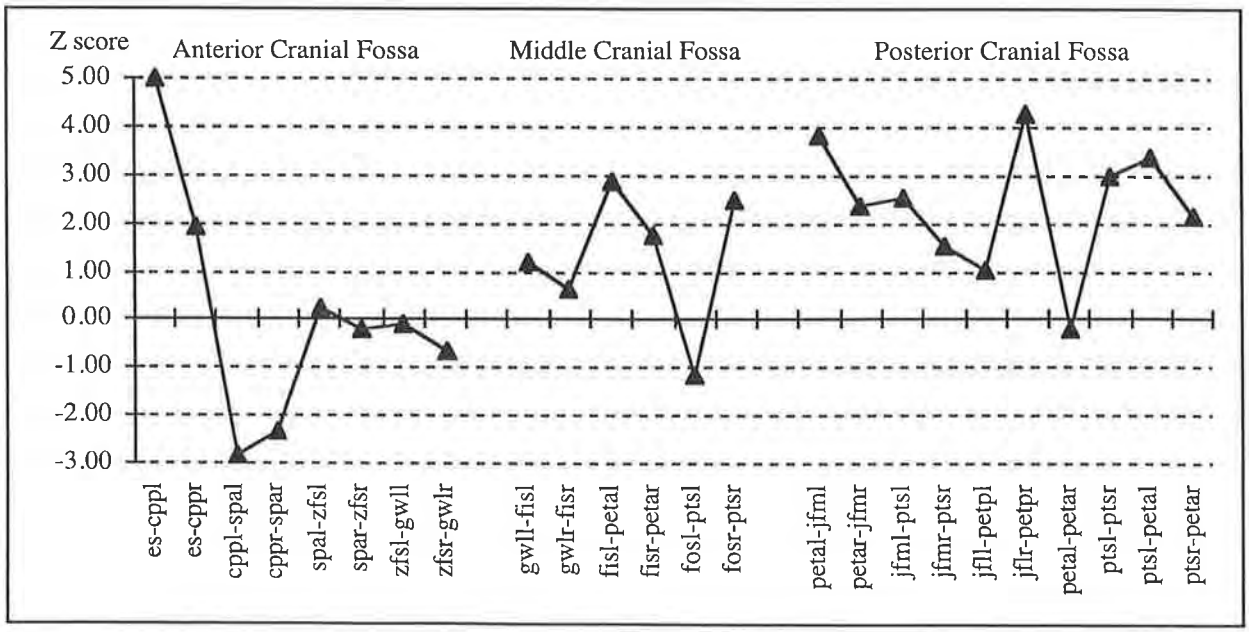

3.4.18.13 The Craniofacial Dimensions and Angles of Patient AY

Dimensions and Angles (Figure 3.32(r)): The patient's mouth was open during the CT scan making the measurements of the facial height and SNB angle (s-n-sm) invalid. The SNA (s-n-ss) angle was reduced. The cranial base angle (ba-s-n) showed a tendency to be more acute in this patient. The cranial base dimensions were not significantly different from the experimental standard.

Discussion: The maxilla was retruded with the cranial base angle borderline reduced in this patient.

Figure 3.32(r) Z Scores of the Craniofacial Dimensions and Angles for Patient AY compared with the 6 Year Old Experimental Standard

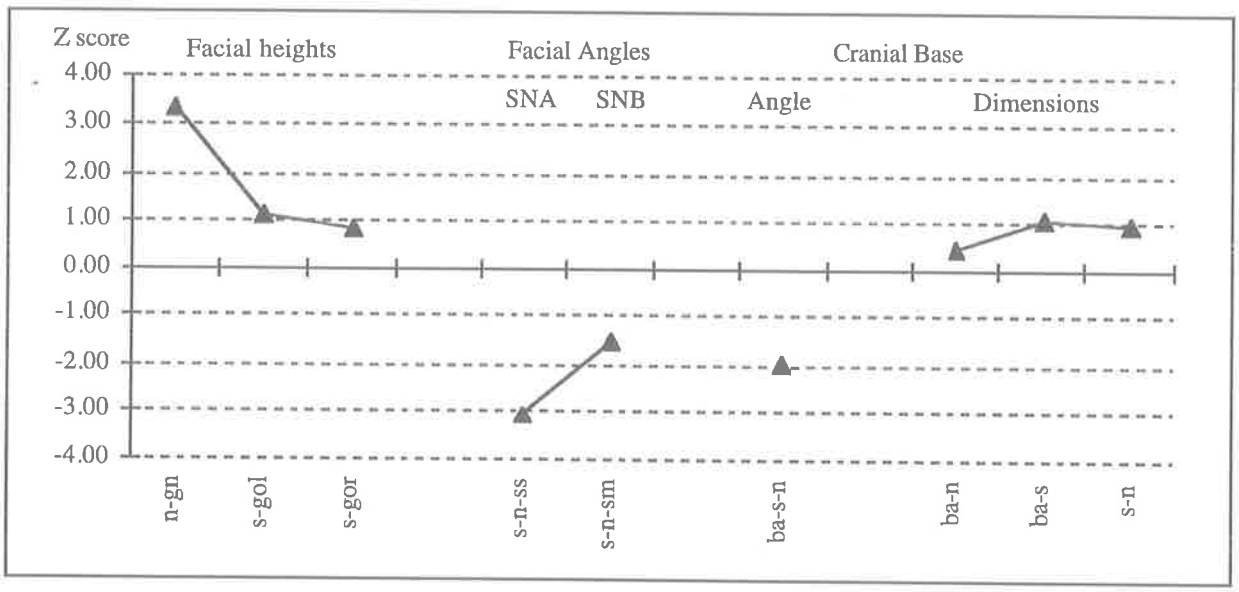

3.4.19 Clinical and Radiographic Findings for Patient HC

Clinical Features

This patient was first seen at the ACFU at the age of 12 years and was reviewed again at the age of 15 years (Figure 3.7). No family history was available due to his orphan status. At the age of 10 he had undergone a fronto-orbital advance elsewhere. The details of the indications and the surgery performed were not available. On review at age 15 years his head shape was brachycephalic with proptosis and mild hypertelorism. A divergent squint and evidence of exposure keratitis were present. He had a moderate degree of conductive deafness with bilateral absent external auditory meati and atresia of the canals. The maxilla was hypoplastic, with a Class III occlusion and hyponasal speech.

Lateral, Antero-Posterior and Basal Radiographs

Lateral, antero-posterior (AP) and basal radiographs had been performed. The lateral radiograph revealed the bony defect in the region of the coronal sutures as a result of the previous surgery. No cranial sutures were seen on the radiographs. The anterior cranial fossa was steep due to the swept up lesser wings of the sphenoid. The sella was large, with a prominent sphenoid sinus and the appearance of fusion of the spheno-occipital synchondrosis. The temporal bone did not show the external auditory meati. A cervical spine fusion of C2-C3 and calcification of the stylohyoid ligament were visible. The occlusion was class III. The AP view revealed the lesser wing swept upwards and prominence of the ethmoid sinuses. Interosseous wires could be seen above the supra-orbital ridges bilaterally. There was a very mild copper-beaten appearance to the calvaria. The nasal septum was deviated to the right.

3D CT Reconstruction

Calvarial bones: Evidence of previous surgery was again noted by the absence of bone along the coronal sutures, and the evidence of wires above the supra-orbital ridge. No calvarial sutures were seen. The external auditory meati were absent.

Cranial base: The anterior cranial fossa revealed that the cribriform plate and the jugum sphenoidale bones were pushed down and thinned. The right side of the cranial base appeared

narrower than the left side, although this may have resulted from the angle of the CT scan. The sella was slightly large and the clivus was steep. The spheno-occipital synchondrosis was not patent. The foramen magnum had a pointed posterior margin.

Orbital: The appearance of the orbital aperture was of a vertical elongation. The medial orbital wall, the lacrimal area and the floor of the orbit demonstrated small bony defects. These were small errors of exclusion seen on the 3D CT bone reconstruction.

Maxilla: The right lateral upper incisor was missing. The anterior maxillary wall also contained an error of exclusion.

3.4.20 Features of the CT Scan and 3D Reconstruction for Patient HC that made Landmark Identification difficult

The calvarial landmarks (l, as, br, spt, spc) could not be identified nor reliably estimated. The peri-orbital sutures and cranial base landmarks were identified from the regional bony contours and junctions defined in the landmarks (Figures 3.15-3.26). Landmarks for the peri-orbital structures were difficult to identify on the 3D CT reconstructions and the 2D axial slices were relied on.

3.4.21 Results and Discussion of the Quantitative Analysis of Patient HC compared with the Adult Experimental Standard

Figures 3.33(a)-(r)

3.4.21.1 The Mandible of Patient HC

Distances (Figure 3.33(a)): The majority of distances were not significantly different from the experimental standard. The left anterior superior body distance (id-em1il) was increased, and the left posterior ramal length (cdl-gol) was reduced.

Dimensions and Angles (Figure 3.33(b)): This patient had the largest number of abnormal dimensions and angles of all the patients. The intercondylar distance (cdl-cdr) and inter-coronoid base distance (cbl-cbr) were decreased. The anterior symphyseal height (gn-id) was increased. The gonial angles (cdl-gol-gn, cdr-gor-gn) were increased bilaterally along with the coronoid base (ctl-cbl-id, ctr-cbr-id) and coronoid dental angles (ctl-cbl-em1il, ctr-cbr-em1ir).

Discussion: The increased anterior symphyseal height was possibly a secondary compensatory change related to the class III occlusion. Deformity at the angle was most pronounced in this patient suggesting a possible primary mandibular deformity. The decreased intercondylar distances suggested a cranial base effect.

Figure 3.33(a) Z Scores of the Distances of the Mandible for Patient HC compared with the Adult Experimental Standard

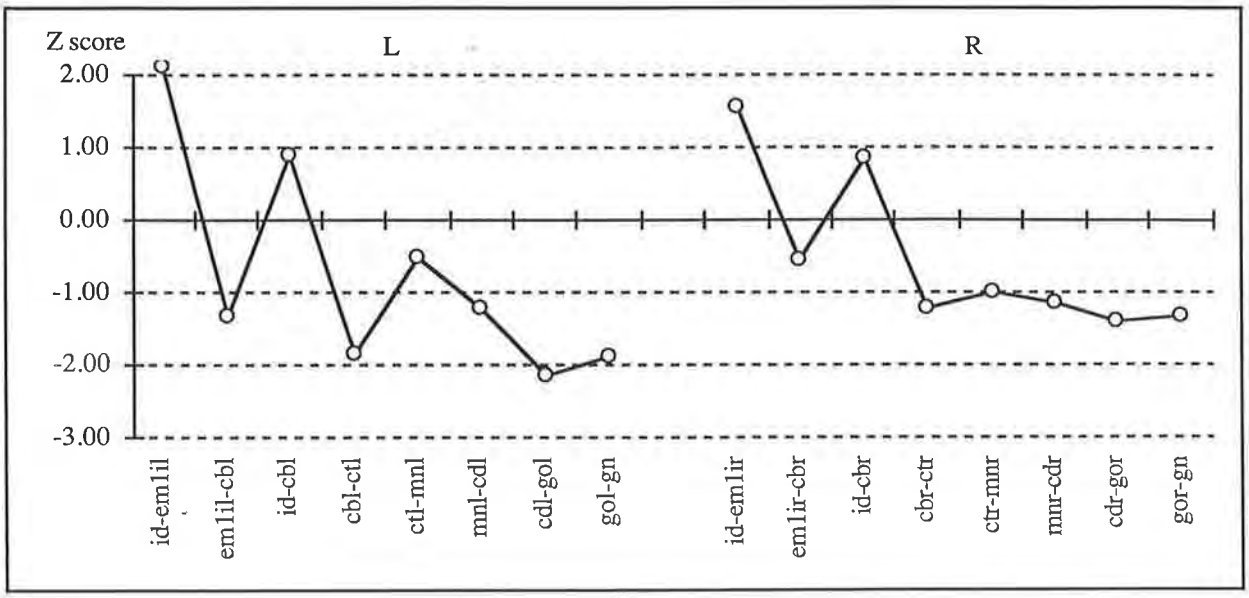

Figure 3.33(b) Z Scores of the Dimensions and Angles of the Mandible for Patient HC compared with the Adult Experimental Standard

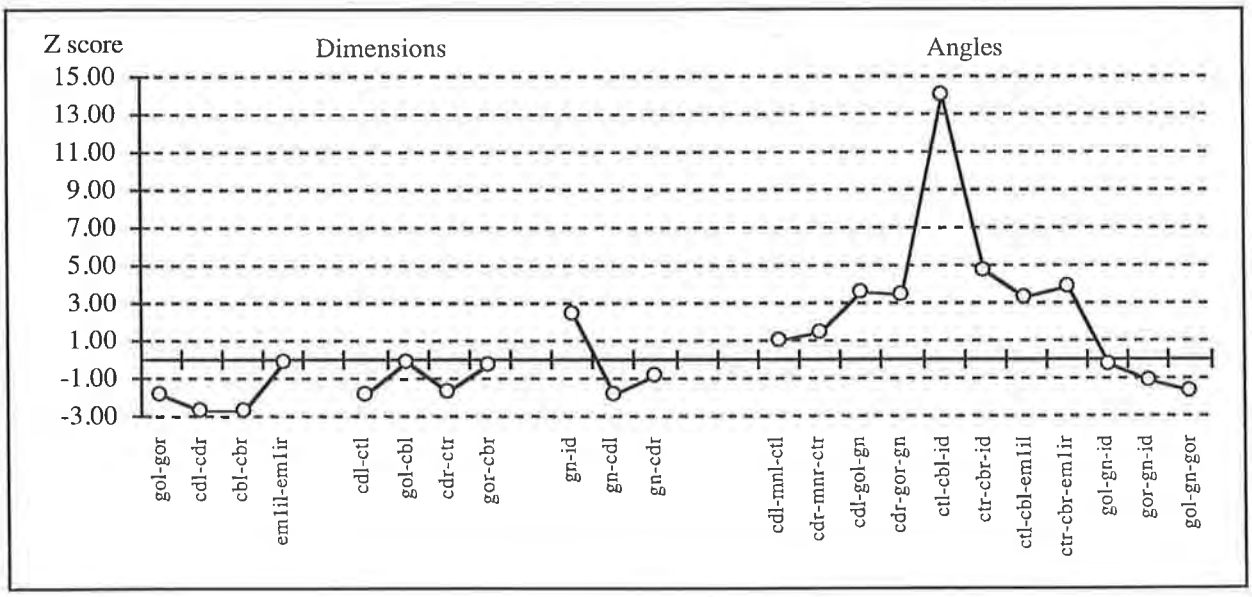

3.4.21.2 The Maxilla of Patient HC

Distances (Figure 3.33(c)): The left anterior border of the lateral ethmoid plate (nlil-morl)was decreased compared with the experimental standard. The posterior lateral orbital floor (msr-iobfr) was increased on the right. The anterior lateral orbital floor (iobfl-orl, iobfr-orr) was decreased on both sides. The left maxillary orbital rim (orl-nlil) was increased in length. The anterior alveolar margin (em1sl-pr, em1sr-pr) was decreased in length. The right upper pyriform margin distance (alr-inmr) was increased. The anterior alveolar height was increased (pr-ans). The right posterior alveolar margin (em1sr-mxtr) was reduced in length and the posterior palatal height (em1sl-gpfl, em1sr-gpfr) was reduced bilaterally.

Dimensions and Angles (Figure 3.33(d)): The dimensions of the lateral height (morr-em1sr) and posterior height (gpfr-msr) on the right side were increased. The width of the nasal aperture was reduced (all-alr). The superior/occlusal angle (snml-msl/em1sl-pr) and the palatal/occlusal angle (ans-pns/em1sl-pr) on the left were increased. The maxillary arch angle (gpfl-pr-gpfr) was increased.

Discussion: The maxilla of Patient HC was not small. Most significant measurements showed an increase in the posterior distances. The anterior measurements particularly around the orbit, and the teeth were reduced. The pattern of deformity of the maxilla in Patient HC was of a broad orbital region with increased height to the maxilla posteriorly and laterally (right side). The anterior alveolar height was increased. The maxilla confirms the impression of a broad maxilla with increased height and lacking corresponding anterior projection.

Figure 3.33(c) Z Scores of the Distances of the Maxilla for Patient HC compared with the Adult Experimental Standard

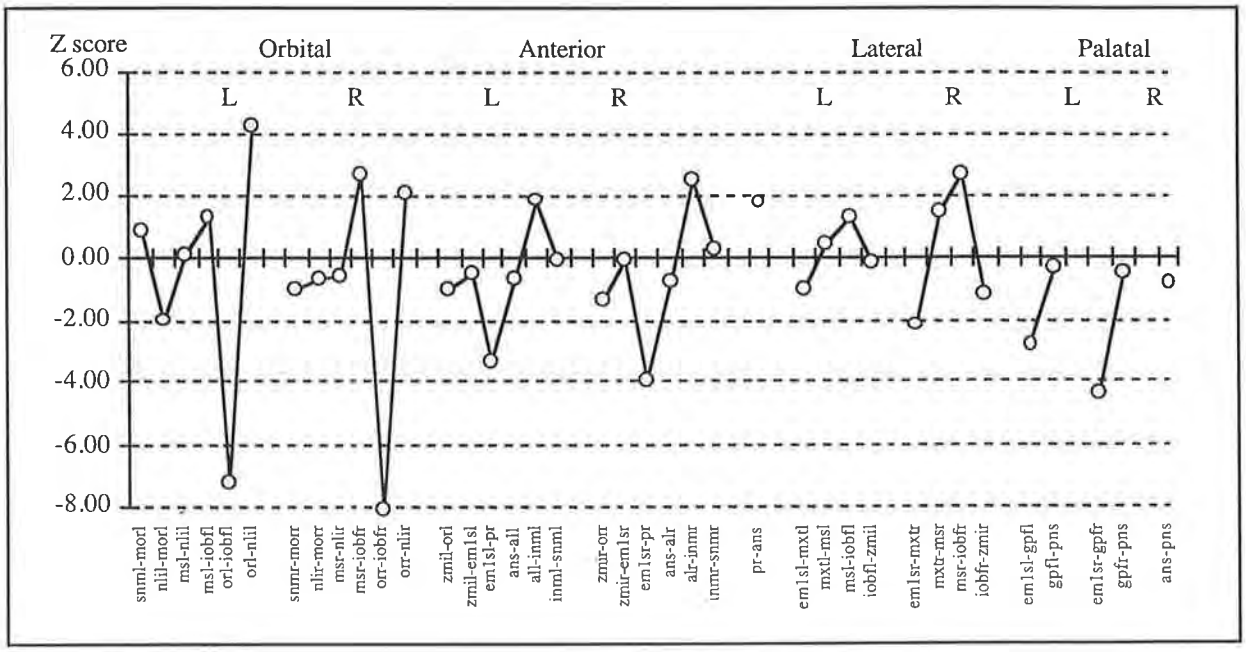

Figure 3.33(d) Z Scores of the Dimensions and Angles of the Maxilla for Patient HC compared with the Adult Experimental Standard

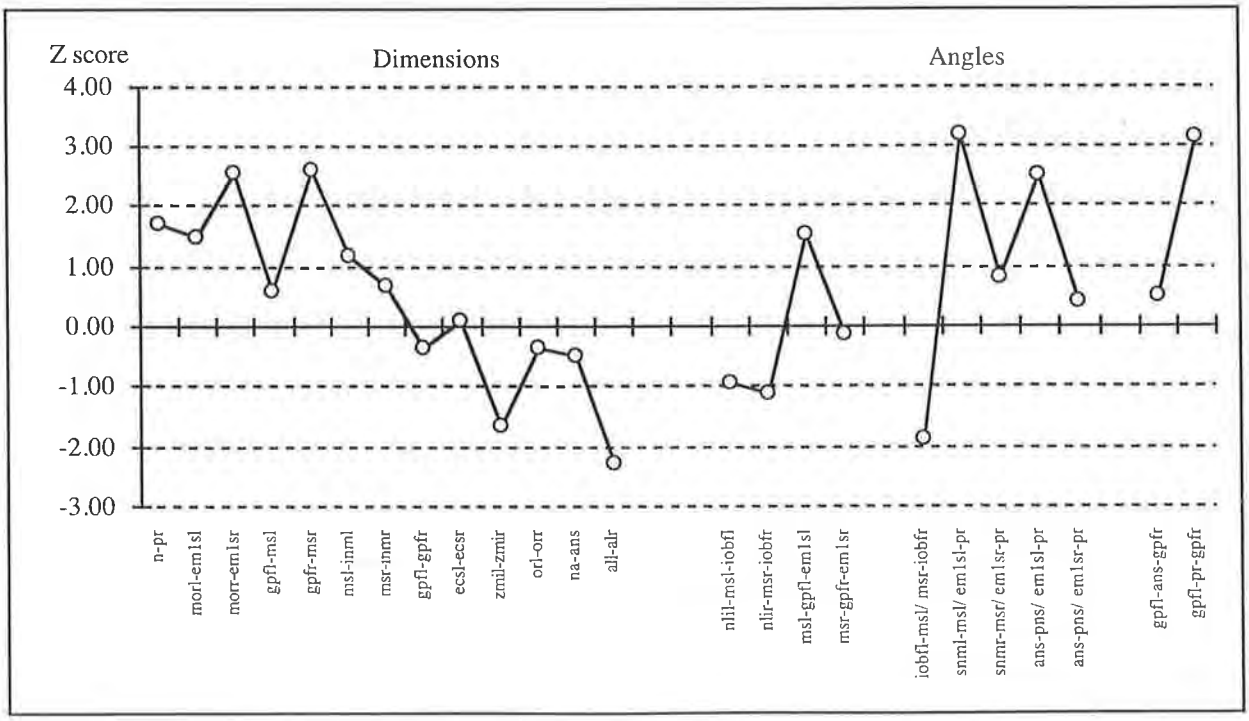

3.4.21.3 The Nasal Bones of Patient HC

Distances, Dimensions and Angles (Figure 3.33(e)): The nasal length (na-n) was increased compared with the experimental standard. The other distances and dimensions in this region were not significantly different from the experimental standard. The only significant angle was the nasal/anterior cranial base angle (s-n-na) which was reduced.

Discussion: The measurements of the nasal bones confirmed the trend of the pathology in this region. The increased length of the midline nasal bone and the reduced nasal/cranial base angle were consistent with the maxillary deformity of increased height and lack of anterior projection.

Figure 3.33(e) Z Scores of the Measurements of the Nasal Bones for Patient HC compared with the Adult Experimental Standard

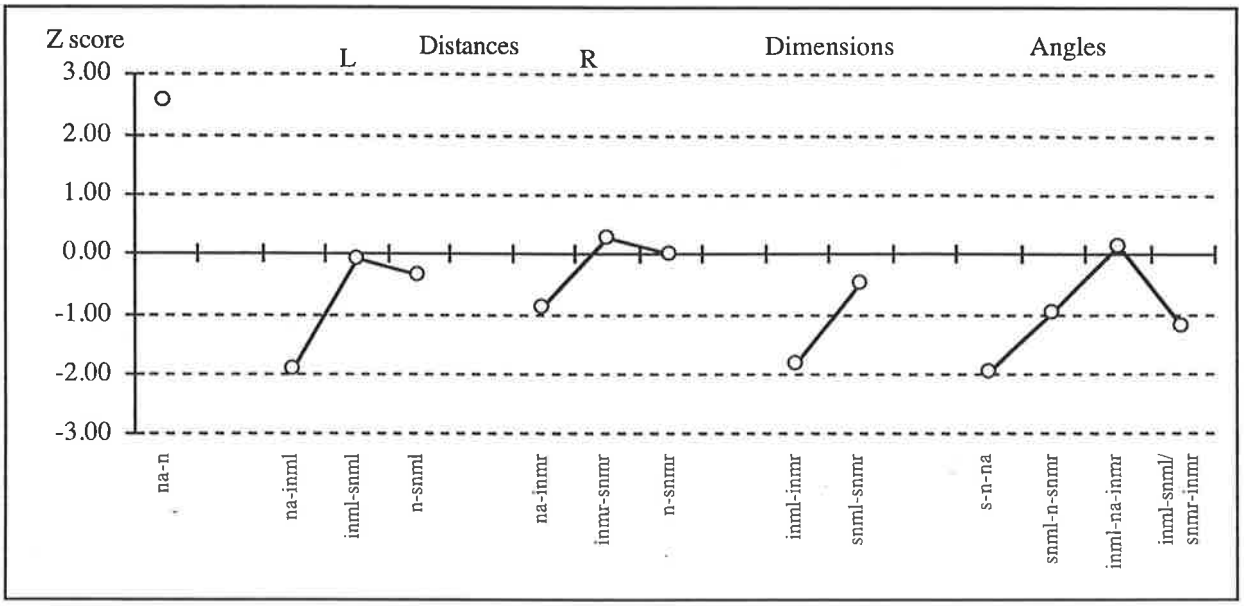

3.4.21.4 The Frontal Bone of Patient HC

Distances (Figure 3.33(f)):

Supra-orbital Region: The majority of the supra-orbital distances were not significantly different from the experimental standard. The supero-medial length of the orbital rim (morr-sorr) was increased on the right with a similar trend seen on the left side. The left lateral fronto-zygomatic suture (zfl-zfsl) was reduced.

Ethmoid Attachment: The nasal root projection (n-fc) was significantly reduced while the lateral length of the ethmoid plate at the frontal ethmoid attachment (cpal-cppl, cpar-cppr) was significantly increased in length. The width of the attachment at the ethmoid posteriorly (cppl-ofaml, cppr-ofamr) was reduced as was the orbital frontal ethmoid attachment (morl-ofaml, morr-ofamr).

Sphenoid Attachment: The attachment to the sphenoid bone had distances which were not significantly different from the experimental standard. The parietal attachment (spc-br) and sphenoid attachments (zfs-spc and spc-spa) were not recordable due to the fusion of sutures and hence poor visibility of landmarks in this region.

Dimensions (Figure 3.33(f)): The depth of the anterior cranial fossa (spal-sorl, spar-sorr) was decreased bilaterally. The anterior superior orbital width was increased (sorl-sorr) as was the posterior width between the tips of the lesser wings (spal-spar).

Discussion: This patient had a fronto-orbital advance performed some 5 years previously leading to some distortion of the primary pathology in this region. Despite this, many of the ethmoid and sphenoid distances should be minimally affected by this surgery. The measurements still reveal a broadening of the frontal bone, both anteriorly and posteriorly, with a reduced depth of the anterior cranial fossa, and suggest the deformity is again present. Medially, however, the projection of the frontal bone was not significantly different from the experimental standard. The overall prominence of the frontal region was normal as measured from the sella to the gnathion. There was an increased length of the frontal ethmoid attachment cranially with reduced width at the orbital level. The narrow frontal ethmoid attachment correlated with a normal interorbital distance (see ethmoid bone).

In summary, the assessment in this region was complicated by the previous surgery. The measurements confirm the features of a broad frontal bone with a shallow anterior cranial fossa and a shape disturbance in the region of the ethmoid.

Figure 3.33(f) Z Scores of the Distances and Dimensions of the Frontal Bone for Patient HC compared with the Adult Experimental Standard

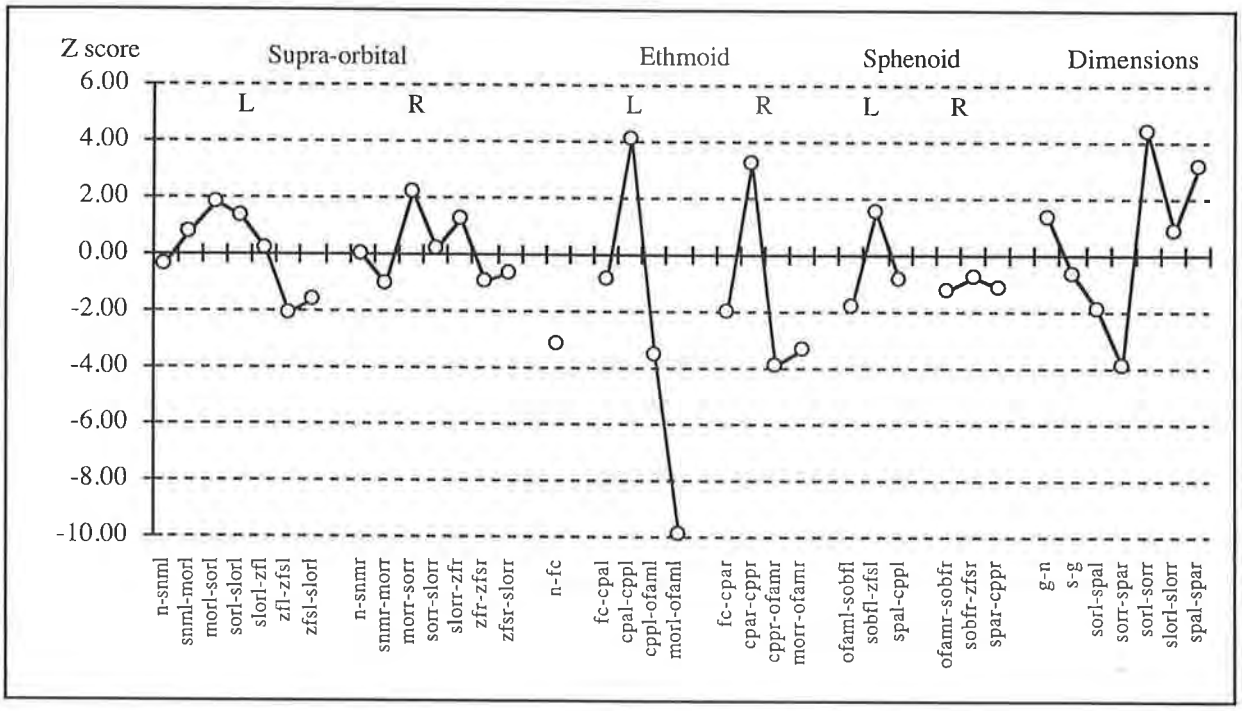

3.4.21.5 The Zygomatic Bone of Patient HC

Distances (Figure 3.33(g)): Several measurements were outside the experimental standard range. The zygo-maxillary suture (orl-iobfl, orr-iobfr) was significantly reduced bilaterally. The anterior height of the inferior orbital fissure (iobfr-gwlr) was increased on the right. The spheno-zygomatic suture (gwll-zfsl, gwlr-zfsr) was increased in length bilaterally. The height of the frontal process was decreased (zfr-ztr) on the right side. The inferior length of the zygomatic arch (parl-zmil, parr-zmir) was reduced bilaterally.

Dimensions (Figure 3.33(g)): The dimensions showed some variance from normal limits. The length of the zygomatic bone (parl-orl) was reduced on the left with a similar trend on the right. The lateral depth of the zygomatic bone (gwll-ilorl, gwlr-ilorr) was also reduced bilaterally.

Discussion: Lengthening and presumed fusion of the spheno-zygomatic suture produced a pattern of deformity where there was a reduction in the anterior-posterior dimension of the zygomatic bone. Fusion of the zygo-maxillary suture would limit anterior growth of the maxilla and promote increased height.

Figure 3.33(g) Z Scores of the Distances and Dimensions of the Zygomatic Bone for Patient HC compared with the Adult Experimental Standard

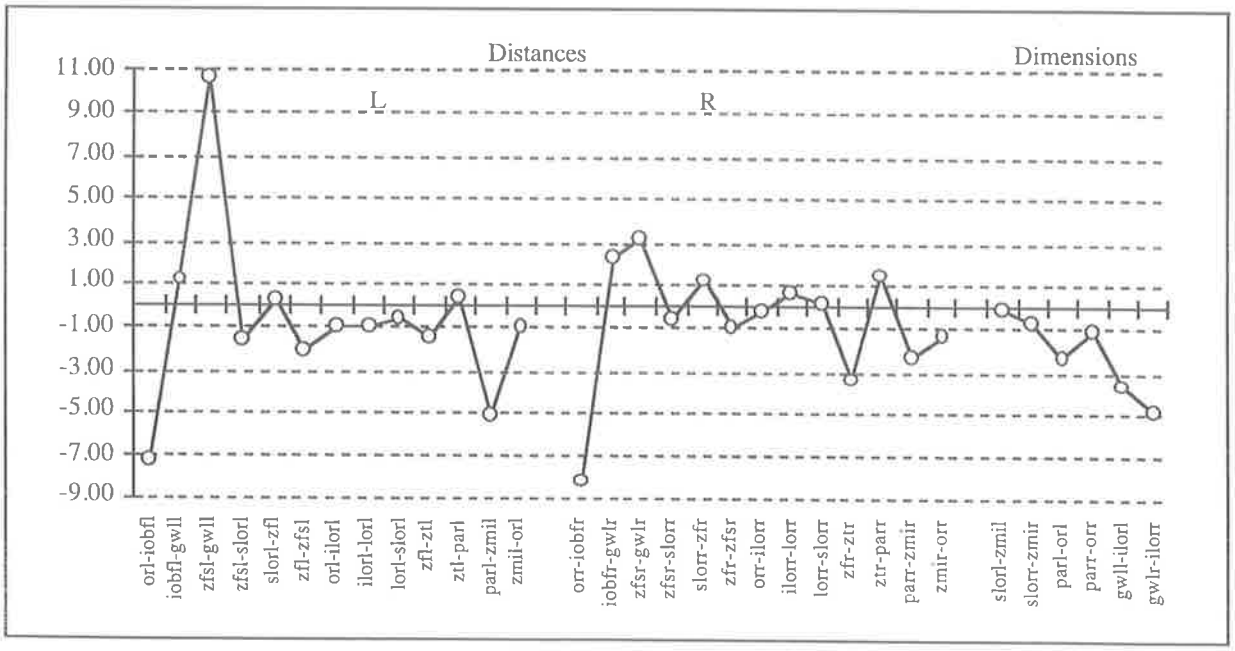

3.4.21.6 The Vomerine Bone of Patient HC

Distances, Dimensions and Angles (Figure 3.33(h)): Most distances were not significantly different from the experimental standard except the ethmoid-vomerine junction (vei-ves) which was reduced in length. The vomerine length (h-ans) was also reduced. The angle of the vomer relative to the cranial base (s-n/h-ans) was significantly increased. This may have resulted from the cranial base deformity.

Discussion: In this patient the vomer showed a tendency to be smaller and angled further inferior from the cranial base. This reflected a lack of forward growth in preference for downward growth which may then have directed the position of the maxilla.

Figure 3.33(h) Z Scores of the Measurements of the Vomer for Patient HC compared with the Adult Experimental Standard

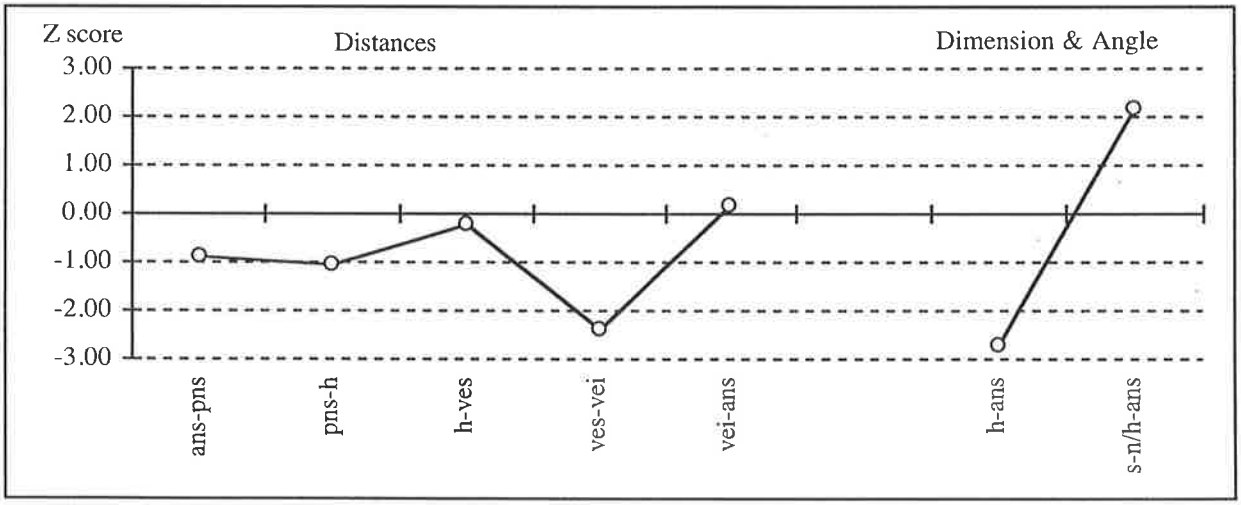

3.4.21.7 The Ethmoid Bone of Patient HC

Lateral Ethmoid Plate (Figure 3.33(i)):

Distances: The lateral ethmoid plate distances, forming the medial orbital wall, were reduced in height and in length. The anterior border of the lateral plate (nlil-morl) was reduced on the left and the posterior border of the lateral plate (ofamr-msr) was reduced on the right. The orbital border of the frontal ethmoid attachment (ofaml-morl, ofamr-morr) was significantly reduced bilaterally. Additionally, the anterior (morl-cpal, morr-cpar) and posterior (cppl-ofaml, cppr-ofamr) frontal ethmoid attachment were reduced in width bilaterally (see frontal bone).

Dimensions and Angles: The inter-orbital dimension (morl-morr) and the posterior superior width between the optic canals (ofaml-ofamr) were not significantly different from the experimental standard however the dimensions between the anterior and posterior inferior lateral plate (nlil-nlir and msl-msr) were reduced. The splay of the lateral plate was decreased posteriorly and anteriorly (nlil-morl/morr-nlir, msl-ofaml/ofamr-msr).

Figure 3.33(i) Z Scores of the Measurements of the Lateral Ethmoid Plate for Patient HC compared with the Adult Experimental Standard

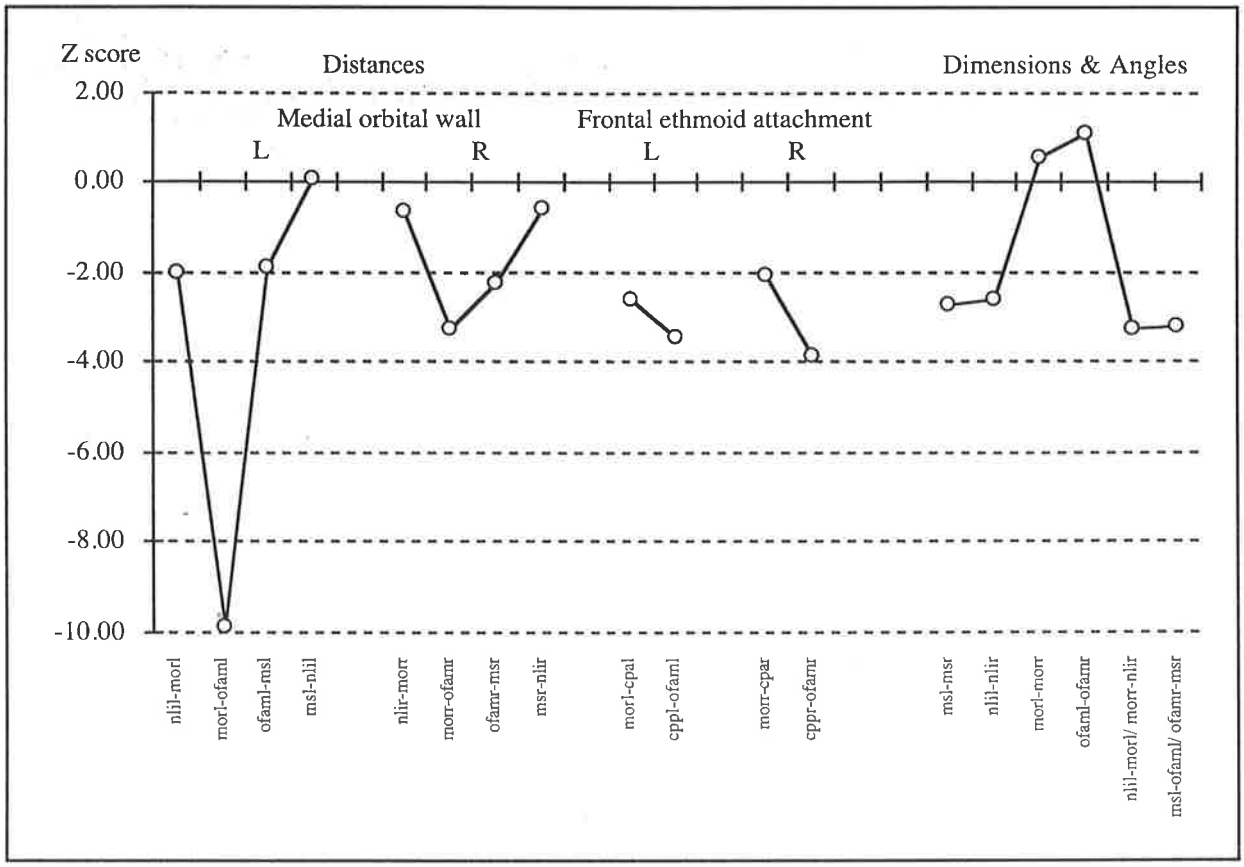

3.4.21.7 The Ethmoid Bone of Patient HC (continued)

Cribriform Plate (Figure 3.33(j)):

Distances: The length of the cribriform plate (cpal-cppl, cpar-cppr) was increased bilaterally. The cribriform plate posterior width at the spheno-occipital synchondrosis (es-cppl, es-cppr) was increased bilaterally. The right anterior cribriform plate width (fc-cpar) was reduced in length.

Angles: The lateral angle of the cribriform plate was increased on the right side (s-n/cpar-cppr) but not on the left and was probably related to the reduced anterior width of the cribriform plate (fc-cpar).

Medial Ethmoid Plate (Figure 3.33(j)):

Distances: The medial plate had a reduced length at its articulation with the vomer (ves-vei) (see vomer) and in its nasal root projection (n-fc).

Dimensions: The dimensions were within the limits of the experimental standard

Discussion: The lateral plate was reduced in size and contributed to the reduced orbital size. The fronto-ethmoid junction was reduced in width and may be related to the decreased lateral plate size and orbital pathology. The decreased size in this region corresponded with a lack of hypertelorism and was adjacent to the previous surgical site. The cribriform plate shows an increase in width posteriorly and an increased length. This may be due to suture abnormality or bone resorption which gives the appearance of a larger cribriform plate region. The medial plate was normal or reduced in its dimensions. Anteriorly, the inter-orbital distance was normal. The findings of the ethmoid bone in this patient may be influenced by the previous surgery. Distances and dimensions such as the inter-orbital distance, the anterior part of the lateral plate and the anterior region of the cribriform plate such as the foramen caecum may all be distorted. Without knowing the exact nature of the original regional pathology, and the precise placement of the surgical cuts in the fronto-orbital advance, and the distance advanced, it was difficult to interpret the anterior results meaningfully. Regardless of this, the spheno-ethmoid synchondrosis was widened and the size and splay of the lateral plates were decreased, as the principal posterior pathology of the ethmoid bone had not been addressed surgically.

Figure 3.33(j) Z Scores of the Measurements of the Cribriform and Medial Ethmoid Plates for Patient HC compared with the Adult Experimental Standard

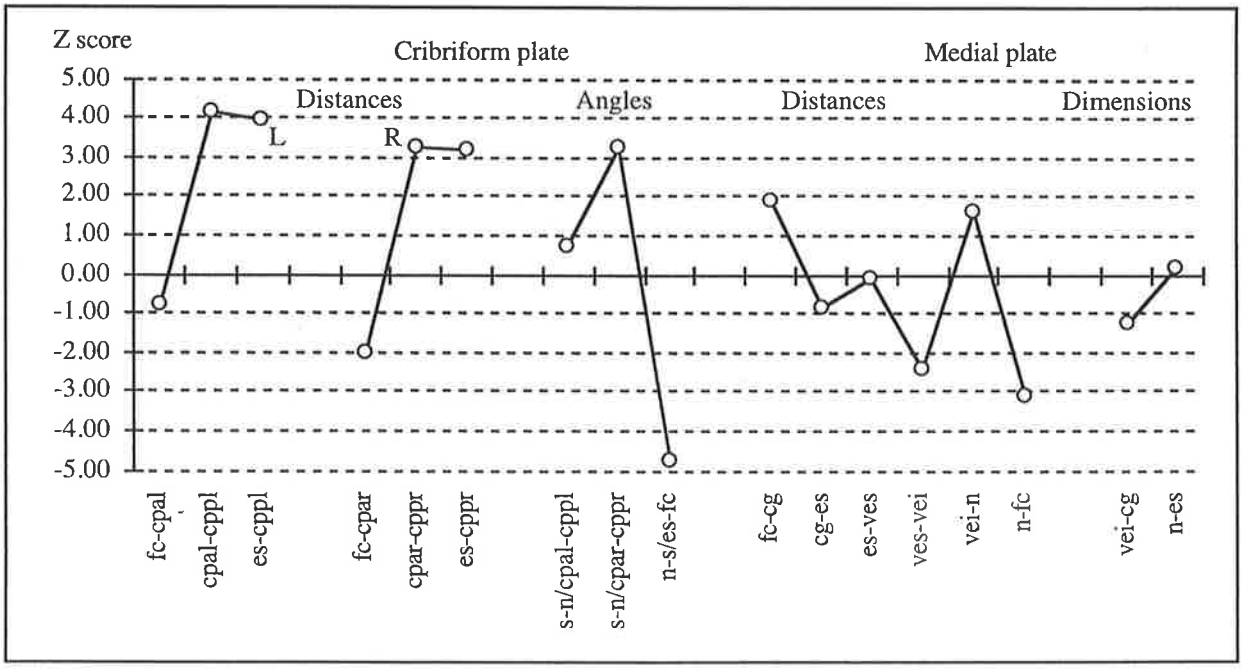

3.4.21.8 The Sphenoid Bone of Patient HC

Lesser Wing (Figure 3.33(k)):

Distances: The length of the lesser wing was increased posteriorly (acl-spal, acr-spar) and anteriorly (spar-es) on the right side compared with the experimental standard.

Dimensions and Angles: The maximum width of the lesser wings (spal-spar) was increased with an increase in the angle between the lesser wings (spal-es-spar). The other distances and angles of the lesser wings were not significantly different from the experimental standard.

Pterygoid Plate (Figure 3.33(k)):

Distances and Angles: The length of the left lateral pterygoid plate (ptll-fool) was significantly reduced compared with the experimental standard. The angles of the pterygoid axis were significantly increased (s-n/ptsl-hpl, s-n/ptsr-hpr) implying a lateral and posterior splay to the pterygoid plates.

Greater Wing (Figure 3.33(l)):

Distances: The measured lateral and orbital distances were not significantly different from the experimental standard with the exception of the spheno-zygomatic suture (gwll-zfsl, gwlr-zfsr) which was increased in length bilaterally (see also zygomatic bone). Landmarks on the squamous sphenoid bone (spt and spc) could not be identified bilaterally, due to fusion of the calvarial bone in this region and hence all the distances of the lateral part of the bone could not be measured. The posterior part of the greater wing was increased at the posterior floor of the middle cranial fossa (fosl-petal) on the left side.

Dimensions and Angles: The posterior sphenoid width (fosl-fosr) was reduced. While the angles of protrusion were increased (zfsl-gwml/gwmr-zfsr, gwll-gwml/gwmr-gwlr), the angle of the floor of the greater wing was normal (zfsl-gwml-ptsl, zfsr-gwmr-ptsr). This would be accounted for by a narrowing of the body of the sphenoid bone posteriorly (see sphenoid body). The posterior angle of the greater wing showed a tendency to be reduced (fosl-petal/petar-fosr).

Figure 3.33(k) Z Scores of the Measurements of the Lesser Wing and Pterygoid Plate of the Sphenoid for Patient HC compared with the Adult Experimental Standard

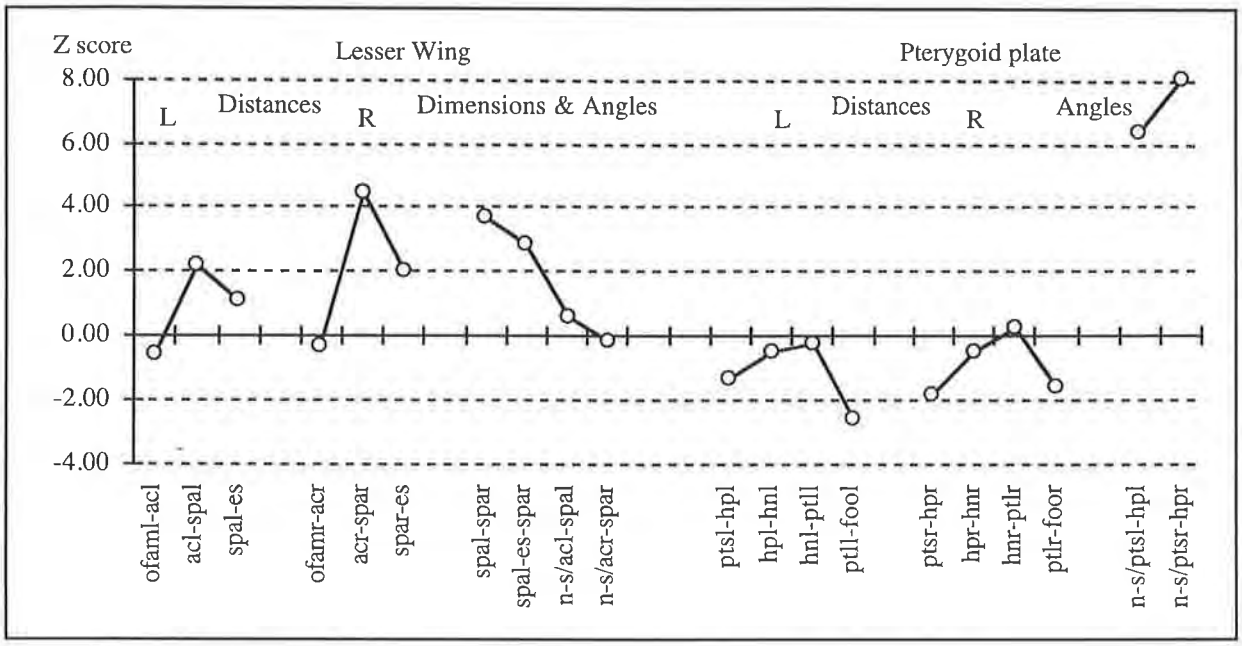

Figure 3.33(l) Z Scores of the Measurements of the Greater Wing of the Sphenoid for Patient HC compared with the Adult Experimental Standard

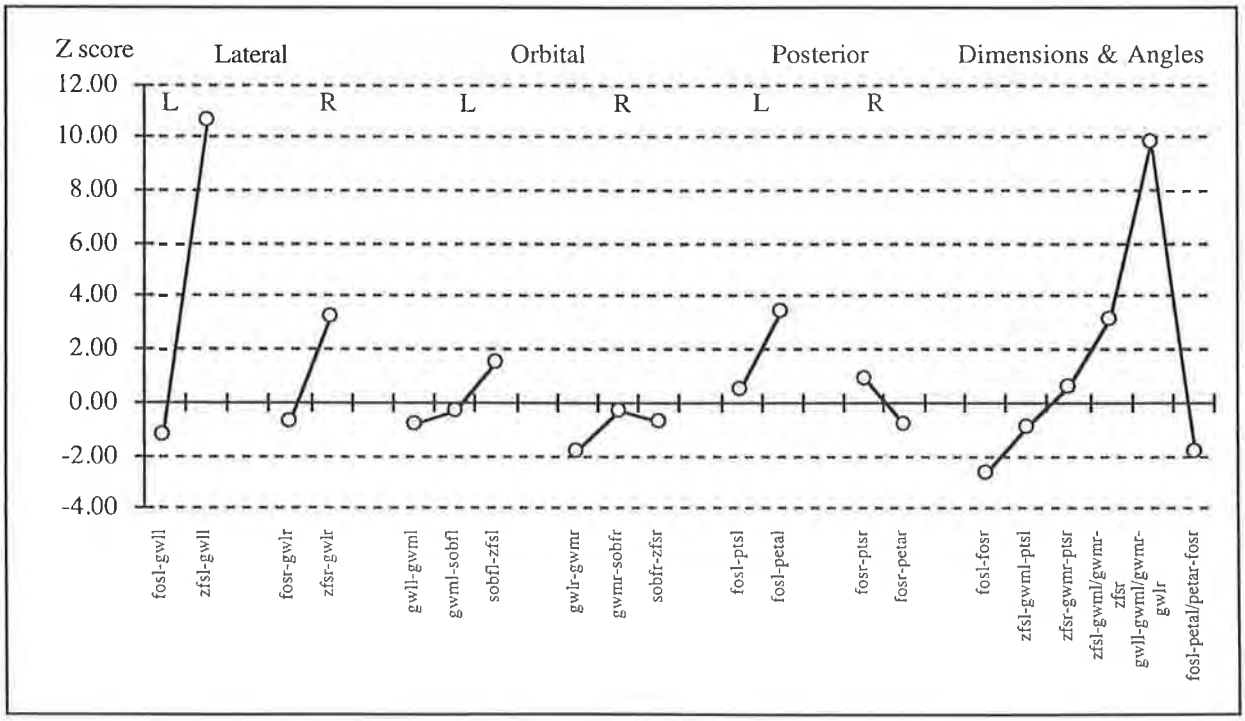

3.4.21.8 The Sphenoid Bone of Patient HC (continued)

Body of Sphenoid (Figure 3.33(m)):

Distances: The body dimensions were varied between and within regions. The lateral distances were not significantly different from the experimental standard including the lateral height of the spheno-occipital synchondrosis bilaterally (ptsl-petal, ptsr-petar). The anterior body showed increased distances at the spheno-ethmoid synchondrosis (es-cppl, es-cppr), and reduced distances at the posterior frontal ethmoid attachment (cppl-ofaml, cppr-ofamr) and the anterior lateral body (cppl-ofpml, cppr-ofpmr). The right lateral sella length (ofpmr-petar) was increased. The distances of the floor were not significantly different from the experimental standard except the posterior widths which were reduced (ptsl-h, ptsr-h).

Dimensions and Angles: The dimensions revealed a normal anterior inferior body width (gwml-gwmr) and anterior superior body width (ofaml-ofamr). The inferior spheno-occipital synchondrosis (ptsl-ptsr) and the superior spheno-occipital synchondrosis (petal-petar) were reduced in length (the lateral spheno-occipital synchondrosis was normal) (see also cranial base sutures). The height of the body (acr-gwmr) was reduced on the right side. The angles of the lateral protrusion of the body from the midline were reduced superiorly on the right (s-n/ofpmr-petar).

Discussion: This sphenoid bone in this patient had slightly enlarged lesser wings with an increased angle of inferior protrusion. The spheno-ethmoid synchondrosis was elongated, and the sella was enlarged slightly. An increased angle of lateral protrusion of the greater wings was present with lengthening of the spheno-zygomatic sutures and some involvement of the spheno-temporal sutures. The spheno-occipital synchondrosis was reduced in width. This may have some bearing on the temporal bone development and the atresia of the auditory canal seen on the right in this patient (see temporal bone).

Figure 3.33(m) Z Scores of the Measurements of the Body of the Sphenoid for Patient HC compared with the Adult Experimental Standard

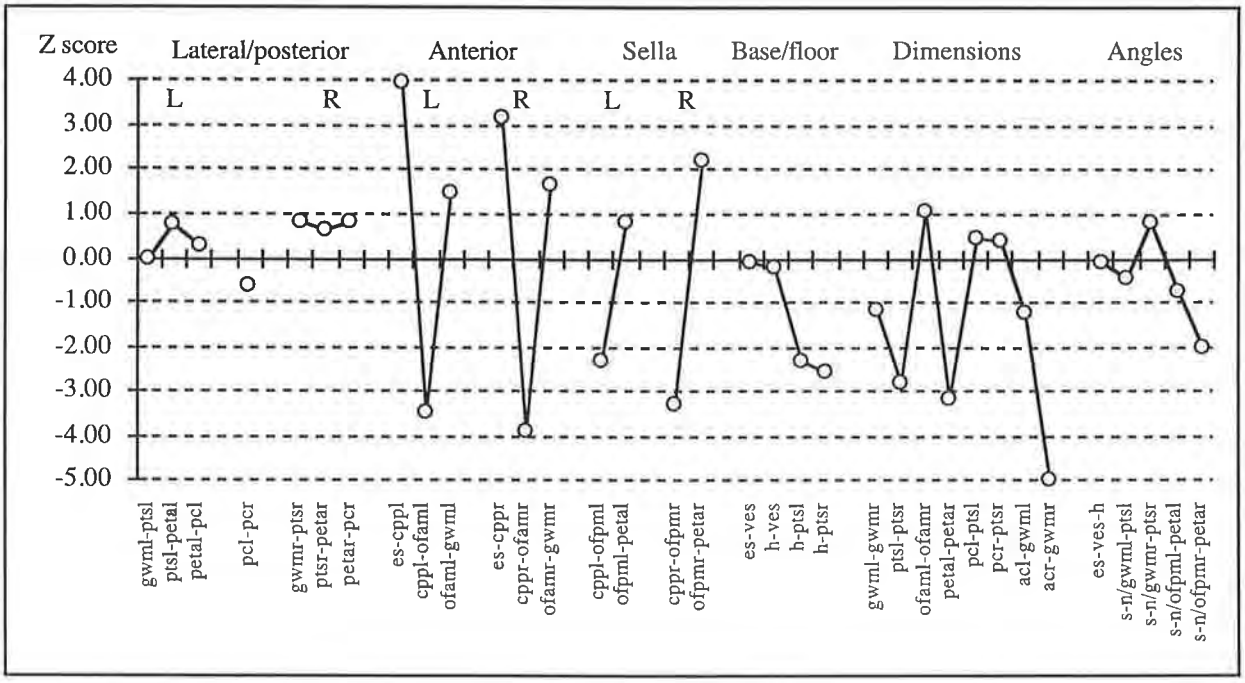

3.4.21.9 The Temporal Bone of Patient HC

Distances (Figure 3.33(n)):

Squamous Temporal Bone: The temporal squamous bone was not fully measurable in this child due to lack of visibility of the asterion (as) and sphenion (spt). The remaining distance (ma-smf) was not significantly different from the experimental standard.

External Auditory Meatus: The external auditory meatus was absent on the left. Only an indistinct outline was visible in the region of the external auditory meatus on the temporal bone and thus was not recorded. The right superior anterior rim (por-eamar) was decreased.

Zygomatic Process: The zygomatic process was generally within the normal range. The length of the zygomatic arch (ztl-aul) was decreased on the left and the height of the articular fossa (afl-ael, afr-aer) was normal.

Petrous Temporal Bone (Figure 3.33(o)): The spheno-petrous temporal suture (superior) (fisr-petar) was significantly decreased in length on the right. The jugular foramen width was not significantly different from the experimental standard (jfll-jfml, jflr-jfmr). Increased distances were recorded at the occipital mastoid suture (inferior) (mal-jfll) on the left, along with the left medial temporo-occipital suture (inferior) (jfml-ptsl).

Dimensions (Figure 3.33(o)): The length of the petrous temporal ridge (petal-petpl, petar-petpr) was normal bilaterally. The dimension between the internal auditory meati (iaml-iamr) and the mastoidale points (mal-mar) was decreased. The angle of the zygoma projection (petal-aul-ztl, petar-aur-ztr) and the angle between the auditory canals (pol-iaml/iamr-por) were reduced. The petrous temporal bone (petpl-petal/petar-petpr) angle was within the normal range.

Discussion: The pattern of measurements of the petrous temporal bone differ in this patient with atresia of the left external auditory meatus from the other patients with Crouzon syndrome. The sphenoid sutures with the petrous temporal bone were not increased but rather decreased. The jugular foramen was of normal size, (although the trend was for it to be reduced). The sutural distances laterally were increased or normal. The distance between the petrous temporal bones was reduced. In summary, the temporal bone measurements demonstrated hypoplasia of the petrous bone with a resultant atresia on the left side.

Figure 3.33(n) Z Scores of the Distances of the Temporal Bone for Patient HC compared with the Adult Experimental Standard

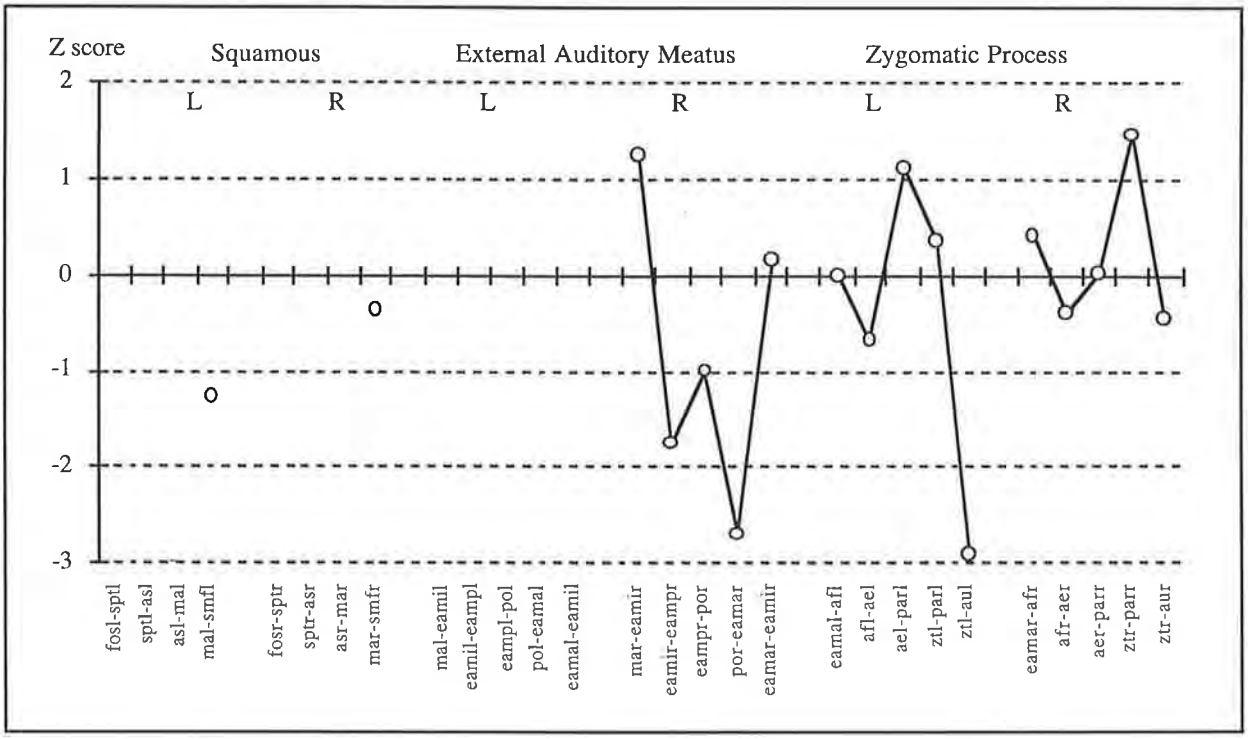

Figure 3.33(o) Z Scores of the Measurements of the Temporal Bone for Patient HC compared with the Adult Experimental Standard

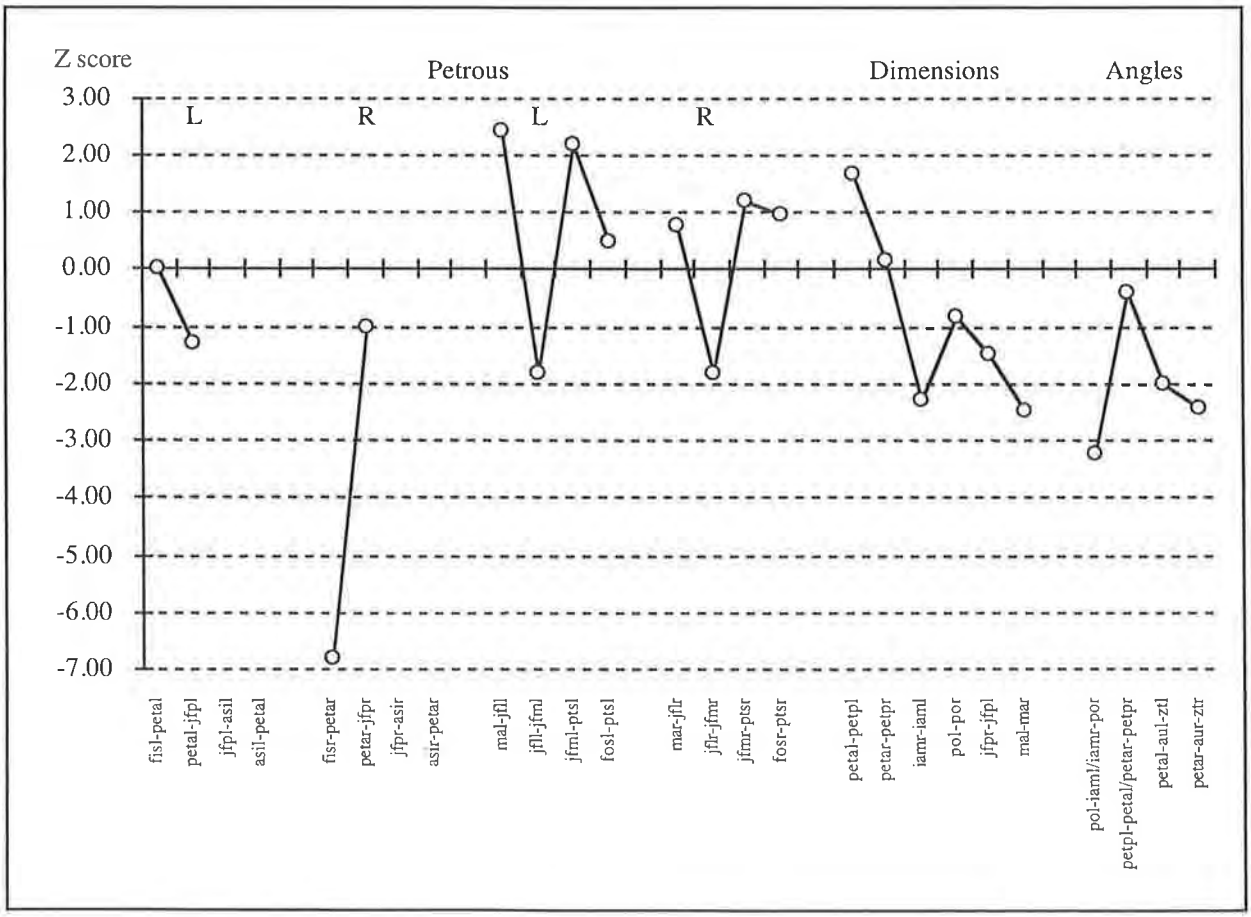

3.4.21.10 The Parietal Bone of Patient HC

Distances: The key landmarks for the parietal bone for Patient HC were not visible due to suture fusion and could not be reliably estimated. Therefore the parietal bone was not measured and a pattern profile of Z scores was not generated. The measurement data for the experimental standard are reported in Appendix 2.

3.4.21.11 The Occipital Bone of Patient HC

Distances (Figure 3.33(p)): The distances around the occipital bone and involving the foramen magnum were not significantly different from the experimental standard except for the medial temporo-occipital suture (inferior) (jfml-ptsl, jfmr-ptsr), which was increased in length on the left with a tendency for an increase on the right. The inferior spheno-occipital synchondrosis length (ptsr-ptsl) was decreased.

Dimensions (Figure 3.33(p)): The dimensions were not significantly different from the experimental standard.

Discussion: The occipital bone suture with the temporal bone was lengthened, the jugular foramen was normal and the spheno-occipital synchondrosis was reduced in length.

Figure 3.33(p) Z Scores of the Measurements of the Occipital Bone for Patient HC compared with the Adult Experimental Standard

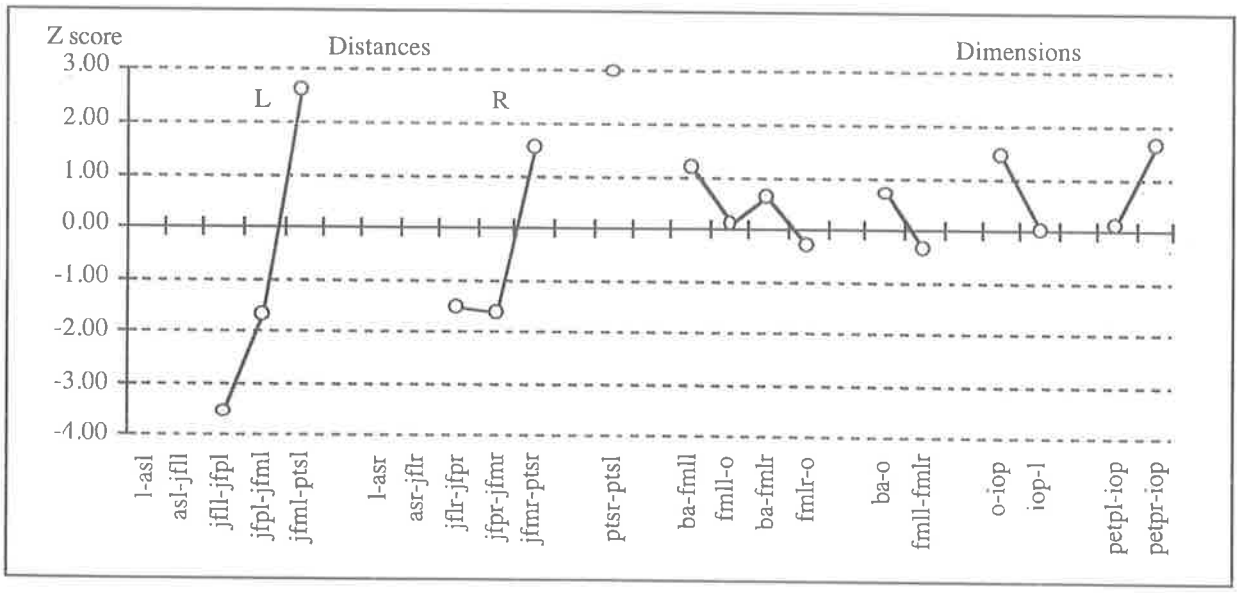

3.4.21.12 The Cranial Base Sutures of Patient HC

Anterior Cranial Fossa (Figure 3.33(q)): The spheno-ethmoid synchondrosis (es-cppl, es-cppr) was increased in length. The spheno-frontal sutures in the anterior cranial fossa (cppl-spal, cppr-spar) and orbit (spal-zfsl, spar-zfsr) were normal. The spheno-zygomatic suture (zfsl-gwll, zfsr-gwlr) was increased in length.

Middle Cranial Fossa (Figure 3.33(q)): The sutures were relatively normal with the right inferior sphenoid-petrous temporal suture (fisr-petar) reduced in length.

Posterior Cranial Fossa (Figure 3.33(q)): The left inferior medial temporo-occipital suture (jfml-ptsl) was slightly increased in length. Laterally the sutures were not significantly different from the experimental standard. The superior and inferior parts of the spheno-occipital synchondrosis (petal-petar, ptsl-ptsr) were reduced in length, while the lateral part of the synchondrosis (ptsl-petal, ptsr-petar) was normal in height.

Discussion: A common pattern of deformity was found in Patient HC, with spheno-ethmoid synchondrosis length increased medially and zygomatic suture lengthened laterally. The middle cranial fossa was relatively spared while a mixed pattern of suture deformity was found posteriorly. Lengthening of the spheno-occipital synchondrosis with hypoplasia of the medial petrous temporal bone was linked with atresia of the external ear canal on the left side.

Figure 3.33(q) Z Scores of the Dimensions of the Cranial Base Sutures for Patient HC compared with the Adult Experimental Standard

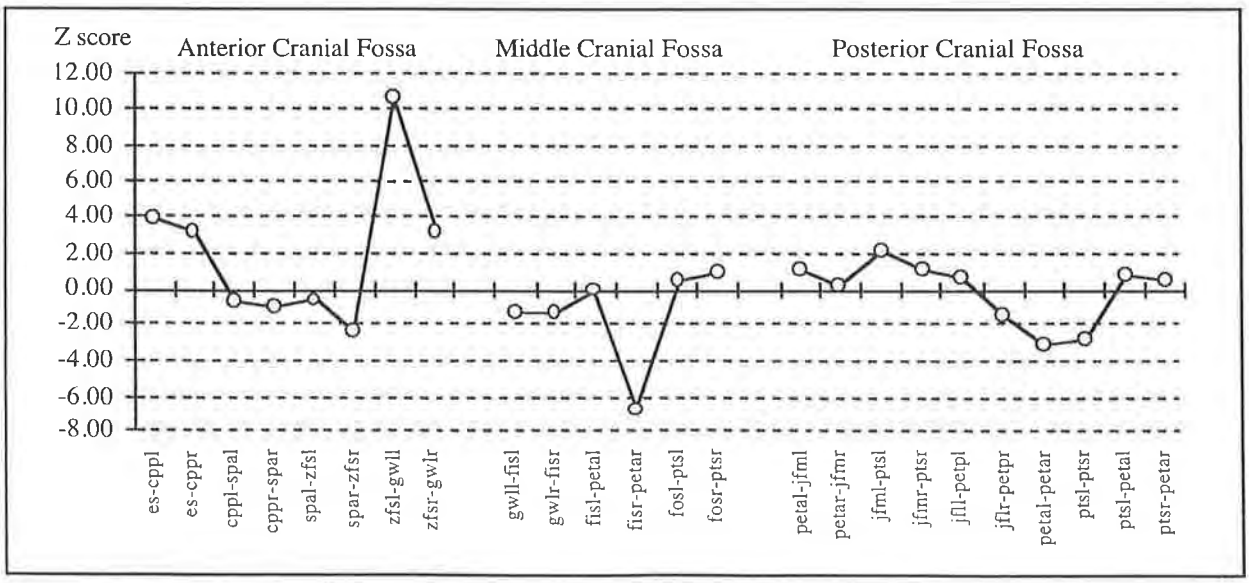

3.4.21.13 The Craniofacial Dimensions and Angles of Patient HC

Dimensions and Angles (Figure 3.33(r)): The anterior facial height (n-gn) was increased (mouth closed during CT scan). Laterally the height was not significantly different from the experimental standard. The SNA (s-n-ss) and SNB (s-n-sm) angles were reduced. The cranial base angle (ba-s-n) was more obtuse in this patient. The cranial base dimensions were not significantly different from the experimental standard.

Discussion: The cranial base angle was increased in this patient. This may contribute to a reduction in the facial angles. However, the decreased facial angles would be expected due to the maxillary hypoplasia alone. The SNB angle may be decreased due in part to the increased gonial angle of the mandible.

Figure 3.33(r) Z Scores of the Craniofacial Dimensions and Angles for Patient HC compared with the Adult Experimental Standard

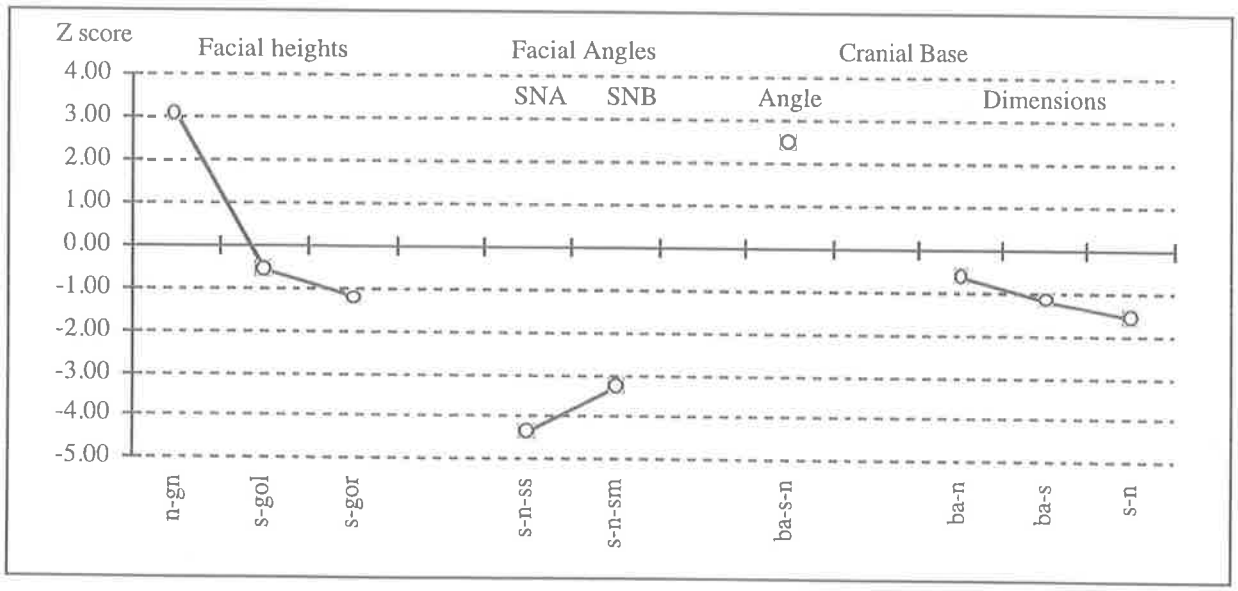

3.4.22 Clinical and Radiographic Findings for Patient TS

Clinical Features

This 27 year old man presented from overseas having had no previous surgery and with no family history (Figure 3.8). He had turricephaly, a prominent supra-orbital ridge, with proptosis, hypertelorism, a divergent squint and corneal ulceration with keratitis. Maxillary hypoplasia was present with a class III occlusion. The speech was hypo- and hyper-nasal.

Lateral, Antero-Posterior and Basal Radiographs

Lateral, anterior-posterior and basal views had been performed. The faint outline of the coronal suture could be seen bilaterally. No other cranial sutures were visible. There was a copper-beaten appearance to the calvaria along with a very prominent frontal sinus and frontal gibbosity. The nasal bones were prominent. The lesser wings were swept up with a prominent enlarged sella. The spheno-occipital synchondrosis could not be seen. Extensive aeration of the mastoid air cells was present. The occlusion was class III. The orbital aperture were elongated in the vertical or slightly oblique direction. This was related to the prominent frontal, ethmoid and maxillary sinuses.

3D CT Reconstruction

Calvarial bones: The most striking feature was the prominent supra-orbital ridge, with a relative flattening of the frontal bone above this. The calvarial sutures could not be visualised. The head shape was relatively normal posteriorly.

Cranial base: The cribriform plate and medial frontal bone were clearly very thin and attenuated, and appeared to be pushed down and laterally. This produced the impression of excessive endocranial bone resorption in this region. Anteriorly, there was an impression in the bone of the anterior cranial fossa made by the globes of the orbit, suggesting a constriction of the orbit by the frontal bone. The sella appeared relatively narrowed. Posteriorly the clivus was steep. The petrous temporal bones were not prominent, and gave the impression of being affected by bone resorption as well. The foramen magnum was unremarkable. The posterior cranial fossa showed areas of thin attenuated bone. The mastoid prominences were enlarged.

Orbital: The orbital shape was oblique, being narrowed medially by protrusion of the lateral ethmoid plate into the orbit. Laterally, the opening of the orbit was increased in height. The roof had a serpentine appearance, being pushed downwards posteriorly and curving upwards and forwards in its anterior half. The greater wing of the sphenoid was prominent in the lateral wall of the orbit. The superior orbital fissure was reduced in length.

Maxilla and Mandible: The maxilla appeared to be narrowed with poor anterior projection and the typical class III occlusion. The height of the maxilla appeared to be normal. The anterior nasal spine was prominent along with the nasal bones and naso-frontal processes of the maxilla. The size of the nasal aperture was subsequently reduced. The zygomatic bone appeared to be small at the region of the zygo-maxillary suture, while the frontal process was increased in height. The angles of the mandible were prominent laterally.

3.4.23 Features of CT Scan and 3D Reconstruction of Patient TS that made landmark identification difficult

While this patient showed several areas of bony resorption on the internal cranial skeleton, increased growth or bony apposition was found externally. Bony prominences included the frontal supra-orbital ridge, the mastoid processes, para-nasal bones and the gonial angles of the mandible. The frontal and mastoid regions were associated with increased sinus air cells. Repeated 3D CT reconstruction at a lower threshold did not remove the bony defects entirely, implying the bone was thin and attenuated. Lower threshold CT scan reconstruction began to occlude foraminae in the cranial base and orbit. The calvarial landmarks (l, as, br, spt, spc) could not be identified nor reliably estimated. The peri-orbital sutures and cranial base landmarks were identified from the regional bony contours and junctions defined in the landmarks (Figures 3.15-3.26).

3.4.24 Results and Discussion of the Quantitative Analysis of Patient TS compared with the Adult Experimental Standard

Figures 3.34(a)-(r)

3.4.24.1 The Mandible of Patient TS

Distances (Figure 3.34(a)): The left superior body distance (id-cbl) was increased, and the left anterior ramal height (cbl-ctl) was increased compared with the experimental standard. The left inferior body distance (gol-gn) was increased. The distances on the right hand side were not significantly different from the experimental standard.

Dimensions and Angles (Figure 3.34(b)): The intergonial distance (gol-gor) and the distance between the coronoid bases (cbl-cdr) was increased. The anterior symphyseal height (gn-id) was increased. The total length of the mandible (gn-cdl) on the left was increased. The right coronoid base angle (ctr-cdr-id) was significantly reduced. The anterior mandibular angle (gol-gn-gor) was significantly increased.

Discussion: Deformity around the region of the angle was pronounced in this patient. The gonial angles were flared out laterally although the measurement of the angles (cd-go-gn) themselves were not changed. The anterior symphyseal height was increased in a similar manner to the other three older patients (see Patients LW, AY and HC).

Figure 3.34(a) Z Scores of the Distances of the Mandible for Patient TS compared with the Adult Experimental Standard

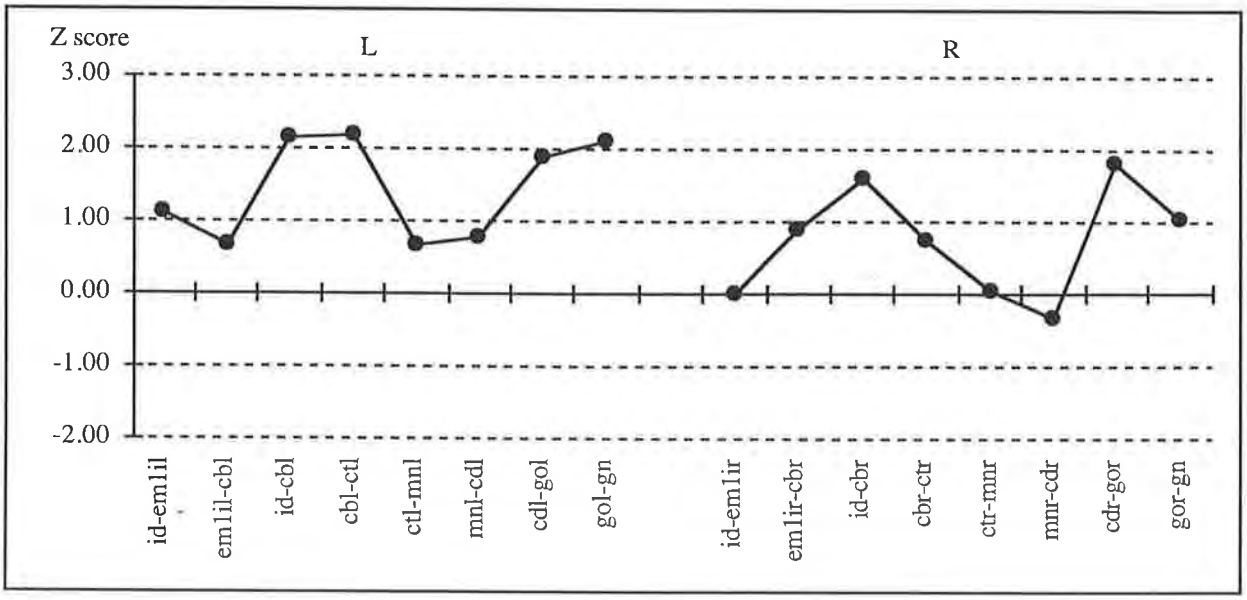

Figure 3.34(b) Z Scores of the Dimensions and Angles of the Mandible for Patient TS compared with the Adult Experimental Standard

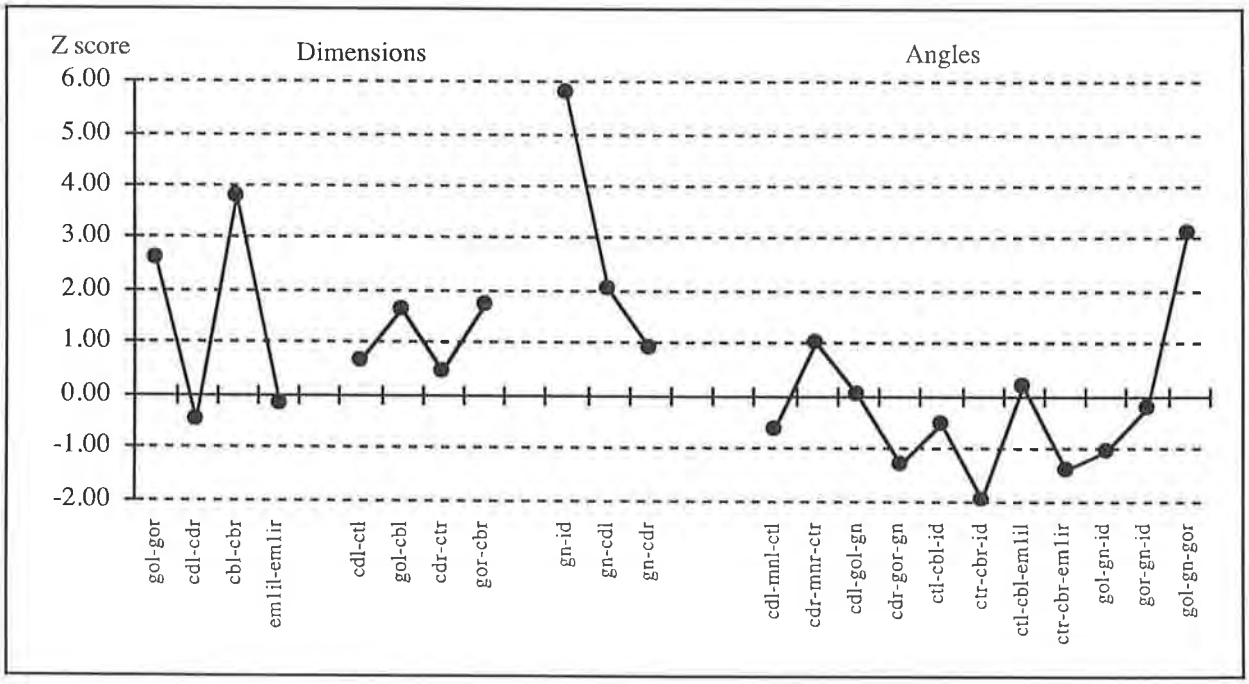

3.4.24.2 The Maxilla of Patient TS

Distances (Figure 3.34(c)): The anterior lateral orbital floor distance (orl-iobfl, orr-iobfr) was reduced bilaterally compared with the experimental standard. The maxillary orbital rim distance (orl-nlil, orr-nlir) was increased bilaterally. The right anterior border of the lateral ethmoid plate (nlir-morr) was reduced. The left lateral distance (zmil-em1sl) was increased on the left. The anterior alveolar margin (em1sl-pr) on the left was reduced, but normal on the right. The naso-maxillary suture length (inml-snml, (inmr-snmr) was increased bilaterally. The anterior alveolar height (pr-ans) was increased. The posterior alveolar margin (em1sl-mxtl) on the left was increased in length, but normal on the right. The posterior maxillary wall height (mxtl-msl, mxtr-msr) was significantly increased bilaterally. The palatal distances were normal.

Dimensions and Angles (Figure 3.34(d)): The dimensions representing the height of the maxilla were significantly increased (n-pr, morl-em1sl, morr-em1sr, gpfl-msl). The widths of the maxilla were normal except for the superior (inter-orbital) width (orl-orr) which was increased. The height of the nasal aperture (na-ans) was reduced. The measured angles of the maxilla were normal.

Discussion: The height of the maxilla was generally greater than for the experimental standard. Measurements recorded in the anterior-posterior direction were normal or reduced. The position of the molar teeth from the prosthion was reduced suggesting crowding of the dental arch. The measurements reflect a lack of anterior development of the maxilla with an over-development in the vertical direction.

Figure 3.34(c) Z Scores of the Distances of the Maxilla for Patient TS compared with the Adult Experimental Standard

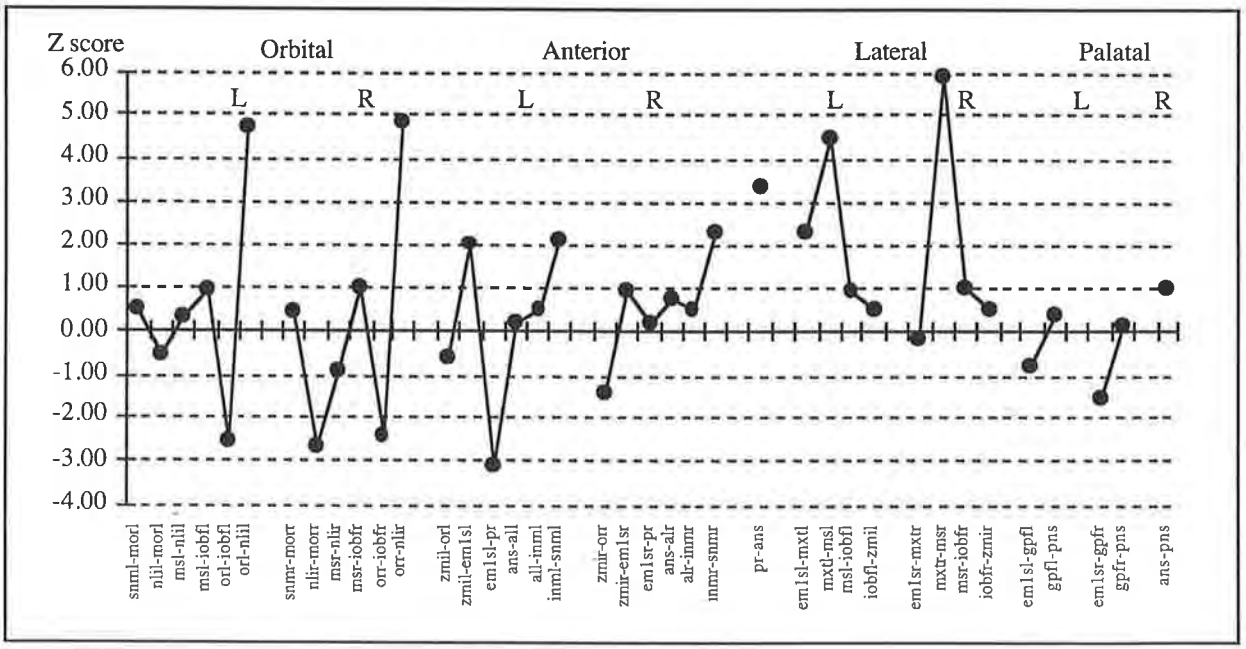

Figure 3.34(d) Z Scores of the Dimensions and Angles of the Maxilla for Patient TS compared with the Adult Experimental Standard

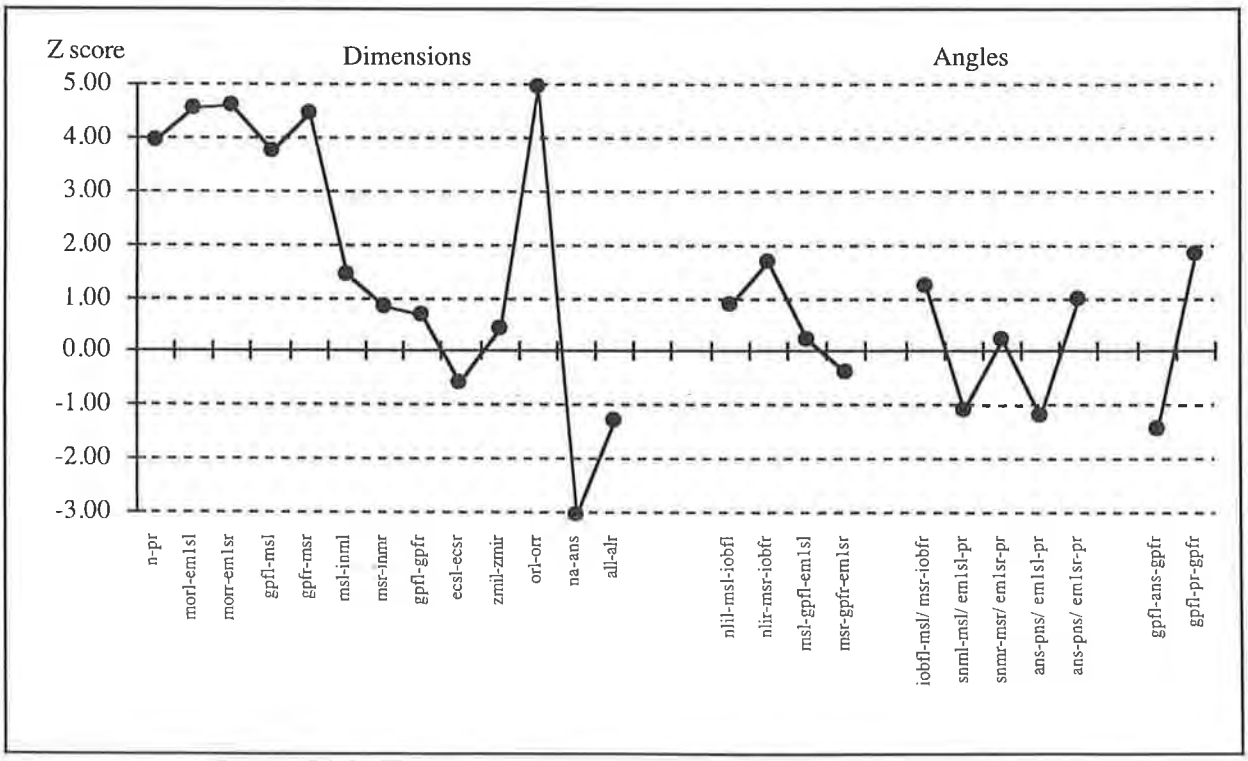

3.4.24.3 The Nasal Bones of Patient TS

Distances, Dimensions and Angles (Figure 3.34(e)): The length of the naso-maxillary sutures (inml-snml, inmr-snmr) were increased bilaterally. The width of the nasal bones was not significantly different from the experimental standard, however, the angle from the cranial base (s-n-na) was decreased.

Discussion: The nasal bones were increased in length and were at an inferiorly placed angle from the cranial base skeleton. The inferiorly placed angle of the nasal bones corresponds with the lack of anterior projection of the maxilla and increased vertical height of the maxilla (see maxilla).

Figure 3.34(e) Z Scores of the Measurements of the Nasal Bones for Patient TS compared with the Adult Experimental Standard

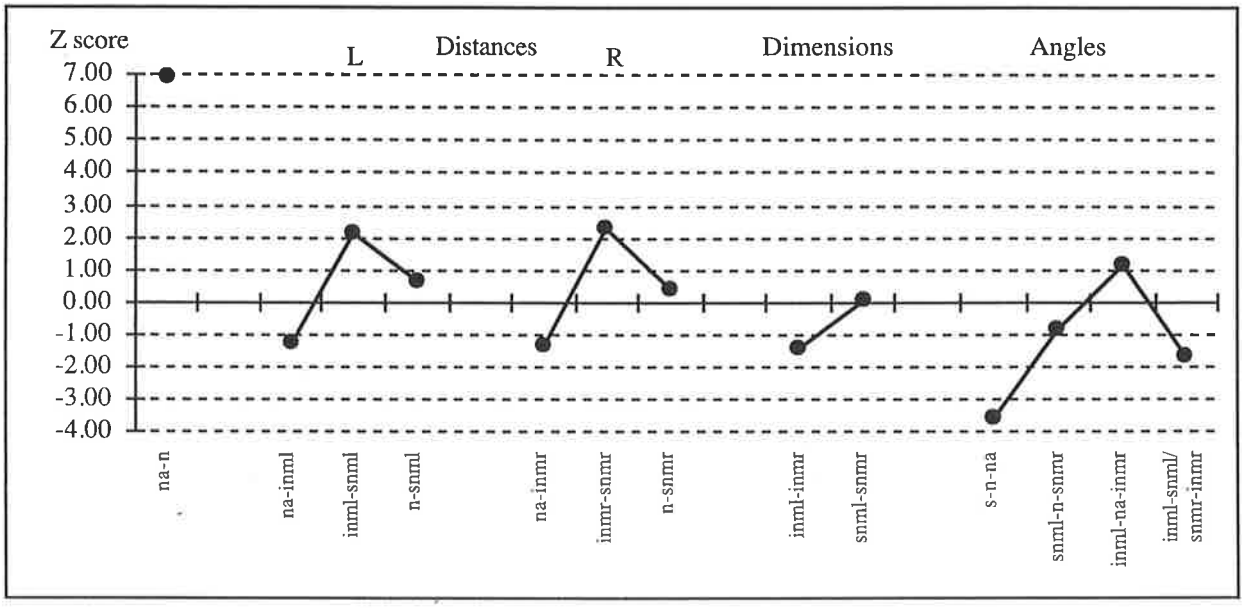

3.4.24.4 The Frontal Bone of Patient TS

Distances (Figure 3.34(f)):

Supra-orbital Region: The majority of measurements were not significantly different from the experimental standard with the exception of the increased distance of the superior lateral orbital rim (sorl-slorl, sorr-slorr) bilaterally.

Ethmoid Attachment: Significant discrepancies were found in the region of the ethmoid. The fronto-ethmoid articulation was reduced in length in the anterior cranial fossa (cpal-cppl, cpar-cppr). The width however, was significantly increased anteriorly (fc-cpal, fc-cpar) and posteriorly (cppl-ofaml, cppr-ofamr). These findings were in direct contrast to the findings in Patient HC.

Sphenoid Attachment: The lesser wing length was increased on the right (spar-cppr). The remaining suture distances of the fronto-sphenoid junction were not significantly different from the experimental standard. The parietal attachment (spc-br) and sphenoid attachments (zfs-spc and spc-spa) were not recorded due to the fusion of sutures and hence poor visibility of landmarks in this region.

Dimensions (Figure 3.34(f)): The medial prominence (g-n, s-g) and depth of the anterior cranial fossa (sorl-spal, sorr-spar) of the frontal bone was within the experimental standard range. The anterior supero-lateral orbital width (slorl-slorr) of the frontal bone was significantly increased compared with the experimental standard. The posterior width between the tips of the lesser wings (spal-spar) was significantly increased.

Discussion: The deformity in this patient can be localised to the frontal ethmoid region and antero-laterally to the region of the fronto-zygomatic and calvarial articulations. The role of the sphenoid lesser wing in the production of the frontal bone deformity was not great, as determined from the measurements. The broad frontal ethmoid attachment with a reduced length was not seen in the other patients. Fusion of the sutures lateral to the spheno-ethmoid synchondrosis and cribriform plate at the frontal ethmoid attachment could produce this pattern of deformity. The calvarial suture abnormalities seen qualitatively, contributed to the distortion of the lateral orbital rim and influenced the morphology of the frontal bone.

Figure 3.34(f) Z Scores of the Distances and Dimensions of the Frontal Bone for Patient TS compared with the Adult Experimental Standard

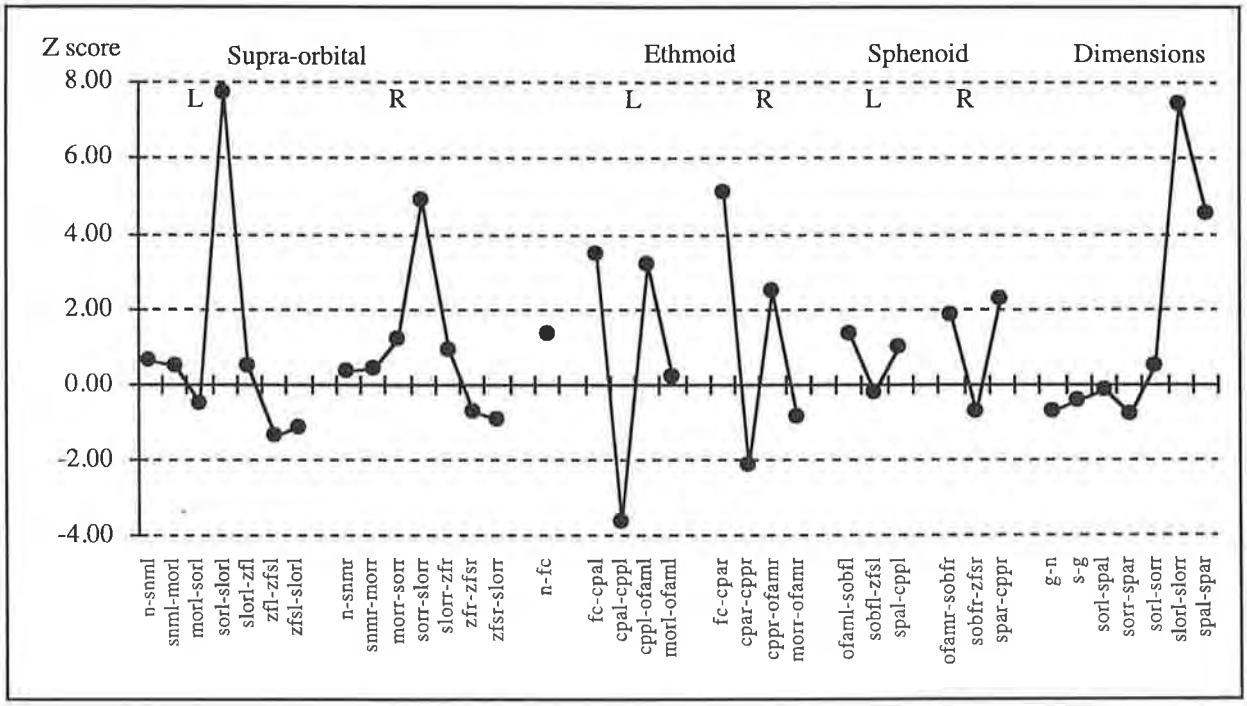

3.4.24.5 The Zygomatic Bone of Patient TS

Distances (Figure 3.34(g)): The orbital zygo-maxillary suture (orl-iobfl, orr-iobfr) was reduced in length bilaterally compared with the experimental standard. The inferior orbital fissure height (iobfl-gwll, iobfr-gwlr) was also reduced. The spheno-zygomatic suture (gwll-zfsl, gwlr-zfsr) was increased in length bilaterally. The lateral height of the frontal process was decreased (zfr-ztr) on the right side. On the left side, the inferior length of the zygomatic arch (parl-zmil) was reduced and the zygomatico-temporal suture (ztl-parl) was increased. A similar trend was seen on the right side.

Dimensions (Figure 3.34(g)): The height of the zygomatic bone (slorr-zmir) was increased on the right compared with the experimental standard with a similar trend on the left. The lengths of the left and right zygomatic bones (parl-orl, parr-orr) also showed a trend to be reduced, but were not statistically significant.

Discussion: The pattern of morphology of the zygomatic bone appeared to be determined by the spheno-zygomatic suture. This suture was increased in length and was presumed to be fused. The development of the zygomatic bone was therefore reduced in the AP direction with an increase in dimensions in the vertical direction.

Figure 3.34(g) Z Scores of the Distances and Dimensions of the Zygomatic Bone for Patient TS compared with the Adult Experimental Standard

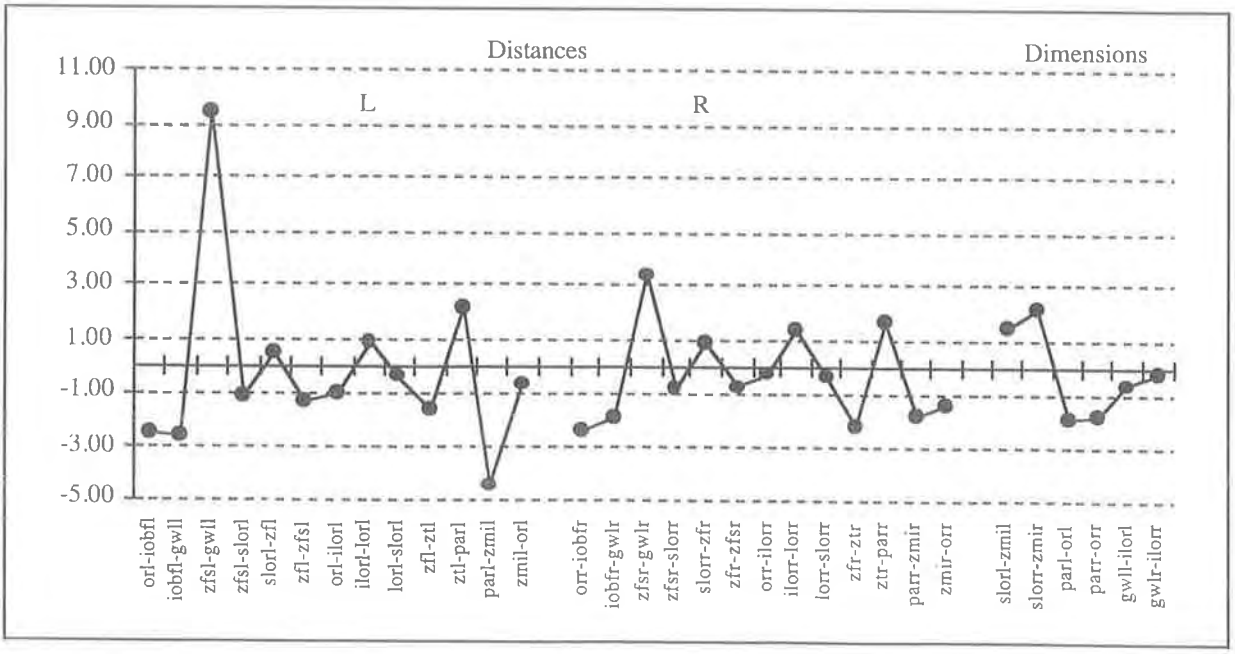

3.4.24.6 The Vomerine Bone of Patient TS

Distances, Dimensions and Angles (Figure 3.34(h)): The length of the spheno-vomerine junction (h-ves) was reduced. The remaining distances were not significantly different from the experimental standard. The longitudinal dimension was normal. The angle of the vomer (s-n/h-ans) relative to the cranial base was significantly increased.

Discussion: In this patient the vomer showed a mild tendency to be smaller and was angled further inferiorly. This corresponds with a lack of forward growth of the vomer and may direct the position of the maxilla.

Figure 3.34(h) Z Scores of the Measurements of the Vomer for Patient TS compared with the Adult Experimental Standard

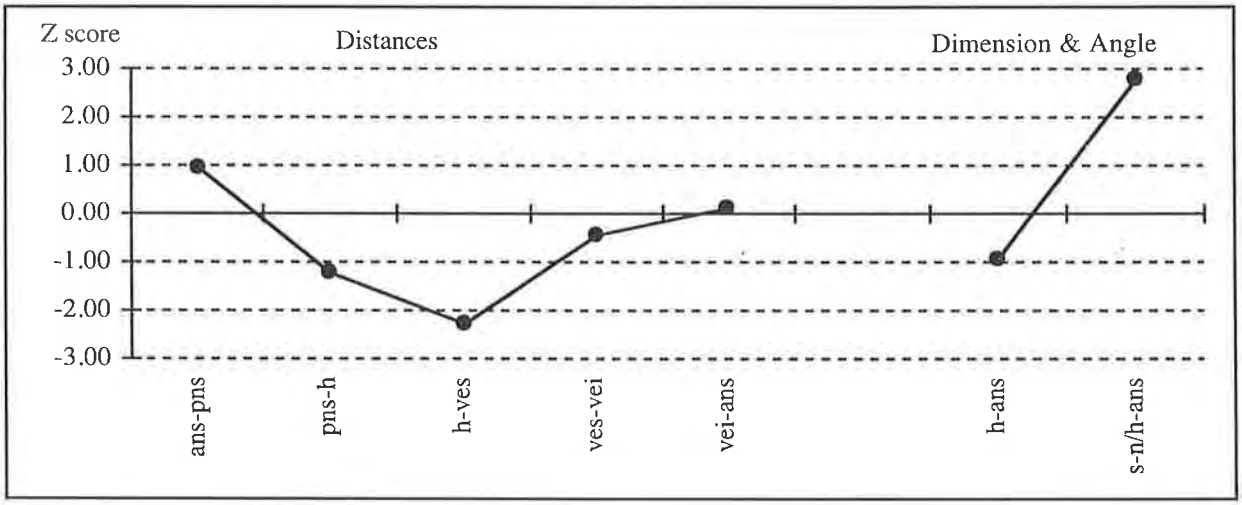

3.4.24.7 The Ethmoid Bone of Patient TS

Lateral Ethmoid Plate (Figure 3.34(i)):

Distances: The lateral ethmoid plate distances, forming the medial orbital wall, were reduced in height but not in length. The height of the medial orbital wall posteriorly (ofaml-msl, ofamr-msr) was reduced bilaterally and the anterior border of the lateral plate (nlir-morr) was reduced on the right side. The posterior frontal ethmoid attachment (cppl-ofaml, cppr-ofamr) was increased in distance bilaterally.

Dimensions and Angles: The inter-orbital distance (morl-morr) and posteriorly between the optic canals (ofaml-ofamr) were significantly increased. The splay of the lateral plate was decreased anteriorly (nlil-morl/morr-nlir), however was increased posteriorly (msl-ofaml/ofamr-msr).

Cribriform Plate (Figure 3.34j):

Distances: The anterior cribriform plate width (fc-cpal, fc-cpar) was increased bilaterally. The posterior widths at the spheno-ethmoid synchondrosis (es-cppl, es-cppr) were not significantly different from the experimental standard. The length of the cribriform plate was reduced bilaterally (cppl-cpal, cppr-cpar).

Angles: The cribriform plate lateral angles (s-n/cpal-cppl, s-n/cpar-cppr) were increased significantly.

Medial Ethmoid Plate (Figure 3.34j):

Distances: The spheno-ethmoid junction (es-ves) and the septal junction (vei-n) were increased.

Dimensions: The height of the medial plate (vei-cg) was increased.

Discussion: The lateral plate was reduced in height. The cribriform plate showed an increase in width anteriorly and decreased length, while the medial plate was increased in height. The spheno-ethmoid synchondrosis was not involved in this patient however the frontal ethmoid attachment was increased in width (see frontal bone). The splay of the lateral plates anteriorly, but not posteriorly, were decreased. Normal growth at the spheno-ethmoid synchondrosis would fit with the more normal posterior splay to the lateral plate. The spheno-ethmoid synchondrosis, when involved in the pathology, appears to push the superior part of the lateral plates further laterally and thus decreasing the angle of lateral splay.

Figure 3.34(i) Z Scores of the Measurements of the Lateral Ethmoid Plate for Patient TS compared with the Adult Experimental Standard

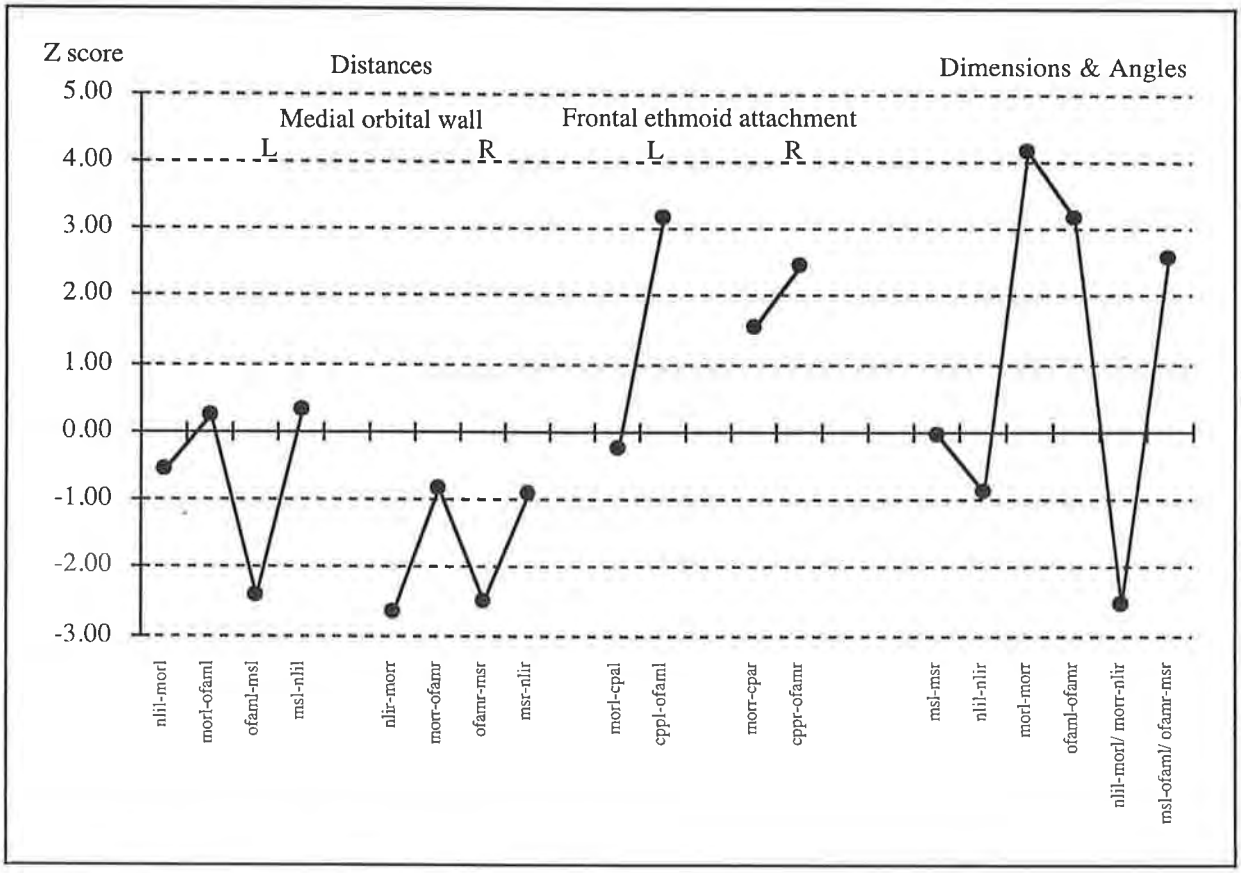

Figure 3.34(j) Z Scores of the Measurements of the Cribriform and Medial Ethmoid Plates for Patient TS compared with the Adult Experimental Standard

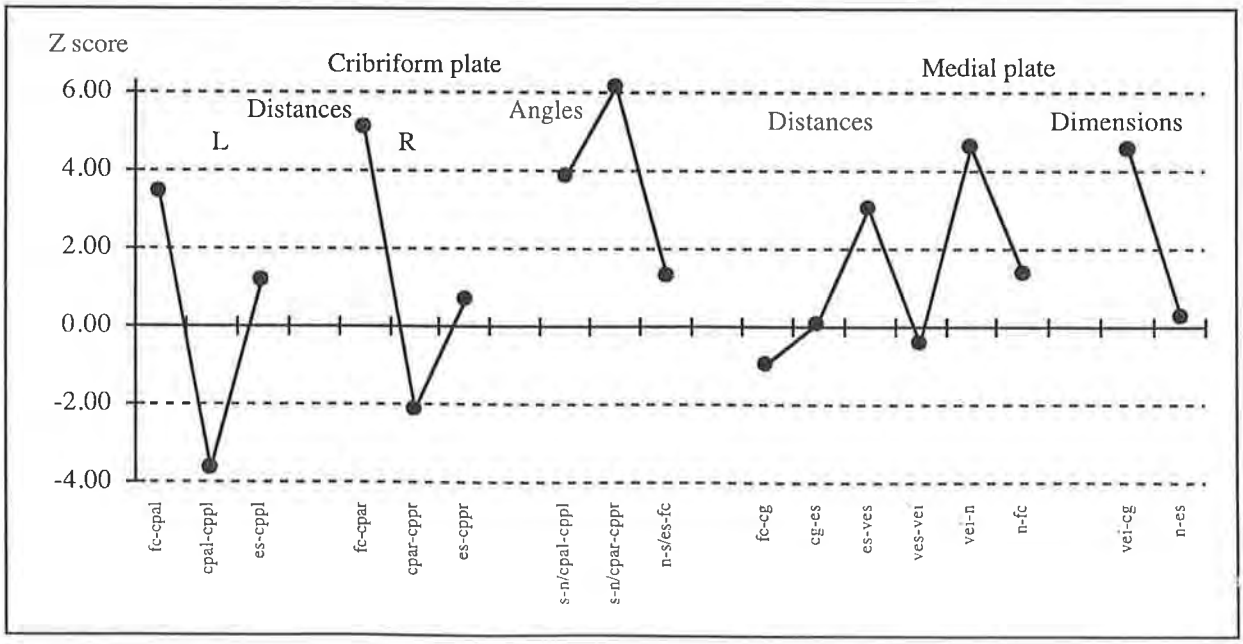

3.4.24.8 The Sphenoid Bone of Patient TS

Lesser Wing (Figure 3.34(k)):

Distances: The medial part of the lesser wing (ofaml-acl, ofamr-acr) was reduced in length compared with the experimental standard. The posterior length of the lesser wing (acl-spal) on the left and the anterior length of the lesser wing (spal-es, spar-es) bilaterally were increased.

Dimensions and Angles: The distance between the tips of the lesser wing was increased (spal-spar), with an increase in the angle between the lesser wings (spal-es-spar). The other distances and angles of the lesser wings were not significantly different from the experimental standard.

Pterygoid Plate (Figure 3.34(k)):

Distances and Angles: The pterygoid plate distances were not significantly different from the experimental standard. The angles of pterygoid axis, however, were significantly increased (s-n/ptsl-hpl, s-n/ptsr-hpr).

Greater Wing (Figure 3.34(l)):

Distances: The lateral and orbital distances were normal with the exception of the spheno-zygomatic suture (zfsl-gwll, zfsr-gwlr) which was increased in length bilaterally (see zygomatic bone). The distance of the anterior floor of the middle cranial fossa was increased (fosr-gwlr) on the right. The length of the inferior orbital greater wing of sphenoid was reduced (gwml-gwll) on the left with a similar trend on the right. The posterior part of the greater wing was increased at the posterior floor of the middle cranial fossa (fosl-petal) on the left side (adjacent the spheno-petrous temporal suture (superior) (fisl-petal). Landmarks on the squamous sphenoid bone (spt and spc) could not be identified bilaterally, due to fusion of the calvarial bone in this region and hence the distances of the lateral part of the bone could not be measured.

Dimension and Angles: While the angles of protrusion of the greater wing were increased (zfsl-gwml/gwmr-zfsr, gwll-gwml /gwmr-gwlr), the angle of the floor of the greater wing was normal (zfsl-gwml-ptsl, zfsr-gwmr-ptsr). The remainder of the distances and angles were normal.

Figure 3.34(k) Z Scores of the Measurements of the Lesser Wing and Pterygoid Plate of the Sphenoid for Patient TS compared with the Adult Experimental Standard

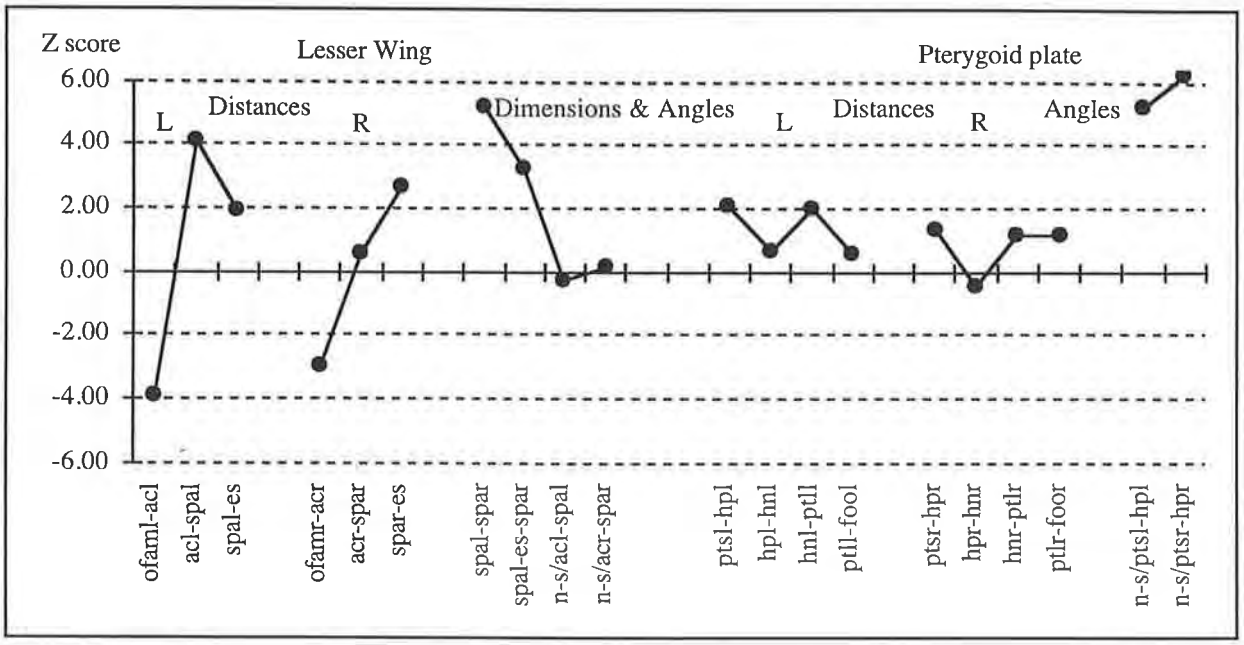

Figure 3.34(l) Z Scores of the Measurements of the Greater Wing of the Sphenoid for Patient TS compared with the Adult Experimental Standard

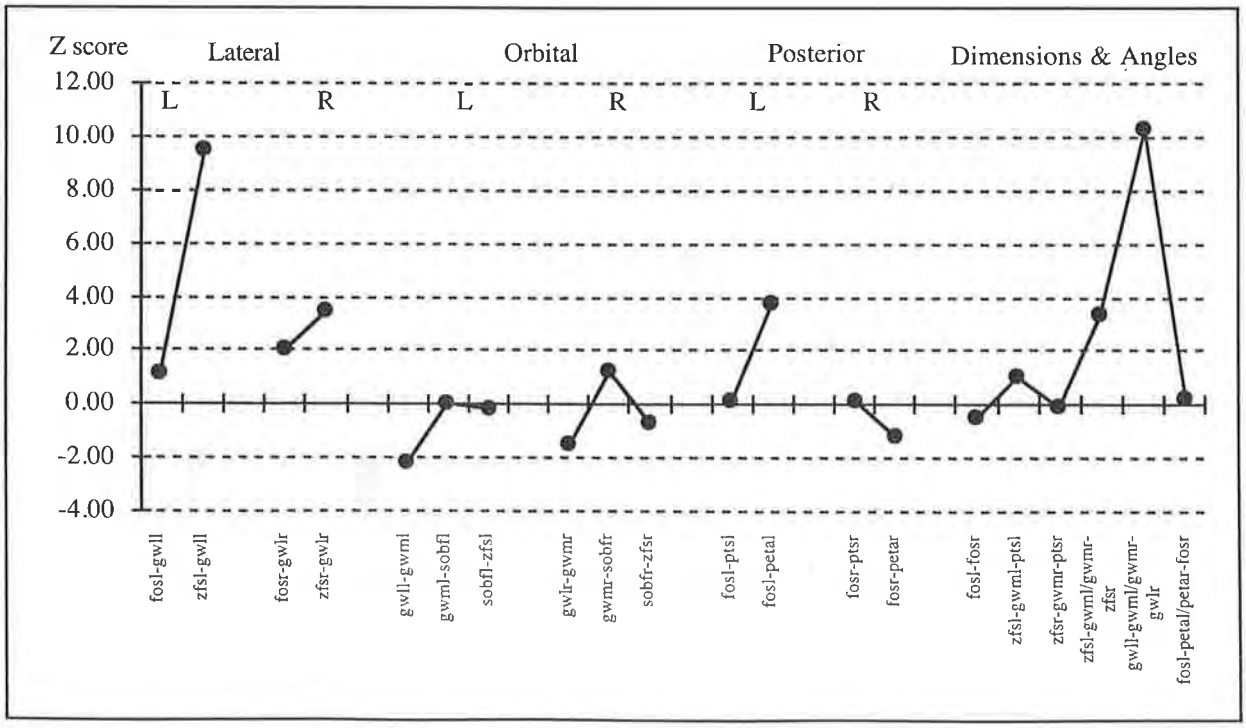

3.4.24.8 The Sphenoid Bone of Patient TS (continued)

Body of Sphenoid (Figure 3.34(m)):

Distances: The lateral distances were not significantly different from the experimental standard with the exception of the increased anterior inferior margin of the sphenoid body (gwml-ptsl, gwmr-ptsr). The lateral height of the spheno-occipital synchondrosis bilaterally (ptsl-petal, ptsr-petar) was normal. The anterior body distances at the spheno-ethmoid synchondrosis (es-cppl, es-cppr) were normal, while the anterior superior length (ofamr-gwmr) on the right was reduced. The posterior border of the frontal ethmoid attachment (cppl-ofaml, cppr-ofamr) was increased. The distances of the floor were increased at the spheno-ethmoid medial plate junction (es-ves), reduced at the spheno-vomerine junction (h-ves) and increased in width on the left posterior side (ptsl-h).

Dimensions: The dimensions revealed an increased distance at the anterior inferior body (gwml-gwmr) and the anterior superior body width (ofaml-ofamr) between the anterior optic foramina. The superior spheno-occipital synchondrosis (petal-petar) was reduced in length while the inferior spheno-occipital synchondrosis (ptsl-ptsr) was normal (see cranial base sutures). The height of the anterior body was reduced on the right side (acr-gwmr). The angles of the lateral protrusion of the body from the midline were reduced bilaterally (s-n/ofpml-petal, s-n/ofpmr-petar).

Discussion: This sphenoid bone in this patient had slightly enlarged lesser wings. The spheno-ethmoid synchondrosis was normal, but there was deformity lateral to this with broadening of the anterior sphenoid, frontal and lateral ethmoid junctions. An increased angle of protrusion of the greater wings was present with lengthening of the spheno-zygomatic sutures and some of the spheno-temporal sutures. The region around the spheno-occipital synchondrosis was normal or reduced in length. The pattern of deformity of the body was of an increase in width of the body anteriorly and inferiorly with the posterior portion remaining relatively normal.

Figure 3.34(m) Z Scores of the Measurements of the Body of the Sphenoid for Patient TS compared with the Adult Experimental Standard

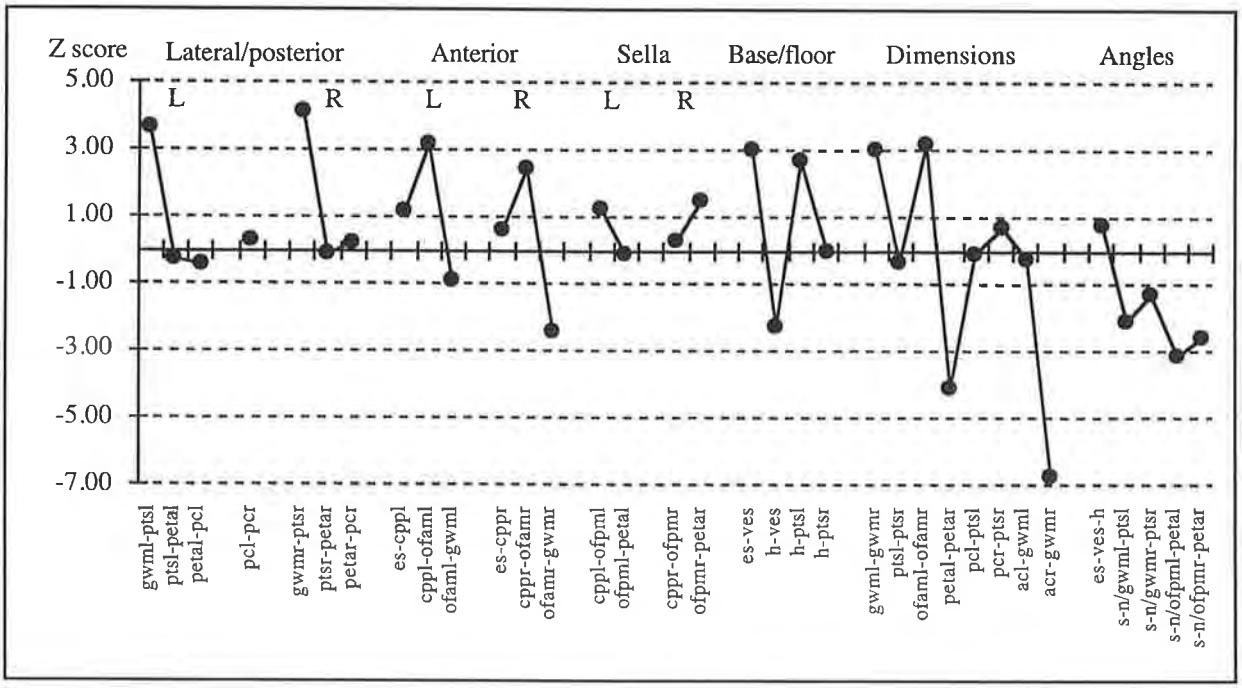

3.4.24.9 The Temporal Bone of Patient TS

Distances (Figure 3.34(n)):

Squamous Temporal Bone: The squamous temporal bone was not fully measurable in this child due to lack of visibility of the asterion (as) and sphenion (spt). The remaining distance of medial mastoid prominence (mal-smfl, mar-smfr) was increased bilaterally.

External Auditory Meatus: The lateral mastoid prominence (mal-eamil, mar-eamir) from the external auditory meatus was increased. The anterior inferior rim (eamal-eamil, eamar-eamir) bilaterally and the right inferior posterior rim (eamir-eampr) were reduced in length.

Zygomatic Process: The zygomatic process was generally within the normal range and symmetrical. The zygomatico-temporal suture distance (ztl-parl) was increased on the left. The height of the articular fossa (afl-ael, afr-aer) was normal.

Petrous Temporal Bone (Figure 3.34(o)): A trend at the apex of the petrous ridge was identified from the pattern profiles. The sphenoid-petrous temporal suture (fisr-petar) was significantly increased in length on the right, with a relative trend to be increased on the left. The petrous temporal-occipital suture length (petal-jfpl) was reduced on the left with a relative trend to be reduced on the right. The jugular foramen width was not significantly different from the experimental standard (jfll-jfml, jflr-jfmr). Increased distance of the occipital mastoid suture (mal-jfll) was found on the left side.

Dimensions (Figure 3.34(o)): The petrous temporal ridge dimension (petal-petpl, petar-petpr) was increased in length bilaterally. The distances between the internal auditory meati points (iaml-iamr) and the jugular foramina (jfpl-jfpr) were normal, with significantly increased distances between the porion points (pol-por). The measured angles were not significantly different.

Discussion: The mastoid process was prominent in this patient with some minor discrepancies in the region of the external auditory meatus. The increased zygomatico-temporal suture length contributes to the increased height and reduced length of the zygomatic bone (see zygomatic bone). The abnormality of the petrous temporal bone was more complex. Increased suture lengths were identified medially with the sphenoid bone and laterally with the occipital bone. The jugular foramen, however, was normal in this patient.

Figure 3.34(n) Z Scores of the Distances of the Temporal Bone for Patient TS compared with the Adult Experimental Standard

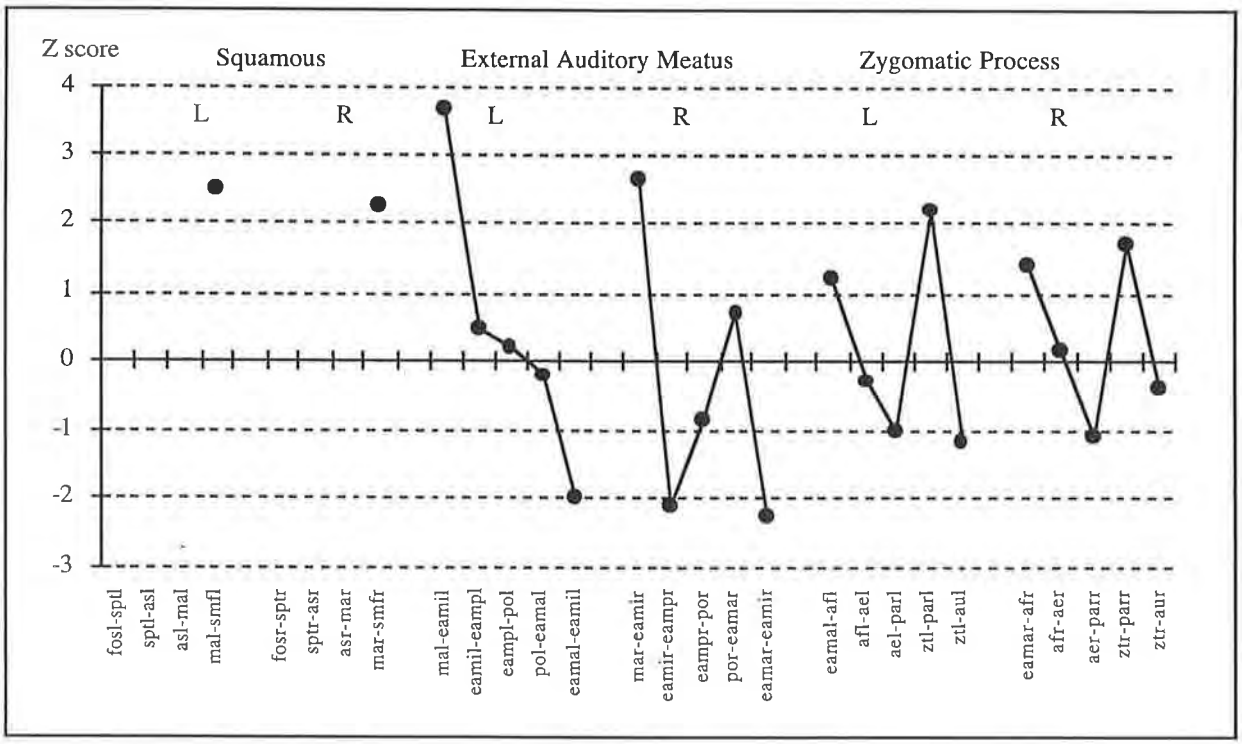

Figure 3.34(o) Z Scores of the Measurements of the Temporal Bone for Patient TS compared with the Adult Experimental Standard

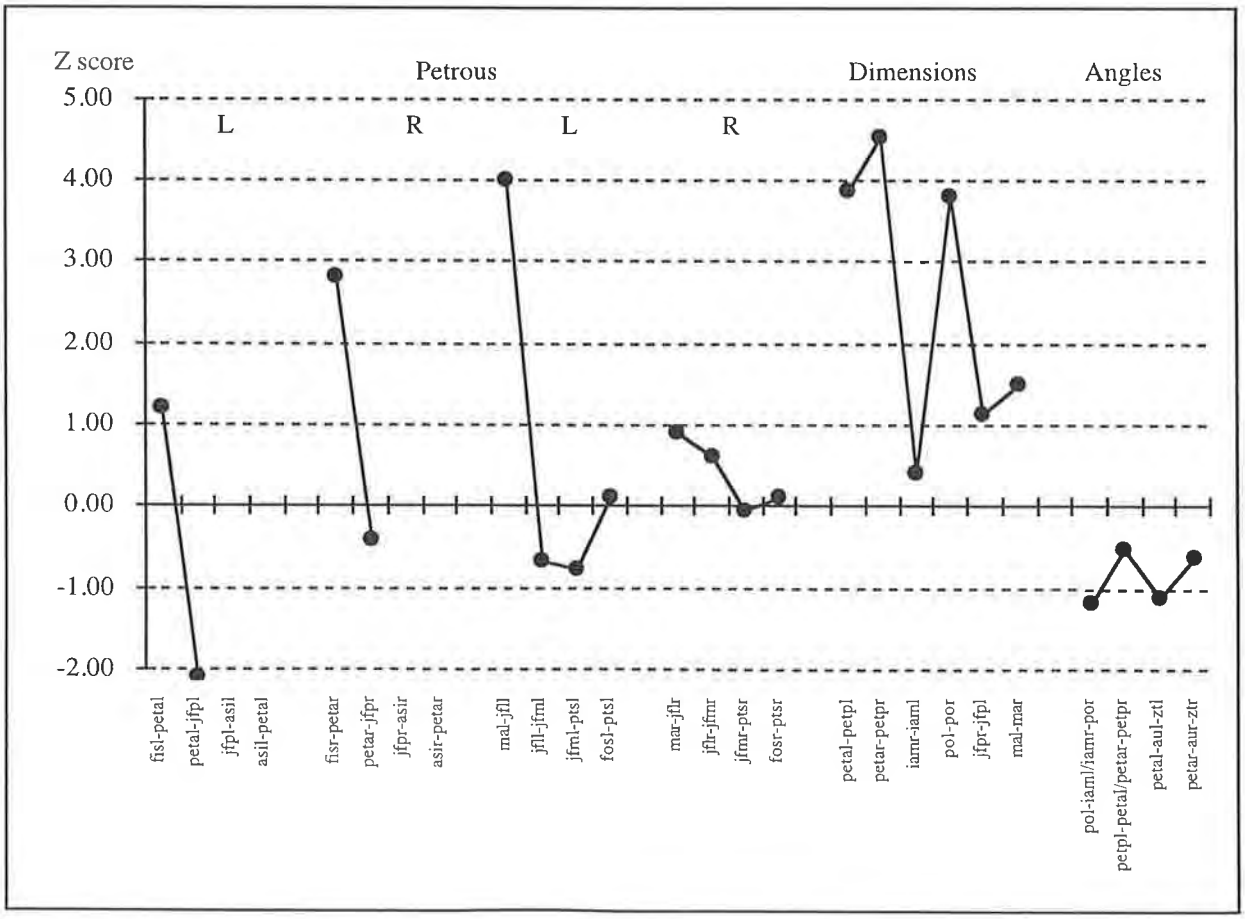

3.4.24.10 The Parietal Bone of Patient TS

Distances: The key landmarks for the parietal bone for Patient TS were not visible due to suture fusion and could not be reliably estimated. Therefore the parietal bone was not measured and a pattern profile of Z scores was not generated. The measurement data for the adult experimental standard are reported in Appendix 2.

3.4.24.11 The Occipital Bone of Patient TS

Distances (Figure 3.34(p)): The distances around the occipital bone were not significantly different from the experimental standard, including the medial temporo-occipital suture (jfml-ptsl, jfmr-ptsr). The spheno-occipital synchondrosis was discussed elsewhere (see sphenoid bone and cranial base sutures). The foramen magnum appeared to be slightly increased in size, with significant increases in length of the left anterior and posterior foramen magnum (ba-fmll, fmll-o).

Dimensions (Figure 3.34(p)): The width of the foramen magnum (fmll-fmlr) was significantly increased. The posterior cranial fossa depth (o-iop) was increased in size and the left posterior fossa length (petpl-iop) was increased.

Discussion: The occipital bone was enlarged at the foramen magnum. The lambdoid sutures could not be measured, however, it appeared calvarial distortion would account for the shape changes to the occipital bone shape.

Figure 3.34(p) Z Scores of the Measurements of the Occipital Bone for Patient TS compared with the Adult Experimental Standard

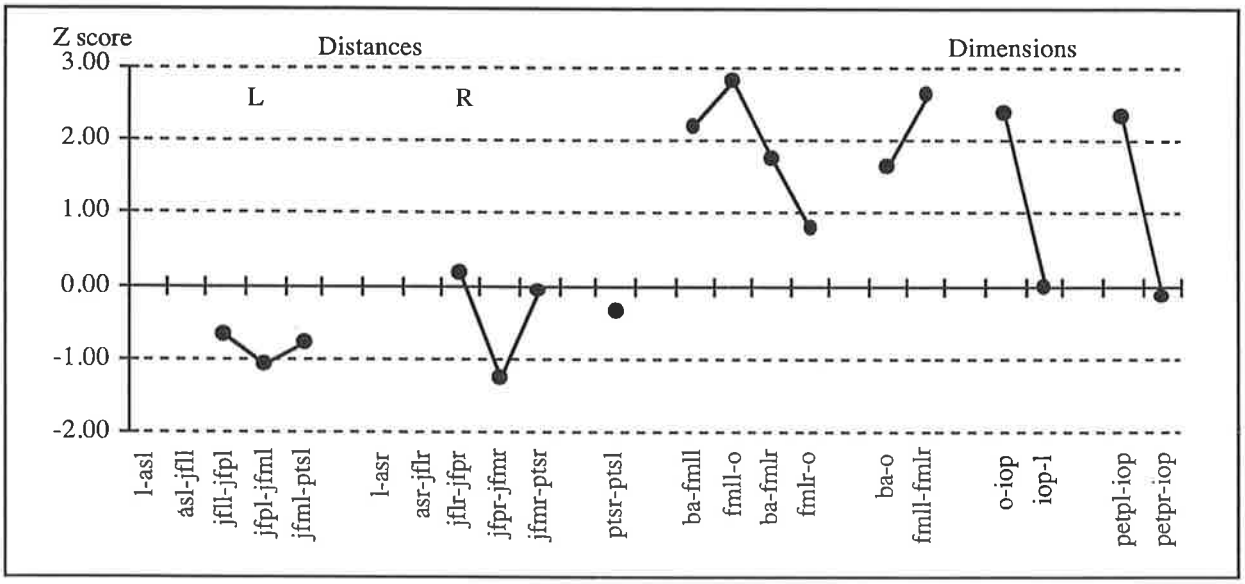

3.4.24.12 The Cranial Base Sutures of Patient TS

Anterior Cranial Fossa (Figure 3.34(q)): The spheno-ethmoid synchondrosis (es-cppl, es-cppr) was of normal length. The spheno-frontal sutures (cppl-spal, cppr-spar) in the anterior cranial fossa show a tendency to be increased and in the orbit (spal-zfsl, spar-zfsr), tend to be reduced. The spheno-zygomatic suture (zfsl-gwll, zfsr-gwlr) was increased in length.

Middle Cranial Fossa (Figure 3.34(q)): The sutures were relatively normal with the right sphenoid-petrous temporal suture (inferior) (fisr-petar) increased.

Posterior Cranial Fossa (Figure 3.34(q)): The lateral occipital mastoid suture (jfll-petpl, jflr-petpr) was increased in length. Laterally the sutures were not significantly different from the experimental standard. The superior part of the spheno-occipital synchondrosis (petal-petar) was reduced in length, while the inferior and lateral parts of the synchondrosis (ptsl-ptsr, ptsl-petal, ptsr-petar) were normal in length and height.

Discussion: The spheno-ethmoid synchondrosis was of normal length. The cranial base sutures were abnormal lateral to the spheno-ethmoid synchondrosis at the frontal ethmoid attachment (see frontal and ethmoid bones). Laterally the spheno-zygomatic suture was abnormal and likely represented a continuation of the calvarial suture abnormality identified qualitatively. Posteriorly the sutural abnormality was identified medially at the spheno-temporal and laterally at the occipital mastoid sutures but did not greatly deform the temporal and occipital bones. Medially the spheno-occipital synchondrosis was deformed with a reduced superior width.

Figure 3.34(q) Z Scores of the Dimensions of the Cranial Base Sutures for Patient TS compared with the Adult Experimental Standard

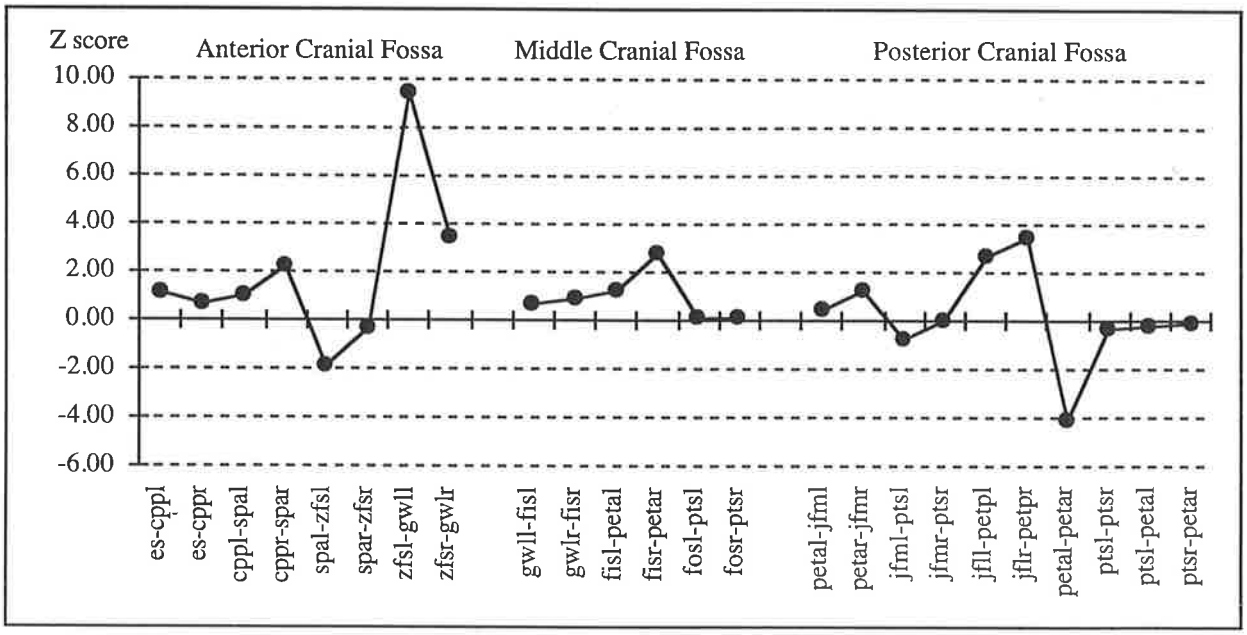

3.4.24.13 The Craniofacial Dimensions and Angles of Patient TS

Dimensions and Angles (Figure 3.34(r)): The anterior facial height (n-gn) was increased. The SNA (s-n-ss) and SNB (s-n-sm) angles were reduced. The cranial base dimensions were not significantly different from the experimental standard. The cranial base angle (ba-s-na) was increased in this patient.

Discussion: The cranial base angle was increased in this patient. The platybasia may reduce the facial angles and was also seen in Patients HC and IP. The cause of the cranial base angle increase is not evident from the measurements.

Figure 3.34(r) Z Scores of the Craniofacial Dimensions and Angles for Patient TS compared with the Adult Experimental Standard

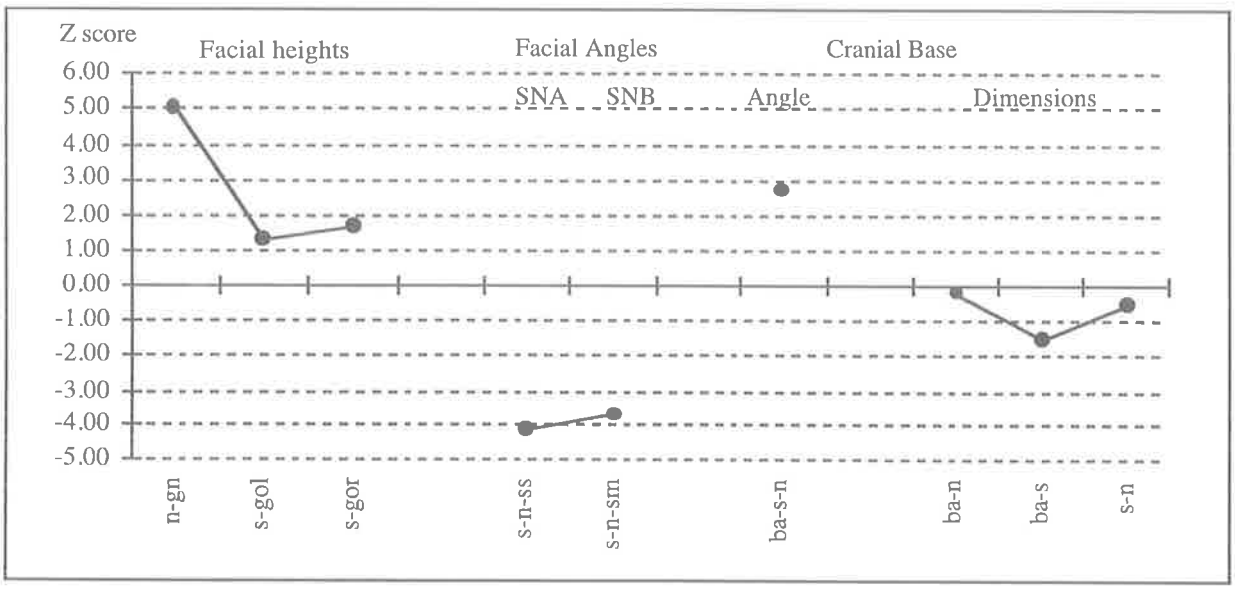

Table 3.3 Summary of Morphological Findings for Eight Patients with Crouzon Syndrome

Table 3.3. SUMMARY OF MORPHOLOGICAL FINDINGS

BONE & REGION	Patient RN	Patient SH	Patient JS	Patient IP
MANDIBLE	• majority normal • ↑ gonial angle	• majority normal	• majority normal	• ↑ intercondylar distance
MAXILLA				
• Orbital	• ↑ orbital angle	• widened orbital apex (↑ sup. maxillary splay)	• normal	• broad frontal process • ↓ orbital length • broad orbital rim
• Anterior	• ↓ depth • ↑ rim size	• normal	• ↑ ant. zygo-maxillary suture	• ↑ ant. zygo-maxillary suture • ↑ height of maxilla
• Lateral	• ↑ post. zygo-maxillary suture	• normal	• ↓ maxillary tuberosity height	• ↑ post. zygo-maxillary suture • ↑ height of maxilla • ↑ width maxilla superiorly
• Palatal	• ↑ palatal angle	• ↑ palatal angles	• ↑ palatal length • narrow palatal angles	• relatively normal
NASAL	• ↑ nasomaxillary length (L)	• ↑ nasomaxillary length • broad inferiorly	• ↑ frontal width • broad inferiorly with ↓ splay inferiorly	• all nasal lengths ↑ • broad with ↓ splay & projection
FRONTAL				
• Calvarial	• not recorded	• not recorded	• not recorded	• not recorded
• Supraorbital Region	• mild shape distortion • sup. orbital points laterally	• mild shape distortion • sup. orbital points medially • ↑ naso-frontal suture • ↑ fronto-zygomatic suture	• mild shape distortion • sup. lat. orbital points laterally	• severe shape distortion • sup. orbital points laterally • ↑ width & ↓ ant. cranial fossa depth
• Ethmoid Attachment	• ↑ length frontal ethmoid attachment	• normal	• ↑ length frontal ethmoid attachment • ↓ width	• broad anteriorly • ↓ length
• Sphenoid Attachment	•↓ lesser wing attachment	•↓ sup. orbital fissure • ↑ spheno-frontal suture	• normal	• ↑ sup. orbital fissure length
ZYGOMATIC	• ↑ spheno-zygomatic suture length	• ↑ fronto-zygomatic suture length	• zygo-maxillary suture lengthened	• ↑ spheno-zygomatic suture • ↑ fronto-zygomatic suture but less severe
VOMER	• normal	• normal	• normal	• angled inferiorly
ETHMOID				
• Lateral plate	• broad anteriorly • narrow posteriorly	• slightly broad anteriorly	• narrow posteriorly • ↓ height and length	• significantly ↓ size of plate • broad anteriorly
• Cribriform plate	• ↑ length frontal ethmoid attachment	• normal	• ↑ length frontal ethmoid attachment	• ↑ width anteriorly and posteriorly (spheno-ethmoid synchondrosis)
• Medial plate	• normal	• normal	• ↑ length	• ↑ height
SPHENOID				
• Lesser wing	• ↓ length swept up anteriorly	• minimal distortion	• broad & splayed laterally	• ↑ length • swept up
• Pterygoid plate	• normal	• normal	• normal	• ↓ size (L) • splayed posteriorly & laterally

Table 3.3. SUMMARY OF MORPHOLOGICAL FINDINGS continued:-

Patient LW	Patient AY	Patient HC	Patient TS
• majority normal • ↑ symphyseal height	• ant. molar • narrow ant. mandible • ↑ symphyseal height • ↑ gonial angles	• majority normal • ↓ intercondylar dist. • ↓ intercoronoid base dist. • ↑ symphyseal height • ↑ gonial angles	• laterally displaced gonial angles • (↑ intergonial distance) • (gonial gibbosity) • ↑ symphyseal height
• short broad frontal process • hypoplastic orbital rim • ↑ orbital floor angle (L)	• broad frontal process • ↑ lat. orbital length • broad orbital rim • ↑ orbital angle (L)	• ↑ inf. orbital fissure length • broad orbital rim medially	• ↑ inf. orbital fissure length • broad orbital rim
• ↓ ant. zygo-max. suture • prominent naso-maxilla • ↑ height of maxilla	• ant. molar	• ant. molar • ↑ height of nasal aperture • ↑ ant. alveolar height	• ↑ ant. alveolar height • ↓ height of nasal aperture
• ↑ height of maxilla • broad superiorly • ↑ post. maxillary angle	• ↑ post. height (R) • ↑ sup. dimension • ↑ post. maxillary angle (L)	• ↑ lat. & post. maxillary heights (R) • ↑ angles between sup., palatal & occlusal planes	• ↑ lat. & post. heights • ↑ ant. sup. width of maxilla
• ↑ palatal length • ↓ palatal angle	• ant. molar	• ↑ maxillary arch angle	• normal measurements
• ↓ naso-max. length (R) • narrow superiorly • ↑ angle nasal prominence • ↑ lateral splay	• ↑ naso-frontal length (R)	• ↑ length of midline • borderline ↓ widths • ↓ nasal/cranial base angle	• ↑ naso-maxillary length • nasal bones angled inferiorly (↓ nasal/cranial base angle)
• not recorded	• not recorded	• not recorded	• not recorded
• mild shape distortion • ↑ fronto-maxillary suture • sup. orbital points lateral • ↑ width anteriorly & posteriorly in ant. cranial fossa	• minimal shape distortion • widening of naso & maxillary frontal region • ↑ fronto-zygomatic suture • ↑ width anteriorly	• mild shape distortion • sup. orbital points laterally • ↑ width anteriorly & posteriorly in ant. cranial fossa • ↓ depth	• mild shape distortion • sup. lat. orbital points laterally • ↑ width anteriorly & posteriorly in ant. cranial fossa
•↑ length frontal ethmoid attachment • slightly narrow posteriorly	• normal	• ↑ length frontal ethmoid attachment but narrowed	• ↓ length frontal ethmoid attachment • ↑ width anterior cribriform plate
• ↓ sup. orbital fissure • ↑ spheno-frontal suture	• ↓ sup. orbital fissure (L) • ↓ spheno-frontal suture (cranial)	• ↓ borderline sup. orbital fissure (L) • ↓ spheno-frontal suture (cranial)	• ↑ spheno-frontal suture (cranial R)
• ↑ fronto-zygomatic suture • ↓ spheno-zygomatic and zygo-max. suture length • ↑ lat. height of zygoma	• ↑ fronto-zygomatic suture • ↑ zygo-temp. suture (R)	• ↑ spheno-zygomatic suture • ↓ zygo-maxillary suture • ↓ projection of zygoma	• ↑ spheno-zygomatic suture • (↑ height ↓ length of zygomatic bone)
• angled anteriorly	• angled slightly ant.	• angled inferiorly	• angled inferiorly
• ↓ height & sup. length • ↑ inf. length • plates broadly separated by cribriform plate	• ↓ height • broadly separated	• ↓ length superiorly • ↓ width of fronto-ethmoid attachment • ↓ separation inferiorly • relatively broad superiorly	• ↓ height of lat. plate • ↑ height of frontal ethmoid attachment • ↑ separation superiorly • relatively narrow post.
• ↑ lat. cribriform plate • ↑ width post. (spheno-ethmoid synchondrosis) • plate depressed	• ↑ width post. (spheno-ethmoid synchondrosis)	• ↑ lat. cribriform plate length • ↑ width post. (spheno-ethmoid synchondrosis)	• ↑ anterior width • ↓ length of plate
• normal	• normal	• majority normal • foramen caecum ant. (previous surgery)	• ↑ height of medial plate
• ↑ length • splayed posteriorly	• relatively normal • prominent (L) anterior clinoid	• ↑ length • splayed more inferiorly and posteriorly	• ↑ length • splayed more inferiorly and posteriorly
• splayed anteriorly & medially	• normal	• normal size • splayed posteriorly & laterally	• normal size • splayed posteriorly & laterally

Table 3.3 continued:-

BONE & REGION	Patient RN	Patient SH	Patient JS	Patient IP
SPHENOID cont.				
• **Greater Wing**	• ↑ length spheno-zygomatic suture	• ↓ sup. orbital fissure • ↑ sphenofrontal suture • ↑ lat. splay of bones	• ↑ lat. splay of bones	• ↑ length spheno-zygomatic suture • ↑ sup. orbital fissure • sphenofrontal suture normal or ↓ • ↑ lat. splay of bones
• **Body**	• constricted orbital apex • hyperplastic base	• ↑ post. clinoid width • ant. clinoid ↑ (R) • hypoplastic base	• constricted orbital apex • ↓ widths anteriorly • ↓ spheno-occipital synchondrosis (sup.) • ↓ angles of body splay from midline (ie. narrowed)	• ↑ length body superiorly & inferiorly • ↑ spheno-occipital synchondrosis (lat.) • ↑ ant. height • ↑ spheno-ethmoid synchondrosis • ↓ width slightly
TEMPORAL				
• **Squamous temporal bone**	• abnormal	• normal	• incompletely recorded	• incompletely recorded
• **Ext. auditory meatus**	• shape distortion (↑ post. lat. distance)	• shape distortion (↑ post. lat. distance)	• normal	• severe shape distortion
• **Zygomatic process**	• ↓ length • ↑ height	• ↓ length • angled laterally	• ↓ length • ↑ height • angled laterally	• ↓ length
• **Petrous temporal**	• normal	•↓ spheno-petrous temporal suture	• ↓ jugular foramen (R) • ↑ occipital mastoid suture • ↑ petrous ridge length • splay of bones more post. & narrowed	• ↓ jugular foramen • ↑ occipital mastoid suture • ↑ petrous ridge lengths • ↑ widths of bones • ↑ splay of bones posterior
PARIETAL	• not recorded	• not recorded	• not recorded	• not recorded
OCCIPITAL				
• **Calvarial**	• not recorded	• not recorded	• not recorded	• not recorded
• **Cranial base**	• minor deformity	• normal	• ↓ jugular foramen (R) • foramen magnum shape asymmetric	• ↓ jugular foramen • ↑ temporo-occipital suture (inf.) • foramen magnum shape asymmetric
CRANIAL BASE SUTURES				
• **Anterior Fossa**	• ↑ frontal ethmoid • ↓ spheno-frontal • ↑ spheno-zygomatic	• normal	• ↑ frontal ethmoid attachment	• ↑ spheno-ethmoid synchondrosis •↓ spheno-frontal (orbital) suture (R) • ↑ spheno-zygo suture
• **Middle Fossa**	• normal	•↓ spheno-petrous temporal suture (sup.)	• ↑ spheno-squamous temporal suture (L)	• ↑ spheno-squamous temporal suture (L)
• **Posterior Fossa**	• normal	• ↑ temporo-occipital suture (sup.) •↓ inf. spheno-occipital synchondrosis	• ↑ temporo-occipital suture (sup.) (R) •↓ sup. spheno-occipital synchondrosis	• ↑ temporo-occipital suture (inf.) • ↑ occipital mastoid suture • ↑ spheno-occipital synchondrosis (lat.)
CRANIOFACIAL DIMENSIONS and ANGLES				
• **Facial Heights**	• not measurable	• not measurable	• not measurable	• not measurable
• **Facial Angles** **SNA** **SNB**	• borderline ↓ • not measurable	• normal • not measurable	• normal • not measurable	• decreased • not measurable
• **C-Base Angle**	• normal	• acute	• normal	• obtuse
• **C-Base Dimensions**	• normal	• normal	• normal	• ↑ length

Table 3.3 continued:-

Patient LW	Patient AY	Patient HC	Patient TS
•↓ spheno-zygomatic suture •↓ sup. orbital fissure • sphenofrontal (orbital) suture normal • ↑ lat. splay of bones •↓ spheno-petrous temporal suture (sup.)	• rel normal distances • borderline ↓ sup. orbital fissure •↑ lat. splay of bones • ↑ spheno-petrous temporal. suture (inf. R) (sup. L)	• ↑ spheno-zygomatic suture • ↑ lat. splay of bones • ↑ petrous temporal suture (sup. L) • narrowed posteriorly	• ↑ spheno-zygomatic suture • ↓ width of greater wing (L) • ↑ lat. splay of bones • ↑ petrous temporal suture (sup. L)
• ↑ body length • ↑ spheno-occipital synchondrosis (lat.) • orbital apex ant. • ↑ spheno-ethmoid synchondrosis • broad anteriorly	• ↑ body length • ↑ spheno-occipital synchondrosis (lat.) • ↑ spheno-ethmoid synchondrosis • broad anteriorly • sella ↑ in size • ↑ spheno-occipital synchondrosis (inf.)	• body length normal • ↑ spheno-ethmoid synchondrosis • sella ↑ in size •↓ spheno-occipital synchondrosis (sup. & inf.) (narrow posteriorly)	• ↑ body length • ↑ ant. length • (sella enlarged) •↓ spheno-occipital synchondrosis (sup.) • broad anteriorly • ↓ height anteriorly (R)
• incompletely recorded • prominent mastoid	• incompletely recorded	• incompletely recorded	• incompletely recorded • prominent mastoid
• slight shape distortion • (↓ sup. ant. distance (R))	• shape distortion • (↑ sup. ant. distance)	• atretic EAM (L) • shape distortion (R) • (↓ sup. ant. distance)	• shape distortion • (↓ inf. distances)
• ↓ length	• relatively normal • minimal asymmetry	• ↓ length (L) • angled medially	• relatively normal
• ↓ jugular foramen (R) • ↑ spheno-petrous temporal suture (sup.) (R) • ↑ occipital mastoid suture • ↑ temporo-occipital suture (inf.) (L) • ↑ length petrous ridge	• borderline ↓ jugular foramen • ↑ spheno-petrous temporal suture (sup.) (L) • ↑ occipital mastoid suture • ↑ temporo-occipital suture (inf.) (L) • ↑ length petrous ridge • ↑ distance between EAM	• borderline ↓ jugular foramen •↓ spheno-petrous temporal suture (sup.) (R) • ↑ occip. mastoid suture (L) • ↑ temporo-occipital suture (inf.) (L) • petrous ridge normal length	• jugular foramen distorted • ↑ spheno-petrous temporal suture (sup.) (R) • ↑ occipital mastoid suture (L) • ↑ length petrous ridge • ↑ distance between temporal bones
• not recorded	• not recorded	• not recorded	• not recorded
• not recorded	• not recorded	• not recorded	• not recorded
• ↓ jugular foramen (R) • ↑ temporo-occipital suture (inf.) (L)	• ↓ jugular foramen • ↑ temporo-occipital suture (inf.) (L) • ↑ spheno-occipital synchondrosis (inf.)	• ↓ jugular foramen (L) • ↑ temporo-occipital suture (inf.) (L) • ↑ spheno-occipital synchondrosis (inf.)	• jugular foramen distorted • sutures & synchondroses normal • except ↓ spheno-occipital synchondrosis (sup.)
• ↑ spheno-ethmoid synchondrosis • ↑ spheno-frontal (ant. fossa) suture •↓ spheno-zygomatic suture	• ↑ spheno-ethmoid synchondrosis •↓ spheno-frontal (ant. fossa) suture	• ↑ spheno-ethmoid synchondrosis •↓ spheno-frontal (orbital) suture (R) • ↑ spheno-zygomatic suture	• ↑ spheno-frontal (ant. fossa) suture (R) • ↓ spheno-frontal (orbital) suture (L) • ↑ spheno-zygo suture
• ↑ spheno-petrous temporal suture (sup.) (R)	• ↑ spheno-petrous temporal suture (sup.) (L) • ↑ spheno-petrous temporal suture (inf.) (R)	•↓ spheno-petrous temporal suture (sup.) (R)	• ↑ spheno-petrous temporal suture (sup.) (R)
• ↑ temporo-occipital suture (inf.) • ↑ occipital mastoid suture • ↑ spheno-occipital synchondrosis (lat.)	• ↑ temporo-occipital suture (sup., inf. & L) • ↑ occipital mastoid suture (R) • ↑ spheno-occipital synchondrosis (inf. & lat.)	• ↑ temporo-occipital suture (inf.) (L) • occipital mastoid suture normal •↓ spheno-occipital synchondrosis (inf. & sup.)	• ↑ occipital mastoid suture •↓ spheno-occipital synchondrosis (sup.)
• not measurable	• not measurable	• increased	• increased
• normal • normal	• decreased • not measurable	• decreased • decreased	• decreased • decreased
• acute	• borderline acute	• obtuse	• obtuse
• normal	• normal	• normal	• normal

3.5 Quantitative Analysis by Anatomical Unit in the Eight Patients with Crouzon Syndrome

3.5.1 The Morphology of the Mandible in the Eight Patients with Crouzon Syndrome

Distances: The majority of the distances measured from the 3D CT reconstructions of the mandibles in this group of patients with Crouzon syndrome were not significantly different from the experimental standard although many of the measurements were above the mean suggesting a tendency towards enlargement of this bone. Of the total number of 128 distances measured (16 measurements per patient), 13 were significantly increased and 7 were decreased compared with the appropriate age-matched control. Many abnormal measurements resulted from an anterior position of first molar suggesting crowding of the dentition.

Dimensions and Angles: The majority of the dimensions of the mandible were not significantly different but a similar trend towards larger mandibles was again suggested by the majority of measurements being greater than the mean. There was no consistent increase or decrease in the widths of the mandible. Ramus dimensions were generally larger than the mean. The anterior mandibular height at the symphysis was significantly greater in the 4 older patients. This may reflect either a compensatory overgrowth, to obtain a functional occlusion, or a primary growth abnormality. The gonial angle was increased in 3 patients. The angles based around the coronoid base and first molar showed the widest positive and negative significant Z scores. This was in part due to the variable anterior position during growth of the molar in the patients.

In general, the width of the mandible at the level of the gonial angles was decreased, with a reduced anterior mandibular angle, except in the oldest patient (Patient TS) in which these dimensions and angles were increased. Clinically, this patient had very broad and coarse features associated with a frontal gibbosity and flaring of the mandibular angles, not seen in the other patients. The distances between the condyles in all patients were not significantly different from the experimental standard or reduced, except in the patient with the most marked clinical deformity (Patient IP), where this measurement was increased. The significant distortion of the temporal bone in this patient would appear to make the greatest contribution to the condylar

position. These 2 patients may represent different subtypes of Crouzon syndrome. In the majority of patients, there was a tendency towards a minimally longer and more slender mandible, with an increased gonial angle and compensatory symphyseal growth. The changes became more apparent in the older patients.

Discussion: Major growth disturbance of the mandible does not typically occur in Crouzon syndrome. Minor abnormalities of shape and position along with either prognathism or retrognathism have been described in case reports, and in greater detail in quantitative studies (Kreiborg, 1981; Costaras-Volarich and Pruzansky, 1984).

Kreiborg's cephalometric measurements of the mandible revealed three main findings in patients with Crouzon syndrome. Firstly, the gonial angle was slightly greater than in the controls but still within the normal range. This finding was confirmed in the patients studied here, using slightly different definitions of the landmarks, where the measurements were often found to be statistically increased. Kreiborg also found that the mandibular length and height were significantly smaller than controls in the female Crouzon population, but normal in the male population. The sample of patients studied here was too small to determine any differences with respect to sex. Both mandibular length and height were within, and evenly spread across the normal range. The significant findings were one patient with a short left ramus and another with a long left body. Despite a slightly more obtuse gonial angle, the total mandibular length was not increased.

In a cephalometric analysis of 30 Crouzon syndrome patients, Costaras-Volarich and Pruzansky (1984) found that the mandibular body length was significantly shorter and the mandibular ramus tended to be long but not statistically so. They described the ratio of ramus height to body length approaching 1:1, compared with 2:3 in the normal population. The total mandibular length was not significantly different from the experimental standard but tended to be short. This finding was not confirmed in this study.

Kreiborg also found that the mandible was retrognathic in relation to the cranial base. This relationship was not investigated in this study. It is possible that a posterior position of the mandible contributes to a narrow upper airway in many cases.

It is clear the mandible undergoes subtle changes in patients with Crouzon syndrome. Based on this study, 3 patterns of mandible were identified (Figure 3.35).

1. Primary Crouzon Mandible (Patients RN, SH, HC, JS, LW and AY): This is the commonest form of mandible and is represented by the majority of studies which show a slightly increased gonial angle, and tendency to increased symphyseal height. The ramal and body lengths are usually not significantly different from the experimental standard. The gonial angle increase may be a primary growth abnormality or related to the cranial base and soft tissue attachments. The symphyseal height may be compensatory for the increased angle and deficient maxilla.

2. Secondary Crouzon Mandible (Patient IP): This mandible is distorted due to cranial base deformity directly affecting the position of the mandibular condyles. This presents with a broad condyle and ramus and increased intercondylar distances.

3. Gibbous Mandible (Patient TS): This deformity is due to a localised overgrowth of bone in the region of the mandibular angle and may be associated with a frontal gibbosity and bony overgrowth in other areas.

3.5.2 The Morphology of the Maxilla in the Eight Patients with Crouzon Syndrome

Distances: The measurements of the distances between the landmarks of the maxilla extended above and below the normal range, with such variability as to make it difficult to find any recurrent patterns. This is somewhat surprising as a hypoplastic maxilla is one of the major features of Crouzon syndrome and some uniformity of the distances might be expected. The size and shape of the maxilla is also influenced by the secondary deforming forces of the cranial base and the surrounding bony structures such as the zygomatic, frontal and nasal bones. Variable distortions of growth in these regions contributes to the variable pattern of deformity of the maxilla.

Dimensions and Angles: The majority of dimensions were either enlarged or not significantly different from the experimental standard. An increase in vertical height was found at the

expense of anterior growth. The height and width of the maxilla were generally greater than for the experimental standard, while measurements in the anterior-posterior direction were reduced.

Discussion: The maxilla in Crouzon syndrome is clinically described as hypoplastic. This refers to the flat appearance of the midface and is due to the reduced anterior growth of the maxilla. This is most commonly evident during late childhood and early adolescence when maxillary growth is maximal. The infants, 2 year old children and 6 year old children would therefore be expected to have most variables within the normal range. In this study the infants showed minimal deformity of the maxilla, as did one of the 2 year old children (Patient JS). The other 2 year old child, Patient IP, showed marked involvement which correlated with the severe clinical deformity. The 6 year old children also showed marked measurement abnormalities. The 2 adult patients would be expected to show predominantly hypoplasia of the mandible. The adult patients demonstrated some reduced anterior distances with increased lateral and posterior distances. The pattern was one of a broad and tall posterior maxilla with a small anterior maxilla.

The relationship with the cranial base was not examined in this study and would have provided additional information about the posterior maxilla. In Kreiborg's study (1981), the maxilla was found to be retrognathic and inclined upwards and backwards and the lateral and AP widths were reduced, as well as the height.

Many posterior measurements in cephalometric analysis of the maxilla rely on points not found on the bone itself, such as the sella and the apex of the pterygomaxillary fissure. This latter point commonly belongs to the junction of greater wing of the sphenoid with the pterygoid. The true highest point of the maxilla in the deformed skull of Crouzon syndrome is more medial and often higher than can be identified on cephalograms. The landmark can be readily be seen on the CT coronal slices. This problem may account for the reduced posterior dimensions of the maxilla described by Kreiborg, conflicting with the data in this study. On the other hand, it enables Kreiborg to make valid statements about the relationship of the position of the maxilla to the cranial base. The broad and high posterior maxilla described in this study, often with normal or increased dimensions, is clearly related to the development of the ethmoid and cranial base and will be discussed in the relevant sections.

Growth of the palatal sutures in the normal maxilla have been shown to occur up until adolescence (Persson, 1973). Kreiborg found the maxilla of Crouzon syndrome was smaller in all the dimensions measured and he related this to premature synostosis of the maxillary sutures. Previous studies (Kreiborg and Bjork, 1982) on a dried skull with Crouzon syndrome showed premature synostosis of the transverse and mid palatal sutures and of the vertical squamous sutures between the palatine bones. Early synostosis was also seen at the fronto-maxillary and zygo-maxillary sutures. In this study, increased suture length suggesting premature fusion was found at the fronto-maxillary, naso-maxillary and zygo-maxillary sutures. No common pattern was found implying that sutures were involved with variable severity.

Eight patients in Kreiborg's series had metallic implants inserted to allow assessment of maxillary sutural growth. Premature sutural arrest was found in 7 of these cases, occurring as early as 2 years of age in 1 patient (7 - 12 years in remaining patients). Lack of anterior growth with an overall decrease of downward growth was characteristic. Remodelling of the maxilla as a result of this process was observed but was not assessed statistically. Characteristics described by Kreiborg included: decreased bone apposition at the maxillary tuberosity, increased bone apposition at the maxillary spine, resorptive lowering of the posterior nasal floor and excessive alveolar height. The orbital surface of the maxilla revealed signs of bone resorption and the relative width of the dental arch decreased with growth. In this study, increased anterior alveolar height (pr-ans) was found in 1 adult with a tendency to be increased in the other. The maxillary dental arch width (gpfl-gpfr, ecsl-ecsr) was normal, although the anterior maxillary angles (gpfl-ans-gpfr, gpfl-pr-gpfr) were increased in 3 patients (including the 2 adults) and decreased in 2 patients.

It is suggested, based on data from this study, that the maxilla in patients with Crouzon syndrome has 3 predominant features (Figure 3.36) although a larger number of patients are needed to confirm this.

1. Increased maxillary height.

2. Increased maxillary width.

3. Reduced anterior-posterior distances and dimensions.

This deformity was measurable in the adult patients, children at 6 years of age and in a severely affected child aged 2. The maxilla was found to be extending up into the inter-orbital region at its junction with the ethmoid resulting in an increased height posteriorly. Increase in inter-orbital distances also makes the maxilla broad at its superior margin. In addition, the increased intra-orbital component of the maxilla contributes to the proptosis and hypertelorism. This leaves a reduced volume of sub-orbital maxilla, a feature which is seen clinically and encountered at surgery. The majority of the sub-orbital height of the maxilla is made up of alveolar bone, with a close relationship of the palate to the cranial base.

3.5.3 The Morphology of the Nasal Bones in the Eight Patients with Crouzon Syndrome

Distances, Dimensions and Angles: The measurements of the nasal bones in this group of patients with Crouzon syndrome demonstrated increases in the lengths of the naso-maxillary sutures, suggesting some prominence to the lateral part of the nasal bones (Figure 3.36). In many patients, the bones were broad inferiorly and also splayed laterally and inferiorly. In several patients the projection of the nasal bones was also reduced (Patients IP and TS). The only patient with a normal or decreased maxillary suture length with a prominent nasal angle had a correspondingly normal clinical appearance to the nose (Patient LW, Figure 3.5).

Discussion: The typical feature of the nasal structures in Crouzon syndrome is the so-called "parrot beak" deformity. This is characterised by a lack of cartilaginous projection for the nose. This produces a retruded tip with overhang, giving a beaked appearance to the structure. Clearly the nasal deformity in Crouzon syndrome is a component of both nasal bone structure as well as cartilaginous support. The nasal bone deformity has been described above and usually shows some downward and lateral growth characteristics. The growth of the septal cartilage is directed by the medial plate of the ethmoid and the vomer. In this study, these structures were relatively normal but showed a tendency for downward angulation, particularly in the older patients (Patients AY, HC and TS). It is interesting to note that the patient with the more normal nasal bones and in particular, the prominent nasal angle (s-n-na) had a correspondingly more normal appearance and therefore presumably a more normal cartilaginous

framework support (Patient LW). The position of the nasal tip is also influenced by the lack of anterior projection of the maxilla. The relationship of the fronto-nasal and naso-maxillary sutures may alter the role of the nasal bones in determining the extent of parrot beaking but this cannot be definitely concluded from this study. In summary, the nasal deformity is related to the length and prominence of the nasal bones, the size and angle of projection of the medial ethmoid plate and vomer, and the amount of anterior growth of the maxilla. The variation in appearance of the nose may be attributed to the severity of involvement in each bony region, and of the sutures between these structures.

3.5.4 The Morphology of the Frontal Bone in the Eight Patients with Crouzon Syndrome

Distances: For the purposes of this study, the frontal bone was analysed as 4 separate regions: the frontal bone; the calvarial component, which contributes to the atypical head shape; the supra-orbital region, which typically provides inadequate superior cover for the globes in these patients; the junction with the ethmoid bone medially and the junction with the sphenoid bone posteriorly and laterally. Deformity of this bone is part of the classical presentation of Crouzon syndrome and its analysis is particularly important.

Calvarial Region: Premature fusion precluded identification of the sutures and as a result the calvarial distances and dimensions were not measured. The range of clinical calvarial abnormalities found in this study is presented in Chapter 2 and the deformity in each patient is presented with the qualitative data in Chapter 3. Fusion of the calvarial sutures influences the shape and position of surrounding structures such as the supero-lateral orbital rim of the frontal bone, the zygomatic bone, the temporal bone and the sphenoid greater wing. While this region is important in the overall deformity this study has focussed on the cranial base and facial bones.

Supra-orbital Region: All patients exhibited some shape distortion of the supra-orbital region. The typical finding was a more rectangular shape to the superior orbital rim. Either the superior orbital point or the supero-lateral orbital point was more laterally placed and accounted for this deformity. (The angle of the superior orbital rim was not measured and may have provided greater information on the discrepancy in this region). The deformity of the supra-orbital region

was mild in some cases but was very severe in others where the lateral wall was greatly swept up and the height of the lateral orbital wall was increased (Patients RN and IP). This deformity was found in conjunction with the spheno-zygomatic pattern of the zygomatic bone (Section 3.5.5 Zygomatic Bone). A moderate deformity was also seen in Patient HC. Increased width across the frontal supra-orbital ridge was recorded in the older and severely involved patients (Patients IP, RN, AY, HC, TS) and was related to pathology of both the medial and lateral orbital walls (Figure 3.37) and corresponded with the predominant pattern of deformity of the maxilla.

Ethmoid Attachment: The frontal ethmoid attachment was represented by the lateral part of the cribriform plate and the supero-medial part of the orbit. Three patterns were identified:

1. Lengthening of the frontal ethmoid attachment with a corresponding constriction in dimensions at the orbital apex (Patients RN, JS, LW and HC).

2. Normal frontal ethmoid attachment (Patients SH and AY).

3. Reduced frontal ethmoid attachment length with a broad anterior attachment (Patients IP and TS).

The increase in the frontal ethmoid attachment length appeared to be related to the increased dimensions of the cribriform plate. The overall clinical deformity in the patients with a normal ethmoid junction was less severe. A greater degree of significant pathology in the region of sphenoid bone was found in those patients with reduction in the length of frontal ethmoid attachment (Section 3.5.8 Sphenoid bone).

Sphenoid Attachment: The principal finding in the majority of patients was a reduction in the length of the superior orbital fissure. This usually occurred in those patients with an increased frontal ethmoid attachment length. Those with a reduced frontal ethmoid attachment length had significant increase or tendency to be increased in the superior orbital fissure length (Patients IP and TS).

Discussion: Fusion of the frontal and parietal sutures with extensions into the zygomatic bone have been previously demonstrated (Kreiborg and Bjork, 1982). The concept of a coronal ring

of sutures extending into the cranial base was suggested by Burdi et al. (1986). In this study several patterns of deformity of the supra-orbital, ethmoid and sphenoid sections of the frontal bone emerged from the measurements. It was unfortunate this could not be correlated with measurements of the calvarial deformity. The involvement of frontal and zygomatic bones altered the superior orbital rim laterally and produced a more rectangular appearance. Medially and posteriorly, along the junction of the ethmoid and sphenoid bones, a range of deformity was seen. Lengthening of the ethmoid attachment and shortening of the superior orbital fissure was identified in one group of patients. A normal or less severe type of this deformity was seen in another, smaller group. In the third group, shortening of the ethmoid attachment with lengthening of the superior orbital fissure was found. The pattern of the medial deformity here did not appear to be related to the clinical or measured deformities in the region of the facial skeleton, but appeared to be more a product of the cranial base pathology. As with the calvarial pathology, it may be that the type of deformity is determined by which region of sutures is involved and to what extent. Due to the complex nature of the frontal bone, posterior deformities (that is, in the region of the sphenoid bone) may influence the position of other anterior structures. The effects of intracranial pressure, which are noted to be significant in the region of the sella (Kreiborg et al., 1993), may also exert deforming forces on the ethmoid, the wings of the sphenoids and the frontal bone directly.

3.5.5 The Morphology of the Zygomatic Bone in the Eight Patients with Crouzon Syndrome

Distances: The distances measured in this region are very informative as they are made up of a large number of sutures and reflect the position of the lateral orbital wall and the prominence of the cheek. Two dominant patterns emerged, depending upon whether the spheno-zygomatic suture or the fronto-zygomatic suture was involved. Four patients (Patients RN, IP, HC and TS) had increased distances at the spheno-zygomatic suture. These patients included the children with the more severe disease and the 2 adults with the established deformity, all with greater clinical deformity around the orbit. The other group (Patients SH, LW and AY) had increased distances at the fronto-zygomatic suture and normal or decreased distances at the spheno-zygomatic suture. These sutural measurements were normal in one patient (Patient JS) with correspondingly normal zygomatic bone measurements and dimensions. Only 2

measurements were increased in this patient, one related to the height of the lateral orbital wall and the other associated with the zygo-maxillary suture on one side.

Dimensions: The dimensions reflected, to some extent, the abnormal suture patterns. The spheno-zygomatic group tended to have increased zygomatic height and decreased length. The fronto-zygomatic group tended to have normal overall dimensions. This may have been predicted given their young age and lack of severity.

Discussion: The patterns of deformity of the zygomatic bone (Figure 3.38) were, in order of severity:

1. Minimal change (Patient JS)

2. Fronto-zygomatic suture pattern (Patients SH, LW and AY)

3. Spheno-zygomatic suture pattern (Patients RN, IP, HC and TS)

The morphology of the zygomatic bone demonstrates very well the role of adjoining bones and the interplay of the sutures in determining the size and shape of the bone. A strong association between suture dimension and bone shape was shown. The sutures with the sphenoid and frontal bones appeared to be more relevant than the sutures with the maxilla or temporal bone as variable involvement of the zygo-maxillary suture and zygomatico-temporal suture (Section 3.5.9 Temporal Bone) was present.

3.5.6 The Morphology of the Vomer in the Eight Patients with Crouzon Syndrome

Distances: All distances were not significantly different from the experimental standard in the younger children. In the adult patients the vomer tended to be smaller than the experimental standard.

Dimensions and Angles: The angle of the vomer relative to the cranial base was significantly increased in the severely affected and older patients (Patients IP, HC, TS). This may be partly a result of the influence of the cranial base deformity on the angle however, the inferiorly angled

vomer strongly suggests the lack of forward growth in favour of downward growth (Figure 3.39).

Discussion: Studies have suggested that the lack of midface growth is due to a lack of nasal septal drive (Enlow, 1975). While it is difficult to determine if the disturbed vomerine growth is a primary or secondary event, it would appear to make up an important contribution to the characteristics of the Crouzon midface. The increasingly significant results with increasing age suggest a primary developmental problem in view of the timing of midface growth and the importance of nasal septal development in maxillary development.

3.5.7 The Morphology of the Ethmoid Bone in the Eight Patients with Crouzon Syndrome

Deformity of the ethmoid bone in Crouzon syndrome has classically been described as broad with depression of the cribriform plate (Bertelsen, 1958). As the name suggests (ethmoid: Greek *ethmos* sieve; sievelike), most attention has been focused on the cribriform plate. This study has examined other areas and divided the ethmoid into the lateral plate, the cribriform plate and the medial plate and examined the relationships with the surrounding bones.

Lateral Ethmoid Plate: The lateral plate comprises the medial wall of the orbit. A typical finding was a reduction in the size of the plate, in particular the height. The separation of the two lateral plates was variable, with the overall tendency to be broadly separated. A wedge shape to the ethmoid was found when the lateral plates were separated broadly anteriorly, but were more narrowly separated posteriorly (Patients RN, SH, JS, TS).

Cribriform Plate: In the majority of cases the cribriform plate was increased in its dimensions with respect to length and width. An increase in the posterior width represents lengthening of the spheno-ethmoid synchondrosis and was found in 4 patients (Patients IP, LW, AY, HC). These patients did not show the wedge shape to the ethmoid bone. The frontal ethmoid attachment was discussed with the frontal bone (Section 3.5.4).

Medial Ethmoid Plate: The medial plate was normal in the infant and 6 year old age groups and in one adult (Patient HC). In the 2 year old patients and the adult patient TS, increased dimensions of the medial plate was seen. In the oldest patient (TS), the height of the plate was

increased and corresponded to an increase in the vertical dimensions of the medial plate of the ethmoid and the vomer, with a relative lack of AP growth.

Discussion: The findings of the ethmoid bone are consistent with what is known about this structure from previous studies (Bertelsen, 1958; Kreiborg, 1981). The ethmoid bones were broad and contributed to the hypertelorism and the reduction in orbital volume and had a secondary effect of increasing the overall breadth of the face (Figure 3.40). Along with the sphenoid and frontal bones, this bone directs the growth of the roof and lateral wall of the orbit and, along with the maxilla, influences the shape and angle of the floor. Involvement of the spheno-ethmoid synchondrosis has been suggested by other authors (Burdi et al., 1986). This study was able to confirm this in some but not all patients. In those patients without lengthening of the spheno-ethmoid synchondrosis a wedge shaped ethmoid bone was found.

The medial orbital wall was generally reduced in its height and length but with some minor discrepancies in terms of which regions were shortened (that is, anterior-posterior, superior-inferior). The medial plate was less severely involved. The depression of the cribriform plate was not measured along the lines of Bertelsen and Kreiborg. Additional angles representing the splay of the plate and separation from the midline were identified in this study and confirmed the broad and lateral position of the ethmoid. The reduced dimensions of the lateral plate contributed to create the impression of the ethmoid being depressed and protruding into the medial wall of the orbit. The reduced lateral plate size was associated with the increased inter-orbital component of the maxilla. Hence the maxilla may have a greater role in the development of reduced orbital volume and proptosis.

In the case of the ethmoid bone, pathology is related to the sutural and synchondrosis abnormalities between the frontal, sphenoid and ethmoid bones along with deforming bony and soft tissue forces such as increased intracranial pressure.

Patterns of deformity of the ethmoid bone in this study are summarised as:

1 Lateral plate

. normal (Patients RN, SH)

. reduced size (Patients JS, IP, LW, AY, HC, TS)

2. Posterior ethmoid

. spheno-ethmoid synchondrosis lengthened (Patients IP, LW, AY, HC)

. wedge shaped bone (Patients RN, SH, JS, TS)

3. Frontal ethmoid attachment (Section 3.5.4 Frontal bone)

4. Cribriform plate

. not depressed relative to anterior cranial base (all patients)

5. Medial plate

. normal (Patients RN, SH, LW, AY, HC)

. increased size (Patients JS, IP, TS)

3.5.8 The Morphology of the Sphenoid in the Eight Patients with Crouzon Syndrome

The sphenoid is the most intricate and complex bone of the cranial skeleton. The name is derived from the Greek for "wedge". This may be due to its shape, but also to its position between the other craniofacial bones. Via its elaborate processes, the sphenoid articulates with or is in contact with 9 other craniofacial bones. The measurement and determination of its shape is correspondingly complex. In this study the anatomy of the sphenoid bone was subdivided into four regions; the Lesser Wing, the Pterygoid Plate, the Greater Wing and the Sphenoid Body. These regions may present with different patterns of distortion. The summary of major trends is listed.

Lesser Wing: The lesser wing measurements varied (Figure 3.41). The moderate deformity was represented by prominent anterior clinoid processes and relatively normal size of the lesser wing. The more severe deformity showed a reduction in the anterior clinoid presumed due to bone resorption in the region of the sella. The lesser wing was longer and was associated with sweeping up of the lesser wing. This resulted in greater lateral protrusion of the bone contributing to a broad head shape.

Summary of Deformity:

1. Moderate Deformity (Patients RN, SH, JS, LW and AY)

Prominent anterior clinoid

Normal or reduced length of lesser wing

Angles variable

2. Severe Deformity (Patients IP, HC and TS)

Small anterior clinoid

Increased length lesser wing

Increased distance between tips of wings

Angles variable

Pterygoid Plate: The size (distances and dimensions) of the pterygoid plate was generally not significantly different from the experimental standard. The angle of the pterygoid plate from the sella-nasion line was increased in the most severe clinical presentation (Patient IP) and the adult patients (Patients HC and TS) (Figure 3.42). A lateral and posterior position of the pterygoid axis in these patients reduced the anterior position of the maxilla, and accounted for the greater severity of facial deformity in these patients. Muscle development in this region may subsequently be affected and produce deforming forces on other structures such as the mandibular ramus and gonial angle (Section 3.5.1 Mandible).

Summary of Deformity:

1. No deformity (Patients RN, SH, JS, LW and AY)

Normal dimensions and normal axis

2. Deformity (Patients IP, HC and TS)

Normal dimensions

Increased angle of pterygoid axis (lateral and posterior)

Greater Wing: The sphenoid greater wing was splayed more laterally than in the control population (Figure 3.42). The curve of protrusion into the orbit was not measured specifically. The lateral protrusion may be accounted for by the effect of surrounding squamous suture fusion preventing forward growth. Additionally, lateral growth of the ethmoid bone may push the orbit and subsequently the greater wing laterally. Fusion of the spheno-temporal suture may

also contribute to holding back the greater wing. As has already been discussed, the surrounding suture lengths were variably involved, a typical feature of Crouzon syndrome.

Summary of Deformity:

1. Spheno-zygomatic suture involvement (Patients RN, IP, HC and TS - the more severe cases)

2. Distortion of orbital component of greater wing (Patient IP)

3. Increased lateral protrusion of greater wing (All Patients)

4. Spheno-temporal suture involvement (5 older Patients) (Section 3.5.12 Cranial base sutures)

Sphenoid Body: The dimensions of the sella were generally increased as a result of increased bone resorption (Figure 3.43). The spheno-occipital synchondrosis showed 2 patterns. Firstly an increase in lateral height and normal width and secondly, a normal lateral height and reduced width. The measured deformity of the spheno-occipital synchondrosis makes its shape consistent, but size variable. The impact of this shape on the growth of the synchondrosis is not clear, but a reduced or distorted pattern of growth could result. Qualitative examination shows the spheno-occipital synchondrosis to be patent radiographically in the 6 children in this study. The synchondrosis was not visible in the 3D CT reconstruction of any except the 2 youngest patients. What is happening at a cellular level in the cartilage is the most pertinent question, but cannot be answered from this study.

Summary of Deformity:

1. Lateral body tended to be larger (All Patients)

2. Lateral spheno-occipital synchondrosis lengthened (Patients IP, LW and AY)

3. Spheno-occipital synchondrosis (superior, inferior) normal or reduced in length (All Patients)

Discussion: The features of the sphenoid in Crouzon syndrome have been described in the literature from dried specimens and cephalometric examination. Findings have included sweeping up of the lesser wing, increased protrusion of the greater wing into the orbit, enlargement of the sella turcica and variation in the cranial base angle (a feature not solely determined by the sphenoid bone) (Kreiborg, 1981; Kreiborg et al., 1993). Sutural involvement of the spheno-zygomatic, spheno-temporal (calvarial) sutures has also been described (Kreiborg and Bjork, 1982). The spheno-occipital synchondrosis has been shown to not be visualised on 3D CT reconstructions (Kreiborg et al., 1993).

In this study, several features of the natural history of Crouzon syndrome have emerged which are typified by the sphenoid bone (Figures 3.41 - 3.43). The sphenoid bone may be involved in 4 ways. Firstly, the primary growth of the sphenoid may be abnormal. Secondly, the sutures and synchondroses of the sphenoid may influence its subsequent growth. Thirdly, the sutures of other bones and regions may exert distorting influences on the sphenoid. Finally, the pressure effects of the brain will influence the extent of bony apposition and resorption, particularly in the region of the cranial base. Consequently, a range of deformity is seen, with the features being more marked in older patients and those with the more severe disease. Measurement of the distances, dimensions and angles cannot necessarily separate these influences but demonstrate the result of these forces.

The following list comprises the major findings of the sphenoid bone in this study.

1. The spheno-ethmoid synchondrosis is often abnormal
2. Lengthening of the lesser wings
3. Lateral protrusion of the greater wings
4. Variable involvement of the spheno-zygomatic suture and spheno-temporal sutures
5. Tendency for increased size of sella
6. Variable involvement anteriorly at the junction of the sphenoid, frontal and ethmoid bones.

3.5.9 The Morphology of the Temporal Bone in the Eight Patients with Crouzon Syndrome

Temporal Squamous Bone: The temporal squamous bone was only fully measurable in the infants where the landmarks asterion (as) and sphenion (spt) were visible. Premature fusion of sutures and/or reduced visibility of the sutures made the analysis of the superior part of the squamous temporal bone impossible in the other patients. Of the distances that could be measured the distance from the stylomastoid foramen to the mastoid process tip (ma-smf) was increased in 3 of the older 4 patients suggesting increased prominence of this process.

External Auditory Meatus: The external auditory meatus measurements were symmetrical in nearly all patients. Increased distances were usually adjacent to decreased distances, implying a distortion or tilting of the external auditory meatus. In summary, the external auditory meatus measurements showed increased distances in 4 patients (Patients RN, SH, IP and AY), equal increased and decreased distances in 2 patients (Patients JS and LW) and reduced distances in 2 patients (Patients HC and TS). One patient (Patient HC) had atresia of the external auditory meatus and an associated abnormality of the adjacent petrous temporal bone.

Zygomatic Process: The zygomatic process was also symmetrical. The zygomatic arch distance (aul-ztl, aur-ztr) was reduced in the majority of patients and the height of the articular fossa was increased in some patients.

Petrous Temporal Bone: Analysis of the petrous temporal bone revealed that the petrous temporal ridge distance (petar-petpr) was increased in the majority of patients. Suture lengths at the apex of the bone (fis-peta, peta-jfp) varied greatly (Figure 3.44). Distances of the jugular foramen were reduced, to a greater degree on the right side (Figure 3.45). The occipital component of the jugular foramen (jfl-jfp, jfp-jfm) showed a similar trend in the majority of patients. The petrous temporal-occipital suture was reduced on the left with non-significant reduction on the right. Increased distances from the mastoid to jugular foramen were found and may reflect the prominence of the mastoid process in the population as well as the narrowing of the jugular foramen.

Dimensions: The dimensions between the temporal bone were slightly increased, with the exception of Patient HC who had left external auditory canal atresia, and showed reduced distances between the left and right bones, as well as reduced angles. Several other patients showed an increased distance between the internal auditory meati points, the porion points and the jugular foramina. The angles of the petrous temporal bone were normal in 5 patients (Patients SH, IP, LW, AY and TS).

Discussion: The temporal bone in patients with Crouzon syndrome has been described as hypoplastic (Nager and de Reynier, 1948). Fusion of the squamous temporal sutures has been reported (Kreiborg and Bjork, 1982). There is little information in the literature about the detailed pathology of the temporal bone in Crouzon syndrome. In this study, 2 patterns have emerged. The first is the typical pattern, the features of which are listed below. This pattern reflects the dysmorphic growth of the Crouzon cranium. The mechanisms by which the abnormality of the sutures determine the shape of the temporal bone are less clear due to the complex shape of the bone. The shape and position is also influenced by the growth distortion of the surrounding bones.

The sutural patterns of the temporal bone were more difficult to identify than any other bone, particularly laterally where the cranial base meets the calvaria due to their complex pattern. For this reason it was difficult to implicate the sutures as being distorted, although it seems likely that they are.

Narrowing of the jugular foraminae was a consistent finding and may have several effects such as producing a reduced intracranial outflow with reduced reabsorption of cerebrospinal fluid contributing to ventriculomegaly or hydrocephalus. Other extracranial-intracranial venous communications may become more prominent. Bleeding from these regions and from the venous sinuses may be more pronounced during surgery in this population. This has not been clinically recorded, however, brisk bleeding in the region of the orbits and from the dura has been our experience in some cases. It is probable that any changes to intracranial dynamics are relatively subtle and these changes are difficult to measure.

The second pattern of the temporal bone is proposed due to the atypical findings in Patient HC with atresia of the external ear canal. The relevant feature about this patient was that while

deformity was found in all regions of the bone, the dimensions of the bone were reduced. The sutures of the spheno-occipital synchondrosis were shortened and the temporal bones were closer together. The anterior petrous temporal sutures were reduced in length while the posterior sutures were increased, implying a more profound posterior process. The pattern profile was similar to the other patients but translocated to a reduced size position implying hypoplasia of the bone. This may reflect a primary growth abnormality of the petrous bone along the lines of a clefting process. Clearly, analysis of further patients with atresia or stenosis of the external auditory canal is required to determine whether this pattern holds true for others.

Summary of Deformity:

1. Typical Pattern

   Calvarial suture involvement

   Normal or prominent mastoid process

   Distorted external auditory meatus (with increasing age)

   Zygomatic process shortened

   Narrowed jugular foramen

   Cranial base sutures lengthened or normal (variable combinations)

   Generally broad inter-temporal distances

   Variable angles of splay of the bones

2. Atretic Pattern

   Calvarial suture involvement

   Normal or prominent mastoid process

   Stenotic or atretic external auditory meatus

   Zygomatic process normal or lengthened

   Normal or narrow jugular foramen

   Cranial base sutures shortened anteriorly, lengthened posteriorly

   Narrow inter-temporal distances

   Variable angles of splay of the bones

3.5.10 The Morphology of the Parietal Bone in the Eight Patients with Crouzon Syndrome

The sutures outlining the parietal bone could not be identified in the Crouzon population due to the pathology. No reliable landmarks could be identified adjacent to allow any measurements to be accurately recorded. As a result no data has been produced for a region which clearly has pathology.

3.5.11 The Morphology of the Occipital Bone in the Eight Patients with Crouzon Syndrome

Distances: The majority of the measured distances were normal. All the distances in the

2 infants were all in the normal range. Increase in the length of the petrous temporal-occipital suture was found in 4 patients, either bilaterally or unilaterally, with the trend to be increased on the other side. The foramen magnum was reduced in size in 1 patient, yet nearly all patients tended to have reduced distances in this region. The foramen magnum was distorted in 2 patients with some asymmetry of shape.

Dimensions: The internal occipital protuberance was usually normally positioned. On 3 occasions the position was atypical, and reflects some shape variation in the posterior cranial fossa.

Discussion: The occipital bone is a large curved squamous bone which articulates with the sphenoid, temporal and parietal bones. Measurement is made difficult due to difficulty identifying the calvarial sutures. From plain radiographs and qualitative data, the lambdoid suture is the least commonly involved in Crouzon syndrome. Measurement of the dimensions of the posterior fossa is unreliable due to difficulty in landmark location on the large curved surface. The measurements therefore concentrate on the cranial base, the sutures with the temporal bone and the foramina. The relationship with the temporal bone determines the majority of the measurements.

The petrous temporal-occipital suture tended to be variable in length, and was considered in conjunction with the other distances representing the suture (jfm-peta, peta-pts) which are

described in the temporal bone, sphenoid bone and the cranial base sutures (Sections 3.5.8, 3.5.9, 3.5.12 respectively).

The spheno-occipital synchondrosis tended to be reduced in length and increased in height in the older patients (Patients IP, LW, AY, HC and TS). A complete description of the synchondrosis is given in the description of the sphenoid bone (Section 3.5.8) and cranial base sutures (Section 3.5.12).

The jugular foramen consistently had reduced distances, representing narrowing of the foramina. This was also seen qualitatively. Reduction in venous outflow has been considered a possible cause of raised intracranial pressure, hydrocephalus or ventriculomegaly in Crouzon syndrome. Narrowing of the foramina has been statistically demonstrated in some patients. Collection of more data and comparison with ventricular findings may further elucidate any correlation.

Variable asymmetry was seen at the foramen magnum and appeared to represent a distortion of the lateral margins of the foramen. There is no clear explanation for this but bone resorption may be involved and may be increased with raised intracranial pressure. Underlying central nervous system abnormalities such as tonsillar herniation (David et al., 1982) may also distort bony shape. In this study CNS abnormalities were not detected in this region in these patients.

Summary of Deformity:

1. Petrous temporal-occipital suture length variable.
2. Spheno-occipital synchondrosis shape distorted.
3. Narrow jugular foramen.
4. Variable asymmetry at foramen magnum.

3.5.12 The Morphology of the Cranial Base Sutures in the Eight Patients with Crouzon Syndrome

Anterior Cranial Fossa: The commonest region of deformity was at the spheno-ethmoid synchondrosis. This was demonstrated in 4 patients (Patients IP, LW, AY and HC). These

patients were 4 of the 5 oldest in the group. The oldest patient (Patient TS) had no spheno-ethmoid involvement but involvement laterally in the region of the fronto-ethmoid suture was found (Sections 3.5.3 Frontal bone, 3.5.7 Ethmoid bone). The spheno-frontal sutures measured in the anterior cranial fossa and in the orbit showed only slight and infrequent variation from normal. Laterally the spheno-zygomatic suture was increased in length in 4 patients and is discussed in patterns of zygomatic suture involvement (Section 3.5.4 Zygomatic Bone).

Middle Cranial Fossa: The sutures were relatively normal in the floor of the middle cranial fossa, with increased spheno-petrous temporal suture length the commonest finding in the older patients.

Posterior Cranial Fossa: The sutures were lengthened either medially (Patients SH and HC), laterally (Patients JS and TS) or with a combination of both (Patients IP, LW and AY). Patient RN had normal suture lengths. In the older patients, the spheno-ethmoid synchondrosis involvement occurred in a particular pattern. The region was reduced in width and increased in height. This was reflected in the measurements in 2 ways. Firstly, the height was increased and the width was normal (Patients IP, LW and AY). Secondly, the height was normal and the width was reduced (Patients HC and TS), These measurements produce a similar shape but a relative size reduction.

Discussion: A pathological process in Crouzon syndrome occurs both at the suture and synchondrosis. What drives this event is not clear. Its timing and severity are also poorly understood. The cause and effect relationship between the role of cranial bone growth and the sutural fusion in Crouzon syndrome has yet to be determined. Variability of calvarial suture involvement, however, typically occurs. The same can be said of the cranial base sutures and synchondroses. The spheno-ethmoid synchondrosis appears to be involved, and is thought to be instrumental in normal midfacial development (Enlow, 1975; Burdi et al., 1986). The distance representing the spheno-ethmoid synchondrosis was lengthened in 4 patients (Z score > 1.96). The clinical effect of this lengthening and presumed premature fusion was the reduction of the forward growth of the ethmoid with deflection of growth laterally. Thus, the relationship of maxilla with the ethmoid shows it to be broad and positioned superiorly in

Crouzon syndrome when compared with the experimental standard. Clinically the maxilla develops downward to produce a functional occlusion but has reduced growth in the AP direction.

The distance representing the spheno-zygomatic suture was significantly increased in 4 of the patients (Z score > 1.96). Fusion at this suture would account for the lack of AP growth and subsequent increased vertical length of the suture and contribute to the lack of bony support for the globe and thus proptosis. It would also contribute to the lack of forward growth of the greater wing of the sphenoid which may be a primary growth event or related to the involvement of the surrounding sutures such as the spheno-zygomatic, spheno-squamous temporal and, to a lesser extent, the occipital mastoid suture.

Examination of all the cranial base sutural measurements produced a picture of primarily anterior and peripheral sutural involvement (Figure 3 46). The spheno-zygomatic and occipital mastoid sutures are essentially an extension of the calvarial sutures and anteriorly, the sphenoid-ethmoid synchondrosis is intimately related to maxillary development. The spheno-occipital synchondrosis proper, a site thought to play a major role in the cranial base pathology, was distorted but not greatly lengthened.

There was variation in which sutures were involved. This method of analysis allows specific identification of this variation in each patient producing a profile of involved regions. It should be noted that the more severe the deformity (Patient IP) and the older the patients (Patients LW, AY, HC and TS) the greater the chance of identifying abnormal sutural distances. Further population-based study with improved experimental standards is currently needed and provides the focus of ongoing research.

3.5.13 The Morphology of the Craniofacial Dimensions and Angles in the Eight Patients with Crouzon Syndrome

Dimensions: The facial height from nasion to gnathion was increased in the older patients where the landmarks could be reliably assessed. Laterally, the height was closer to normal. The cranial base dimensions were generally not significantly different from the experimental standard, with the exception of Patient IP, who had the most distorted skull.

Angles: The SNA angles were low-normal or reduced and reflected the midface hypoplasia. Additionally, the cranial base angle and the subsequent position of the sella-nasion line, influenced the angle. The SNB angles appeared to follow a similar pattern, although they could not be assessed in the younger patients.

The cranial base angles varied from increased (Patients IP, HC and TS), to normal (Patients RN and JS) to reduced (Patients SH, LW and AY).

Discussion: The cranial base angles vary. This finding has been described previously by others (Kreiborg, 1981). This interesting feature highlights two points. Firstly, the evolution of the pathology may occur at different rates and with different severity at different locations, in a similar way to the varied pathology of the cranial sutures and resultant calvarial shapes. Secondly, we need to look for not a single pattern of clinical and measured deformity in Crouzon syndrome, but rather for a range of patterns. It is probable that some patterns of the deformity are more common than others. This thesis attempts to identify some of these patterns. The significance of the cranial base pathology should be related to the surrounding pathology and resultant deformity. The primary growth of the cranial base may be distorted by a primary growth disturbance of the bones or synchondroses and sutures. Secondary distorting forces include the effect of adjacent bone deformity and the intracranial pressure.

3.6 Theory of Pathogenesis of Craniofacial Morphology in Crouzon Syndrome

The pathogenesis of the deformities in Crouzon syndrome is not fully understood. Two main theories currently exist. The first theory evolved from initial observations of deformity in the simple craniosynostoses and proposes that the primary defect is at the level of the suture. Premature suture fusion results in bony deformation which is readily demonstrable at the calvarial level. In contrast to simple craniosynostosis disorders, the premature suture fusion extends into the cranial base having a compounding effect on the morphology at this level. In addition, raised intracranial pressure exerts forces that alter the dynamic morphology of the cranial base bones. The resultant cranial base changes have a secondary effect on the orbital and maxillary manifestations. Recent 3D CT qualitative descriptions by Kreiborg et al. (1993) have postulated a sutural abnormality and demonstrated secondary cranial base changes from

pressure. This is in contrast to Apert syndrome where a primary defect of cartilaginous bone has been implicated.

The second theory proposes that the premature suture fusion occurs in response to external forces. The postulated primary event is a spatial malpositioning or abnormal dural stresses acting on the calvarial sutures. This theory is based on animal studies and fetal examinations where typical calvarial deformities may be present, but the cranial sutures are patent (Moss, 1959).

This study has demonstrated, by quantification, the pathology of Crouzon syndrome. The results are summarised in Table 3.3 and are represented diagrammatically in Figures 3.35 - 3.46 (comparisons of each patient with the experimental standard are to scale, comparisons between the age groups are not to scale).

The interpretation of the morphological quantification identified the pathology at the level of the suture but at the same time found regions of primary bony dysplasia. Differentiation between the 2 theories of pathogenesis cannot be conclusively demonstrated by qualitative and quantitative assessment, particularly at the level of the cranial base. Primary bone growth and suture function are intimately related and both contribute to morphology. Both of these features can be considered primary abnormalities in Crouzon syndrome (Figure 3.47). The premature suture fusion accounts for the typical shape distortion of the calvarial bones, however, dysplasia of bony elements in the cranial bones has also been identified and is less clearly the result of pathology of adjacent sutures and synchondroses. In addition, the present study identified pathology at some but not all cranial base sutures. In addition, the pattern of distortion of the cranial bases is not uniform. In this study, for example, external auditory meatus atresia seen in 1 patient was correlated with hypoplasia of the petrous temporal bone.

In addition reduced size of foraminal openings was a prominent feature of the disorder. As mentioned above the external auditory meatus may be stenosed or atretic. The jugular foramen was found to be narrowed in virtually all patients. Similarly the superior orbital fissure was shortened in the majority. The diameter of the optic canal was not assessed, due to difficulty in visualisation, but clearly is a relevant dimension in relationship to the progressive optic atrophy

that is found in Crouzon syndrome and of the risk of the optic nerve traction at the time of surgical manipulation.

The abnormal shape of the bones appears to be related to both primary developmental and secondary deforming factors (Figure 3.47). Secondary morphological features complicate the dysmorphology in Crouzon syndrome and these are considered as the interactions between structures. Deformity of one bone exerts a deforming force on its adjacent neighbour not only by its sutural attachment but by its bulk and direction of growth. This is most clearly seen in the zygomatic bone where its position and shape are affected not only by the adjacent sutures but by the projection of the greater wing of the sphenoid and calvarial deformities. The effect of the brain on adjacent bones either at normal or raised intracranial pressure exerts some deforming effect. Endocranial bony resorption and scalloping has been well described. The enlargement of the sella turcica in the body of the sphenoid can be demonstrated on CT scans (Kreiborg et al., 1993) and is presumed due to bony resorption secondary to pressure. Thirdly the effect of the functional matrix (Moss and Salentijn, 1969; Moss, 1971, 1975) has relevance particularly at the occlusal level. Increased alveolar height, and the retroclined position of the mandibular symphysis attempt to form a functional occlusion.

Added to this complex picture are the effects of growth. Calvarial growth is more rapid in infancy and greater deformities are seen at this time. Later in childhood maxillary deformity becomes more evident.

In conclusion, the nature of primary bony abnormality influencing sutural development cannot be determined without histochemical analysis. Several features, however, suggest this interaction exists. Calvarial deformity may exist with the absence of sutural fusion and the pattern of sutural fusion is variable. The growth and development of the cranial base bone is not normal and at times produces deformity not correlated with any detectable suture abnormality. The assessment of the cranial bones is affected by the secondary forces which alter the primary pathology. Further study of all facets of Crouzon syndrome both clinical, radiological, histological, and genetic will lead to the determination of the fundamental pathological process.

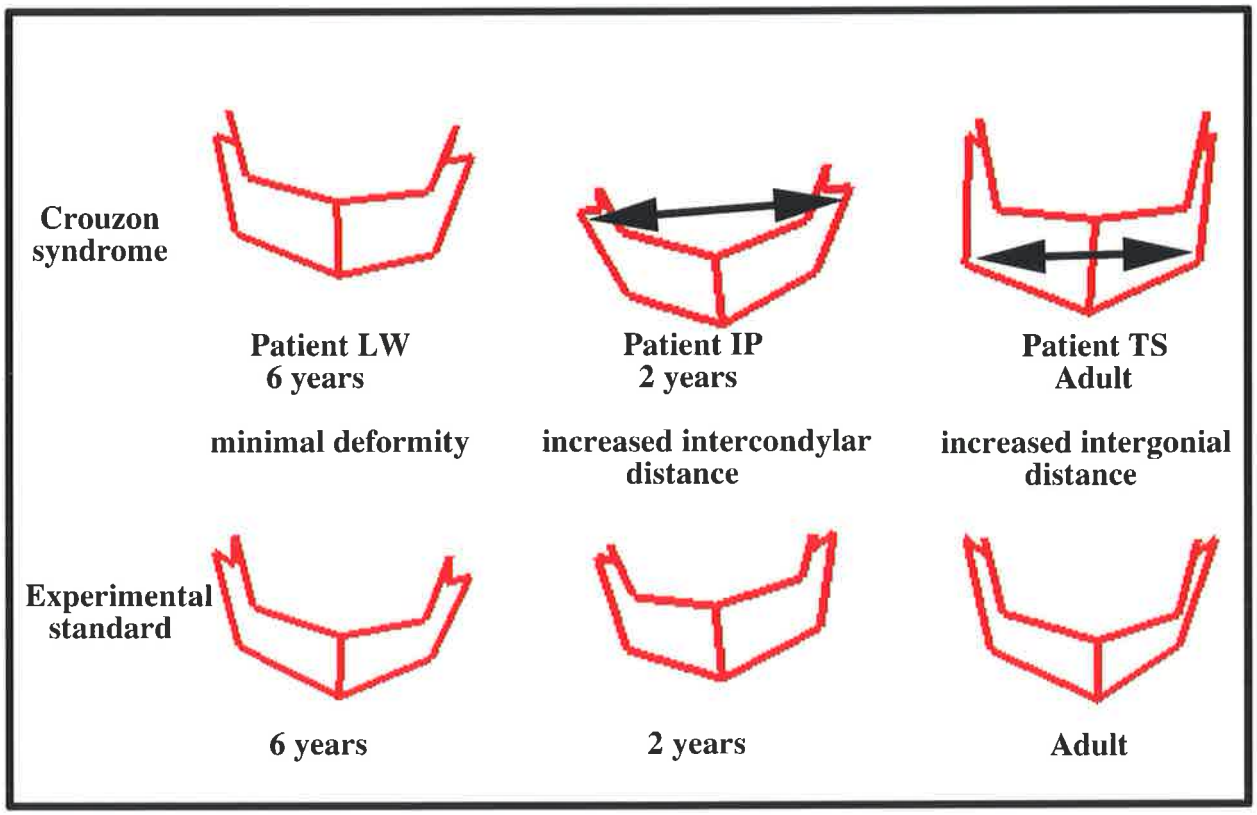

Figure 3.35 Pattern of deformity of the Mandible in Crouzon syndrome. (Each age group independently scaled.)

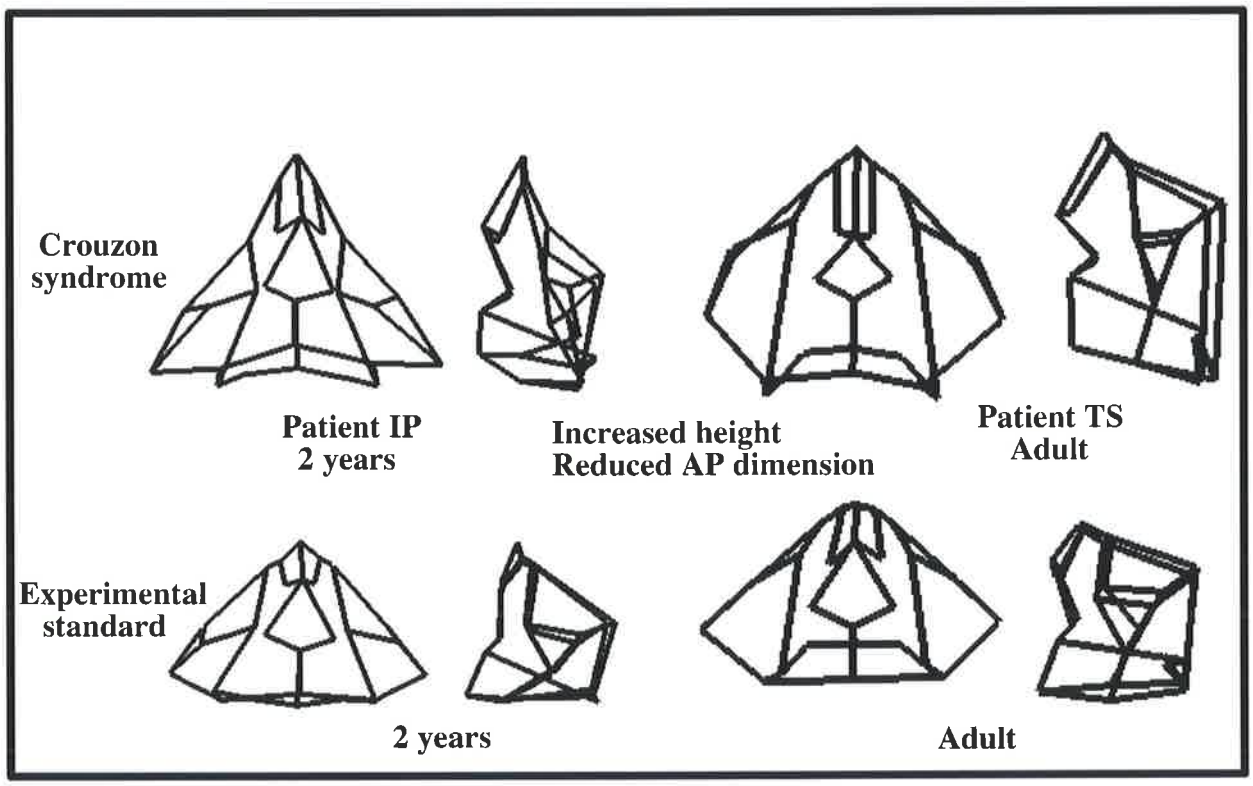

Figure 3.36 Pattern of deformity of the Maxilla in Crouzon syndrome. (Each age group independently scaled.)

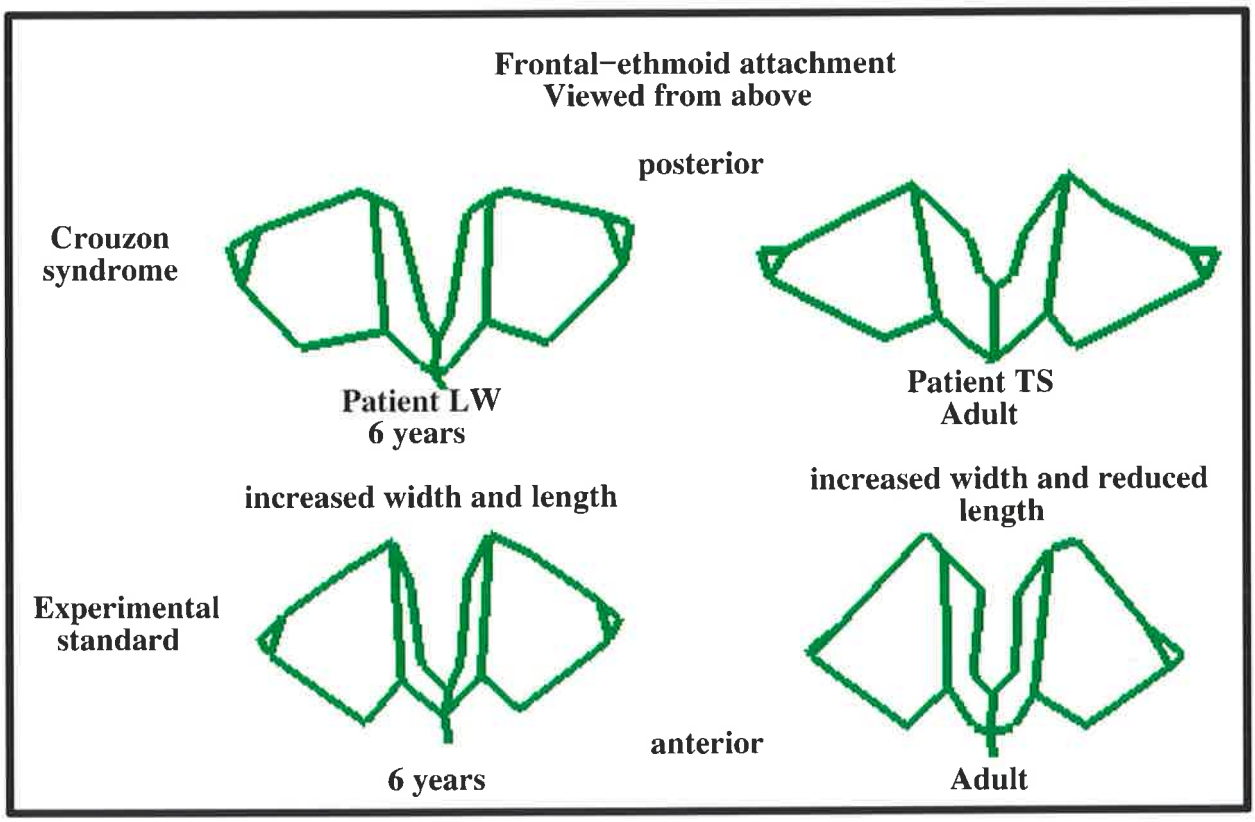

Figure 3.37 Pattern of deformity of the Frontal bone in Crouzon syndrome. (Each age group independently scaled.)

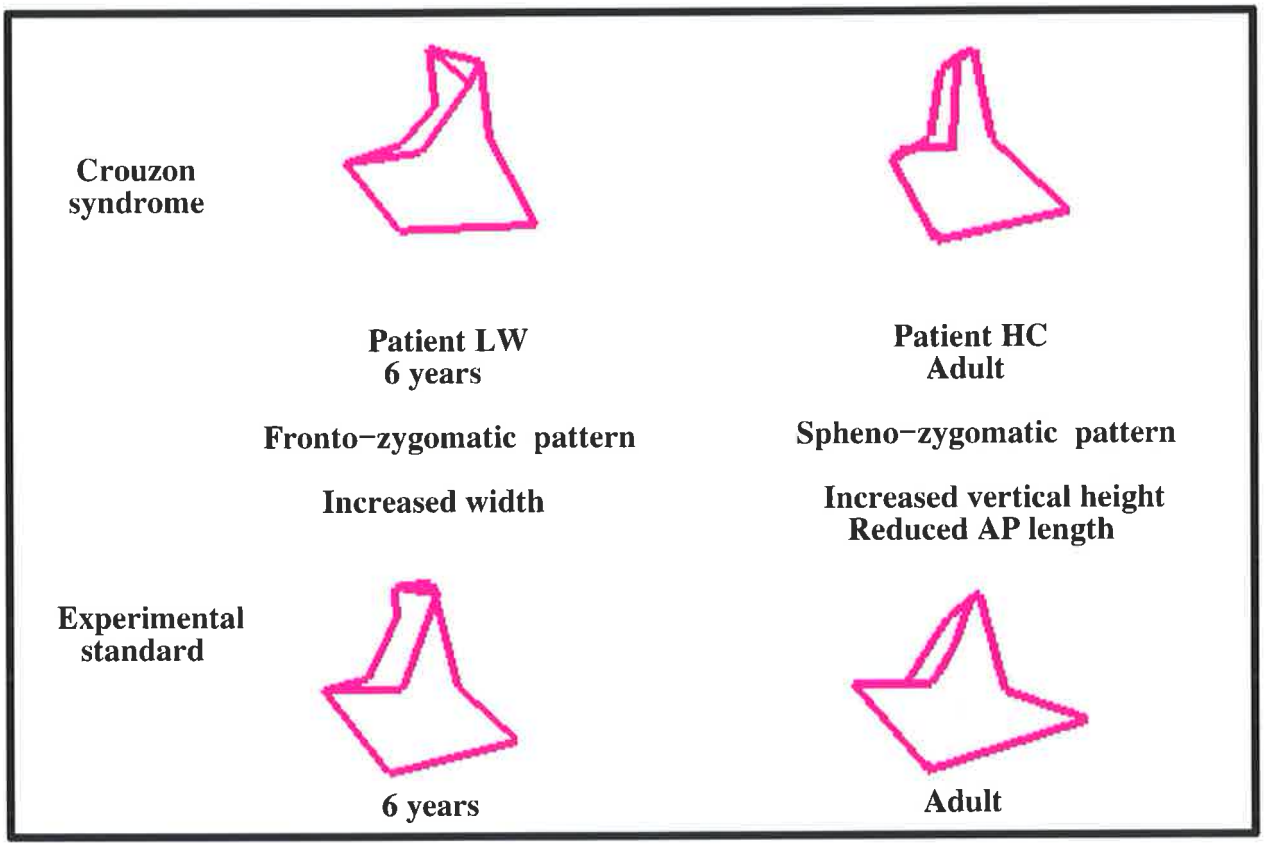

Figure 3.38 Pattern of deformity of the Zygomatic bone in Crouzon syndrome. (Each age group independently scaled.)

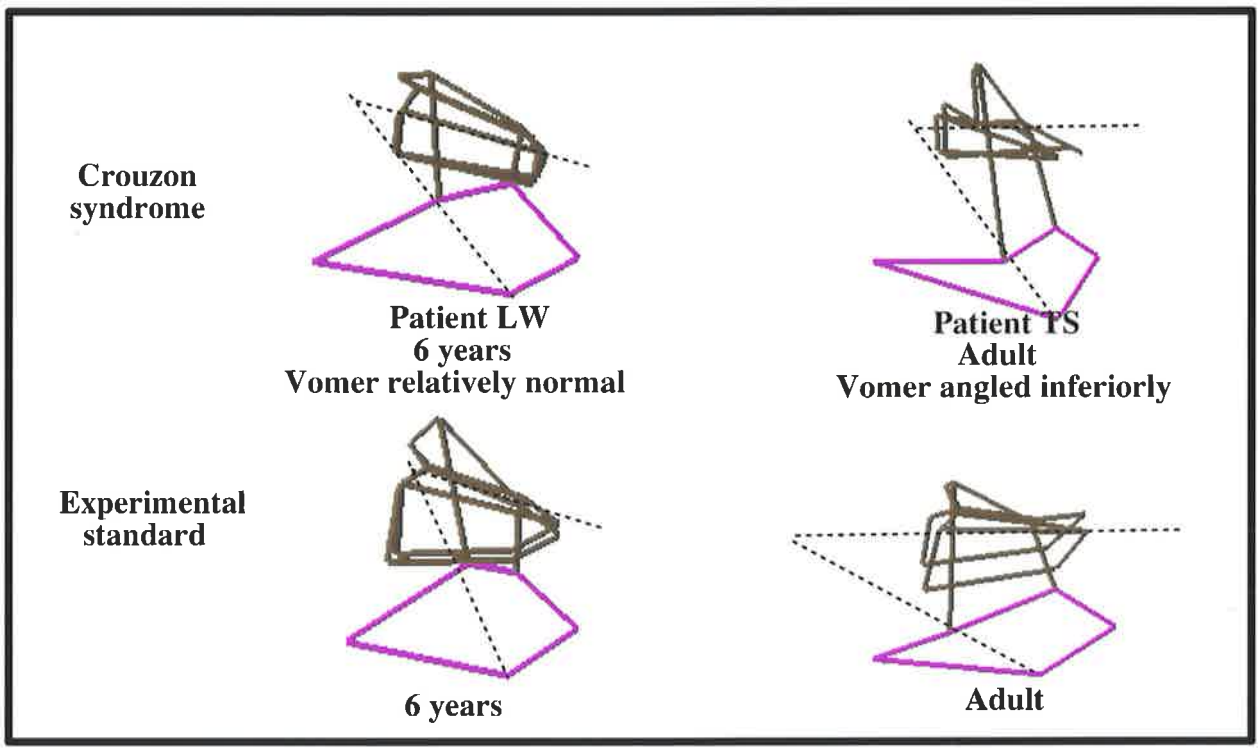

Figure 3.39 Pattern of deformity of the Vomer and Ethmoid bone in Crouzon syndrome. (Each age group independently scaled.)

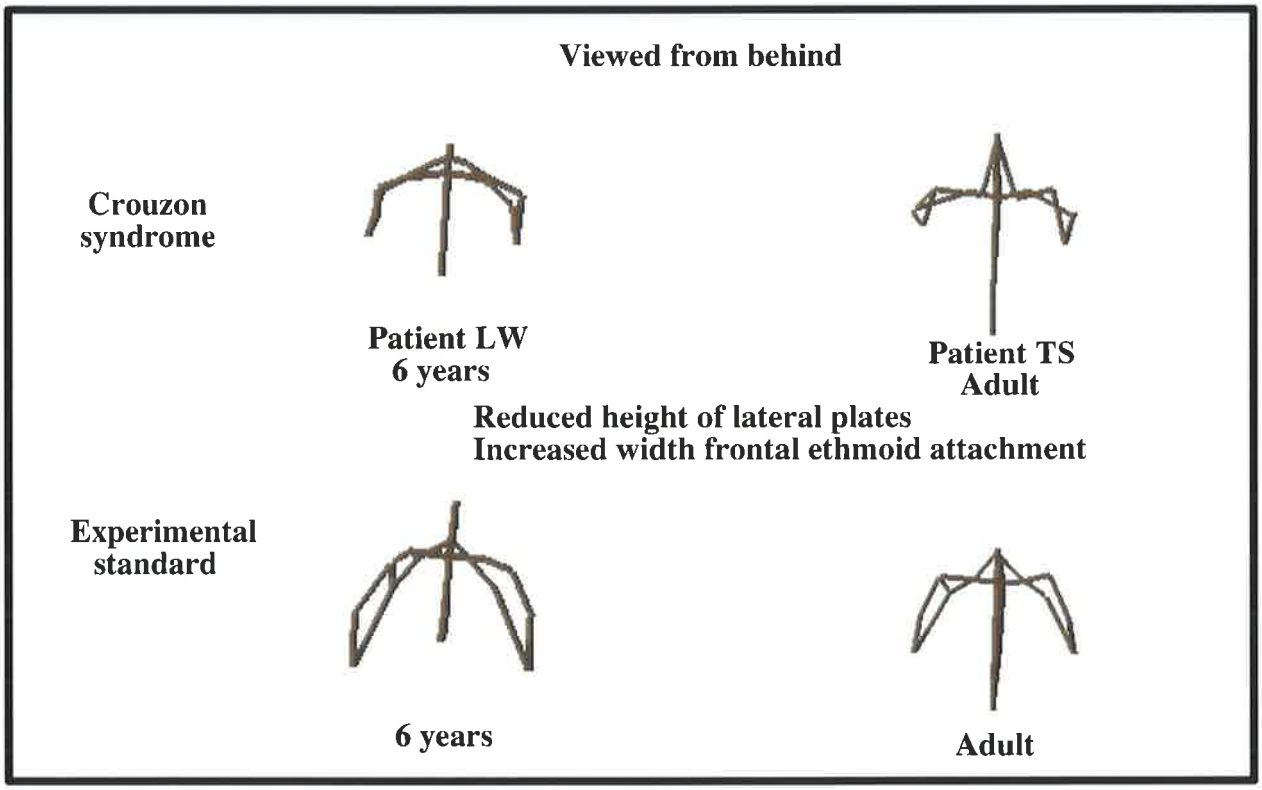

Figure 3.40 Pattern of deformity of the Ethmoid bone in Crouzon syndrome. (Each age group independently scaled.)

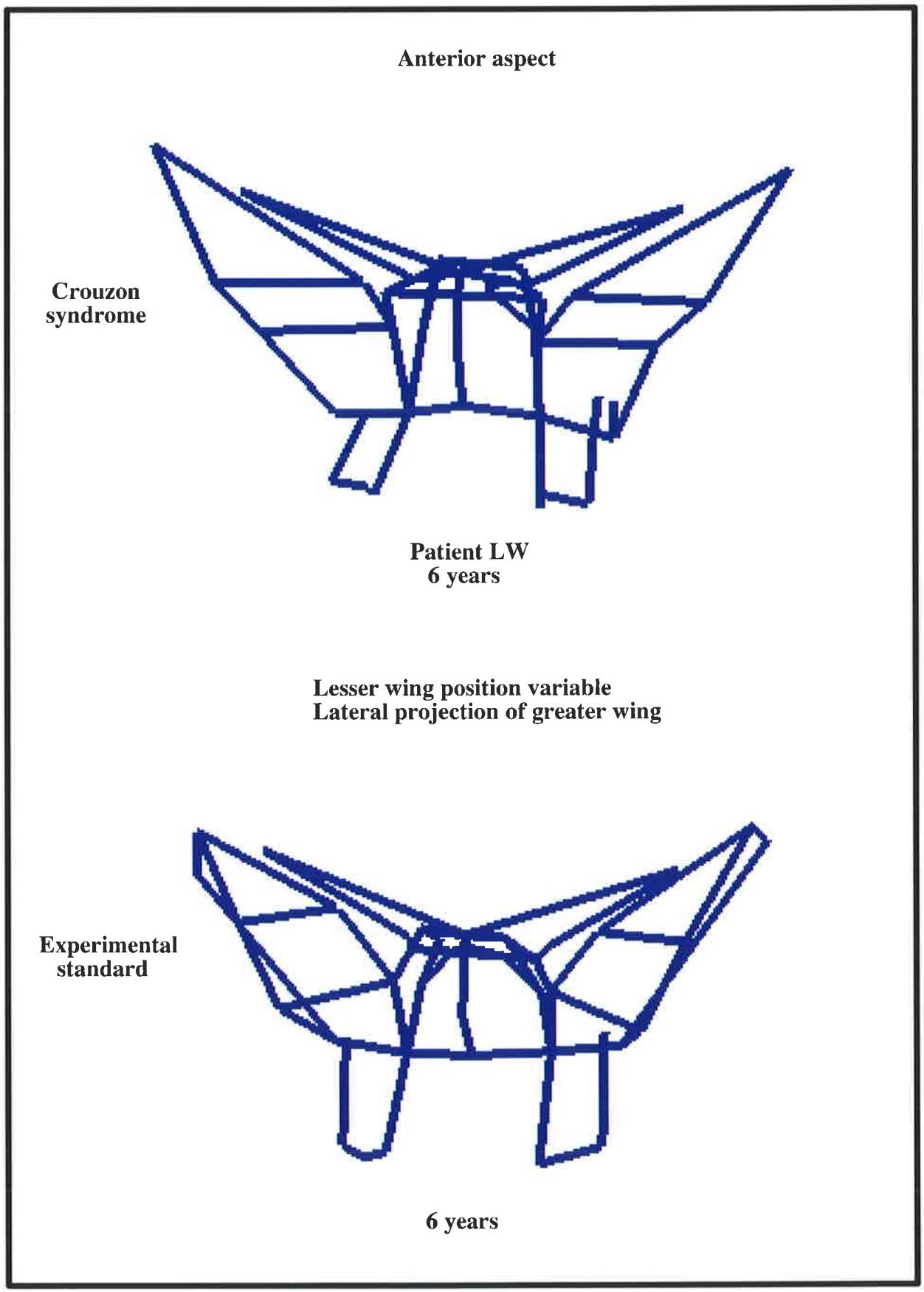

Figure 3.41 Pattern of deformity of the Sphenoid bone in Crouzon syndrome.

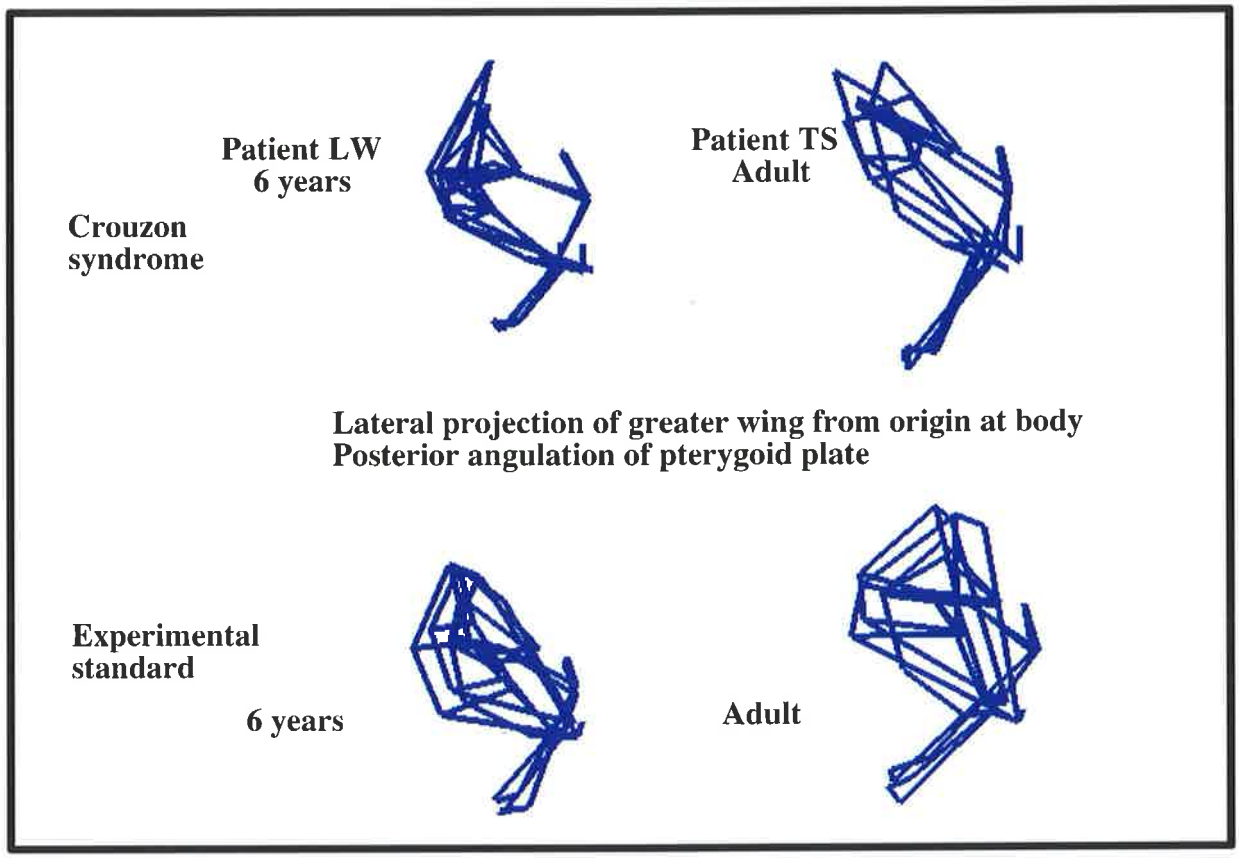

Figure 3.42 Pattern of deformity of the Sphenoid Greater Wing and Pterygoid Plate in Crouzon syndrome. (Each age group independently scaled.)

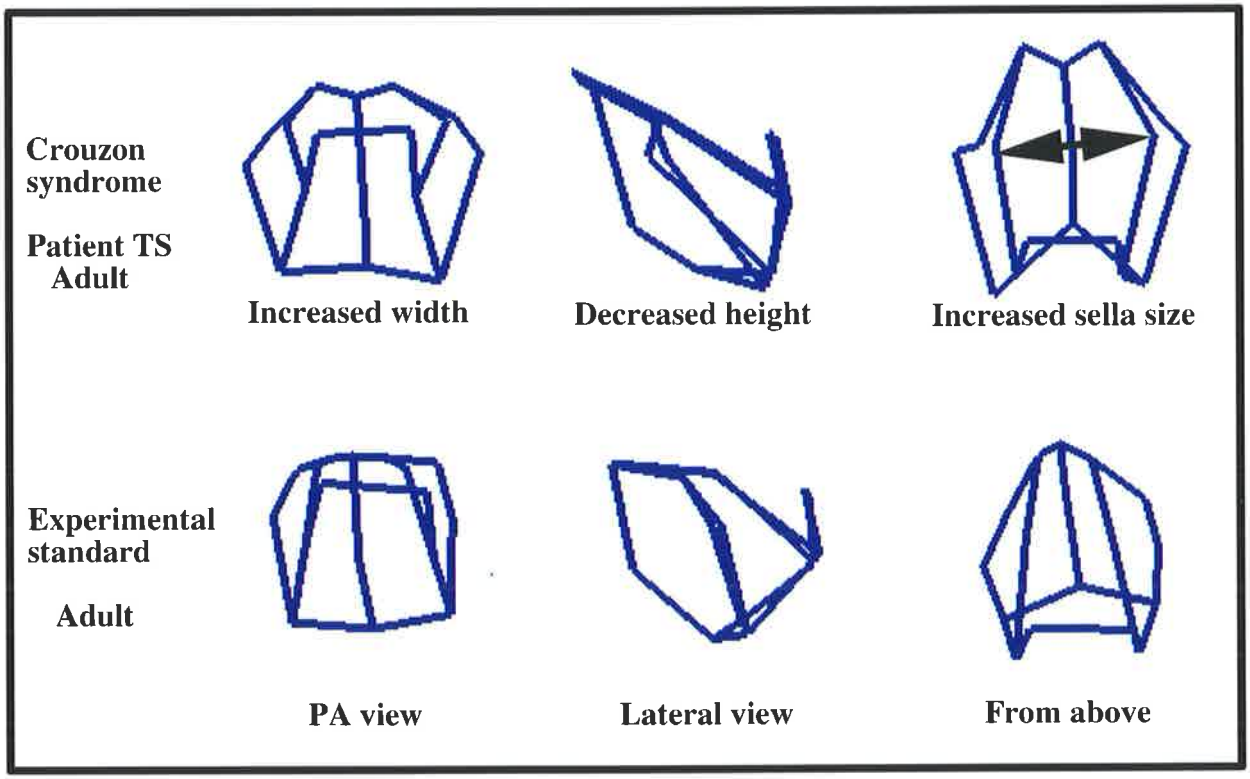

Figure 3.43 Pattern of deformity of the Sphenoid Body in Crouzon syndrome.

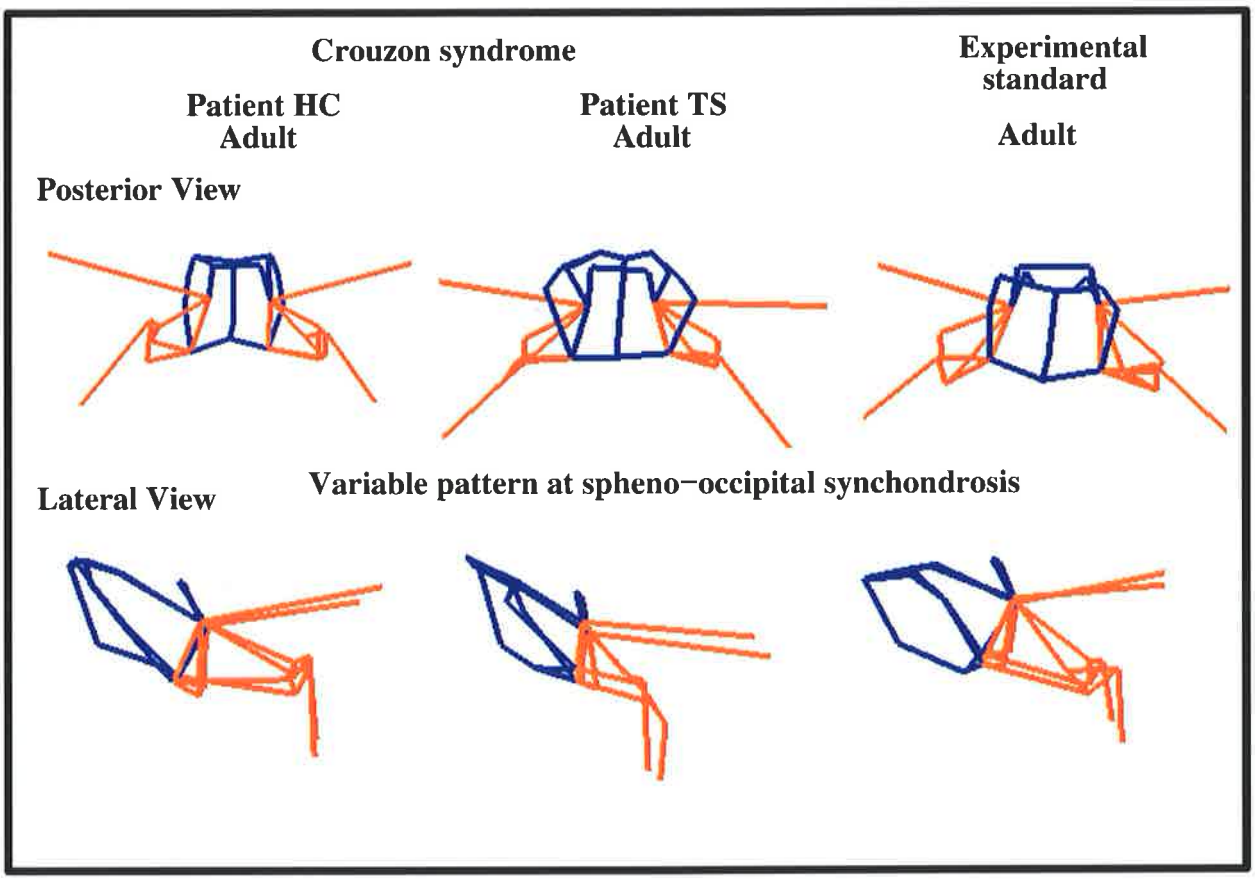

Figure 3.44 Pattern of deformity of the Sphenoid Body and Temporal bone in Crouzon syndrome.

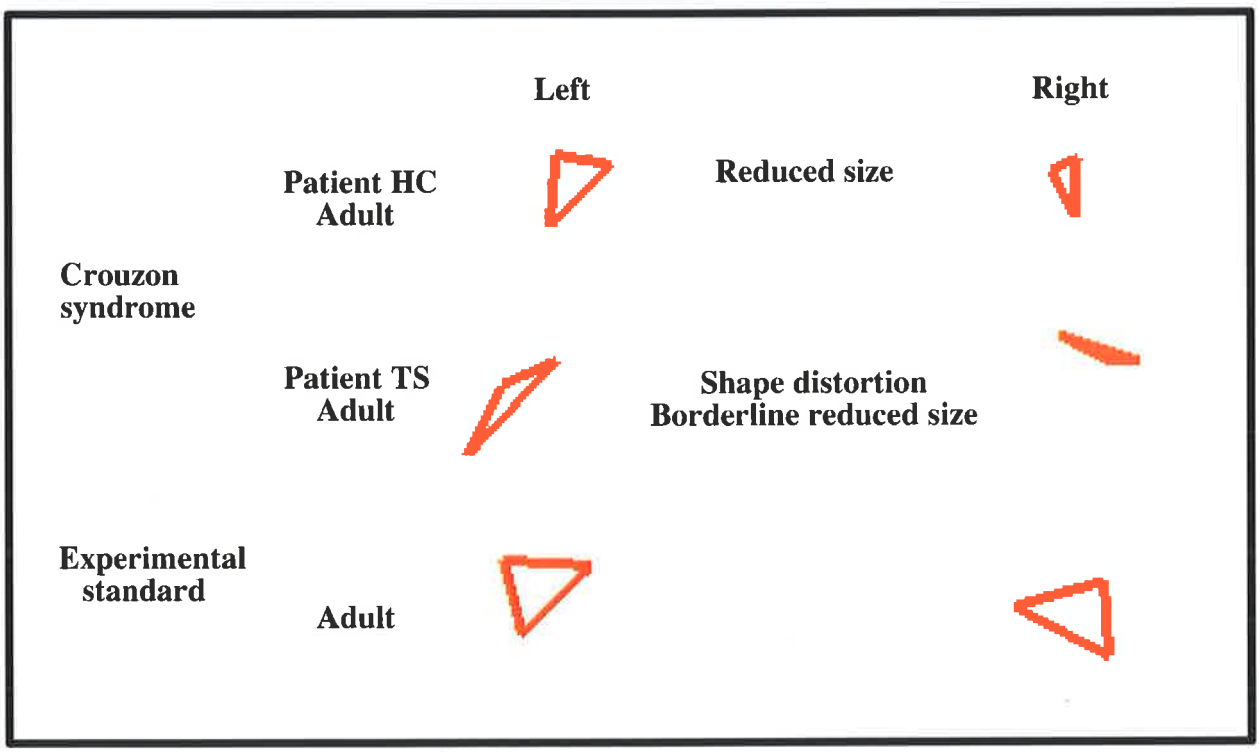

Figure 3.45 Pattern of deformity of the Jugular Foramen in Crouzon syndrome.

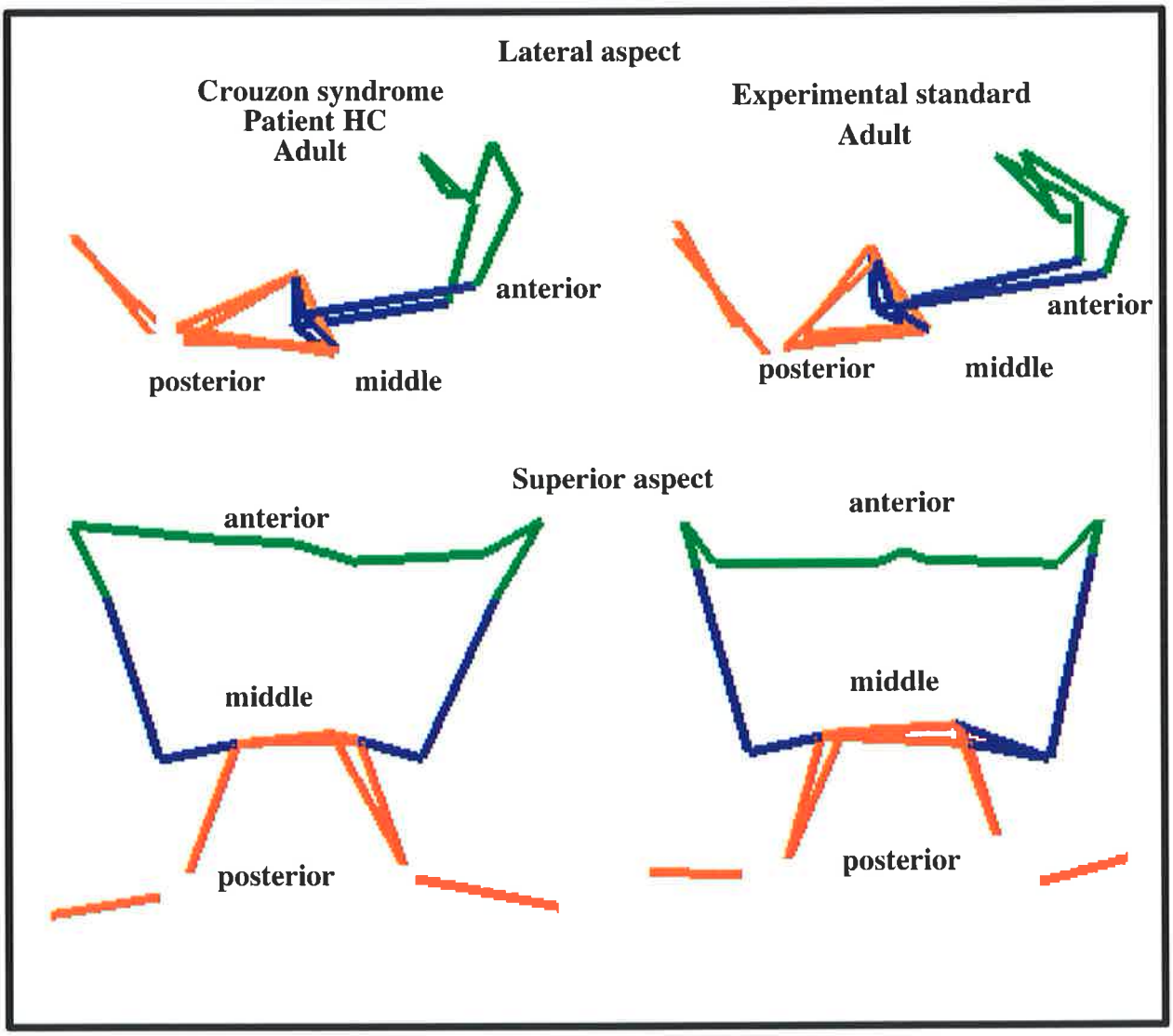

Figure 3.46 Pattern of deformity of the Cranial Base Sutures in Crouzon syndrome.

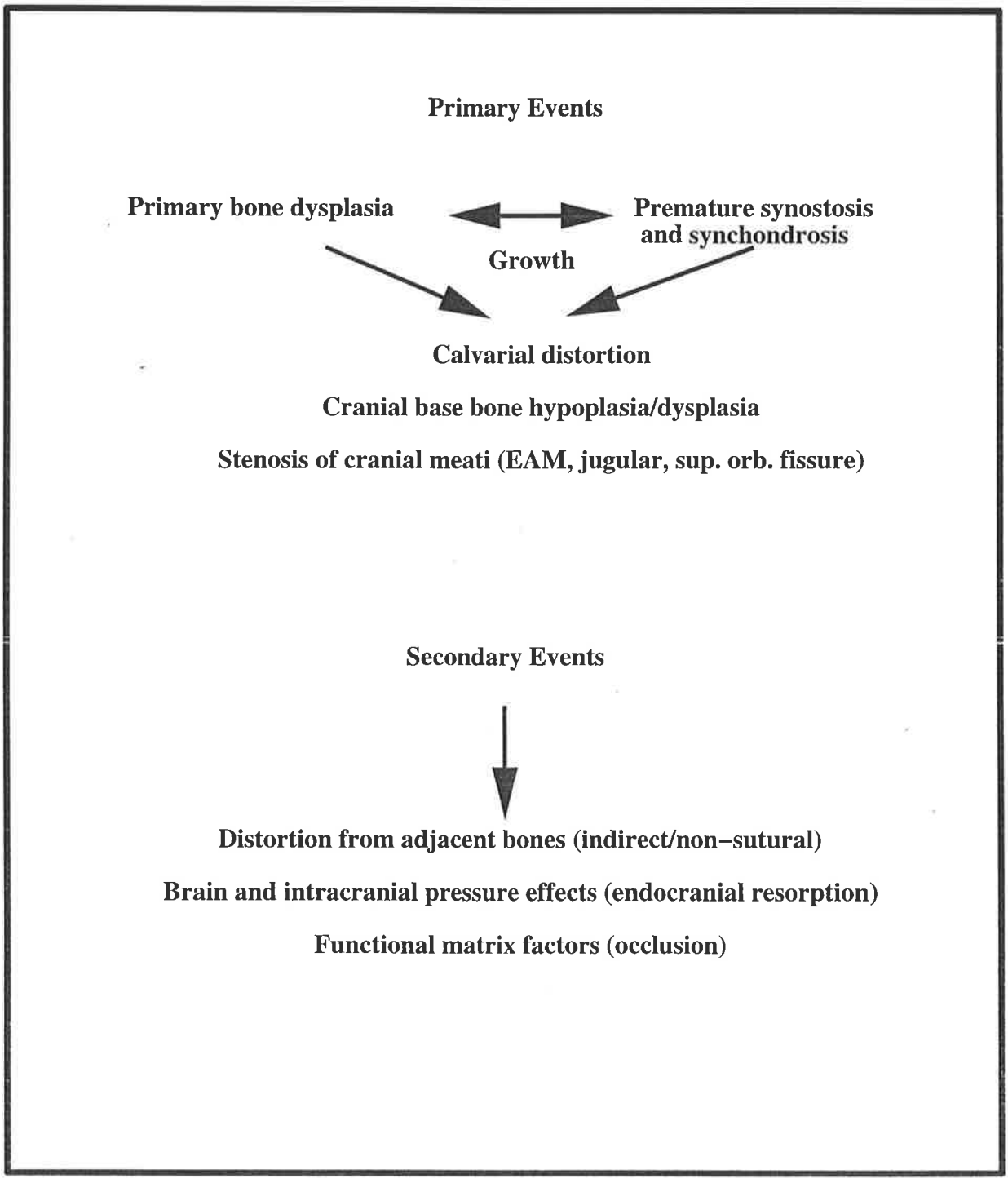

Figure 3. 47 **Theory of Pathogenesis of Morphology in Crouzon Syndrome**

CHAPTER 4

THE THREE DIMENSIONAL QUANTITATIVE ANALYSIS OF THE CRANIOFACIAL MORPHOLOGY BEFORE AND AFTER SURGERY IN CROUZON SYNDROME

4.1 Introduction

Dysmorphology of the craniofacial skeleton in Crouzon syndrome has been extensively examined in the preceding chapter with the aim of analysing the underlying pathology. The quantitative analysis was based on the determination of the position of anatomical landmarks in 3D. This method of analysis has 2 other main applications. These are the assessment of craniofacial growth in this (and other) conditions as well as the normal population and the analysis of the effects of surgical intervention which aim to release sutures and advance craniofacial bony elements. In the group of patients studied, there were no serial CT scans of patients to allow analysis of growth. However, CT scans were performed routinely following surgery and hence this data was available for analysis. The alteration of the craniofacial morphology by surgery, for either functional or aesthetic indications, is assessed in this chapter.

The techniques of craniofacial surgery were pioneered by Paul Tessier, and have since been expanded by many others. Many procedures have been described for functional and aesthetic indications. The broad principles and outline of surgical intervention are described in Chapter 2. The priority of surgery is functional correction of the deformity. The aesthetic correction of the deformity a is desirable but secondary objective. In general, the age of the patient and the extent of the deformity will determine the type and timing of surgery. In infancy the fronto-orbital advance is used to release the calvarial suture and provide protection for the globes. The concept of the floating forehead (Marchac and Renier, 1979) aims to maximise the anterior advancement by allowing brain growth to expand the calvarial bones.

After 3 years of age brain expansion is less rapid and the effect of the floating forehead is less dramatic. The fronto-orbital advance is also used in childhood for raised intracranial pressure and globe protection. Mid-facial surgery is also possible in this age group (McCarthy et al., 1990).

In adults the definitive correction of the aesthetic deformity may be attempted. This has been predominantly done using fronto-facial and Le Fort III advancement. Variable osteotomy sites have been suggested (Gillies and Harrison, 1951; Tessier, 1971b; Tessier, 1976; Ortiz-Monasterio et al., 1978).

Problems with craniofacial surgery in Crouzon syndrome include relapse in the position of bony elements, recurrent synostosis with the growth of the patient and a failure to adequately correct a complex deformity with simple osteotomies. This last problem is highlighted by the difference between the good result in the simple craniosynostosis patients compared with the less satisfactory results in the syndromal synostosis patients.

In the past, assessment of surgery in Crouzon syndrome has been measured by cephalometry (Bachmayer and Ross, 1986; Kaban et al., 1986; Kreiborg and Aduss, 1986; Ousterhout et al, 1986; Tulasne and Tessier, 1986; Ousterhout and Vargervik, 1987; David and Sheen, 1990) and more recently by two dimensional CT (Posnick et al., 1993).

Using the method and experimental standard data described in Chapter 3 of this manuscript, CT analysis was undertaken to provide further information on the craniofacial proportions following surgery. In particular, the pathology of the patient and the region undergoing surgery were analysed. The distance of movement of the surgical region was determined from the post-operative CT scan and the relationship of this new position was compared with the experimental standard data.

This study represents the development of a new method of morphometric analysis of surgery utilising 3D CT reconstructions. The accuracy and the limitations of the method are determined. The analysis aims to provide insights into the pathology and surgical manipulation for a greater understanding of the complex deformity.

4.2 Materials

4.2.1 Patient Selection

Five of the 8 patients whose craniofacial morphology was measured in Chapter 3, had corrective surgery with post-operative CT scans, enabling analysis of the operative procedures. A fronto-orbital advance had been performed in 3 patients (Patients SH, JS, IP). Another patient (Patient LW) had an extended fronto-orbital advance and a 15 year old male (Patient HC) had analysis of a fronto-facial advance (Figures 3.2, 3.3, 3.4, 3.5 and 3.7).

The other 3 patients were not suitable for analysis. The post-operative CT scan for Patient RN was performed at age 10 months while the pre-operative scan was performed at 1 month and these were not considered comparable due to the growth changes during this time period (Figure 3.1). Patient AY had had no surgery due to a mild degree of deformity and Patient TS did not have a satisfactory post-operative CT scan (Figures 3.6 and 3.8). Details of the patients and the surgery performed are shown in Table 4.1.

Table 4.1 Details of 5 Patients with Crouzon Syndrome undergoing Surgery

				Ages		
Category	**Name**	**Sex**	**Surgery**	**Age at CT scan**	**Surgery**	**Post-op CT scan**
6 months	SH	F	FOA	5 months	7 months	8 months
2 years	JS	F	FOA	21 months	21 months	22 months
2 years	IP	M	FOA	21 months	21 months	22 months
6 years	LW	M	Extended FOA	5.5 years	5.7 years	6 years
Adult	HC	M	FFA	15 years	15 years	15 years

There was inadequate CT data available for long term follow up. This was relevant in the adult patient studied where degree of relapse and long term outcome could not be fully assessed. In children and especially in infants assessment of long term follow up may be confounded by growth. Despite these difficulties the assessment of surgery in this study provides immediate information about the surgery performed and allows analysis of whether the surgical aim was achieved in the short term.

4.2.2 Experimental Standard

The experimental standard used in Chapter 3 was utilised for comparison with the pre- and post-operative positions.

4.3 Method

4.3.1 CT Scan Protocols and Reconstructions

The pre- and post-operative CT scans and the experimental standard CT scans were performed according to the protocols outlined in Chapter 3 (Sections 3.3.1 CT Scan Protocols, 3.3.2 3D CT Scan Reconstruction and Interpretation).

4.3.2 Definition of Surgical Units

The bony structure of the region undergoing surgery is represented by the relevant landmarks and lines drawn between the landmarks. This diagrammatic representation is termed the "surgical unit" and are described in the following Sections 4.3.2.1-3 and in Figures 4.1-3.

4.3.2.1 Fronto-orbital Advance

The fronto-orbital advance entails a forward shift of the frontal bone with part of the ethmoid. The aim is to gain a forward advance of between 1-2 cm, thereby releasing the cranial sutures and providing protection for the globes. This is usually in 2 pieces: the frontal bone plate and the fronto-orbital bar (the supra-orbital ridges). Part of the nasal bones, the ethmoid, the zygomatic bone and their relevant sutures may be involved in the surgical cuts to a greater or lesser extent. The area involved cannot be simply described using the previous landmark definitions from Chapter 3. In order to compare the pre- and post-operative structures,

landmarks were identified which could be seen on both pre- and post-operative images and were representative of the surgery performed. It is difficult to visualise the calvarial landmarks of the frontal bone fully, due to fusion of the sutures at the fronto-zygomatic, fronto-sphenoidal and fronto-parietal regions and this region was excluded in this study. However, the supra-orbital ridge has readily reproducible landmarks on pre- and post-operative CT scans and also on the normal standards. A comparison of the position of these landmarks also provides the best guide to the functional success of the operation as the surgical movement of the supraorbital ridge aims to cover the proptosed globes and provide room for forward brain expansion and growth. The fronto-orbital bar was used as the bony component representing the fronto-orbital advance. Landmarks on this area are defined and shown in Figure 4.1. Lines were drawn between the landmarks to provide an outline of the bone component to enable visualisation of the surgical unit.

During surgery remodelling of the shape of the fronto-orbital bar occurs. At operation, the frontal bar is divided in the middle and in the region of the lateral corner of the supra-orbital rim. It is rejoined with a more obtuse angle, centrally and a more acute angle, laterally. This brings the lateral segments forward to a greater extent than the central parts. A change in shape is therefore expected in the post-operative surgical unit.

4.3.2.2 Extended Fronto-orbital Advance

The extended fronto-orbital advance is defined, for the purposes of this project, as the surgical advancement of the supra-orbital ridge, the frontal bone and also the bodies of the zygomatic bones. This procedure has the effect of advancing the lateral orbital wall and the malar eminence, along with the supra-orbital region. The aim is similar to that of the fronto orbital advance in gaining a forward advance of between 1 - 2 cm. The fronto-orbital bar and the zygomatic bones combine to make the bone component of the extended fronto-orbital advance. The frontal bone plate has again been excluded due to difficult calvarial landmark identification. The landmarks for this surgical unit are defined and shown in Figure 4.2.

4.3.2.3 Le Fort III Advance

The Le Fort III advance is an advancement of the maxilla and upper dentition at the level of the orbits and the ethmoid. For the analysis of the Le Fort III advance, landmarks from the facade of the maxilla were recorded to represent the surgical unit. The landmarks are defined and shown in Figures 4.3a and 4.3b. One patient (Patient HC), underwent a fronto-facial advance derived from the addition of the landmarks for the Le Fort III advance to those of the fronto-orbital advance. This procedure was planned using standard orthognathic techniques with an anterior shift at the occlusal level of 14 mm.

4.3.3 Alignment of Surgical Units

Alignment of the surgical units on each other for comparison, required the definition of landmarks which were not involved in the surgical process. These were found most readily in the cranial base.

4.3.3.1 Cranial Base Unit

The cranial base landmarks selected for alignment were readily identifiable points which were equally spaced across the cranial base. These include the foramen magnum, the foramen ovale, the mastoid process, the porion and auriculare points. The landmarks for alignment for the cranial base alignment unit are defined in Figures 4.4a and 4.4b. Virtually any alignment points selected are involved in the pathology in Crouzon syndrome, as demonstrated in Chapter 3. The cranial base points were chosen as they were readily identifiable, remote from the surgical location and therefore not affected by it. They do, however, reflect the cranial base pathology. Compared with the experimental standard, small discrepancies at the level of the cranial base may manifest themselves as larger, more extreme changes, when the alignment is used as the reference for the anterior craniofacial surgical units. This limitation exists whatever landmarks are used for comparison due to the generalised pathology of the craniofacial skeleton in Crouzon syndrome.

4.3.4 ` Landmark Identification and Accuracy

The method and the determination of the accuracy of the landmark identification for the surgical units is the same as that used in Chapter 3 (Sections 3.3.6 Method of Landmark Identification, 3.3.7 Landmark Accuracy). Landmark accuracy for all points is listed in Appendix 1.

4.3.5 Analysis of CT Data

For each of the five patients, landmarks representing the relevant surgical unit for the patient, along with the cranial base alignment unit were recorded from the pre- and post-operative CT scans and from the CT scans of age-matched normal skulls (as discussed in Chapter 3).

A longitudinal study, in three parts, was made by comparing:

a) The pre-operative shape and position of the surgical unit of the patient with that of the corresponding surgical unit of the averaged normal skulls (experimental standard). This analysis provided additional visual and measurement data on the pathological morphology of Crouzon syndrome, described in Chapter 3.

b) The pre-operative shape and position of the surgical unit with the post-operative surgical unit. This assessed the direction and maintenance of the surgical manoeuvre.

c) The post-operative shape and position of the surgical unit with the surgical unit of the experimental standard. This was to determine whether the surgical manoeuvre had shifted the surgical unit any closer to the ideal structure, as represented by the data for the normal skulls.

4.3.6 Comparison of Surgical Unit Data

The data from the measurement of the landmarks of the six normal control dried skulls were averaged, taking into account the error of landmark identification. This produced 1 set of landmark data which was used in the visual and statistical assessments of the surgical comparisons. The CT scan landmarks of each patient were aligned with those of the relevant experimental standard using the cranial base alignment unit (Figure 4.5). This was performed using the least squares (procrustes method) and repeated median methods of alignment (Rohlf

and Slice, 1990; Bookstein, 1991). Having aligned the skulls on their cranial base units, the surgical units being compared were then viewed which enabled immediate appreciation of surgical shifts. In addition to visualisation of the surgical units (Figures 4.5 - 4.11), the differences between the surgical units was measured.

Measurements were made in 2 ways. Firstly, the distance between the same landmark on each surgical unit was measured with the greater differences representing a greater degree of deformity from either normal or from the pre-operative position. Secondly, registration to "best fit" the two surgical units together was performed, using the least squares and repeated median methods. By performing this function, the averaged or mean translocation for one surgical unit to move and align itself on the other was represented. This translocation analysis has been used as an index of mismatch of the two surgical units under comparison. The registration provides the orientation and translation differences. The rotation matrices are near normal (rotations of only a few degrees). The translations are given in Appendix 3. The vectors of displacement are positive when to the right, anterior or superior. Negative displacement vectors are to the left, posterior or inferior. This analysis was performed for the 3 comparisons that were described in the previous section.

In the first analysis (pre-operative surgical unit vs standard surgical unit) the distances and translation represent the deviation of the pre-operative surgical unit from the standard surgical unit. In the second analysis (pre-operative surgical unit vs post-operative surgical unit) the distances and translation represent the movement of the surgical unit following surgery. In the third analysis (post-operative surgical unit vs standard surgical unit) the distances and translations represent the residual deformity of the surgical unit compared with the standard surgical unit.

Figures 4.1 - 4.4 **Diagrammatic representations of the Surgical Units and Alignment Units showing the Landmarks identified**

Legend for Figure 4.1 Fronto-orbital Advance

g	**glabella:** The most prominent point in the mid-sagittal plane between the eyebrow ridges (see frontal bone).
sorl/sorr	**superior orbitale left/right:** The most superior point on the supra-orbital margin (see frontal bone).
slorsl/slorsr	**supero-lateral orbitale superius left/right:** The same point as the supero-lateral orbitale in the unoperated state ie The intersection of the fronto-zygomatic suture with the lateral orbital rim (almost the intersection of the curve of the supra-orbital rim with the lateral orbital rim (see frontal and zygomatic bone). In the post-operative state the point is annotated as 'superius' to differentiate it from the inferior region which may not have been shifted surgically.
smorl/smorr	**supero-mediale orbitale left/right:** The most superior and medial point on the orbital rim midway between the superior and medial orbitale points.
zfsl/zfsr	**zygo-frontale superius left/right:** The same point as the zygo-frontale in the unoperated state ie the point located at the posterior extremity of the fronto-zygomatic suture (see frontal and zygomatic bone). In the post-operative state the point is annotated as 'superius' to differentiate it from the inferior region which may not have been shifted surgically.

Legend for Figure 4.2 Extended Fronto-orbital Advance

g	**glabella:** The most prominent point in the mid-sagittal plane between the eyebrow ridges (see frontal bone).
ilorl/ilorr	**infero-lateral orbitale left/right:** The point is determined approximately mid-way between the sutures limiting the zygomatic bone or, alternatively, at the intersection of the anterior projection of the maxillary border of the inferior orbital fissure with the lateral orbital rim.
orl/orr	**orbitale left/right:** The most inferior point on the infraorbital margin.
parl/parr	**pre-articulare left/right:** The most superior point on the lower border of the zygomatic arch located anterior to point articular eminence.
sorl/sorr	**superior orbitale left/right:** The most superior point on the supra-orbital margin (see frontal bone).
slorl/slorr	**supero-lateral orbitale left/right:** The intersection of the fronto-zygomatic suture with the lateral orbital rim (almost the intersection of the curve of the supra-orbital rim with the lateral orbital rim.
smorl/smorr	**supero-mediale orbitale left/right:** The most superior and medial point on the orbital rim midway between the superior and medial orbitale points.
zfl/zfr	**zygo-frontale left/right:** The point located at the posterior extremity of the fronto-zygomatic suture.
zmil/zmir	**zygomaxillare inferius left/right:** The lowest point on the external suture between zygomatic and maxillary bones.(in the region of the craniometric landmark, zygomaxillare).
ztl/ztr	**zygo-temporale left/right:** The mid-point of the bony concavity formed between the frontal and temporal processes of the zygomatic bone.

Figure 4.1: **Fronto-orbital Advance**
(anterior aspect)
Surgical Unit

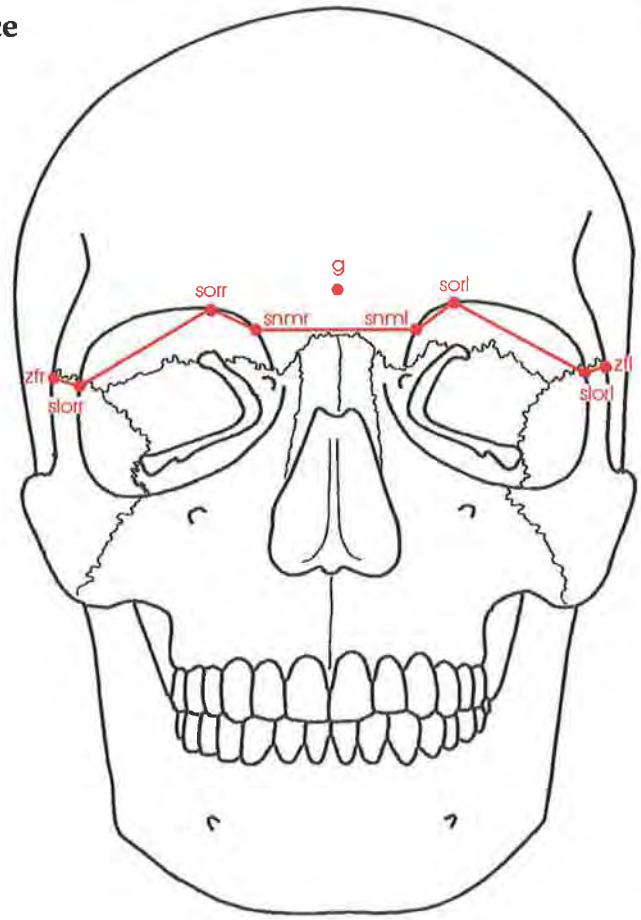

Figure 4.2: **Extended Fronto-orbital Advance**
(anterior aspect)
Surgical Unit

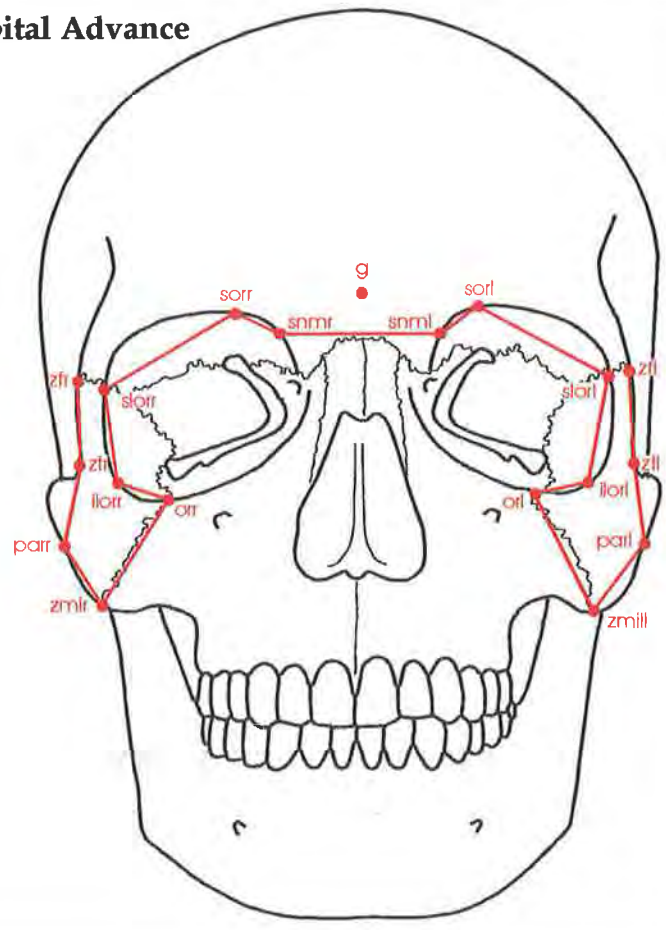

Legend for Figure 4.3 Le Fort III Advance

all/alr **alare left/right:** The most lateral point on the anterior nasal aperture.

ans **anterior nasal spine:** The apex of the anterior nasal spine. (Also known as spinal point (sp) or acanthion (ac)).

csl/csr **canine superius left/right:** The tip of the buccal cusp of the maxillary canine.

dmsl/dmsr **disto-molare superius left/right:** The disto-buccal cusp of the maxillary first molar.

ecsl/ecsr **ecto-canine superius left/right:** The most anterior point on the alveolar ridge, opposite the centre of the maxillary canine.

eicsl/eicsr **ecto-incision central superius left/right:** The most anterior point on the alveolar ridge, opposite the centre of the maxillary central incisor.

em1sl/em1sr **ectomolare 1st superius left/right:** The most lateral point on the alveolar ridge, opposite the centre of the maxillary first molar.

gpfl/gpfr **greater palatine foramen left/right:** The centre of the greater palatine foramen.

isl/isr **incision superius left/right :** The mid-point of the incisal edge of the maxillary central incisor.

ilorl/ilorr **infero-lateral orbitale left/right:** The point is determined approximately mid-way between the sutures limiting the zygomatic bone or, alternatively, at the intersection of the anterior projection of the maxillary border of the inferior orbital fissure with the lateral orbital rim.

lorl/lorr **lateral orbitale left/right:** The most lateral point on the orbital rim.

mxtl/mxtr **maxillary tuberosity left/right:** The most postero-inferior point in the midline of the maxillary tuberosity.

morl/morr **medial orbitale left/right:** The most medial point on the orbital margin in the region of the fronto-lacrimal suture. (Located near the craniometric point Dacryon).

mm1sl/mm1sr **medio-molare 1st superius left/right:** The tip of the medio-buccal cusp of the maxillary first molar.

na **nasale:** The tip of the nasal bone.

n **nasion:** The most anterior point of the frontonasal suture. (If suture not clearly identified then the deepest point on the nasal notch can be substituted in the midline.)

nlil/nlir **naso-lacrimal inferius left/right:** The most antero-inferior point on the margin of the naso-lacrimal groove as it exits the orbit (usually this point is located at the small spicule of bone covering the lateral wall of the naso-lacrimal groove and the inferior orbital rim).

orl/orr **orbitale left/right:** The most inferior point on the infraorbital margin.

pns **posterior nasal spine:** The apex of the posterior nasal spine.

pr **prosthion:** The most antero-inferior point on the maxillary alveolar margin in the mid-sagittal plane.

ss **subspinale:** The most posterior point on the anterior contour of the maxillary alveolar process in the mid-sagittal plane. (Also known as Down's Point A).

snml/snmr **superior naso-maxillare left/right:** The most superior point on the naso-maxillary suture.

slorl/slorr **supero-lateral orbitale left/right:** The intersection of the fronto-zygomatic suture with the lateral orbital rim (almost the intersection of the curve of the supra-orbital rim with the lateral orbital rim.

Figure 4.3(a): **Le Fort III Advance**
(anterior aspect)
Surgical Unit

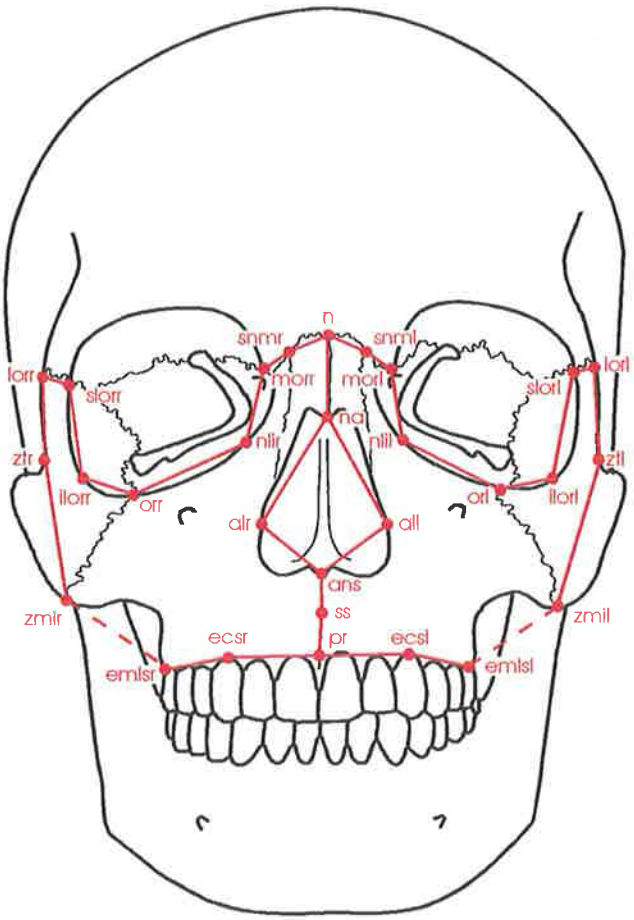

Figure 4.3(b): **Le Fort III Advance**
(left lateral aspect)
Surgical Unit

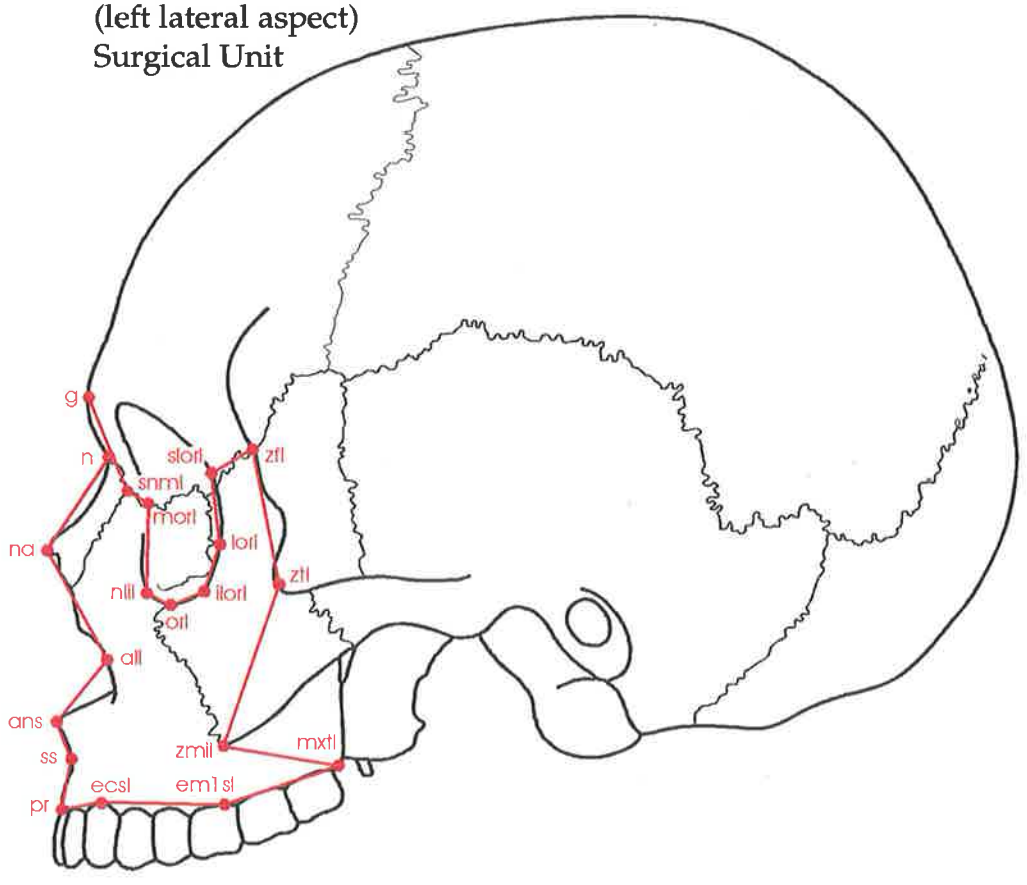

Legend for Figure 4.3 Le Fort III Advance (continued)

zfl/zfr	**zygo-frontale left/right:** The point located at the posterior extremity of the fronto-zygomatic suture.
zmil/zmir	**zygomaxillare inferius left/right:** The lowest point on the external suture between zygomatic and maxillary bones.(in the region of the craniometric landmark, zygomaxillare).
ztl/ztr	**zygo-temporale left/right:** The mid-point of the bony concavity formed between the frontal and temporal processes of the zygomatic bone.

Legend for Figure 4.4 Cranial Base Alignment Unit

acl/acr	**anterior clinoid left/right:** The most posterior point on the anterior clinoid of the lesser wing of the sphenoid bone. In the cases of bridging between the anterior and posterior clinoid the point is determined at the anterior prominence mid-way along the bridge.
aul/aur	**auriculare left/right:** The most superior point on the root of the zygomatic arch nearest to craniometric point porion.
ba	**basion:** The mid-sagittal point on the anterior margin of the foramen magnum (determined as the point of maximum convexity on the clivus of the skull at the anterior margin of the foramen magnum).
pol/por	**external auditory meatus superius (ie porion) left/right:** The most superior point on the margin of the external auditory meatus.
fmll/fmlr	**foramen magnum lateralis left/right:** The most lateral point on the margin of the foramen magnum.
foil/foir	**foramen in ovale left/right:** The mid point of the internal opening of the foramen ovale.
fool/foor	**foramen out ovale left/right:** The mid point of the external opening of the foramen ovale, at the level of the skull base.
mal/mar	**mastoidale left/right:** The most inferior point on the mastoid process.
o	**opisthion:** The mid-sagittal point on the posterior margin of the foramen magnum.
pcl/pcr	**posterior clinoid left/right:** The most superior and lateral point on the posterior clinoid.
s	**sella:** The centre of the sella turcica.

Figure 4.4(a): **Cranial Base Alignment** (superior cranial base) Landmarks

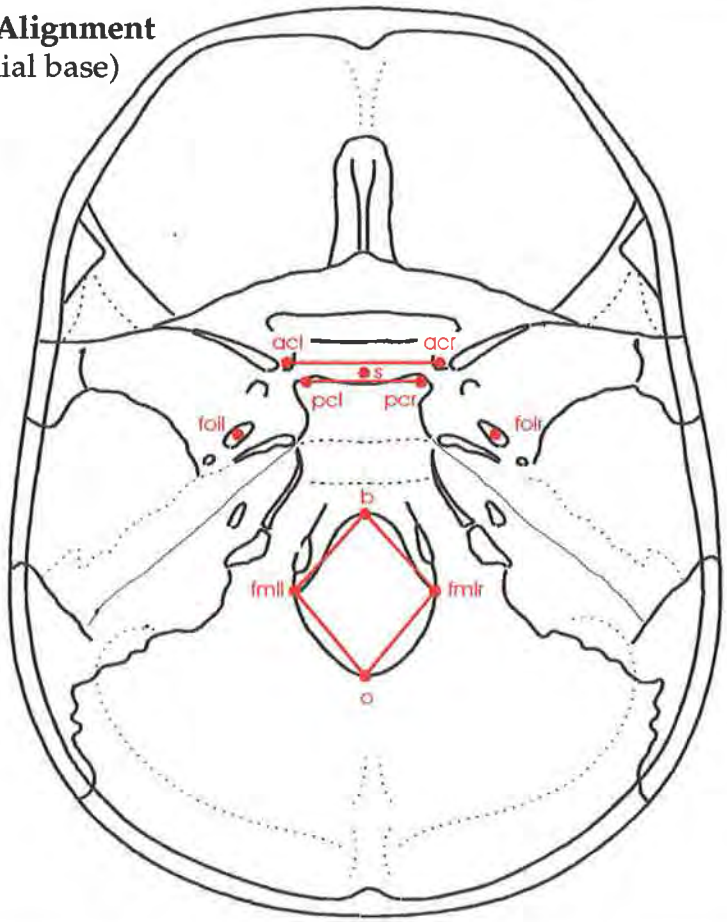

Figure 4.4(b): **Cranial Base Alignment** (inferior cranial base) Landmarks

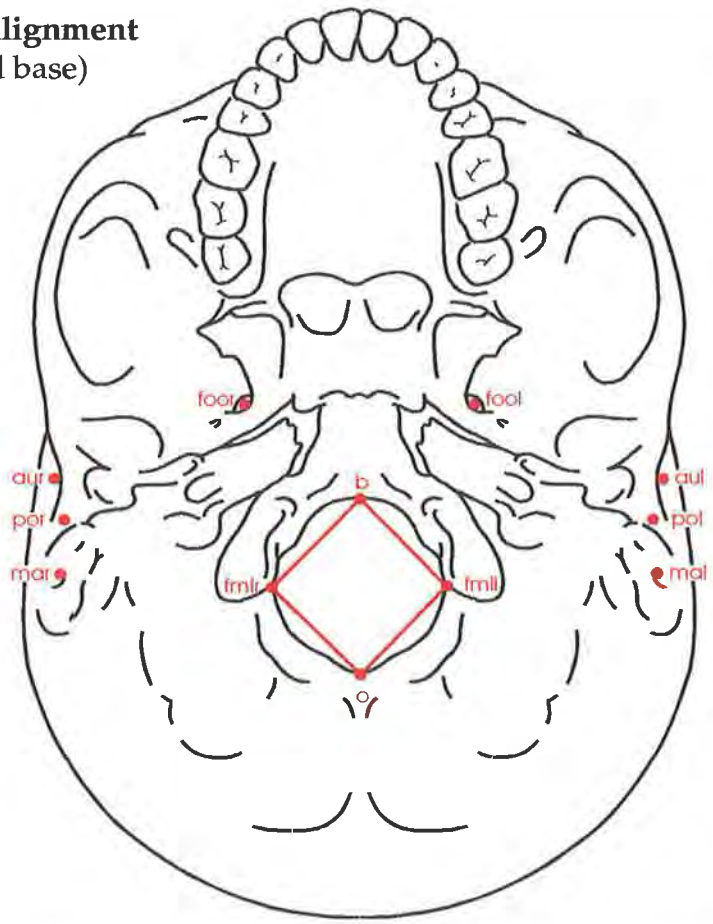

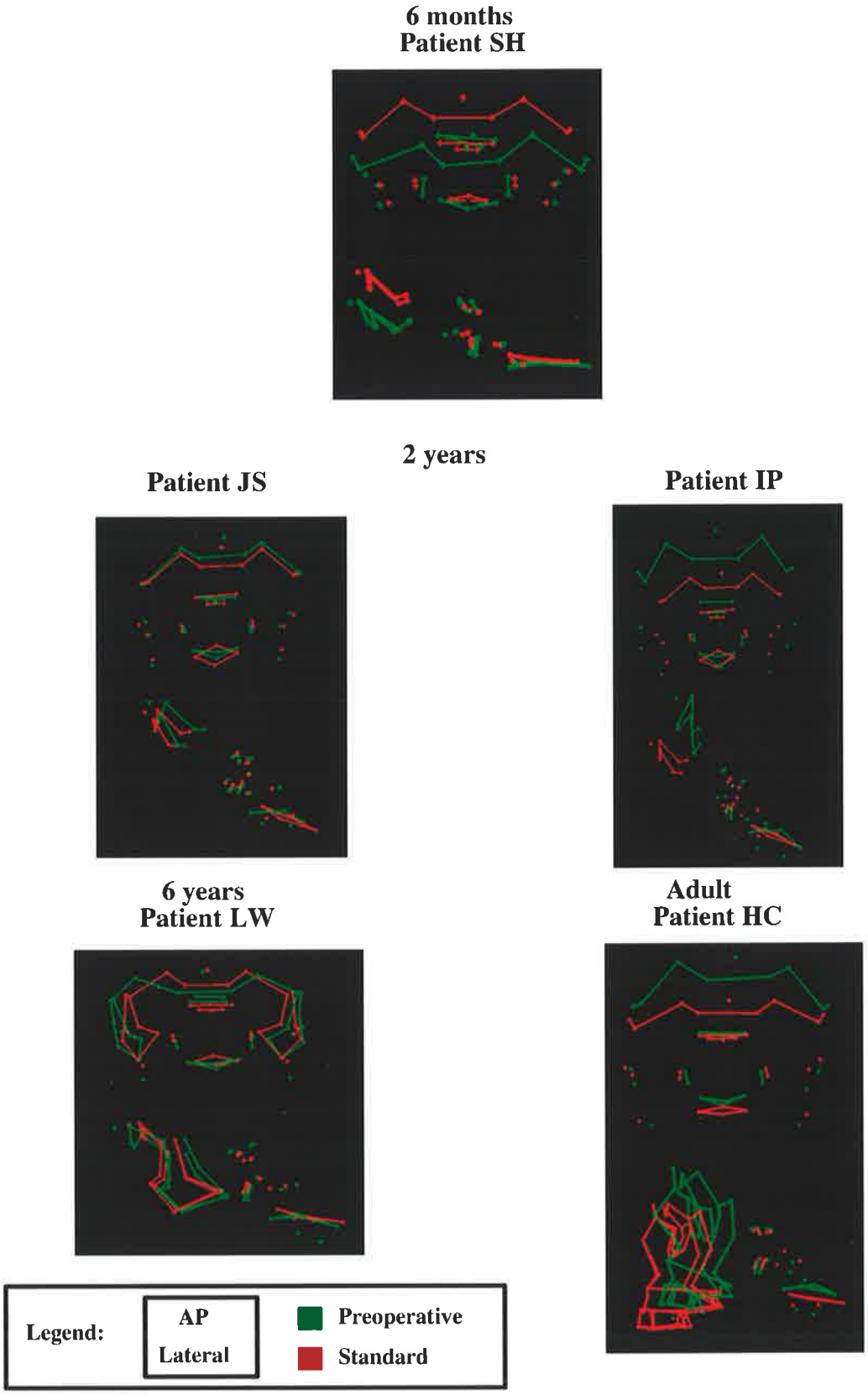

Figure 4.5 Cranial base alignment and surgical units for five patients with Crouzon syndrome.
Alignment performed on cranial base unit showing relative position of pre-operative (Crouzon) surgical unit (green) and experimental standard unit (red).

4.4 Results

4.4.1 Analysis of the Pre- and Post-operative Morphology of Patient SH

4.4.1.1 Alignment of the Cranial Base Unit for Patient SH

For this patient, the post-operative scan was taken at 8 months of age, approximately 1 month after the surgery and 3 months after the pre-operative CT scan (Figure 4.5). This represents closer age-matching than for patient RN in the same age group.

4.4.1.2 Comparison of the Surgical Units for Patient SH

Pre-operative Surgical Unit vs Standard Surgical Unit (Figure 4.6a)

The cranial base angle in this patient was significantly reduced compared with the experimental standard (Figure 3.5). Alignment of the surgical units using the cranial base resulted in an inferior position of the surgical unit for Patient SH. Measurement distances between corresponding surgical unit points were between 8.0 mm and 15.1 mm (Appendix 3). The index of mismatch had a magnitude of 11.8 mm where the pre-operative surgical unit was displaced 2.9 mm to the left, 0.3 mm anteriorly and 11.4 mm inferiorly from the standard surgical unit.

Pre-operative Surgical Unit vs Post-operative Surgical Unit (Figure 4.6b)

As seen on the lateral view and view from above, the post-operative surgical unit was advanced anteriorly a short distance only, relative to the pre-operative position. Measurements of between 4.7 mm and 13.8 mm were recorded, but the index of mismatch had a magnitude of 8.5 mm and was predominantly due to a superior displacement of 7.6 mm (Appendix 3). There was a 3.3 mm anterior displacement and a 1.5 mm displacement to the right. The lateral points were moved further than the medial points due to intra-operative bone reshaping. Due to the short delay between pre- and post-operative CT scans, the cranial base alignment units were very similar.

Post-operative Surgical Unit vs Standard Surgical Unit (Figure 4.6c)

The post-operative surgical unit was anterior to the standard surgical unit by between 8.2 mm and 12.3 mm with a mismatch of magnitude 10.0 mm (Appendix 3). This was comprised of an anterior displacement of 9.3 mm with 3.7 mm to the right and 0.1 mm superiorly. Based on the images seen here, the surgical manoeuvre appeared to have advanced the supra-orbital bar into a satisfactory position. The superior surgical advancement compensated for the reduced cranial base angle.

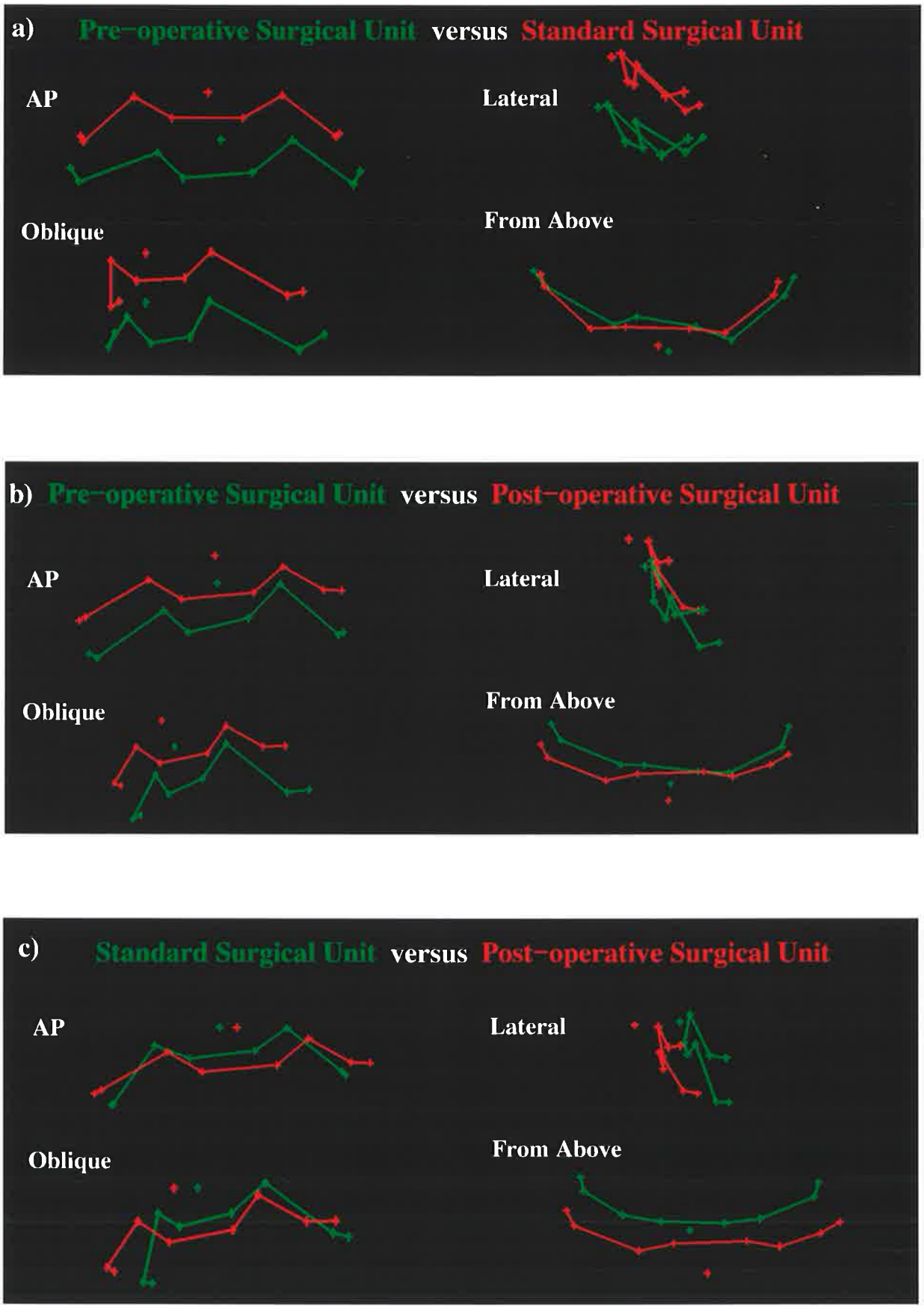

Figure 4.6 Comparison of Surgical Units for Fronto-Orbital Advance in Patient SH.

4.4.1.3 Summary of the Surgical Findings for Patient SH

The analysis in this patient was more successful than for Patient RN as the pre- and post-operative CT scans were performed temporally closer together. The size of the patient's pre- and post-operative surgical units were close to the experimental standard, tending to improve the comparison. The relationship between the cranial base pathology and the surgical unit resulted in the craniofacial facade being positioned below the experimental standard. However, surgery shifted the facade up (and forward) and could therefore be considered to have resulted in a more favourable anatomical result, although not necessarily clinically apparent. The superior displacement of the surgical unit may have been due to operative positioning of the surgical unit, the stability of the fixation method and/or the effects of scalp closure. Surgery altered only the facade of the craniofacial skeleton. The cranial base deformity persists and may further distort growth.

4.4.2 Analysis of the Pre- and Post-operative Morphology of Patient JS

4.4.4.1 Alignment of the Cranial Base Unit for Patient JS

The alignment of the cranial base in this patient was good with respect to both size and position (Figure 4.5).

4.4.2.2 Comparison of the Surgical Units for Patient JS

Pre-operative Surgical Unit vs Standard Surgical Unit (Figure 4.7a)

The pre-operative surgical unit lay posterior and slightly superior to the standard surgical unit. Distances between the landmarks of the surgical units of 4.9 mm and 7.4 mm were recorded (Appendix 3). The index of mismatch had a magnitude of 5.1 mm, where the pre-operative surgical unit was displaced by 0.2 mm to the left, 4.3 mm posteriorly and 2.7 mm superiorly.

Pre-operative Surgical Unit vs Post-operative Surgical Unit (Figure 4.7b)

The position of the post-operative surgical unit was anterior to the pre-operative position. A slight superior displacement of the supra-orbital ridge was also seen. Measurements of between 7.1 mm and 18.6 mm were recorded (Appendix 3). The index of mismatch had a magnitude of 10.5 mm, where the post-operative surgical unit was displaced by 0.7 mm to the right, 10.0 mm anteriorly and 3.0 mm superiorly.

Post-operative Surgical Unit vs Standard Surgical Unit (Figure 4.7c)

The post-operative surgical unit lay anterior and superior to the normal or standard surgical unit. This represented an improvement from the pre-operative position where the supra-orbital bar was behind the standard surgical unit. Measurements were between 6.3 mm and 13.3 mm, with an index of mismatch of 7.8 mm (Appendix 3), where the post-operative surgical unit was displaced by 0.7 mm to the right, 6.5 mm anteriorly and 4.2 mm superiorly from the standard surgical unit.

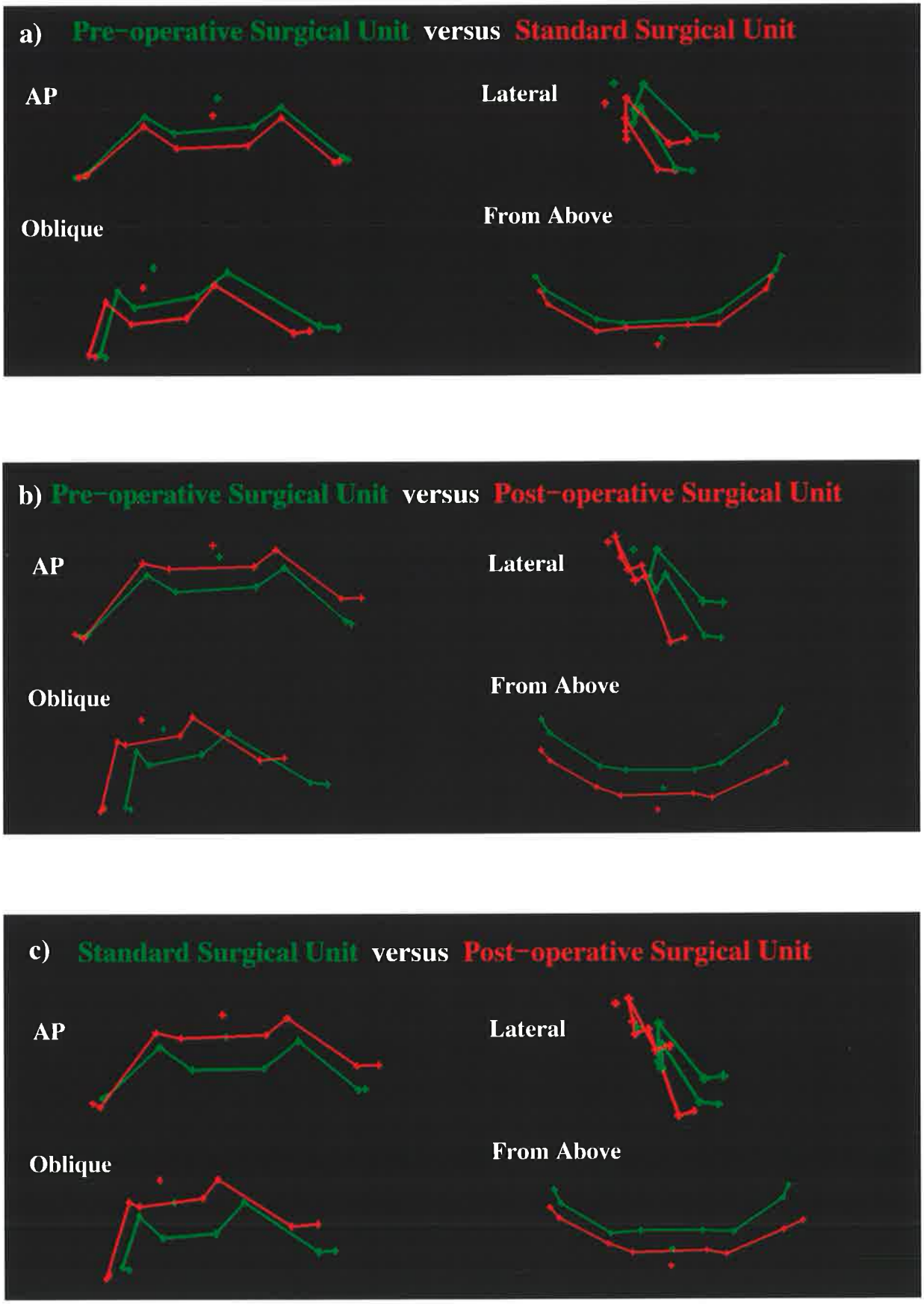

Figure 4.7 Comparison of Surgical Units for Fronto-Orbital Advance in Patient JS.

4.4.2.3 Summary of the Surgical Findings for Patient JS

The posterior position of the pre-operative surgical unit was advanced by surgery beyond the standard surgical unit. This was at the expense of some superior displacement. A satisfactory overcorrection was achieved and was demonstrated in the post-operative photographs (Figure 3.3).

The discrepancies seen in the post-operative positioning demonstrate several points. The fronto-orbital advancement, while it advances the supra-orbital ridge, may also raise it up superiorly, perhaps worsening the degree of superior displacement of this region, compared with the normal. In addition, the lateral wings of the supra-orbital bar are advanced further forward than the medial part, that is, the supra-orbital bar is divided and the lateral elements swung forward. In effect, this over-corrects the situation. In the pre-operative versus the standard figure, the shapes of the supra-orbital bars can be seen to be relatively similar, particularly when viewed from above. When the post-operative position is compared with the standard, the lateral elements are lateral and more anterior as a result of the surgical manoeuvre. Clinically, this structural change results in squaring of the frontal region. This feature was also seen in the pre- and post-operative comparison where the anterior movement was recorded. Fixation was maintained with miniplates and screws and more closely matches the desired anterior translocation of 1-2 cm.

4.4.3 Analysis of the Pre- and Post-operative Morphology of Patient IP

4.4.3.1 Alignment of the Cranial Base Unit for Patient IP

This patient had severe calvarial and cranial base deformities and the cranial base angle was increased. Subsequently, the alignment of the cranial base posteriorly was reasonable, but anteriorly, the increased cranial base angle resulted in the anterior craniofacial skeleton being well superior to the standard surgical unit (Figure 4.5).

4.4.3.2 Comparison of the Surgical Units for Patient IP

Pre-operative Surgical Unit vs Standard Surgical Unit (Figure 4.8a)

As mentioned previously, the pre-operative surgical unit lay superior to the standard surgical unit. It was also posterior to the experimental standard. The measurements between the landmarks were between 18.0 mm and 34.5 mm (Appendix 3). The index of mismatch had a magnitude of 24.5 mm where the pre-operative surgical unit was displaced by 2.9 mm to the right, 12.2 mm posteriorly and 21.0 mm superiorly.

Pre-operative Surgical Unit vs Post-operative Surgical Unit (Figure 4.8b)

The pre-operative surgical unit had been advanced a significant distance anteriorly to a position represented by the post-operative surgical unit. Measurements between 19.7 mm up to 27.4 mm were recorded (Appendix 3). The index of mismatch had a magnitude of 22.6 mm and was made up of a displacement from the pre-operative to post-operative position of 3.8 mm to the left, 18.1 mm anteriorly and 13.0 mm superiorly.

Post-operative Surgical Unit vs Standard Surgical Unit (Figure 4.8c)

The post-operative surgical unit was superior and anterior to the standard surgical unit. It was also significantly larger than the standard surgical unit. Measurements between the landmarks were between 33.0 mm and 37.3 mm (Appendix 3). The index of mismatch had a magnitude of an average of 33.6 mm and was made up of a displacement of the post-operative surgical unit from the standard surgical unit of 0.6 mm to the left, 7.5 mm anteriorly and 32.8 mm superiorly.

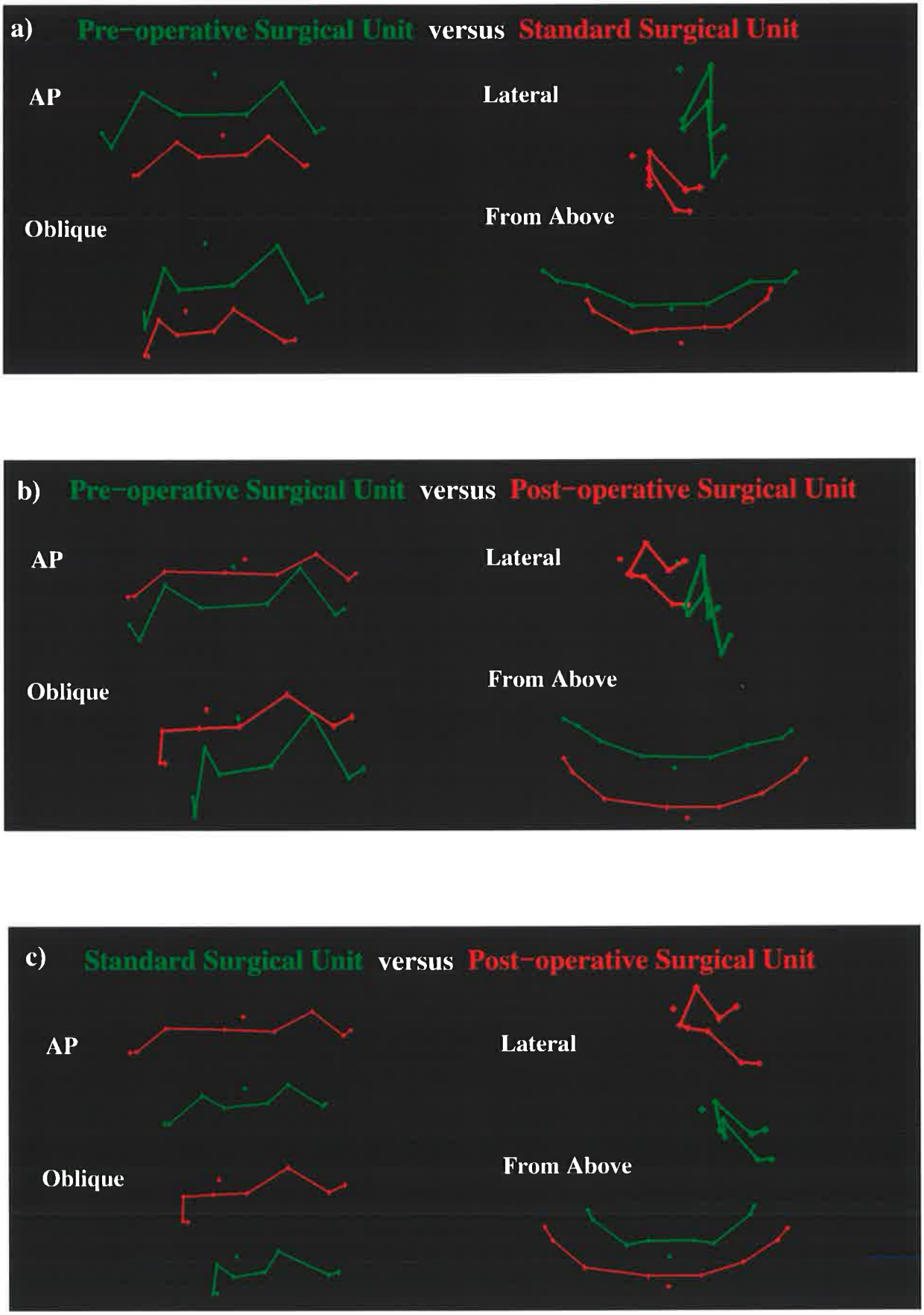

Figure 4.8 Comparison of Surgical Units forFronto-Orbital Advance in Patient IP.

4.4.3.3 Summary of the Surgical Findings for Patient IP

There was gross deformity of the craniofacial skeleton in Patient IP. The supra-orbital region was significantly enlarged and lay superior and posterior to the experimental standard. This region was advanced by surgery but the underlying cranial base pathology was not corrected and considerable deformity remained. Clinically, correction of raised intracranial pressure and protection for the globes was achieved (Figure 3.4). Release of the raised intracranial pressure may also have helped to maintain the anterior position of the frontal advance, although the extent of this effect cannot be quantified.

4.4.4 Analysis of the Pre- and Post-operative Morphology of Patient LW

4.4.4.1 Alignment of the Cranial Base Unit for Patient LW

Cranial base unit alignment was satisfactory (Figure 4.5) with good correlation in the region of the foramen magnum and sella and other points. However, the cranial base angle was reduced, which was demonstrated by the relative anterior position of the basion, compared with the standard. Due to the comparable alignment of the remaining points of the cranial base unit, the projections of the pre-operative surgical unit and standard surgical unit showed close alignment medially, in the region of the nasion. This suggests that the pathology in this region was less severe and is confirmed clinically when viewing the prominent nasion in this patient (Figure 3.5).

4.4.4.2 Comparison of the Surgical Units for Patient LW

Pre-operative Surgical Unit vs Standard Surgical Unit (Figure 4.9a)

The pre-operative surgical unit was anterior to the standard unit in the midline, however posterior to the standard surgical unit laterally. Measurements between the landmarks ranged between 3.6 mm and 16.2 mm (Appendix 3). The forehead was broader and slightly larger than in the control. Despite the often large measurements, the index of mismatch had a magnitude of 1.6 mm where the pre-operative surgical unit was displaced by 0.5 mm to the right, 1.3 mm posteriorly and 0.7 mm inferiorly. Despite achieving a best fit by a translocation of only 1.6 mm, there were many points which were large distances from the corresponding point in the control but which could not be accommodated due to the differing shapes of the structure.

Pre-operative Surgical Unit vs Post-operative Surgical Unit (Figure 4.9b)

A comparison of the position of the post-operative surgical unit with the pre-operative position highlighted the anterior shift of the supra-orbital ridge with a greater anterior shift of the extended part of the fronto-orbital advance, that is, the zygomatic bodies. The distances between landmarks were 1.6 mm for the glabella and up to 20.5 mm for the pre-articulare point on the right. The majority of the measurements were between 3 and 10 mm with the greater distances occurring laterally (Appendix 3). The surgical objective of advancing the lateral elements a greater distance anteriorly was achieved. However, the index of mismatch had a magnitude of 6.1 mm with a 0.8 mm displacement to the right, 5.3 mm anteriorly and 3.0 mm superiorly.

Post-operative Surgical Unit vs Standard Surgical Unit (Figure 4.9c)

The post-operative surgical unit was anterior to the standard surgical unit, and was seen best on the lateral view and in the view from above in Figure 4.9c. The lateral orbital walls and the zygomatic bodies were advanced some distance anteriorly to the standard surgical unit. The distances between the landmarks were between 5.4 mm and 16.1 mm (Appendix 3). The index of mismatch had a magnitude of 4.2 mm (1.8 mm to the right, 3.5 mm anteriorly and 1.4 mm superiorly). There appeared to be a discrepancy due to the significant change in shape of the surgical units so that matching was not as complete as it might otherwise be.

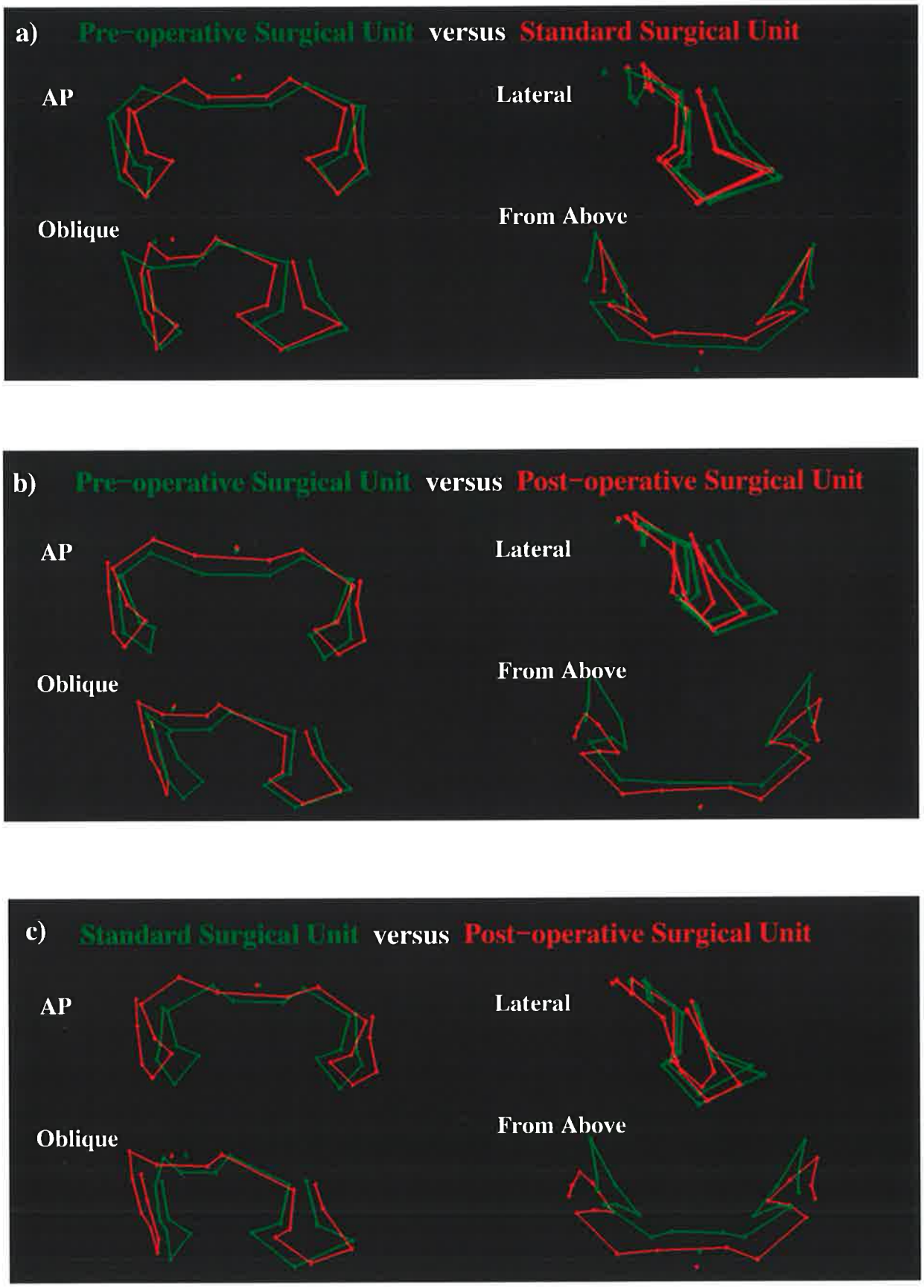

Figure 4.9 Comparison of Surgical Units for Extended Fronto-Orbital Advance in Patient LW.

4.4.4.3 Summary of the Surgical Findings for Patient LW

The pre-operative position of the surgical unit of Patient LW was relatively similar to the position of the standard. Clinically, the relatively normal anterior position of the supra-orbital ridge was demonstrated medially (Figure 3.5), with a more pronounced deficiency seen in the lateral orbital wall. The lateral orbital wall of Patient LW lies at the level of, or just posterior to, the lateral orbital wall of the standard (Figure 4.9a). In this situation, proptosis may have been a result of reduced orbital volume rather than due to deficient anterior growth of the bony orbital rim. At surgery, advancement of the fronto-orbital bar with osteotomy and overcorrection of the lateral elements, was performed.

Plate fixation was also used in this patient, but appeared to have held the lateral elements advanced at the expense of the medial part of the supra-orbital ridge. While the lateral orbital wall and body of the zygomas were brought forward during surgery, the post-operative position demonstrates they were also swung outwards. This resulted in the effect of widening the face with a "less than optimal" result. There are 2 ways to prevent this. Firstly, advancing the zygomatic bodies and lateral orbital walls to the same degree as the supra-orbital ridge would lessen this effect. Alternatively, when the zygomatic bodies are advanced forward they are brought medially as well as anteriorly. Resection of part of the supra-orbital bar and a medial translocation of the zygomatic bodies would readily accommodate this manoeuvre.

4.4.5 Analysis of the Pre- and Post-operative Morphology of Patient HC

4.4.5.1 Alignment of the Cranial Base Unit for Patient HC

The cranial base angle of Patient HC was more obtuse than the standard and had the effect of raising the position of the anterior craniofacial skeleton relative to the standard (Figure 4.5). The pre-operative position of the basion lay anterior to the standard cranial base position. The obtuse cranial base resulted in even further superior movement of the nasion.

4.4.5.2 Comparison of the Surgical Units for Patient HC

Pre-operative Surgical Unit vs Standard Surgical Unit (Figure 4.10a)

The pre-operative surgical unit lay superior to the standard. It also lay in a significantly posterior position and accounted for the class III occlusion in this patient. Measurements varied greatly from 7.6 mm to 27.9 mm (Appendix 3). The index of mismatch between the pre-operative and standard surgical units had a magnitude of 17.3 mm and this was made up of displacement of the pre-operative surgical unit 2.1 mm to the left, 12.4 mm posteriorly and 11.9 mm superiorly, relative to the surgical standard.

Pre-operative Surgical Unit vs Post-operative Surgical Unit (Figure 4.10b)

Significant advancement of the post-operative surgical unit compared with the pre-operative unit was found (best demonstrated in the lateral and superior views). Of note, the lateral view of the surgical shift produced images similar to the cephalometric analyses readily derived from plain radiographic data. Measurements of the surgical advance ranged from 12.6 mm to 22.1 mm (Appendix 3). The index of mismatch was 16.5 mm and was made up of a displacement of 2.3 mm to the left, 15.9 mm anteriorly and 4.0 mm superiorly.

Post-operative Surgical Unit vs Standard Surgical Unit (Figure 4.10c)

The position of the post-operative surgical unit was again distorted by the effect of the cranial base alignment causing it to be positioned superior to the standard. At the occlusal level, the distances between the surgical units were shorter than at the level of the superior orbital ridge. Lengthening of the anterior face during surgery would account for this. The lengthening may be intentional to assist the occlusal relationship, or may be the inadvertent result of surgical osteotomies and manipulation. Measurements made between corresponding landmarks ranged from 8.7 mm to 31.1 mm (Appendix 3). The index of mismatch had a magnitude of 17.2 mm and consisted predominantly of a superior displacement of the post-operative surgical unit of 15.7 mm with displacement 3.2 mm anterior and 6.4 mm to the left.

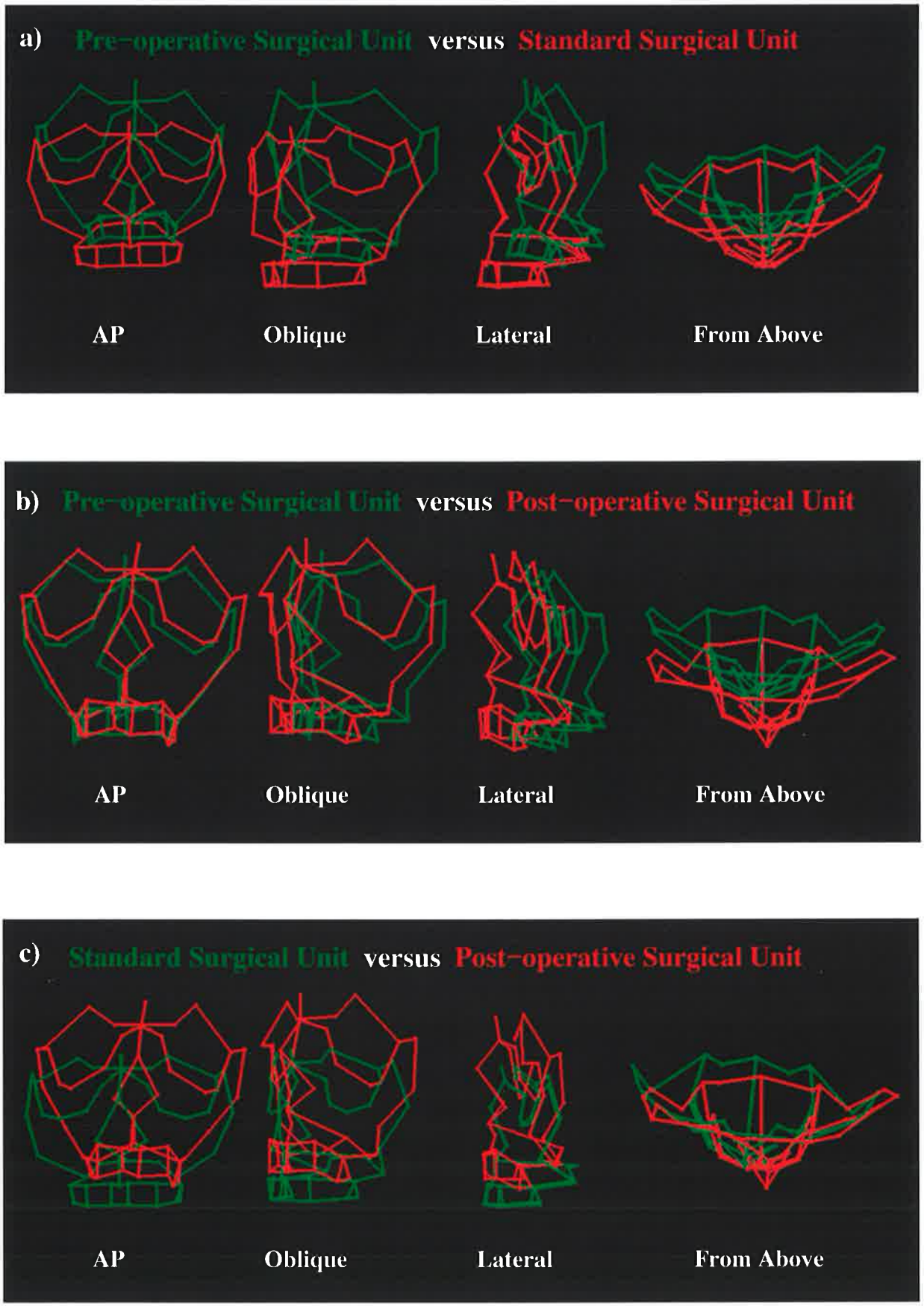

Figure 4.10 Comparison of Surgical Units for Fronto-Facial Advance in Patient HC.

4.4.5.3 Summary of the Surgical Findings for Patient HC

Analysis of the data relevant to the fronto-facial advance, in this patient, provided information in 3 main areas. Firstly, variation in the cranial base angle altered the positioning of the anterior craniofacial skeleton. In anterior translocation orthognathic surgery this effect persists in the post-operative and standard surgical unit comparisons. Secondly, the surgical shift was well demonstrated using this method with graphic pictures showing anterior displacement. Measurement analysis of the occlusal relationship had not been performed but was seen on the clinical images and CT scans (Figure 3.7). The final feature to emerge was the increase in the facial height which can be appreciated on the wire frame images. Variation from the standard surgical unit at the supra-orbital ridge level was greater than the variation at the occlusal level and this was due to the increase in facial height. Given the premorbid increased facial heights in most patients with Crouzon syndrome this surgical alteration should be considered unfavourable relative to the standard.

4.5 Discussion of the Surgical Analysis

Analysis of the comparisons in 3D between the pre-operative, post-operative and standard surgical units in the patients undergoing corrective surgery of Crouzon syndrome demonstrated many new features relevant to the underlying pathology, the type of surgery performed and the effectiveness of this surgery with respect to overall patient appearance (Table 4.2 - 4.4).

4.5.1 Features of Pathology in Crouzon Syndrome determined from Comparison of Pre-operative and Standard Surgical Units

The cranial base was described by Enlow (1975) as the template for the face. Numerous studies have associated the cranial base abnormality with the craniofacial abnormality in Crouzon syndrome (Bennett, 1967: Rosen and Whitaker, 1984). Pathology of the cranial base was demonstrated in cephalometric examinations (Rune et al., 1979; Kreiborg, 1981) and 3D CT scans (Kreiborg et al., 1993) and is more fully described in Chapter 3.

In this study the cranial base angle played an important role in determining the position of the surgical unit. When the cranial base angle was increased, the surgical unit was in a superior

position, compared with the more normal or inferior position of the surgical unit, when the cranial base angle is decreased (Table 4.2, Figure 4.5). This finding highlighted the extent of the pathology involving the cranial base. The widespread involvement of the craniofacial skeleton in the pathology of Crouzon syndrome precluded the identification of any normal reference points to allow a direct comparison with normal points on a standard model.

It could be argued that alternative points should be included and others deleted. Any variable points selected would have had an effect on the alignment position of the surgical unit due to their intrinsic pathological position. In this study, a large number of widely spaced cranial base landmarks were selected as the cranial base unit for alignment.

In the main, the sizes of the pre- and post-operative surgical units compared with the standards were increased. In the patients with the mild to moderate deformity, the "shape" of the fronto-orbital region was relatively normal. Its size and position varied greatly between patients. This becomes relevant when surgical manipulations altered the shape during the fronto-orbital advance procedure. There was very little asymmetry seen.

Table 4.2 Comparison of Pre-operative and Standard Surgical Units

PATIENT	SH	JS	IP	LW	HC
Age at CT scan	5 mo.	21 mo.	21 mo.	5·5 yrs	15 yrs
Cranial base angle	smaller	normal	larger	smaller	larger
Surgical unit - Size	normal	normal	much larger	slightly larger	normal
- Shape	good	good	distorted superiorly	slightly broad laterally	good, slightly narrow anteriorly
- Position (mean translation of patient relative to standard (mm))	left (2.9) posterior (0.3) inferior (11.4)	left (0.2) posterior (4.3) superior (2.7)	right (2.9) very posterior (12.2) very superior (21.0)	right (0.5) posterior (1.3) inferior (0.7)	left (2.1) very posterior (12.4) very superior (11.9)

4.5.2 Results of Surgery in Crouzon Syndrome determined from Comparison of Pre-operative and Post-operative Surgical Units

At operation, several factors may have altered the result as measured in this analysis. The age at which the post-operative CT scan was performed was significantly more important in the infant population due to the rapid bony growth of the calvaria. The results of Patient RN were strongly influenced by this phenomenon with the pre-operative scan taken at 1 month and the post-operative scan at 10 months. The results for this patient were therefore excluded.

Reshaping the fronto-orbital bar by swinging the lateral elements anteriorly, following a medial osteotomy, had the effect of flattening the supra-orbital bar and producing a square appearance to the fronto-orbital region. This surgical procedure was performed with the intention of providing increased coverage for the globes. The effect of this reshaping was seen when examining the position of the post-operative surgical unit compared with the standard (Section 4.5.3). When considering the effect on the directional shifts of the surgical unit, the reshaping increased the lateral distances shifted compared with the midline. In the summary table (Table 4.3) the mean distances of the directional shifts are recorded.

Bony fixation was with wire in 2 patients and plates in the other 3. In general, wire fixation is preferred in the young to maximise the floating forehead principal (Marchac and Renier, 1979). The use of plates in young patients has been a subject of controversy due to the inward migration of plates with growth (Munro, 1993). Plate and screw fixation is more rigid and particularly useful for orthognathic work. It may contribute to the stability of the peri-orbital surgical shift, particularly when anchoring 3 points such as the temporal region to the lateral orbital rim bilaterally and at the nasal bones medially. In this small group of patients, plate fixation resulted in a reduced surgical shift superiorly with a preference for an anterior maintenance of position. (Table 4.3; Patients JS and LW.) The long term effects of the plates and the positions of fixation are unknown.

The precise positioning of the surgical unit at the time of surgery, rather than the type of fixation performed, may be equally relevant. This analysis was not able to address this issue, although this data suggested that this might be an area of further study. Similarly, the effects of soft tissue closure on the bony position have not been determined.

Table 4.3 Comparison of Pre-operative and Post-operative Surgical Units

PATIENT	SH	JS	IP	LW	HC
Surgery	FOA	FOA	FOA	Extended FOA	FFA
Reshaping of lateral bar	Yes	Yes	Yes	Yes	Yes
Method of bony fixation	wire	plates	wire	plates	plates
Age at post-op CT scan	8 mo.	22 mo.	22 mo.	6 yrs	15 yrs
Surgical unit (mean translation of pre-operative to post-operative position (mm))	right (1.5) anterior (3.3) superior (7.6)	right (0.7) anterior (10.0) superior (3.0)	left (3.8) anterior (18.1) superior (13.0)	right (0.8) anterior (5.3) superior (3.0)	left (2.3) anterior (15.9) superior (4.0)

4.5.3 Residual Deformity in Crouzon Syndrome determined from Comparison of Post-operative and Standard Surgical Units

The results of surgery, as demonstrated by the comparison of the post-operative surgical unit with the standard surgical unit, revealed 3 main features. In each patient, the size of the surgical unit was essentially unchanged. Secondly, the shape of the surgical unit was altered by the swing of the lateral wings anteriorly. This had the effect of providing further coverage for the orbits as can be seen in the figures of the wire frame diagrams of the patients' skulls (Figures 4.6 - 4.10). The manoeuvre changed the shape of the fronto-orbital bar away from the normal standard. Based on this limited data, consideration should be given to advancing the lateral orbital walls and/or zygomatic bodies to the same degree as the rest of the supra-orbital ridge in order to lessen this effect. Alternatively, they may be brought medially following osteotomy, as well as forward, to reduce lateral splaying of the lateral orbital wall.

Thirdly, as demonstrated in the surgical directional shift measurements, all the landmarks of the post-operative surgical units lay anterior to the standard with minor asymmetry. The position of the supra-orbital bar was generally superior, in patients where the cranial base angle was

decreased. When wire fixation was used (Patient SH), the surgical shift placed the supra-orbital bar in a position at the level of the normal experimental standard (Table 4.4 and Figure 4.7).

Table 4.4 Comparison of Post-operative and Standard Surgical Units

PATIENT	SH	JS	IP	LW	HC
Surgical unit - Size	increased	slightly increased	greatly increased	increased	normal
- Shape	broad laterally	slightly broad laterally	less distorted	more broad laterally	slightly broader laterally
- Position (mean translation of patient relative to standard (mm))	right (3.7) anterior (9.3) superior (0.1)	right (0.7) anterior (6.5) superior (4.2)	left (0.6) anterior (7.5) superior (32.8)	right (1.8) anterior (3.5) superior (1.4)	left (6.4) anterior (3.2) superior (15.7)

In summary, the present study used the cranial base for alignment to enable assessment of the region undergoing surgery. Not only the relative size of the pre-operative surgical unit, but its shape and position in space, were determined from the 3D CT analysis. The shape, size and position of the surgical unit following the surgical shift have also been assessed. The comparison of the post-operative position with the experimental standard data was performed in the early post-operative phase. At this stage, an improvement in the position of the surgical unit has been demonstrated.

Based on the trends identified in this study, a new set of questions may be asked, challenging the current surgical techniques to produce a reconstruction which is individualised for each patient's variable pathology, accurate in its execution with an appropriate method of fixation and with limited morbidity.

CHAPTER 5

DISCUSSION AND SUMMARY OF MAJOR FINDINGS

5.1 The Clinical and Radiographic Features of a Population with Crouzon Syndrome

This thesis has contributed to the understanding of the variation and severity of the clinical manifestations of Crouzon syndrome by the analysis of the clinical and radiographic pathology and the natural history and treatment of a population of 59 patients.

Crouzon syndrome is clasically described as having fusion of the calvarial sutures, shallow orbits with proptosis and maxillary hypoplasia leading to a class III malocclusion, all with variable severity. These findings and others in this population are summarised in Table 2.21. Many are similar to those described by Kreiborg (1981) in the only other large population studied, such as variation in head shape, suture patency and copperbeaten appearance.

New findings from this study were a birth prevalence of 24.2 per million which was higher than other studies of 15.5 per million (Martinez-Frias et al., 1991) and 16.5 per million (Cohen and Kreiborg, 1992). Seventy-five percent of patients presenting represented new mutations of Crouzon syndrome while 25% had a positive family history. The new mutation rate is much higher than other studies (56% in Kreiborg's series (1981)) and while increased paternal age may be a factor the exact cause of this is not clear.

For the first time CT examination of the central nervous system of a large population of patients with Crouzon syndrome was reviewed and revealed a high rate of ventriculomegaly, a distortion and dilation of the ventricles which is not necessarily a functional problem. This was considered mild in 51% of patients, moderate in 11% and severe with functional significance in 9% of patients (Proudman et al., 1995). Schizencephaly in one patient was a finding not previously reported in Crouzon syndrome. These findings differ from Apert syndrome central nervous system findings (Cohen and Kreiborg, 1990) where structural abnormality of brain

matter and mental retardation is more common and further confirm the difference between these two syndromes.

Ophthalmological review confirmed the well established findings of proptosis, strabismus, optic atrophy, exposure keratitis, decreased acuity, nystagmus and coloboma of the iris. In addition, ophthalmological findings not usually associated with Crouzon syndrome were found such as orbital dystopia in 10% of patients and ptosis in 14%.

The findings by Kreiborg (1981) of abnormality of the ear, stenosis or atresia of the external ear canal with middle ear disease and hearing loss were confirmed, however only 1 palatal deformity (bifid uvula) was found in this population compared with up to 10% in other studies (Kreiborg, 1981). Occlusal abnormalities were also examined confirming the established high incidence of class III occlusion.

For the first time in a large population with Crouzon syndrome, examination of the speech highlighted the high rates of articulation disorder (90%), hyponasality (88%) and hypernasality (10%). Abnormality of the nasopharyngeal airway was manifest in the extreme by obligatory mouth breathing in 38% of patients, similar to the findings of Kreiborg (1981). In addition, oxygen desaturation was recorded in 8% of patients and may be of significance in infants where it may not be detected. Further detailed longitudinal studies of the airway in all Crouzon patients will provide the necessary data on which appropriate treatment may be based.

Investigation of non-craniofacial features of Crouzon syndrome confirmed cervical spine fusions, predominantly in the upper cervical spine (C-2,3) compared with Apert syndrome in the lower cervical spine (Kreiborg, 1987; Hemmer et al., 1987). Stylohyoid ligament calcification, elbow stiffness with radius subluxation and ankylosis were also seen in this study. Minor hand abnormality was found in 10% of patients, a finding rarely reported before (Garcin et al., 1932; Kaler et al., 1982).

The surgical intervention in this population with Crouzon syndrome was also recorded (Section 2.4.10) and documents the indications, types of procedures, secondary procedures and complications. This follows the regimens outlined by Tessier and others (Tessier, 1971a, 1971b; David et al., 1982). All patients survived surgery. At this stage, Le Fort III osteotomy

in childhood is justified for medical reasons. Further investigation will determine whether it should be routinely implemented for psycho-social reasons.

Four patients of the 59 patients studied died. One suffered atlantoaxial subluxation with spinal cord compression and 3 infants with severe deformity died from respiratory difficulties.

This population data collected represents a large addition to the body of information of the natural history and treatment of the condition. These data are consistent with the concept that Crouzon syndrome is a dysplastic condition which affects chondral and bone growth. The condition shows great variation in presentation. This may be related to the timing of, and possibly the rate of synchondrosis and synostosis. The late onset of the calvarial deformity and the early onset of the maxillary involvement seen in some patients support this concept. The gradual onset of the cervical spine fusion, elbow deformity and stylohyoid calcification suggest that the dysplastic bony condition is progressive. What directs the synchondrosis is not clear.

Crouzon syndrome shares many features with other craniostenotic conditions. It would seem that while they each have a distinct genetic pattern, and possibly pathological processes at the level of the bone and cartilage, the resultant structural abnormalities produce similar functional and aesthetic problems.

The concept of a primary abnormality of bone and cartilage development producing all the features is a valid hypothesis. Some evidence does suggest, however, the CNS and the soft tissues of the face and palate may also be primarily affected. The genetic and embryological implications of this are not readily apparent.

5.2 The Three Dimensional Quantitative Analysis of the Craniofacial Morphology of Crouzon Syndrome

Developments in CT imaging and analysis enabled the variable and complex clinical presentation of this disorder to be defined by detailed measurement of the craniofacial skeleton (Abbott, 1988). 3D CT reconstructions of 8 patients with Crouzon syndrome were analysed using Persona 3D medical imaging and analysis software. Landmarks representing each craniofacial bone were identified, allowing measurement of distances, dimensions and angles for each bone (anatomical units). The measurements were compared with age-matched

experimental data and statistically significant regions of deformity were identified in each patient. This study enabled, for the first time, the identification of patterns of deformity for each craniofacial bone in Crouzon syndrome. The results should be reviewed in light of the small number and varying age of the patients studied. These new findings are summarised here.

This study identified a typical pattern of deformity of the mandible with increased gonial angle and increased symphyseal height. An increased gonial angle supported Kreiborg's findings of a tendency to an increase in the angle (1981). In addition to the typical findings it was found that the position of the condyles of the mandible could also be distorted by deformity of the cranial base. Localised overgrowth at the gonial angles was also identified in one patient.

The maxilla in Crouzon syndrome is clinically described as hypoplastic, however in this study the maxilla was hypoplastic only in its anterior-posterior dimensions, and increased in its height and width. This finding was more common in the older patients and is in contrast to the findings of others (Kreiborg, 1981). This increased height and width was identified in the interorbital region, a site usually considered to be broad due to downward displacement of the ethmoid bone. CT examination and measurement clearly identified the maxilla and its antrum encroaching into the interorbital region.

The nasal bones tended to be increased in length and angled inferiorly, which was consistent with the length and facial form of the maxilla and mandible.

Prior studies have focussed on the calvarial dimensions of the frontal bone which was not measured in this study. In this study the supraorbital ridge, ethmoid and sphenoid attachments have been quantified for the first time. The frontal bone supraorbital ridge was increased in width in the majority of patients. The frontal ethmoid attachment length varied greatly and was related to deformity in the surrounding bones. An increase in the frontal ethmoid attachment length appeared to be related to increased dimensions of the cribriform plate. The overall clinical deformity in the patients with a normal frontal ethmoid junction was less severe. A greater degree of pathology in the region of the sphenoid bone was found in those patients with reduction in the length of the frontal ethmoid attachment (Section 3.5.8 Sphenoid bone). The superior orbital fissure was commonly reduced in length.

Deficiency of the lateral orbital wall has been described and related to the posterior position of the zygomatic bone due to fusion of the squamous and temporal calvarial sutures (Kreiborg and Bjork, 1982). The involvement of suture fusion and the resulting pattern of the bone has been further described in this study as presenting with minimal involvement (1 patient) or as one of 2 distinct patterns. The fronto-zygomatic pattern was characterised by suture lengthening producing a normal or slightly wide zygomatic bone. The spheno-zygomatic pattern, a more severe deformity with lengthening of the suture, produced a decrease in length but increase in height of the zygomatic bone.

The vomerine bone has not previously been considered in isolation but as part of the developing nasal capsule. In this study the vomer was often smaller and angled inferiorly, particularly in the older patients, consistent with downward growth at the expense of anterior growth of the facial skeleton and supports the previously held concepts of the development of this bone.

Deformity of the ethmoid bone in Crouzon syndrome has classically been described as broad with depression of the cribriform plate (Bertelsen, 1958). In this study the ethmoid bone was examined by region and again demonstrated variable patterns of deformity. The size of the lateral ethmoid plate was normal in some patients but more often was reduced in size. Involvement of the spheno-ethmoid synchondrosis has been suggested by other authors (Burdi et al., 1986). This study was able to confirm this in some but not all patients. The posterior ethmoid was increased in width at the spheno-ethmoid synchondrosis in half the patients, but normal or reduced in width in the other half, producing a wedge shaped bone in the latter group. The frontal ethmoid attachment was reported with the frontal bone (see above). The cribriform plate was broad and the medial ethmoid plate was normal or increased in size.

The sphenoid bone has been well described qualitatively from cephalometric radiographs and 3D CT reconstructions (Kreiborg, 1981; Kreiborg et al., 1993). In this study, the sphenoid bone was again divided into regions. Severity of abnormality of the sphenoid bone correlated with the degree of clinical severity of Crouzon syndrome. In cases with mild clinical involvement the lesser wing showed a moderate deformity with prominent anterior clinoids and normal or reduced length of the lesser wing. The more severely involved patients showed a reduced size of the anterior clinoid and increased length of the lesser wing. The pterygoid plates

were generally normal in size and position. An increased lateral and posterior angle of the pterygoid plate was identified in those patients with more severe clinical deformity and may influence the position and projection of the maxilla. The greater wing of the sphenoid was angled laterally. Lengthening of the spheno-zygomatic and spheno-temporal sutures was commonly identified, consistent with fusion as described by Kreiborg and Bjork (1982). The measurements of the sphenoid body were larger in size than the experimental standard in most cases. This finding was consistent with raised intracranial pressure causing endocranial resorption of the sella turcica and distortion of the lateral walls and confirmed the qualitative findings of Kreiborg et al. (1993). The spheno-occipital synchondrosis was distorted in shape (increased height with normal width or normal height with reduced width) but the significance of this finding remains unclear.

There is little information in the literature about the detailed pathology of the temporal bone in Crouzon syndrome. The temporal bone in patients with Crouzon syndrome has been described as hypoplastic (Nager and de Reynier, 1948). Fusion of the squamous temporal sutures has been reported (Kreiborg and Bjork, 1982). In this study several new findings emerged. The shape of the external auditory meatus of the temporal bone was distorted. The zygomatic process was often reduced in length with an increased height of the articular fossa. The jugular foramen was narrowed with lengthening of the surrounding cranial base sutures. One patient with atresia of the external auditory meatus exhibited a similar pattern to the other patients but with reduced measurements implying a degree of hypoplasia of the petrous temporal bone.

The parietal bone and squamous temporal bone were not analysed fully in this study, while limited measurements of the remaining basal occipital bone showed minimal additional abnormality.

The major cranial base sutures were measured for the first time to determine what, if any, pattern emerged. While the pattern of suture involvement was variable, the sutures were lengthened primarily anteriorly and laterally. Suture lengthening may imply suture fusion with growth along the line of the suture, not always matching the involvement seen clinically in the calvaria but allowing a suture profile to be determined for each patient.

The craniofacial dimensions and angles confirmed the increase in facial height with a reduction in the maxillary projection anteriorly. The cranial base angles were quite variable, consistent with previous studies (Kreiborg, 1981) and confirmed that the morphology of this region reflects both primary and secondary forces.

From the data generated from this study and based on the theories previously postulated (Virchow, 1851; Moss, 1959; Kreiborg, 1981) craniofacial morphology in Crouzon syndrome is due to a combination of primary and secondary pathological events. The craniofacial bones have a primary developmental abnormality with premature suture fusion of variable severity that becomes manifest with time. As with the variable calvarial shapes in Crouzon syndrome, different regions of the craniofacial bones are affected, producing the patterns of deformity in these bones described above. Morphology of these bones is secondarily affected by 3 factors: the deformity in adjacent growing bones, raised intracranial pressure causing endocranial bone resorption and the effect of the functional matrix on the occlusion (Figure 3.47).

5.3 The Three Dimensional Quantitative Analysis of the Morphology before and after Surgery in Crouzon Syndrome

Three-dimensional measurement studies of surgical manoeuvres in infants and children with Crouzon syndrome are infrequent in the literature. Previous studies of cephalometric radiographs (Kreiborg, 1981; Kreiborg and Aduss, 1986) and dry skull examinations (Kreiborg and Bjork, 1982; Burdi et al., 1986) demonstrated the pathology in the fronto-orbital and zygomatic regions. Carr et al. (1992) made CT scan-based measurements of the cranial orbital zygomatic region in unoperated Crouzon and Apert infants. A detailed description of the craniofacial pathology in patients with Crouzon syndrome is reported in Chapter 3 of this manuscript. Attempts at measurement of forehead morphology was performed by Friede et al. (1986) using digitised cephalometric radiographs.

A more recent study by Posnick et al. (1993) examined 14 measurements in 14 patients with Crouzon syndrome who underwent surgery. The measurements were all in the cranio-orbito-zygomatic region and were measured by callipers from 2D axial CT scan images. No analysis of cranial base pathology was incorporated in the study. The findings suggested that whilst

anterior movement of landmarks was performed, the post-operative measurements at one year were still significantly abnormal.

3D CT reconstructions of 5 patients with Crouzon syndrome undergoing fronto-orbital or fronto-facial surgery were extensively analysed. The fronto-orbital bar and Le Fort III components (surgical units) were analysed using Persona 3D medical imaging and analysis software.

The position of the pre-operative and post-operative surgical units were compared with each other and with age-matched experimental standard data. This was performed by alignment of the surgical units using cranial base landmarks not in the operative field, and least squares and repeated median methods to measure the distances between the surgical units. The severity of the pathology, the effect of the surgical manipulation and the residual deformity were all examined.

The effect of the cranial base pathology on the alignment of the pre-operative and standard surgical units demonstrated that the pathology in Crouzon syndrome extended throughout the craniofacial skeleton. In general, the pre-operative surgical units were posterior to the experimental standard. The superior or inferior relationship of the pre-operative surgical unit to the standard surgical unit was related to changes in the cranial base angle.

Assessment of the surgery to the pre-operative surgical unit demonstrated an anterior translocation in all patients. However, several new findings emerged from the analysis. When this anterior translocation was small, it was at the expense of superior translocation of the post-operative surgical unit. The degree of superior displacement of the post-operative surgical unit varied, occurring with both wire and plate fixation and may have been related to the effects of soft tissue closure.

In addition, reshaping of the fronto-orbital bar with increased lateral orbital advancement to assist in globe projection, accentuated the broad and flattened appearance of the forehead which may not be desirable aesthetically. Fronto-facial surgery however, in adults, resulted in a more reliable anterior translocation of the bones, but with a slight increase in the facial height.

Further analysis is required to determine the degree and rate of relapse. Posnick et al. (1993) do not comment on possible factors influencing the degree of relapse. Extended population studies, possibly in the form of controlled trials, may help unravel this multifactorial dilemma.

In conclusion, this study correlates cranial base position with that of the surgical unit and vividly demonstrates that surgery in Crouzon syndrome (and other craniosynostosis syndromes) is a surgery of the facial facade. Variables affecting the facial surgery and which may be manipulated, are osteotomy of the lateral orbital walls, the 3D positioning of the bone, the method of fixation and the tightness of skin closure. A more complete analysis of a large population of pre- and post-operative patients with Crouzon syndrome would help define these variables further as well as the patterns of deformity in both operated and unoperated patients.

5.4 Scope for Further Studies

The analysis of 3D CT reconstructions of other populations with Crouzon syndrome would help to confirm or add to the patterns of deformity found in this study. The analysis of the craniofacial skeleton of other craniofacial deformities using this method, including a comparison with Crouzon syndrome would provide additional information on the range of craniofacial deformity. Further collection of data for the experimental standard would provide more information about the craniofacial skeleton of the normal population and enable greater statistical power for comparison studies.

Specific studies which could be addressed in Crouzon syndrome include structural, growth and surgical analyses. Regions of structural abnormality of interest not addressed in detail in this study include the dimensions of the optic foramen, calvarial abnormalities and occlusal relationships. Further measurement of the spheno-occipital synchondrosis and temporal bones may help define the dysmorphology of these regions. Narrow slice CT data would be needed for close examination of some of these areas.

Growth studies in Crouzon syndrome, by the collection and analysis of serial CT scans, would produce further information on primary developmental changes in Crouzon syndrome as well as on growth following surgery. Parallel detailed growth studies of the normal population could also theoretically be undertaken.

The assessment of surgical intervention could also be extended. Using the analysis as a pre-operative assessment of the individual patient deformity, surgery could be tailored to the sites of pathology identified. The results of this surgical intervention could then be analysed.

The present investigation has demonstrated the detailed clinical and radiographic features of the craniofacial morphology of Crouzon syndrome. Quantification from 3D CT reconstructions provides a greater understanding of the pathological morphology and enables analysis of the effects of surgical manipulation. This detailed analysis of the pathology and present day surgical management of Crouzon syndrome expands our current understanding and provides the framework for future developments in this field.

BIBLIOGRAPHY

Abbott AH (1988) The acquisition and analysis of craniofacial data in three dimensions. Ph.D. Research Thesis. Adelaide, Australia: The University of Adelaide.

Abbott AH, Netherway DJ, David DJ, Brown T (1990a) Application and comparison of techniques for three-dimensional analysis of craniofacial anomalies. *J Craniofac Surg* 1 (3): 119-134.

Abbott AH, Netherway DJ, David DJ, Brown T (1990b) Craniofacial Osseous Landmark Determination from Stereo Computer Tomography Reconstructions. *Ann Acad Med* 19 (53): 595-604.

Atkinson FRB (1937) Hereditary Cranio-Facial Dysostosis, or Crouzon's Disease. *Med Press Circ* 195: 118-124.

Bachmayer DI, Ross RB (1986) Stability of Le Fort III advancement in children with Crouzon's, Apert's and Pfeiffer's syndromes. *Cleft-Palate J* Suppl (Dec): 69-74.

Bachmayer DI, Ross RB, Munro IR, Chir B (1986) Maxillary growth following Le Fort III advancement surgery in Crouzon, Apert and Pfeiffer syndromes. *Am J Orthod Dentofacial Orthop* 90(5): 420-430.

Baldwin JL (1968) Dysostosis craniofacialis of Crouzon. A summary of recent literature and case reports with emphasis on the ear. *Laryngoscope* 78: 1660-1676.

Baxter BS, Sorenson JA (1981) Factors affecting the measurement of size and CT number in computed tomography. *Investigative Radiology* 16 (4): 337-341.

Bennett KA (1967) Craniostenosis: a review of the etiology and a report of new cases. *Amer J Phys Anthrop* 27: 1-10.

Bergland O (1963) The bony naso-pharynx. Roentgen Craniometric Study. *Acta Odontol Scand* 21: Suppl 135: 1-137.

Bertelsen TI (1958) The premature synostosis of the cranial sutures. *Acta Ophthalmol* Suppl 51: 1-176.

Bite U, Jackson IT, Forbes GS, Gehring DG (1985) Orbital volume measurements in enophthalmos using three-dimensional CT imaging. *Plast Reconstr Surg* 75 (4): 502-507.

Bjork A (1966) Sutural growth of the upper face studied by the implant method. *Acta Odontol Scand* 24: 109-127.

Bookstein FL 1987 Describing a craniofacial anomaly: finite elements and the biometrics of landmark location. *Am J Phys Anthropol* 74: 495-509.

Bookstein FL 1991 Morphometric tools for landmark data. Cambridge University Press, New York.

Boyd E (1980) Origins of the study of Human Growth. University of Oregon Health Sciences Foundation. Oregon.

Breitbart AS, Eaton C, McCarthy JG (1989) Crouzon's syndrome associated with acanthosis nigricans: ramifications for the craniofacial surgeon. *Ann Plast Surg* 22: 310-315.

Broadbent BH (1931) A new x-ray technique and its application to orthodontia. *Angle Orthod* 1: 45.

Brown T, Abbott AH (1989) Computer-assisted location of reference points in three dimensions for radiographic cephalometry. *Am J Orthod Dentofacial Orthop* 95: 490-498.

Burdi AR, Kusnetz AB, Venes JL, Gebarski SS (1986) The natural history and pathogenesis of the cranial coronal ring articulations: implications in understanding the pathogenesis of the Crouzon craniostenotic defects. *Cleft Palate J* 23 (1): 28-39.

Carmel PW, Luken MG, Ascheri GF (1981) Craniosynostosis: Computed tomographic evaluation of skull base and calvarial deformities and associated intracranial changes. *Neurosurg* 9: 366-372.

Carr M, Posnick JC, Pron G, Armstrong D (1992) Cranio-Orbito-Zygomatic Measurements from Standard CT scans in unoperated Crouzon and Apert Infants: Comparison with Normal Controls. *Cleft Palate-Craniofacial J* 29 (2): 129-136.

Chatelin C (1914) La dysostose cranio-faciale hereditaire. *Ann de med.*, Paris. ii 55-71.

Christiansen EL, Thompson JR, Kopp S (1986) Intra- and inter-observer variability and accuracy in the determination of linear and angular measurements in computed tomography. *Acts Odontol Scand* 44: 221-229.

Coccaro PJ, McCarthy JG, Epstein FJ, Wood-Smith D, Converse JM (1980) Early and late surgery in craniofacial dysostosis: a longitudinal cephalometric study. *Am J Orthod* 77: 421-436.

Cohen MM Jr (1975) An etiological and nosological overview of craniosynostosis syndromes. *Birth Defects* 11: 137-189.

Cohen MM Jr (1979) Craniosynostosis and syndromes with craniosynostosis: Incidence, genetics, penetrance, variability, and new syndrome updating. *Birth Defects* 15: 13-63.

Cohen MM Jr (ed.) (1986) Craniosynostosis; diagnosis, evaluation and management. New York. Raven Press.

Cohen MM Jr, Kreiborg S (1990) The central nervous system in the Apert syndrome. *Amer J Med Genet* 35: 36-45.

Cohen MM Jr, Kreiborg S (1992) Birth prevalence studies of the Crouzon syndrome: comparison of the direct and indirect methods. *Clin Genet* 41: 12-15.

Cohn ER, Ormond Hesky EM, Bradley WF Jr, McWilliams BJ, Hurwitz DJ, Brown Wallace S (1985) Life response to Crouzon's disease. *Cleft Palate J* 22: 123-131.

Comby J (1926) Un cas de dysostose craniofaciale non hereditaire ni familial. *Bull et Mém Soc méd de Hôp de Paris* 3 s, 1: 1327.

Corey JP, Caldarèlli DD, Gould HJ (1987) Otopathology in craniofacial dysostosis. *Am J Otology* 8: 14-17.

Costaras-Volarich M, Pruzansky S (1984) Is the mandible intrinsically different in Apert and Crouzon syndromes? *Am J Orthod* 85 (6): 475-487.

Craig CL, Goldberg MD (1977) Calcaneocuboid coalition in Crouzon's syndrome (craniofacial dysostosis) *J Bone Joint Surg* 59A(6): 826-827.

Crouzon O (1912) Dysostose cranio-faciale héréditaire. *Bull Soc Med Hop Paris* 33: 545-555.

Crouzon O, Regnault F (1933) Les variations de forme du crane dans la dysostose cranio-faciale hereditaire. *Vol. jubilaire. Marinesco.* 169-179.

Cutting C, Bookstein FL, Grayson B, Fellingham L, McCarthy JG (1985) Three-dimensional computer-assisted design of craniofacial procedures: optimization and interaction with cephalometric and CT-based models. *Plast Reconstr Surg* 77(6): 877-885.

Cutting C, Bookstein FL, Grayson B, Fellingham L, McCarthy JG (1986) Computer-aided planning and evaluation of facial and orthognathic surgery. Computers in Plastic Surgery. *Clin Plast Surg* 13(3): 449-462.

David DJ (1977) Cranio-facial surgery: The team approach. *Aust NZ J Surg* 47: 193-198.

David DJ, Cooter RD (1987) Craniofacial infections in ten years of transcranial surgery. *Plast Reconstr Surg* 80 (2): 213-223.

David DJ, Cooter RD, Edwards TJC (1991) Crouzon twins with cloverleaf skull malformations. *J Craniofac Surg* 2 (2): 56-60.

David DJ, Hemmy DC, Cooter RD (1990) Cranio-Facial Deformities: atlas of three dimensional reconstruction from computed tomography. Springer-Verlag, New York.

David DJ, Poswillo DE, Simpson DA (1982) The craniosynostoses; causes, natural history and management. Berlin. Springer-Verlag.

David DJ, Sheen R (1990) Surgical correction of Crouzon syndrome. *Plast Reconstr Surg* 85 (3): 344-354.

Devine P, Bhan M, Feingold M, Leonidas J, Wolpert S (1984) Completely cartilaginous trachea in a child with Crouzon syndrome. *Am J Dis Child* 138: 40-43.

Ellis RWB (1937) Craniofacial dysostosis (Crouzon's syndrome). *Proc R Soc Med* 30: 1187-1188.

Enlow DH (1968) The human face. First edition. Hoeber Medical Division, Harper and Row, New York.

Enlow DH (1975) Handbook of Facial Growth. Saunders, Philadelphia, Pennsylvania.

Eshbaugh D (1948) Relation of the changes in the brain to those in the skull of Crouzon's and similar diseases; with a report of a case. *J Neuropathol Exp Neurol* 7: 328-343.

Faber HK, Towne EB (1927) Early craniectomy as a preventive measure in oxycephaly and allied conditions with special reference to prevention of blindness. *Am J Med Sci* 173: 701-711.

Farkas LG (1978) Ear morphology in Treacher Collins, Apert's and Crouzon's syndromes. *Arch Otorhinolaryngol* 220: 153-157.

Fishman MA, Hogan GR, Dodge PR (1971) The concurrence of hydrocephalus and craniosynostosis. *J Neurosurg* 34: 621-629.

Flippen JH Jr (1950) Cranio-facial dysostosis of Crouzon: Report of a case in which the malformation occurred in four generations. *Paediatrics* 5: 90-96.

Friede H, Lilja J, Lauritzen C, Andersson H, Johanson B (1986) Skull morphology after early craniotomy in patients with premature synostosis of the coronal suture. *Cleft Palate J* 23 (Supp 1): 1-8.

Fullerton GD, White DR (1979) Anthropomorphic test objects for CT scanners. *Radiology* 133: 217-222.

Garcin R, Chevallèy M, Bize R (1934) Étude anatomique d'un cas de dysostose cranio-faciale (maladie de Crouzon) *Bull Mem Soc Med Hop Paris* 1178-1188.

Gillies H, Harrison SH (1951) Operative correction by osteotomy of recessed malar maxillary compound in a case of oxycephaly. *Br J Plast Surg* 3: 123-127.

Golabi M, Chierici G, Ousterhout DK, Vargervik K (1984) Radiographic abnormalities of Crouzon syndrome: A survey of 23 cases. *Proc Greenwood Genetic Center* 3: 102-103.

Golabi M, Edwards MSB, Ousterhout DK (1987) Craniosynostosis and hydrocephalus. *Neurosurg* 21: 63-67.

Gross H (1959) Zur kenntnis der beziehungen zwischem gehirn und schädelkapsel bei den turricephalen, craniosynostischen dysostosen. *Virchows Arch* 330: 365-383.

Hanieh A, Sheen R, David DJ (1989) Hydrocephalus in Crouzon's syndrome. *Child's Nerv Syst* 5 (3): 188-189.

Healy MJR, Tanner JM (1981) Size and shape in relation to growth and form. *Symposia Zool Soc Lond* 46: 19-335.

Hemmer KM, McAlister WH, Marsh JL (1987) Cervical spine anomalies in the craniosynostosis syndromes. *Cleft Palate J* 24: 328-333.

Hemmy DC, David DJ, Herman GT (1983) Three dimensional reconstruction of craniofacial deformity using computed tomography. *Neurosurg* 13(5): 534-541.

Hemmy DC, Tessier P (1985) CT of dry skulls with craniofacial deformities: accuracy of three-dimensional reconstruction. *Radiology* 157: 113-116.

Herman GT, Liu HK (1977) Display of three-dimensional information in computed tomography. *J Comput Assist Tomogr* 1: 155-160.

Hounsfield GN (1973) Computerised transverse axial scanning (tomography): Part 1. Description of system. *Br J Rad* 46: 1016-1022.

Hunter AGW, Rudd NL (1977) Craniosynostosis: II. Coronal synostosis: Its familial and associated clinical findings in 109 patients lacking bilateral polysyndactyly or syndactyly. *Teratology* 15: 301-310.

Ingraham FD, Alexander E Jr, Matson DD (1948) Clinical studies in craniosynostosis. Analysis of 50 cases and description of a method of surgical treatment. *Surgery* 24: 518-541.

Jabs EW, Muller U, Li X, Ma L, Luo W, Haworth IS, Klisak I, Sparkes R, Warman ML, Mulliken JB, Snead ML, Maxson R (1993) A mutation in the homeodomain of the human MSX2 gene in a family affected with autosomal dominant craniosynostosis. *Cell* 75: 443-450.

Jackson CE, Weiss L, Reynolds WA, Forman TF, Peterson JA (1976) Craniosynostosis, mid-facial hypoplasia, and foot abnormalities: An autosomal dominant phenotype in a large Amish kindred. *J Paediatr* 88: 963-968.

Jones KL, Smith DW, Harvey MAS, Hall BD, Quan L (1975) Older paternal age and fresh gene mutation: Data on additional disorders. *J Paediatr* 86: 84-88.

Kaban LB, Conover M, Mulliken JB (1986) Midface position after Le Fort III advancement: a long-term follow-up study. *Cleft-Palate J* Suppl (Dec): 75-77.

Kaler SG, Bixler D, Yu PL (1982) Radiographic hand abnormalities in fifteen cases of Crouzon syndrome. *J Craniofac Genet Dev Biol* 2(3): 205-213.

Koehler PR, Anderson RE, Baxter B (1979) The effect of computed tomography viewer controls on anatomical measurements. *Radiology* 130: 189-194.

Koizumi H, Tomoyori T, Sato KC, Ohkawara A (1992) An association of acanthosis nigricans and Crouzon syndrome. *J Dermatol* 19: 122-126.

Kolar JC, Munro IR, Farkas LG (1988) Patterns of dysmorphology in Crouzon syndrome: an anthropometric study. *Cleft Palate J* 25: 235-244.

Kreiborg S (1981) Crouzon Syndrome. A clinical and roentgen cephalometric study. *Scand J Plast Reconstr Surg* Suppl 18: 11-198.

Kreiborg S (1987) Apert's and Crouzon's syndrome contrasted: qualitative craniofacial x-ray findings. In Proceedings of the First International Congress of the International Society of Cranio-Maxillo-Facial Surgery. Marchac D (ed.) Berlin. Springer-Verlag. 91-95.

Kreiborg S, Aduss H (1986) Pre- and post-surgical growth in patients with Crouzon's and Apert's syndromes. *Cleft Palate J* 23 (Suppl): 78-90.

Kreiborg S, Bjork A (1982) Description of a dry skull with Crouzon syndrome. *Scand J Plast Reconstr Surg* 16: 245-253.

Kreiborg S, Jensen BL (1977) Variable expressivity of Crouzon's syndrome within a family. *Scand J Dent Res* 85: 175-184.

Kreiborg S, Marsh JL, Cohen MM Jr, Liversage M, Pedersen H, Skovby F, Børgesen SE, Vannier MW (1993) Comparative three-dimensional analysis of CT-scans of the calvaria and cranial base in Apert and Crouzon syndromes. *J Cranio-Maxillo-Fac Surg* 21: 181-188.

Kushner J, Alexander E Jr, Davis CH Jr, Kelly DL Jr, Kushner AH (1972) Crouzon's disease (craniofacial dysostosis). Modern diagnosis and treatment. *J Neurosurg* 37: 434-441.

Laitinen LV (1956) Craniosynostosis. Premature fusion of the cranial sutures. An experimental, clinical and histological investigation with particular reference to the pathogenesis and etiology of the disease *Annul Aln Paed Fenn* 2: Suppl 6.

Li X, Lewanda AF, Eluma F, Jerald H, Choi H, Alozie I, Proukakis C, Talbot CC Jr, Kolk CV, Bird LM, Jones MC, Cunningham M, Clarren SK, Pyeritan RE, Weissenbach J, Jackson CE, Jabs EW (1994) Two craniostenotic syndroma loci, Crouzon and Jackson-Weiss, map to chromosome 10q23-q26. *Genomics* 22: 418-424.

Marchac D, Renier D (1979) The floating forehead. *Ann Chir Plast* 24: 121-126.

Marchac D, Renier D (1982) Craniofacial surgery for craniosynostosis. Boston. Little Brown.

Marsh JL, Vannier MW (1983) The "third" dimension in craniofacial surgery. *Plast Reconstr Surg* 71:759-767.

Marsh JL, Vannier MW (1985) Comprehensive care for craniofacial deformities. St Louis. CV Mosby.

Marsh JL, Vannier MW, Bresina S, Hemmer KM (1986) Application of computer graphics in craniofacial surgery. Computers in Plastic Surgery. *Clin Plast Surg* 13(3): 441-448.

Martinez-Frias ML, Cereijo A, Bermejo E, Lopez M, Sanchez M, Gonzalo C (1991) Epidemiological aspects of Mendelian syndromes in a Spanish population sample: I. Autosomal dominant malformation syndromes. *Am J Med Genetics* 38: 622-625.

McCarthy JG, LaTrenta GS, Breitbart AS, Grayson BH, Bookstein FL (1990) The Le Fort III advancement osteotomy in the child under 7 years of age. *Plast Reconstr Surg* 86: 633-646.

McCullough EC (1977) Factors affecting the use of quantitative information from a CT scanner. *Radiology* 124: 99-107.

Mixter RC, David DJ, Perloff WH, Green CG, Pauli RM, Popic PM (1990) Obstructive sleep apnoea in Apert's and Pfeiffer's syndromes: More than a craniofacial abnormality. *Plast Reconstr Surg* 86 (3): 457-463.

Moore MH, Tan E, Reilly PL, David DJ (1991) Frontofacial advancement with a free flap: deadspace versus drainage. *J Craniofac Surg* 2 (1): 33-37.

Moorrees CFA, Fanning EA, Hunt EE Jr (1963a) Formation and resorption of three deciduous teeth in children. *Am J Phys Anthropol* 21: 205-213.

Moorrees CFA, Fanning EA, Hunt EE Jr (1963b) Age variation of formation stages for ten permanent teeth. *J Dent Res* 42: 1490-1502.

Moss ML (1954) Growth of the calvaria in the rat. *Am J Anat* 94: 333-362.

Moss ML (1957) Premature synostosis of the frontal suture in the cleft palate skull. *Plast Reconstr Surg* 20: 199-205.

Moss ML (1958) Fusion of the frontal suture in the rat. *Am J Anat* 102: 141-166.

Moss ML (1959) The pathogenesis of premature cranial synostosis in man. *Acta Anat* 37: 351-370.

Moss ML (1971) Functional cranial analysis and the functional matrix. *Amer Speech Hear Ass Rep* 6: 5-18.

Moss ML (1975) Functional anatomy of cranial synostosis. *Child's Brain* 1: 22-33.

Moss ML, Salentijn L (1969) The primary role of functional matrices in facial growth. *Am J Orthod* 55: 566-577.

Mühlbauer W, Anderl H, Heeckt P, Schmidt A, Zenker J, Hopner F, Schaarschmidt B (1989) Early operation in Craniofacial Dysostosis. *World J Surg* 13: 362-372.

Munro I (1975) Orbito-cranio-facial surgery: the team approach. *Plast Reconstr Surg* 55: 170-176.

Munro I (1993) in Craniofacial Surgery 5. Proceedings of the International Congress of Craniofacial Surgery. Ortiz-Monasterio F (Ed.) Monduzzi Editore, Bologna, Italy.

Nager FR, de Reynier JP (1948) Das gehörgan bei den angeborenen kopfmissildungen. *Pract Oto-rhino-larynx* Supp 2: 1-128.

Noetzel MJ, March JL, Palkes H, Gado M (1985) Hydrocephalus and mental retardation in craniosynostosis. *J Paediatr* 107: 885-892.

Ortiz-Monasterio F, del Campo AF, Carillo A (1978) Advancement of the orbits and midface in one piece combined with frontal repositioning for the correction of Crouzon's deformities. *Plast Reconstr Surg* 61: 507-516.

Ousterhout DK, Vargervik K (1987) Aesthetic improvement resulting from craniofacial surgery in craniosynostosis syndrome. *J Cranio-Max-Fac Surg* 15: 189-197.

Ousterhout DK, Vargervik K, Clark S (1986) Stability of the maxilla after Le Fort III advancement in craniosynostosis syndromes *Cleft-Palate J* Suppl (Dec): 91-101.

Pantke OA, Cohen MM Jr, Witkop CJ, Feingold M, Schaumann B, Pantke HC, Gorlin RJ (1975) The Saethre-Chotzen syndrome. *Birth Defects* 11(2): 190-225.

Persson M (1973) Structure and growth of facial sutures. *Odont Rev* 24, Suppl 26: 1-146.

Peterson SJ, Pruzansky S (1974) Palatal anomalies in the syndromes of Apert and Crouzon. *Cleft Palate J* 11: 394-403.

Polinelli U, Imoda E (1963) Un caso di malattia de Crouzon. *Minerva Paediatr* 15: 1304-1307.

Posnick JC, Bite U, Nakano P, Davis J, Armstrong D (1992) Indirect intracranial volume measurements using CT scans: clinical applications for craniosynostosis. *Plast Reconstr Surg* 89 (1): 34-45.

Posnick JC, Lin KY, Jhawar BJ, Armstrong D (1993) Crouzon syndrome: quantitative assessment of presenting deformity and surgical results based on CT scans. *Plast Reconstr Surg* 92 (6): 1027-1037.

Preston RA, Post JC, Keats BJB, Aston CE, Ferrell RE, Priest J, Losken HW, Morris CA, Hurrt MR, Mulvihill JJ, Erhlich GD (1994) A gene for Crouzon craniofacial dysostosis maps to the long arm of chromosome 10. *Nature Genet* 7: 149-153.

Proudman TW, Abbott AH, Netherway DJ, David DJ (1994) New dimensions in Crouzon syndrome. In Craniofacial Surgery 5. Proceedings of the 5th International Congress of the International Society of Cranio-Facial Surgery Congress. Ortiz-Monasterio, F (Ed.), Monduzzi Editore, Bologna, Italy. Ch 4.

Proudman TW, Moore MH, Abbott AH, David DJ (1994) Noncraniofacial manifestations of Crouzon's disease. *J Craniofac Surg* 5: 218-222.

Proudman TW, Clark BE, Moore MH, Abbott AH, David DJ (1995) Central nervous system imaging in Crouzon syndrome. *J Craniofac Surg* 6(5): 401-405.

Reardon W, Winter RM, Rutland P, Pulleyn LJ, Jones BM, Malcolm S (1994) Mutations in fibroblast growth factor receptor gene 2 cause Crouzon syndrome. *Nature Genet* 8: 98 -103.

Renier D, Saint-Rose C, Marchac D, Hirsch J-F (1982) Intracranial pressure in craniosynostosis. *J Neurosurg* 57: 370-377.

Riolo ML, Moyers RE, McNamara JA , Hunter WS (1974) An atlas of craniofacial growth: cephalometric standards from the University School Growth Study, The University of Michigan. Monograph Number 2 Craniofacial Growth Series, Center for Human Growth and Development.

Rohlf FJ, Slice D (1990) Extensions of the procrustes method for the optimal superimposition of landmarks. *Syst Zool* 39(1): 40-59.

Rosen HM, Whitaker LA (1984) Cranial base dynamics in craniofacial dysostosis. *J Max-fac Surg* 12: 56-62.

Rune B, Selvik G, Kreiborg S, Sarnäs K-V, Kagström E (1979) Motion of bones and volume changes in the neurocranium after craniectomy in Crouzon's disease. A roentgen stereometric study. *J Neurosurg* 50: 494-498.

Salyer KE, Taylor DP, Billmire DE (1986) Three dimensional CAT scan reconstruction - paediatric patients. Computers in Plastic Surgery. *Clin Plas Surg* 13(3): 463-474.

Scammon RE (1930) The measurement of the body in childhood. In: Harris JA, Jackson CM, Paterson DG, Scammon RE. The Measurement of Man. University of Minnesota Press, Minneapolis, University of Minnesota. 171-215.

Schmaus H (1901) Grundriss der Pathologischen Anatomie, 6th Edition. Bergmann, Wiesbaden. p 648-649.

Scott JH (1956) Growth of the facial sutures. *Am J Orthod* 42: 381-387.

Selle G, Jacobs HG (1977) Cleft palate in two syndromes. *Cleft Palate J* 14: 230-233.

Shands AR, Bundens WD (1956) Congenital deformities of the spine. An analysis of the roentgenograms of 700 children. *Bull Hosp Joint Disease* 17: 110-133.

Shiller JG (1959) Craniofacial dysostosis of Crouzon: A case report and pedigree with emphasis on heredity. *Paediatrics* 23: 107-112.

Sicher H (1952) Oral anatomy,. Second edition, CV Mosby, St Louis.

Siegel AF (1982) Robust regression using repeated medians. *Biometrica* 69: 242-244.

Sneath PHA (1967) Trend-surface analysis of transformation grids. *J Zool Lond* 151: 65-122.

Solomon LM, Medenica M, Pruzansky S, Kreiborg S (1973) Apert syndrome and mucopolysaccharides. *Teratology* 8: 287-291.

Suslak L, Glista B, Gertzman GB (1985) Crouzon syndrome with periapical cemental dysplasia and acanthosis nigricans: the pleiotrophic effect of a single gene? *Birth Defects* 21: 127-134.

Tessier P (1971a) Relationship of craniostenosis to craniofacial dysostosis, and to faciostenosis. A study with therapeutic implications. *Plast Reconstr Surg* 48: 224-237.

Tessier P (1971b) The definitive plastic surgical treatment of the severe facial deformities of craniofacial dysostosis: Crouzon's and Apert's diseases. *Plast Reconstr Surg* 48: 419-442.

Tessier P (1976) Recent improvements in treatment of facial and cranial deformities of Crouzon's disease and Apert's syndrome. In: Tessier P, Callahan A, Mustardé JC, Salyer K (Eds) Symposium on plastic surgery in the orbital region. *Proc Symp Educ Found Am Soc Plast Reconstr Surg* 12. CV Mosby, St Louis. 271-303.

Tessier P (1986) Craniofacial Surgery. In: Craniosynostosis; Diagnosis, evaluation and management. Cohen MM Jr (ed.) New York. Raven Press. Ch 12.

Tulasne JF, Tessier PL (1986) Long-term results of Le Fort III advancement in Crouzon's syndrome. *Cleft-Palate J* Suppl (Dec): 102-109.

Van Limborgh J (1970) A new view on the control of the morphogenesis of the skull. *Acta Morphol Neerl Scand* 8: 143-160.

Vannier MW, Marsh JL, Warren JO (1984) Three dimensional CT reconstruction images for craniofacial surgical planning and evaluation. *Radiology* 150: 179-184.

Virchow R (1851-1852) Über den Cretinsimus, namentlich in Franken, und über pathologische Schädelformen. *Verh Phys Med Ges Wurzburg* 2: 230-271.

Waitzman AA, Posnick JC, Armstrong DC, Pron GE (1992a) Craniofacial Skeletal Measurements Based on Computed Tomography: Part 1. Accuracy and Reproducibility. *Cleft Pal-Craniofac J* 29 (2): 112-117.

Waitzman AA, Posnick JC, Armstrong DC, Pron GE (1992b) Craniofacial Skeletal Measurements Based on Computed Tomography: Part 2. Normal Values and Growth Trends. *Cleft Pal-Craniofac J* 29 (2): 118-128.

Walker J, Wybar K (1975) Ocular motility problems in cranio-facial dysostosis. In: Orthoptics: past, present, future. Moore S, Mein J, Stockbridge L (eds.) Boston. Stratton Intercontinental Medical Book Corporation.

Wood-Smith D, Epstein F, Morello D (1976) Transcranial decompression of the optic nerve in the osseous canal in Crouzon's disease. *Clin Plast Surg* 3(4): 621-623.

Appendix 1

Accuracy of Landmark Identification

Double Determinations of the landmarks were performed for:

1 Crouzon Syndrome Population (n=8)

Pooled landmark relocation error = 1.3 mms
Median landmark relocation error = 1.0 mms
Minimum = 0.4 mms for sphenion t left
Maximum = 5.3 mms for vertex

2 Sample of Dried Skull Population (n=10)

Pooled landmark relocation error = 1.2 mms
Median landmark relocation error = 0.9 mms
Minimum = 0.3 mms for crista galli
Maximum = 2.8 mms for sphenion t left

Appendix 1 Accuracy of Landmark Identification:

Crouzon Syndrome Patients:

Landmark	n	Landmark Relocation Error x	y	z	|xyz|
alare left	8	0.5	0.9	0.9	1.4
alare right	8	0.3	0.6	0.4	0.8
anterior clinoid left	8	0.4	0.3	0.8	0.9
anterior clinoid right	8	0.3	0.3	0.8	0.8
anterior nasal spine	8	0.3	0.3	0.4	0.6
articular eminence left	8	0.4	0.7	0.3	0.8
articular eminence right	8	0.3	0.4	0.1	0.6
articular fossa left	8	0.6	1	0.3	1.2
articular fossa right	8	0.4	0.6	0.4	0.8
asterion inner left	2	0	0.4	0.3	0.5
asterion inner right	2	0.4	0	0.6	0.7
asterion left	2	0	0.8	0.3	0.8
asterion right	2	0	0.4	0.6	0.7
auriculare left	8	0.3	0.9	0.5	1.1
auriculare right	8	0.2	0.9	0.5	1
basion	8	0.6	0.4	1.1	1.3
bregma	1	1.8	1.6	0.5	2.5
canine inferius left	5	0.2	0.4	0.3	0.5
canine inferius right	5	0.2	0.2	0.2	0.4
canine superius left	6	0.4	0.2	0.3	0.5
canine superius right	6	0.3	0.4	0.5	0.7
condylion laterale left	8	0.3	0.3	0.5	0.7
condylion laterale right	8	0.2	0.3	0.5	0.6
coronoid base left	8	0.6	0.6	0.6	1.1
coronoid base right	8	0.7	0.5	1.1	1.4
coronoid tip left	8	0.4	0.3	0.1	0.5
coronoid tip right	8	0.4	0.6	0.3	0.8
cribriform plate anterius left	8	1.4	0.7	0.7	1.7
cribriform plate anterius right	8	0.7	0.7	0.7	1.2
cribriform plate posterius left	8	0.3	0.7	0.5	0.9
cribriform plate posterius right	8	0.3	0.4	0.8	1
crista galli	7	0.1	0.3	0.5	0.6
disto-molare inferius left	6	0.4	0.6	0.3	0.8
disto-molare inferius right	6	0.5	0.4	0.6	0.9
disto-molare superius left	6	0.5	0.5	0.4	0.8
disto-molare superius right	6	0.5	0.3	0.8	1
ecto-canine inferius left	8	0.6	0.4	0.3	0.8
ecto-canine inferius right	8	0.7	0.3	0.8	1
ecto-canine superius left	8	0.4	0.5	0.9	1.1
ecto-canine superius right	8	0.9	0.7	0.9	1.4
ecto-incision central inferius left	8	0.2	0.5	1	1.2
ecto-incision central inferius right	8	0.3	0.7	0.9	1.2
ecto-incision central superius left	8	0.3	0.6	0.8	1
ecto-incision central superius right	8	0.4	0.6	0.7	1
ectomolare 1st inferius left	8	0.4	0.5	0.7	0.9
ectomolare 1st inferius right	8	0.4	0.5	0.6	0.9

Appendix 1 Accuracy of Landmark Identification:

Crouzon Syndrome Patients (continued):

Landmark	n	Landmark Relocation Error x	y	z	|xyz|
ectomolare 1st superius left	8	0.5	0.8	0.7	1.2
ectomolare 1st superius right	8	0.7	0.8	0.8	1.3
ethmoid spine	8	0.4	0.7	0.3	0.8
euryion left	5	0	1.5	0.6	1.6
euryion right	5	0.1	0.8	0.6	1
external auditory meatus anterius left	7	1	0.3	0.7	1.2
external auditory meatus anterius right	8	1.1	0.8	0.5	1.5
external auditory meatus inferius left	7	0.7	0.9	0.7	1.3
external auditory meatus inferius right	8	1.1	0.5	1	1.6
external auditory meatus posterius left	7	1.5	0.3	0.7	1.6
external auditory meatus posterius right	8	1.1	0.4	0.7	1.4
ext aud meatus superius (ie porion) L	8	0.7	0.7	0.3	1.1
ext aud meatus superius (ie porion) R	8	0.7	0.5	0.1	0.9
foramen caecum	7	0.3	0.3	0.5	0.6
foramen in ovale left	8	0.7	0.5	0.5	1
foramen in ovale right	8	0.6	0.9	0.6	1.3
foramen in spinosum left	8	0.2	0.3	0.4	0.5
foramen in spinosum right	8	1.1	0.8	0.7	1.6
foramen magnum lateralis left	8	0	0.5	0.5	0.7
foramen magnum lateralis right	8	0.3	0.5	0.4	0.7
foramen out ovale left	8	0.5	0.5	1	1.2
foramen out ovale right	8	0.6	0.5	0.6	0.9
foramen out spinosum left	8	0.3	0.6	0.9	1.1
foramen out spinosum right	8	0.8	0.5	1	1.4
glabella	8	0.5	0.3	0.4	0.7
gnathion	8	0.7	0.3	0.3	0.8
gonion left	8	0.3	0.4	0.5	0.7
gonion right	8	0.2	0.5	0.9	1
greater palatine foramen left	8	0.8	0.5	0.9	1.3
greater palatine foramen right	8	1.2	0.4	1.2	1.7
greater wing laterale left	8	0.4	0.4	0.3	0.6
greater wing laterale right	8	0.5	0.7	0.8	1.2
greater wing mediale left	8	0.3	0.5	0.7	0.9
greater wing mediale right	8	0.7	0.4	0.4	0.9
hamular notch left	8	0.4	0.5	0.4	0.8
hamular notch right	8	0.3	0.5	0.3	0.7
hamular process left	8	0.5	0.4	0.4	0.7
hamular process right	8	0.6	0.4	0.8	1.1
hormion	8	0.3	0.7	0.4	0.8
incision inferius left	6	0.3	0.4	0.2	0.5
incision inferius right	6	0.4	0.2	0.2	0.5
incision superius left	6	0.5	0.4	0.6	0.9
incision superius right	6	0.3	0.4	0.5	0.7
inferior naso-maxillare left	8	0.2	0.4	0.7	0.8
inferior naso-maxillare right	8	0.6	0.8	1.1	1.5
inferior orbital fissure left	8	0.3	0.4	0.6	0.8
inferior orbital fissure right	8	0.7	0.7	0.4	1.1

Appendix 1 Accuracy of Landmark Identification:

Crouzon Syndrome Patients (continued):

Landmark	n	Landmark Relocation Error x	y	z	|xyz|
infero-lateral orbitale left	8	0.5	0.4	0.5	0.8
infero-lateral orbitale right	8	1	0.3	0.6	1.2
infradentale	8	0.4	0.5	0.3	0.7
infra-orbital foramen inferior left	2	0.8	0.4	0.8	1.2
infra-orbital foramen inferior right	2	0.4	0.8	0.3	0.9
infra-orbital foramen lateral left	2	0.8	1.9	0.3	2
infra-orbital foramen lateral right	2	0.8	1.5	1.1	2.1
infra-orbital foramen left	2	0.3	0.2	0.3	0.5
infra-orbital foramen medial left	2	0.4	0.8	0.5	1
infra-orbital foramen medial right	2	0.4	0.4	0.9	1
infra-orbital foramen right	2	0.2	0.4	0.4	0.6
infra-orbital foramen superior left	2	0.4	0.5	0.8	1
infra-orbital foramen superior right	2	0.4	0.4	0.1	0.5
internal auditory meatus left	8	0.4	0.4	0.4	0.7
internal auditory meatus right	8	0.7	0.3	0.6	1
internal occipital protuberance	8	1.5	1.3	0.5	2.1
jugular foramen lateralis left	8	0.3	0.7	0.6	0.9
jugular foramen lateralis right	8	0.4	0.8	0.4	1
jugular foramen medial left	8	1.3	1.1	0.8	1.8
jugular foramen medial right	8	0.4	1.1	0.6	1.3
jugular foramen posterius left	8	0.7	0.9	0.7	1.3
jugular foramen posterius right	8	1.5	0.7	1	1.9
lambda	2	0.1	0.4	0.8	0.9
lambda inner	2	0.5	1.2	0.7	1.4
lateral orbitale left	8	0.8	0.4	0.7	1.1
lateral orbitale right	8	0.3	0.3	0.7	0.8
latero-frontale left	6	0.9	3.1	2	3.8
latero-frontale right	6	1.4	2.3	2.2	3.5
mandibular canal left	7	0.3	0.4	0.3	0.6
mandibular canal right	7	0.3	0.2	0.2	0.4
mandibular notch left	8	0.3	0.6	0.3	0.8
mandibular notch right	8	0.3	0.6	0.2	0.7
mastoidale left	8	0.4	0.9	0.5	1.1
mastoidale right	8	1	1.1	0.4	1.5
maxillare superius left	8	0.5	0.9	1.3	1.6
maxillare superius right	8	0.3	0.7	0.7	1
maxillary tuberosity left	8	0.6	0.9	2.1	2.3
maxillary tuberosity right	8	0.8	0.6	1.6	1.9
medial orbitale left	8	0.4	0.9	0.7	1.2
medial orbitale right	8	0.4	0.7	1.1	1.4
medio-molare 1st inferius left	6	0.2	0.4	0.3	0.6
medio-molare 1st inferius right	6	0.4	0.3	0.9	1
medio-molare 1st superius left	6	0.4	0.4	0.6	0.8
medio-molare 1st superius right	6	0.4	0.3	0.6	0.8
mental foramen left	3	0	0.5	0.6	0.8
mental foramen right	3	0.4	0.4	0.2	0.6
nasale	8	0.3	0.3	0.4	0.6

Appendix 1 Accuracy of Landmark Identification:

Crouzon Syndrome Patients (continued):

Landmark	n	Landmark Relocation Error x	y	z	|xyz|
nasion	8	0.2	0.6	0.6	0.9
naso-lacrimal inferius left	8	0.6	0.4	0.9	1.1
naso-lacrimal inferius right	8	1	0.8	1.6	2
odontoid	6	0.1	0.2	0.7	0.7
opisthion	8	0.4	0.4	1.2	1.3
opisthocranion	6	0.3	0.1	0.5	0.6
optic foramen a inferior left	8	0.5	0.4	0.7	0.9
optic foramen a inferior right	8	0.3	0.3	0.4	0.6
optic foramen a lateral left	8	0.7	0.7	0.7	1.2
optic foramen a lateral right	8	0.8	0.5	0.5	1.1
optic foramen a left	8	0.4	0.3	0.5	0.6
optic foramen a medial left	8	0.3	0.6	0.5	0.9
optic foramen a medial right	8	0.4	0.8	0.2	0.9
optic foramen a right	8	0.2	0.4	0.3	0.5
optic foramen a superior left	8	0.5	0.6	0.3	0.8
optic foramen a superior right	8	0.5	0.6	0.6	1
optic foramen p inferior left	8	0.8	0.9	1	1.6
optic foramen p inferior right	8	0.9	0.9	1	1.6
optic foramen p lateral left	8	0.6	1	1.1	1.6
optic foramen p lateral right	8	0.4	0.7	0.8	1.1
optic foramen p left	8	0.3	0.5	0.8	1
optic foramen p medial left	8	0.6	0.6	0.9	1.2
optic foramen p medial right	8	0.5	0.9	1	1.4
optic foramen p right	8	0.3	0.4	0.7	0.9
optic foramen p superior left	8	0.6	0.6	0.7	1.1
optic foramen p superior right	8	0.2	0.3	0.5	0.6
orbitale left	8	1.3	0.3	0.3	1.4
orbitale right	8	0.7	0.3	0.3	0.8
petrous posterius left	8	0.6	1.4	0.4	1.6
petrous posterius right	8	0.7	0.9	1.8	2.1
petrous sup-anterius left	8	0.7	0.3	0.3	0.8
petrous sup-anterius right	8	0.3	0.5	0.3	0.7
pogonion	8	0.5	0.4	0.6	0.9
posterior clinoid left	8	0.5	0.5	0.5	0.9
posterior clinoid right	8	0.5	0.6	0.4	0.9
posterior nasal spine	8	0.3	0.3	0.3	0.5
pre-articulare left	8	0.3	1	0.3	1.1
pre-articulare right	8	0.3	0.9	0.5	1.1
prosthion	8	0.4	0.8	0.7	1.2
pterygo-lateralis left	8	0.3	0.4	0.5	0.7
pterygo-lateralis right	8	0.3	0.5	0.5	0.7
pterygo-superius left	8	0.9	0.6	0.5	1.2
pterygo-superius right	8	0.9	0.7	0.7	1.4
sella	8	0.5	0.5	0.9	1.1
sphenion c left	2	0.5	0.5	0.7	1
sphenion c right	2	0.8	0.8	0.7	1.3
sphenion t left	2	0.4	0	0.1	0.4

Appendix 1 Accuracy of Landmark Identification:

Crouzon Syndrome Patients (continued):

Landmark	n	Landmark Relocation Error x	y	z	|xyz|
sphenion t right	2	0.8	0.8	1	1.5
sphenoidale anterior left	8	0.7	0.5	0.6	1.1
sphenoidale anterior right	8	0.7	0.3	1.3	1.5
stylomastoid foramen left	5	1.2	1.5	0.5	2
stylomastoid foramen right	5	0.1	0.5	0.7	0.8
subspinale	8	0.4	0.5	0.7	0.9
superior naso-maxillare left	8	0.4	0.5	0.6	0.9
superior naso-maxillare right	8	0.4	0.4	0.6	0.8
superior orbital fissure left	8	0.7	0.5	0.7	1.1
superior orbital fissure right	8	0.6	1.2	0.4	1.5
superior orbitale left	8	1	0.5	0.4	1.2
superior orbitale right	8	0.5	0.7	0.4	1
supero-lateral orbitale left	8	0.1	0.4	0.6	0.7
supero-lateral orbitale right	8	0.3	0.6	0.5	0.8
supero-lateral orbitale superius left	3	0.1	1.6	0.7	1.7
supero-lateral orbitale superius right	3	0.3	0.8	1.4	1.6
supero-medial orbitale left	4	2.3	0.9	2	3.2
supero-medial orbitale right	4	2.9	1.4	2.1	3.8
supramentale	7	0.6	0.6	0.5	1
vertex	5	1.2	5.2	0.6	5.3
vomo-ethmoid inferius	8	0.2	1.4	1.2	1.9
vomo-ethmoid superius	8	0.5	1	0.8	1.4
zygion left	8	0	0.6	0.4	0.7
zygion right	8	0.2	0.8	0.5	0.9
zygo-frontale left	8	0.3	0.4	0.6	0.8
zygo-frontale right	8	0.3	0.4	1.2	1.3
zygo-frontale sphenoidale left	8	0.4	0.4	0.9	1.1
zygo-frontale sphenoidale right	8	0.4	0.4	0.9	1.1
zygo-frontale superius left	3	1.2	1.5	0.8	2.1
zygo-frontale superius right	3	0	1	0.9	1.4
zygo-maxillare inferius laterale left	1	0.1	0.5	0.4	0.6
zygo-maxillare inferius laterale right	1	2.2	0	0.7	2.3
zygo-maxillare inferius left	8	0.7	0.9	0.6	1.3
zygo-maxillare inferius right	8	1.1	0.7	0.5	1.4
zygo-temporale left	8	0.2	0.8	0.8	1.1
zygo-temporale right	8	0.3	0.3	0.3	0.6

Appendix 1 Accuracy of Landmark Identification:

Dried Skulls:

Landmark	n	Landmark Relocation Error x	y	z	|xyz|
alare left	10	0.3	0.4	0.8	1
alare right	10	0.3	0.3	0.6	0.7
anterior clinoid left	10	0.4	0.3	0.8	1
anterior clinoid right	10	0.3	0.4	0.5	0.7
anterior nasal spine	10	0.3	0.2	0.4	0.5
articular eminence left	10	0.6	0.6	0.3	0.9
articular eminence right	10	0.8	0.7	0.2	1
articular fossa left	10	0.8	0.7	0.4	1.1
articular fossa right	10	0.4	0.5	0.3	0.7
asterion inner left	10	0.7	1.2	1.2	1.8
asterion inner right	10	0.6	1.2	2.1	2.5
asterion left	10	0.7	0.9	1	1.5
asterion right	10	0.7	1.2	2.1	2.5
auriculare left	10	0.2	1.5	0.4	1.5
auriculare right	10	0.4	1.4	0.6	1.6
basion	10	0.2	0.3	0.5	0.6
bregma	8	0.5	2.7	0.5	2.8
canine inferius left	7	0.3	0.4	0.6	0.8
canine inferius right	5	0.3	0.6	0.4	0.8
canine superius left	8	0.3	0.3	0.4	0.5
canine superius right	8	0.3	0.4	0.3	0.6
condylion laterale left	10	0.2	0.3	0.5	0.6
condylion laterale right	10	0.2	0.3	0.4	0.5
coronoid base left	10	0.2	0.3	0.7	0.8
coronoid base right	10	0.9	0.7	0.9	1.4
coronoid tip left	10	0.2	0.7	0.2	0.8
coronoid tip right	10	0.3	0.2	0.7	0.8
cribriform plate anterius left	10	0.7	1.4	1.1	1.9
cribriform plate anterius right	10	0.8	1.3	1.3	2
cribriform plate posterius left	10	0.5	1	0.4	1.2
cribriform plate posterius right	10	0.7	1.1	0.5	1.4
crista galli	10	0.2	0.2	0.2	0.3
disto-molare inferius left	6	0.4	0.5	0.6	0.8
disto-molare inferius right	6	0.7	0.7	1.1	1.5
disto-molare superius left	7	0.5	0.5	0.4	0.8
disto-molare superius right	7	0.3	0.4	0.3	0.6
ecto-canine inferius left	10	0.4	0.5	0.5	0.8
ecto-canine inferius right	10	0.5	0.6	0.6	1
ecto-canine superius left	10	0.3	0.3	0.5	0.7
ecto-canine superius right	10	0.6	0.5	0.6	1
ecto-incision central inferius left	10	0.4	0.6	1	1.2
ecto-incision central inferius right	10	0.3	0.6	1	1.2
ecto-incision central superius left	10	0.8	0.3	0.7	1.1
ecto-incision central superius right	10	0.5	0.5	1	1.3
ectomolare 1st inferius left	10	0.5	0.3	0.4	0.7
ectomolare 1st inferius right	10	0.5	0.3	0.5	0.8
ectomolare 1st superius left	10	0.3	0.5	0.4	0.7

Appendix 1 Accuracy of Landmark Identification:

Dried Skulls (continued):

Landmark	n	Landmark Relocation Error x	y	z	|xyz|
ectomolare 1st superius right	10	0.4	0.7	0.7	1.1
ethmoid spine	10	0.4	0.6	0.3	0.8
euryion left	9	0.4	0.8	1.3	1.6
euryion right	9	0.4	0.6	2	2.1
external auditory meatus anterius left	10	0.4	0.4	0.7	0.9
external auditory meatus anterius right	10	0.3	0.4	0.8	0.9
external auditory meatus inferius left	10	1.1	0.4	0.5	1.2
external auditory meatus inferius right	10	0.7	0.4	0.4	0.9
external auditory meatus posterius left	10	0.9	0.3	0.7	1.2
external auditory meatus posterius right	10	0.7	0.5	1	1.4
ext aud meatus superius (ie porion) L	10	1	0.4	0.2	1.1
ext aud meatus superius (ie porion) R	10	0.8	0.3	0.2	0.9
foramen caecum	10	0.4	0.4	0.4	0.7
foramen in ovale left	10	0.3	0.3	0.5	0.7
foramen in ovale right	10	0.4	0.3	0.3	0.6
foramen in spinosum left	10	1.1	1.2	0.5	1.7
foramen in spinosum right	10	0.9	0.4	0.4	1.1
foramen magnum lateralis left	10	0	0.3	0.7	0.8
foramen magnum lateralis right	10	0	0.2	0.5	0.5
foramen out ovale left	10	0.3	0.5	0.2	0.6
foramen out ovale right	10	0.4	0.5	0.5	0.8
foramen out spinosum left	10	1.3	1.1	1	1.9
foramen out spinosum right	10	0.6	1.2	0.7	1.5
glabella	10	0.4	0.2	0.4	0.6
gnathion	10	0.6	0.5	0.3	0.9
gonion left	10	0.2	1.1	0.8	1.4
gonion right	10	0.4	1.2	0.9	1.6
greater palatine foramen left	10	0.3	0.2	0.4	0.5
greater palatine foramen right	10	0.3	0.6	0.7	1
greater wing laterale left	10	0.4	0.3	0.2	0.5
greater wing laterale right	10	0.3	0.3	0.3	0.5
greater wing mediale left	10	0.6	0.4	1	1.3
greater wing mediale right	10	0.6	0.5	1.2	1.4
hamular notch left	10	0.3	0.5	0.4	0.7
hamular notch right	10	0.5	0.5	0.1	0.7
hamular process left	10	0.5	0.5	0.3	0.7
hamular process right	10	0.3	0.2	0.4	0.6
hormion	10	0.2	0.5	0.7	0.9
incision inferius left	10	0.4	0.5	0.5	0.8
incision inferius right	8	0.4	0.2	0.7	0.8
incision superius left	9	0.3	0.3	0.3	0.5
incision superius right	9	0.4	0.3	0.2	0.6
inferior naso-maxillare left	10	0.6	0.4	0.9	1.1
inferior naso-maxillare right	10	0.4	0.4	0.4	0.7
inferior orbital fissure left	10	0.5	0.7	0.2	0.9
inferior orbital fissure right	10	0.3	0.2	0.1	0.4
infero-lateral orbitale left	10	0.7	0.7	0.7	1.2

Appendix 1 Accuracy of Landmark Identification:

Dried Skulls (continued):

Landmark	n	Landmark Relocation Error x	y	z	|xyz|
infero-lateral orbitale right	10	0.8	0.8	0.8	1.4
infradentale	10	0.3	0.2	0.5	0.7
infra-orbital foramen inferior left	6	0.6	0.3	1	1.2
infra-orbital foramen inferior right	6	0.4	0.3	0.6	0.8
infra-orbital foramen lateral left	6	0.5	0.4	0.5	0.8
infra-orbital foramen lateral right	6	0.6	0.5	0.8	1.1
infra-orbital foramen left	10	0.2	0.1	0.4	0.5
infra-orbital foramen medial left	6	0.5	0.7	0.6	1.1
infra-orbital foramen medial right	6	0.4	0.6	0.5	0.8
infra-orbital foramen right	10	0.2	0.3	0.3	0.5
infra-orbital foramen superior left	6	0.5	0.2	0.3	0.6
infra-orbital foramen superior right	6	0.4	0.3	0.5	0.7
internal auditory meatus left	10	0.3	0.3	0	0.4
internal auditory meatus right	10	0.5	0.3	0.3	0.7
internal occipital protuberance	10	1.4	0.8	0.6	1.7
jugular foramen lateralis left	10	0.1	0.3	0.2	0.4
jugular foramen lateralis right	10	0.4	0.3	0.4	0.7
jugular foramen medial left	10	1.1	0.7	1	1.7
jugular foramen medial right	10	0.9	0.2	0.8	1.2
jugular foramen posterius left	10	0.3	0.2	0.6	0.7
jugular foramen posterius right	10	0.5	0.2	0	0.5
lambda	10	1.2	0.5	1.3	1.8
lambda inner	10	0.8	0.5	1.4	1.7
lateral orbitale left	10	0.2	0.8	1.6	1.8
lateral orbitale right	10	0.4	0.6	2	2.1
latero-frontale left	9	0.6	2.1	1.1	2.4
latero-frontale right	9	0.8	1.7	1.1	2.2
mandibular canal left	10	0.2	0.3	0.4	0.6
mandibular canal right	10	0.2	0.3	0.3	0.5
mandibular notch left	10	0.2	0.4	0.2	0.5
mandibular notch right	10	0.3	0.6	0.2	0.7
mastoidale left	10	0.6	1.1	0.4	1.3
mastoidale right	10	1.3	0.5	0.6	1.5
maxillare superius left	10	0.8	1	0.4	1.3
maxillare superius right	10	0.7	0.5	0.4	1
maxillary tuberosity left	10	0.5	0.6	0.6	1
maxillary tuberosity right	10	0.8	0.8	0.5	1.3
medial orbitale left	10	0.2	0.6	0.7	1
medial orbitale right	10	0.4	0.4	1.1	1.2
medio-molare 1st inferius left	6	0.9	0.3	0.3	1
medio-molare 1st inferius right	6	0.2	0.4	0.9	1
medio-molare 1st superius left	7	0.4	0.3	0.5	0.7
medio-molare 1st superius right	7	0.2	0.2	0.3	0.4
mental foramen left	9	0.4	0.5	0.4	0.8
mental foramen right	9	0.5	0.3	0.3	0.7
nasale	10	0.6	0.3	0.4	0.7
nasion	10	0.3	0.2	0.8	0.8

Appendix 1 Accuracy of Landmark Identification:

Dried Skulls (continued):

Landmark	n	Landmark Relocation Error x	y	z	|xyz|
naso-lacrimal inferius left	10	0.4	0.6	0.4	0.8
naso-lacrimal inferius right	10	0.8	0.5	0.4	1
opisthion	10	0.4	0.3	0.7	0.9
opisthocranion	9	0.6	0.2	0.7	1
optic foramen a inferior left	10	0.3	0.7	0.6	0.9
optic foramen a inferior right	10	0.5	0.4	0.4	0.7
optic foramen a lateral left	10	0.8	0.5	0.4	1.1
optic foramen a lateral right	10	0.5	0.5	0.6	0.9
optic foramen a left	10	0.2	0.3	0.2	0.4
optic foramen a medial left	10	1	0.7	0.3	1.2
optic foramen a medial right	10	0.3	0.6	0.3	0.8
optic foramen a right	10	0.3	0.3	0.3	0.5
optic foramen a superior left	10	0.3	0.7	0.2	0.8
optic foramen a superior right	10	0.6	0.7	0.3	0.9
optic foramen p inferior left	10	0.6	0.2	0.2	0.7
optic foramen p inferior right	10	1.2	0.3	0.5	1.4
optic foramen p lateral left	10	0.5	0.9	0.6	1.2
optic foramen p lateral right	10	0.7	1.5	0.4	1.7
optic foramen p left	10	0.2	0.4	0.3	0.5
optic foramen p medial left	10	0.6	1.1	0.7	1.4
optic foramen p medial right	10	0.9	1	0.5	1.4
optic foramen p right	10	0.5	0.5	0.3	0.8
optic foramen p superior left	10	0.5	0.6	0.3	0.9
optic foramen p superior right	10	0.4	0.9	0.6	1.2
orbitale left	10	0.7	0.4	0.3	0.9
orbitale right	10	0.8	0.4	0.2	1
petrous posterius left	10	0.5	2	0.9	2.2
petrous posterius right	10	0.5	1.4	1.1	1.8
petrous sup-anterius left	10	0.3	0.9	0.3	1
petrous sup-anterius right	10	0.4	0.5	0.5	0.8
pogonion	10	0.4	0.2	0.8	0.9
posterior clinoid left	10	0.5	0.3	0.3	0.7
posterior clinoid right	10	0.5	0.5	0.5	0.9
posterior nasal spine	10	0.5	0.7	0.6	1.1
pre-articulare left	10	0.3	1	0.2	1
pre-articulare right	10	0.2	0.8	0.3	0.9
prosthion	10	0.3	0.4	0.6	0.8
pterygo-lateralis left	10	0.4	0.7	0.5	0.9
pterygo-lateralis right	10	0.2	0.5	0.5	0.8
pterygo-superius left	10	1.2	0.8	0.3	1.5
pterygo-superius right	10	0.7	0.4	0.3	0.8
sella	10	0.5	0.2	0.8	1
sphenion c left	10	1.2	1.4	1.7	2.5
sphenion c right	10	1	1	1.4	2
sphenion t left	10	1.5	1.2	2	2.8
sphenion t right	10	0.7	1.4	1.5	2.2
sphenoidale anterior left	10	1.2	0.3	0.7	1.5

Appendix 1 Accuracy of Landmark Identification:

Dried Skulls (continued):

Landmark	n	Landmark Relocation Error x	y	z	|xyz|
sphenoidale anterior right	10	0.9	0.3	0.5	1.1
stylomastoid foramen left	10	0.7	0.6	0.3	0.9
stylomastoid foramen right	10	1	0.9	0.3	1.3
subspinale	10	0.6	0.5	1.1	1.3
superior naso-maxillare left	10	0.8	0.5	0.7	1.2
superior naso-maxillare right	10	0.5	0.3	0.8	1
superior orbital fissure left	10	0.3	0.3	0.2	0.5
superior orbital fissure right	10	0.2	0.3	0.3	0.4
superior orbitale left	10	0.2	0.5	0.4	0.7
superior orbitale right	10	0.5	0.4	0.3	0.7
supero-lateral orbitale left	10	0.4	0.4	0.5	0.8
supero-lateral orbitale right	10	0.3	0.4	0.4	0.6
supramentale	10	0.3	0.3	1.2	1.3
vertex	9	0.7	2.4	0.4	2.5
vomo-ethmoid inferius	10	0	0.3	0.7	0.7
vomo-ethmoid superius	10	0.4	1.6	0.5	1.8
zygion left	10	0.2	0.3	0.4	0.5
zygion right	10	0.2	0.5	0.3	0.6
zygo-frontale left	10	0.4	0.6	0.8	1.1
zygo-frontale right	10	0.5	0.3	0.5	0.8
zygo-frontale sphenoidale left	10	1.2	1	1.7	2.4
zygo-frontale sphenoidale right	10	0.9	1.2	2.2	2.7
zygo-maxillare inferius left	10	1.1	0.6	0.4	1.3
zygo-maxillare inferius right	10	0.9	0.5	0.7	1.3
zygo-temporale left	10	0.1	0.4	0.3	0.5
zygo-temporale right	10	0.4	0.3	0.4	0.7

Appendix 2

Measurements for Dried Skull Experimental Standards and Crouzon Syndrome Patients

---

1. 6 Months of Age
2. 2 years of Age
3. 6 years of Age
4. Adult

Appendix 2 Measurements for the Experimental Standards and the Patients with Crouzon Syndrome:

Six Months of Age:

			6 Month Standard			Patient RN		Patient SH	
Anatomical Unit	**Definition**	**unit**	**mean**	**sd**	**n**	**Value**	**Z**	**Value**	**Z**
MANDIBLE									
Distances									
L anterior superior body	id-em1il	mms	17.8	2.4	5	16.3	-0.62	13.8	-1.67
L posterior superior body	em1il-cbl	mms	14.3	3.9	5	15.7	0.36	14.0	-0.08
L total superior body	id-cbl	mms	30.9	5.6	6	30.6	-0.05	27.2	-0.66
L anterior ramus	cbl-ctl	mms	15.3	2.8	6	14.5	-0.29	16.2	0.32
L anterior mandibular notch	ctl-mnl	mms	8.0	2.1	6	9.1	0.52	7.6	-0.19
L posterior mandibular notch	mnl-cdl	mms	9.2	2.7	6	9.2	0.00	7.6	-0.59
L posterior ramus	cdl-gol	mms	22.1	6.3	6	18.7	-0.54	19.4	-0.43
L inferior body	gol-gn	mms	40.8	6.1	6	34.6	-1.02	38.7	-0.34
R anterior superior body	id-em1ir	mms	18.3	1.3	5	17.1	-0.92	15.2	-2.38
R posterior superior body	em1ir-cbr	mms	14.3	4.4	5	14.7	0.09	14.8	0.11
R total superior body	id-cbr	mms	31.2	5.4	6	30.5	-0.13	29.0	-0.41
R anterior ramus	cbr-ctr	mms	15.0	4.5	6	14.3	-0.16	13.8	-0.27
R anterior mandibular notch	ctr-mnr	mms	8.4	2.0	6	10.1	0.85	7.2	-0.60
R posterior mandibular notch	mnr-cdr	mms	9.6	2.6	6	8.1	-0.58	9.7	0.04
R posterior ramus	cdr-gor	mms	21.7	6.6	6	18.0	-0.56	21.4	-0.05
R inferior body	gor-gn	mms	39.2	6.9	6	34.4	-0.70	36.2	-0.43
Dimensions									
Intergonial dimension	gol-gor	mms	52.5	10.1	6	42.6	-0.98	44.2	-0.82
Intercondylar dimension	cdl-cdr	mms	66.4	9.3	6	63.8	-0.28	58.1	-0.89
Intercoronoid base dimension	cbl-cbr	mms	46.2	8.1	6	46.0	-0.02	40.3	-0.73
Intermolar dimension	em1il-em1ir	mms	30.1	5.3	5	30.2	0.02	25.0	-0.96
L Superior ramus width	cdl-ctl	mms	15.4	3.1	6	16.4	0.32	13.9	-0.48
L inferior ramus width	gol-cbl	mms	17.0	3.1	6	15.4	-0.52	18.4	0.45
R superior ramus width	cdr-ctr	mms	14.6	3.0	6	16.7	0.70	15.1	0.17
R inferior ramus width	gor-cbr	mms	16.8	3.2	6	15.6	-0.37	19.3	0.78
Anterior symphyseal height	gn-id	mms	13.6	3.0	6	16.6	1.00	16.7	1.03
L total mandibular length	gn-cdl	mms	58.8	10.4	6	50.6	-0.79	53.7	-0.49
R total mandibular length	gn-cdr	mms	59.8	11.0	6	50.4	-0.85	53.7	-0.55
Angles									
L mandibular notch angle	cdl-mnl-ctl	deg	118.2	14.8	6	128.0	0.66	131.7	0.91
R mandibular notch angle	cdr-mnr-ctr	deg	118.5	20.0	6	131.3	0.64	127.7	0.46
L gonial angle	cdl-gol-gn	deg	127.2	5.2	6	141.8	2.81	132.0	0.92
R gonial angle	cdr-gor-gn	deg	131.9	2.7	6	145.6	5.07	136.3	1.63
L coronoid base angle	ctl-cbl-id	deg	136.5	4.8	6	122.1	-3.00	138.6	0.44
R coronoid base angle	ctr-cbr-id	deg	134.7	5.0	6	129.6	-1.02	143.8	1.82
L coronoid-dental base angle	ctl-cbl-em1il	deg	138.8	1.4	5	122.9	11.36	141.9	2.21
R coronoid-dental base angle	ctr-cbr-em1ir	deg	135.6	6.0	5	127.2	-1.40	153.4	2.97
L symphyseal angle	gol-gn-id	deg	91.2	9.1	6	89.5	-0.19	79.4	-1.30
R symphyseal angle	gor-gn-id	deg	94.6	4.4	6	89.5	-1.16	87.0	-1.73
Anterior mandibular angle	gol-gn-gor	deg	77.9	5.7	6	76.2	-0.30	72.2	-1.00

Appendix 2 Measurements for the Experimental Standards and the Patients with Crouzon Syndrome:

Six Months of Age (continued):

			6 Month Standard			Patient RN		Patient SH	
Anatomical Unit	**Definition**	**unit**	**mean**	**sd**	**n**	**Value**	**Z**	**Value**	**Z**
MAXILLA									
Distances									
Orbital Region									
L fronto-maxillary suture	snml-morl	mms	5.8	1.6	6	8.8	1.88	5.5	-0.19
L frontal process orbital rim	nlil-morl	mms	10.6	3.0	6	8.1	-0.83	8.6	-0.67
L medial orbital floor	msl-nlil	mms	22.8	3.9	6	15.8	-1.79	17.7	-1.31
L posterior lateral orbital floor	msl-iobfl	mms	15.5	2.5	6	12.3	-1.28	14.7	-0.32
L anterior lateral orbital floor	orl-iobfl	mms	12.3	3.5	6	11.0	-0.37	9.8	-0.71
L maxillary infra-orbital rim	orl-nlil	mms	9.9	1.2	6	11.5	1.33	9.2	-0.58
R fronto-maxillary suture	snmr-morr	mms	6.3	1.9	6	8.0	0.89	7.5	0.63
R frontal process orbital rim	nlir-morr	mms	10.4	2.6	6	6.9	-1.35	7.9	-0.96
R medial orbital floor	msr-nlir	mms	22.0	3.2	6	14.3	-2.41	16.1	-1.84
R posterior lateral orbital floor	msr-iobfr	mms	14.5	2.3	6	12.7	-0.78	15.0	0.22
R anterior lateral orbital floor	orr-iobfr	mms	12.5	3.1	6	11.3	-0.39	10.7	-0.58
R maxillary infra-orbital rim	orr-nlir	mms	10.0	2.3	6	12.5	1.10	13.0	1.30
Anterior Wall									
L anterior zygo-maxillary suture	zmil-orl	mms	16.6	3.3	6	17.6	0.30	13.4	-0.97
L lateral maxillary wall	zmil-em1sl	mms	15.8	3.9	6	17.8	0.51	15.6	-0.05
L anterior alveolar margin	em1sl-pr	mms	20.4	2.1	6	19.7	-0.33	18.1	-1.10
L lower pyriform margin	ans-all	mms	8.1	1.6	6	10.5	1.50	8.3	0.12
L upper pyriform margin	all-inml	mms	11.3	3.3	6	9.6	-0.52	8.6	-0.82
L naso-maxillary suture	inml-snml	mms	11.4	2.7	6	9.3	-0.78	8.8	-0.96
R anterior zygo-maxillary suture	zmir-orr	mms	15.0	3.8	6	19.7	1.24	10.2	-1.26
R lateral maxillary wall	zmir-em1sr	mms	17.6	4.3	6	19.1	0.35	16.0	-0.37
R anterior alveolar margin	em1sr-pr	mms	19.6	2.0	6	21.0	0.70	18.3	-0.65
R lower pyriform margin	ans-alr	mms	9.8	2.1	6	10.4	0.29	11.1	0.62
R upper pyriform margin	alr-inmr	mms	11.2	2.5	6	11.3	0.04	10.5	-0.28
L naso-maxillary suture	inmr-snmr	mms	12.4	3.1	6	9.6	-0.90	8.8	-1.16
Anterior alveolar height	pr-ans	mms	8.5	2.5	6	7.9	-0.24	9.9	0.56
Lateral Wall									
L posterior alveolar margin	em1sl-mxtl	mms	12.3	3.0	6	14.1	0.60	15.0	0.90
L posterior maxillary wall	mxtl-msl	mms	19.0	5.0	6	16.8	-0.44	19.4	0.08
L posterior lateral orbital floor	msl-iobfl	mms	15.5	2.5	6	12.3	-1.28	14.7	-0.32
L posterior zygo-maxillary suture	iobfl-zmil	mms	10.9	1.6	6	14.4	2.19	11.1	0.13
R posterior alveolar margin	em1sr-mxtr	mms	13.4	4.3	6	14.0	0.14	15.3	0.44
R posterior maxillary wall	mxtr-msr	mms	19.1	4.3	6	18.7	-0.09	18.4	-0.16
R posterior lateral orbital floor	msr-iobfr	mms	14.5	2.3	6	12.7	-0.78	15.0	0.22
R posterior zygo-maxillary suture	iobfr-zmir	mms	10.4	1.7	6	15.5	3.00	11.2	0.47
Palate									
L posterior palatal height	em1sl-gpfl	mms	15.8	4.0	6	15.8	0.00	18.6	0.70
L posterior palatal width	gpfl-pns	mms	9.9	1.6	6	11.1	0.75	10.1	0.13
R posterior palatal height	em1sr-gpfr	mms	16.8	4.9	6	15.9	-0.18	18.0	0.24
R posterior palatal width	gpfr-pns	mms	9.9	1.3	6	10.6	0.54	10.4	0.38
Superior palatal length	ans-pns	mms	31.1	5.4	6	26.3	-0.89	27.9	-0.59

Appendix 2 Measurements for the Experimental Standards and the Patients with Crouzon Syndrome:

Six Months of Age (continued):

			6 Month Standard			Patient RN		Patient SH	
Anatomical Unit	**Definition**	**unit**	**mean**	**sd**	**n**	**Value**	**Z**	**Value**	**Z**
MAXILLA (continued)									
Dimensions									
Anterior midline height	n-pr	mms	35.0	7.1	6	32.1	-0.41	31.9	-0.44
L lateral height	morl-em1sl	mms	31.5	6.6	6	27.6	-0.59	26.8	-0.71
R lateral height	morr-em1sr	mms	31.3	7.2	6	25.9	-0.75	26.3	-0.69
L posterior height	gpfl-msl	mms	16.8	3.3	6	15.7	-0.33	17.6	0.24
R posterior height	gpfr-msr	mms	16.7	3.0	6	16.5	-0.07	16.6	-0.03
L superior length	msl-inml	mms	31.3	5.6	6	24.1	-1.29	25.9	-0.96
R superior length	msr-inmr	mms	31.2	5.1	6	23.4	-1.53	24.4	-1.33
Posterior palatal width	gpfl-gpfr	mms	19.1	2.6	6	19.2	0.04	18.8	-0.12
Anterior inter-canine width	ecsl-ecsr	mms	24.8	3.2	6	25.7	0.28	26.8	0.62
Maximum maxillary width	zmil-zmir	mms	60.0	9.7	6	64.1	0.42	52.7	-0.75
Superior (inter-orbital rim) width	orl-orr	mms	37.8	6.9	6	45.6	1.13	43.8	0.87
Nasal aperture height	na-ans	mms	14.2	2.3	6	13.8	-0.17	11.3	-1.26
Nasal aperture width	all-alr	mms	15.1	3.5	6	15.1	0.00	15.6	0.14
Angles									
L orbital floor angle	nlil-msl-iobfl	deg	56.5	3.1	6	66.2	3.13	56.2	-0.10
R orbital floor angle	nlir-msr-iobfr	deg	56.1	9.0	6	75.1	2.11	64.5	0.93
L posterior inferior angle	msl-gpfl-em1sl	deg	110.9	5.7	6	101.3	-1.68	110.3	-0.11
R posterior inferior angle	msr-gpfr-em1sr	deg	109.7	6.1	6	94.4	-2.51	111.7	0.33
Superior maxillary splay	iobfl-msl/msr-iobfr	deg	99.4	11.2	6	129.0	2.64	125.7	2.35
L superior /occlusal angle	snml-msl/em1sl-pr	deg	50.5	8.2	6	56.5	0.73	68.3	2.17
R superior /occlusal angle	snmr-msr/em1sr-pr	deg	48.8	7.2	6	57.7	1.24	57.9	1.26
L palatal/occlusal angle	ans-pns/em1sl-pr	deg	55.5	8.3	6	68.1	1.52	79.8	2.93
R palatal/occlusal angle	ans-pns/em1sr-pr	deg	52.8	6.9	6	63.7	1.58	72.3	2.83
Anterior palatal angle	gpfl-ans-gpfr	deg	39.3	1.9	6	42.4	1.63	38.0	-0.68
Maxillary arch angle	gpfl-pr-gpfr	deg	40.0	1.5	6	49.0	6.00	45.8	3.87
NASAL BONES									
Distances									
Nasal length	na-n	mms	12.2	3.0	6	12.6	0.13	13.0	0.27
L inferior nasal width	na-inml	mms	4.4	1.0	6	5.7	1.30	7.4	3.00
L naso-maxillary suture	inml-snml	mms	11.4	2.7	6	9.3	-0.78	8.8	-0.96
L fronto nasal suture	n-snml	mms	5.1	0.9	6	7.8	3.00	7.6	2.78
R inferior nasal width	na-inmr	mms	3.9	1.3	6	5.3	1.08	8.6	3.62
R naso-maxillary suture	inmr-snmr	mms	12.4	3.1	6	9.6	-0.90	8.8	-1.16
R fronto-nasal suture	n-snmr	mms	5.2	1.5	6	6.7	1.00	8.5	2.20
Dimensions									
Inferior width	inml-inmr	mms	7.7	1.7	6	9.5	1.06	12.9	3.06
Superior width	snml-snmr	mms	8.6	2.1	6	10.4	0.86	10.1	0.71
Angles									
Nasal/anterior cranial base angle	s-n-na	deg	100.3	8.3	6	97.8	-0.30	98.7	-0.19
Superior nasal bone angle	snml-n-snmr	deg	109.8	23.5	6	90.6	-0.82	77.9	-1.36
Inferior nasal bone angle	inml-na-inmr	deg	135.3	18.5	6	119.5	-0.85	107.1	-1.52
Splay of nasal bones	inml-snml/snmr-inmr	deg	5.6	31.5	6	4.9	-0.02	18.0	0.39

Appendix 2 Measurements for the Experimental Standards and the Patients with Crouzon Syndrome:

Six Months of Age (continued):

			6 Month Standard			Patient RN		Patient SH	
Anatomical Unit	**Definition**	**unit**	**mean**	**sd**	**n**	**Value**	**Z**	**Value**	**Z**
FRONTAL									
Distances									
Supra-orbital									
L fronto-nasal suture	n-snml	mms	5.1	0.9	6	7.8	3.00	7.6	2.78
L fronto-maxillary suture	snml-morl	mms	5.8	1.6	6	8.8	1.88	5.5	-0.19
L superior medial orbital rim	morl-sorl	mms	17.8	3.1	6	19.0	0.39	15.4	-0.77
L superior lateral orbital rim	sorl-slorl	mms	22.0	4.2	6	15.9	-1.45	21.8	-0.05
L fronto-zygomatic suture (anterior)	slorl-zfl	mms	4.3	0.5	6	4.0	-0.60	7.6	6.60
L fronto-zygomatic suture (lateral)	zfl-zfsl	mms	4.9	2.0	6	4.1	-0.40	6.1	0.60
L fronto-zygomatic suture (medial)	zfsl-slorl	mms	7.1	2.0	6	3.5	-1.80	10.8	1.85
R fronto-nasal suture	n-snmr	mms	5.2	1.5	6	6.7	1.00	8.5	2.20
R fronto-maxillary suture	snmr-morr	mms	6.3	1.9	6	8.0	0.89	7.5	0.63
R superior medial orbital rim	morr-sorr	mms	17.4	2.9	6	23.4	2.07	9.0	-2.90
R superior lateral orbital rim	sorr-slorr	mms	22.8	4.0	6	16.4	-1.60	23.4	0.15
R fronto-zygomatic suture (anterior)	slorr-zfr	mms	4.1	0.7	6	3.6	-0.71	6.7	3.71
R fronto-zygomatic suture (lateral)	zfr-zfsr	mms	4.5	2.3	6	4.2	-0.13	4.8	0.13
R fronto-zygomatic suture (medial)	zfsr-slorr	mms	6.6	1.8	6	3.8	-1.56	7.8	0.67
Ethmoid									
Nasal root projection	n-fc	mms	5.4	2.3	6			5.5	0.04
L fronto-ethmoid attachment (anterior)	fc-cpal	mms	4.8	0.7	5			5.3	0.71
L fronto-ethmoid attachment (cribriform)	cpal-cppl	mms	16.5	2.5	5	22.8	2.52	19.6	1.24
L fronto-ethmoid attachment (posterior)	cppl-ofaml	mms	8.4	2.5	6	3.0	-2.16	4.4	-1.60
L fronto-ethmoid attachment (orbital)	morl-ofaml	mms	25.8	4.7	6	21.3	-0.96	22.9	-0.62
R fronto-ethmoid attachment (anterior)	fc-cpar	mms	5.1	1.2	6			5.1	0.00
R fronto-ethmoid attachment (cribriform)	cpar-cppr	mms	17.6	2.9	6	23.8	2.14	19.8	0.76
R fronto-ethmoid attachment (posterior)	cppr-ofamr	mms	8.2	2.5	6	2.9	-2.12	5.6	-1.04
R fronto-ethmoid attachment (orbital)	morr-ofamr	mms	26.0	4.7	6	21.8	-0.89	20.3	-1.21
Sphenoid									
L superior orbital fissure	ofaml-sobfl	mms	12.5	2.9	6	11.3	-0.41	4.3	-2.83
L fronto-sphenoid suture (orbital)	sobfl-zfsl	mms	14.3	4.0	6	15.7	0.35	22.8	2.12
L lesser wing length	spal-cppl	mms	27.0	5.3	6	15.9	-2.09	22.4	-0.87
R superior orbital fissure	ofamr-sobfr	mms	11.8	2.0	6	13.7	0.95	5.3	-3.25
R fronto-sphenoid suture (orbital)	sobfr-zfsr	mms	14.1	3.7	6	16.0	0.51	22.1	2.16
R lesser wing length	spar-cppr	mms	25.2	4.5	6	13.2	-2.67	25.1	-0.02
Dimensions									
Glabellar height	g-n	mms	7.6	2.6	6	6.1	-0.58	3.1	-1.73
Glabellar prominence	s-g	mms	48.3	8.5	6	46.2	-0.25	43.5	-0.56
L anterior cranial fossa depth	sorl-spal	mms	28.5	5.8	6	23.5	-0.86	26.9	-0.28
R anterior cranial fossa depth	sorr-spar	mms	28.0	5.2	6	28.4	0.08	29.4	0.27
Anterior superior orbital width	sorl-sorr	mms	37.4	5.0	6	50.4	2.60	33.0	-0.88
Anterior supero-lateral orbital width	slorl-slorr	mms	68.9	10.6	6	66.9	-0.19	69.7	0.08
Posterior width	spal-spar	mms	57.3	9.9	6	37.1	-2.04	53.6	-0.37

Appendix 2 Measurements for the Experimental Standards and the Patients with Crouzon Syndrome:

Six Months of Age (continued):

			6 Month Standard			Patient RN		Patient SH	
Anatomical Unit	Definition	unit	mean	sd	n	Value	Z	Value	Z
ZYGOMATIC BONE									
Distances									
L zygo-maxillary suture (orbital)	orl-iobfl	mms	12.3	3.5	6	11.0	-0.37	9.8	-0.71
L inferior orbital fissure (ant height)	iobfl-gwll	mms	6.9	0.7	6	4.5	-3.43	4.9	-2.86
L spheno-zygomatic suture	zfsl-gwll	mms	10.6	1.5	6	16.2	3.73	8.9	-1.13
L fronto-zygomatic suture (medial)	zfsl-slorl	mms	7.1	2.0	6	3.5	-1.80	10.8	1.85
L fronto-zygomatic suture (anterior)	slorl-zfl	mms	4.3	0.5	6	4.0	-0.60	7.6	6.60
L fronto-zygomatic suture (lateral)	zfl-zfsl	mms	4.9	2.0	6	4.1	-0.40	6.1	0.60
L infero-lateral orbital rim	orl-ilorl	mms	11.3	3.5	6	9.4	-0.54	10.5	-0.23
L infero-lateral orbital rim	ilorl-lorl	mms	8.5	1.1	6	9.7	1.09	5.1	-3.09
L lateral orbital rim	lorl-slorl	mms	3.1	1.7	6	4.0	0.53	4.7	0.94
L lateral frontal process	zfl-ztl	mms	14.3	2.6	6	19.9	2.15	11.0	-1.27
L zygomatico-temporal suture	ztl-parl	mms	12.6	3.2	6	10.8	-0.56	9.0	-1.13
L inferior arch	parl-zmil	mms	15.8	4.6	6	8.8	-1.52	13.8	-0.43
L zygo-maxillary suture	zmil-orl	mms	16.6	3.3	6	17.6	0.30	13.4	-0.97
R zygo-maxillary suture (orbital)	orr-iobfr	mms	12.5	3.1	6	11.3	-0.39	10.7	-0.58
R inferior orbital fissure (ant height)	iobfr-gwlr	mms	6.8	0.9	6	5.3	-1.67	5.3	-1.67
R spheno-zygomatic suture	zfsr-gwlr	mms	11.1	2.8	6	17.9	2.43	6.9	-1.50
R fronto-zygomatic suture (medial)	zfsr-slorr	mms	6.6	1.8	6	3.8	-1.56	7.8	0.67
R fronto-zygomatic suture (anterior)	slorr-zfr	mms	4.1	0.7	6	3.6	-0.71	6.7	3.71
R fronto-zygomatic suture (lateral)	zfr-zfsr	mms	4.5	2.3	6	4.2	-0.13	4.8	0.13
R infero-lateral orbital rim	orr-ilorr	mms	9.6	3.8	6	10.2	0.16	9.6	0.00
R infero-lateral orbital rim	ilorr-lorr	mms	9.6	1.9	6	9.6	0.00	5.2	-2.32
R lateral orbital rim	lorr-slorr	mms	2.3	1.7	6	4.4	1.24	5.6	1.94
R lateral frontal process	zfr-ztr	mms	15.4	3.3	6	19.5	1.24	10.2	-1.58
R zygomatico-temporal suture	ztr-parr	mms	11.7	4.8	6	12.6	0.19	10.4	-0.27
R inferior arch	parr-zmir	mms	15.9	5.3	6	8.2	-1.45	16.5	0.11
R zygo-maxillary suture	zmir-orr	mms	15.0	3.8	6	19.7	1.24	10.2	-1.26
Dimensions									
L zygomatic height	slorl-zmil	mms	23.5	5.0	6	25.9	0.48	23.0	-0.10
R zygomatic height	slorr-zmir	mms	68.6	11.0	6	71.1	0.23	63.0	-0.51
L zygomatic length	parl-orl	mms	29.8	6.4	6	25.2	-0.72	22.7	-1.11
R zygomatic length	parr-orr	mms	27.1	8.0	6	26.9	-0.03	24.2	-0.36
L zygomatic lateral depth	gwll-ilorl	mms	11.8	2.6	6	13.7	0.73	13.0	0.46
R zygomatic lateral depth	gwlr-ilorr	mms	11.6	2.3	6	14.5	1.26	12.5	0.39
VOMER									
Distances									
Palatal length	ans-pns	mms	31.1	5.4	6	26.3	-0.89	27.9	-0.59
Posterior choanal height	pns-h	mms	11.8	4.4	6	8.8	-0.68	10.8	-0.23
Spheno-vomerine junction	h-ves	mms	10.4	5.1	6	4.5	-1.16	9.9	-0.10
Ethmoid-vomerine junction	ves-vei	mms	11.4	3.9	6	14.6	0.82	8.7	-0.69
Septal attachment	vei-ans	mms	17.8	7.5	6	18.0	0.03	21.8	0.53
Dimension and Angle									
Vomerine length	h-ans	mms	39.8	7.8	6	34.1	-0.73	38.0	-0.23
Vomerine angle	s-n/h-ans	deg	20.9	3.7	6	24.5	0.97	17.1	-1.03

Appendix 2 Measurements for the Experimental Standards and the Patients with Crouzon Syndrome:

Six Months of Age (continued):

			6 Month Standard			Patient RN		Patient SH	
Anatomical Unit	**Definition**	**unit**	**mean**	**sd**	**n**	**Value**	**Z**	**Value**	**Z**
ETHMOID									
Lateral Plate									
Distances									
L anterior border lateral plate	nlil-morl	mms	10.6	3.0	6	8.1	-0.83	8.6	-0.67
L frontal ethmoid attachment (orbital)	morl-ofaml	mms	25.8	4.7	6	21.3	-0.96	22.9	-0.62
L posterior border lateral plate	ofaml-msl	mms	8.1	1.9	6	8.4	0.16	5.7	-1.26
L inferior border lateral plate	msl-nlil	mms	22.8	3.9	6	15.8	-1.79	17.7	-1.31
R anterior border lateral plate	nlir-morr	mms	10.4	2.6	6	6.9	-1.35	7.9	-0.96
R frontal ethmoid attachment (orbital)	morr-ofamr	mms	26.0	4.7	6	21.8	-0.89	20.3	-1.21
R posterior border lateral plate	ofamr-msr	mms	7.8	2.8	6	8.6	0.29	4.7	-1.11
R inferior border lateral plate	msr-nlir	mms	22.0	3.2	6	14.3	-2.41	16.1	-1.84
L frontal ethmoid attachment (anterior)	morl-cpal	mms	4.6	0.9	5	6.1	1.67	7.9	3.67
L frontal ethmoid attachment (posterior)	cppl-ofaml	mms	8.4	2.5	6	3.0	-2.16	4.4	-1.60
R frontal ethmoid attachment (anterior)	morr-cpar	mms	4.9	1.1	6	6.6	1.55	9.4	4.09
R frontal ethmoid attachment (posterior)	cppr-ofamr	mms	8.2	2.5	6	2.9	-2.12	5.6	-1.04
Dimensions									
Posterior inferior width	msl-msr	mms	21.2	5.9	6	18.1	-0.53	18.8	-0.41
Anterior inferior width	nlil-nlir	mms	20.8	3.7	6	23.7	0.78	24.7	1.05
Anterior superior width	morl-morr	mms	15.3	2.4	6	21.7	2.67	16.9	0.67
Posterior superior width	ofaml-ofamr	mms	15.6	3.1	6	14.3	-0.42	15.2	-0.13
Ant lateral projection of lateral plate	nlil-morl/morr-nlir	deg	37.1	11.5	6	18.8	-1.59	57.5	1.77
Post lateral projection of lateral plate	msl-ofaml/ofamr-msr	deg	27.8	12.7	6	26.8	-0.08	40.7	1.02
Cribriform Plate									
Distances									
L anterior cribriform plate	fc-cpal	mms	4.8	0.7	5			5.3	0.71
L lateral cribriform plate	cpal-cppl	mms	16.5	2.5	5	22.8	2.52	19.6	1.24
L posterior cribriform plate	es-cppl	mms	4.6	1.5	6	5.2	0.40	6.3	1.13
R anterior cribriform plate	fc-cpar	mms	5.1	1.2	6			5.1	0.00
R lateral cribriform plate	cpar-cppr	mms	17.6	2.9	6	23.8	2.14	19.8	0.76
R posterior cribriform plate	es-cppr	mms	4.4	1.6	6	7.0	1.62	5.2	0.50
Angles									
L angle lateral cribriform plate cf SN	s-n/cpal-cppl	deg	4.9	6.0	5	6.6	0.28	2.2	-0.45
R angle lateral cribriform plate cf SN	s-n/cpar-cppr	deg	8.0	5.7	6	0.9	-1.25	2.9	-0.89
Medial angle of plate cf SN	n-s/es-fc	deg	6.4	3.2	6			6.6	0.06
Medial Plate									
Distances									
Anterior height crista galli	fc-cg	mms	5.2	2.7	6			9.4	1.56
Posterior height crista galli	cg-es	mms	13.8	4.4	6			13.7	-0.02
Spheno-ethmoid medial plate junction	es-ves	mms	10.8	5.0	6	6.5	-0.86	12.0	0.24
Ethmoid-vomerine junction	ves-vei	mms	11.4	3.9	6	14.6	0.82	8.7	-0.69
Septal attachment	vei-n	mms	23.1	7.1	6	22.1	-0.14	22.9	-0.03
Nasal projection	n-fc	mms	5.4	2.3	6			5.5	0.04
Dimensions									
Maximum medial plate height	vei-cg	mms	16.5	7.4	6			15.0	-0.20
Maximum medial plate length	n-es	mms	25.1	4.7	6	29.0	0.83	27.9	0.60

Appendix 2 Measurements for the Experimental Standards and the Patients with Crouzon Syndrome:

Six Months of Age (continued):

			6 Month Standard			Patient RN		Patient SH	
Anatomical Unit	**Definition**	**unit**	**mean**	**sd**	**n**	**Value**	**Z**	**Value**	**Z**
SPHENOID									
Lesser Wing									
Distances									
L medial wing	ofaml-acl	mms	8.2	1.1	6	9.5	1.18	9.9	1.55
L lateral wing (posterior)	acl-spal	mms	25.4	4.1	6	16.9	-2.07	22.8	-0.63
L lateral wing (anterior)	spal-es	mms	31.1	5.4	6	20.7	-1.93	27.4	-0.69
R medial wing	ofamr-acr	mms	8.2	1.1	6	9.8	1.45	12.0	3.45
R lateral wing (posterior)	acr-spar	mms	23.3	4.1	6	14.5	-2.15	19.8	-0.85
R lateral wing (anterior)	spar-es	mms	30.0	5.2	6	20.0	-1.92	28.3	-0.33
Dimensions									
Maximum lesser wing width	spal-spar	mms	57.3	10.0	6	36.9	-2.04	54.0	-0.33
Lesser wing superior angle	spal-es -spar	deg	146.1	6.5	6	129.9	-2.49	150.8	0.72
L lateral projection (anterior angle)	n-s/acl-spal	deg	59.4	3.7	6	49.7	-2.62	54.3	-1.38
R lateral projection (anterior angle)	n-s/acr-spar	deg	58.8	6.0	6	46.2	-2.10	67.2	1.40
Pterygoid Plate									
Distances									
L medial pterygoid plate	ptsl-hpl	mms	15.7	6.0	6	12.9	-0.47	12.6	-0.52
L medial hamular notch	hpl-hnl	mms	3.1	1.1	6	3.3	0.18	4.0	0.82
L lateral hamular notch	hnl-ptll	mms	6.8	10.6	6	8.7	0.18	4.3	-0.24
L lateral pterygoid plate	ptll-fool	mms	14.3	11.4	6	6.6	-0.68	10.4	-0.34
R medial pterygoid plate	ptsr-hpr	mms	14.9	5.4	6	14.4	-0.09	12.6	-0.43
R medial hamular notch	hpr-hnr	mms	3.2	1.5	6	3.8	0.40	4.4	0.80
R lateral hamular notch	hnr-ptlr	mms	7.4	10.6	6	7.2	-0.02	5.1	-0.22
R lateral pterygoid plate	ptlr-foor	mms	12.9	12.2	6	10.6	-0.19	11.2	-0.14
Angles									
L pterygoid axis	n-s/ptsl-hpl	deg	48.6	14.3	6	44.9	-0.26	54.6	0.42
R pterygoid axis	n-s/ptsr-hpr	deg	50.1	14.2	6	46.0	-0.29	55.1	0.35
Greater Wing									
Distances									
Lateral									
L anterior middle cranial fossa	fosl-gwll	mms	23.3	4.6	6	23.0	-0.07	25.0	0.37
L spheno-zygomatic suture	zfsl-gwll	mms	10.6	1.5	6	16.2	3.73	8.9	-1.13
R anterior middle cranial fossa	fosr-gwlr	mms	25.1	4.9	6	26.1	0.20	26.1	0.20
R spheno-zygomatic suture	gwlr-zfsr	mms	11.1	2.8	6	17.9	2.43	6.9	-1.50
Orbital									
L inferior lateral orbital length	gwll-gwml	mms	21.5	5.5	6	16.8	-0.85	18.0	-0.64
L superior orbital fissure height	gwml-sobfl	mms	14.9	6.1	6	13.2	-0.28	1.7	-2.16
L spheno-frontal suture (orbital)	sobfl-zfsl	mms	14.3	4.0	6	15.7	0.35	22.8	2.12
R inferior lateral orbital length	gwlr-gwmr	mms	19.4	4.9	6	16.8	-0.53	19.8	0.08
R superior orbital fissure height	gwmr-sobfr	mms	15.0	4.7	6	15.0	0.00	3.3	-2.49
R spheno-frontal suture (orbital)	sobfr-zfsr	mms	14.1	3.7	6	16.0	0.51	22.1	2.16
Posterior									
L spheno-petrous temporal suture (inf)	fosl-ptsl	mms	10.5	8.7	6	8.9	-0.18	10.8	0.03
R spheno-petrous temporal suture (inf)	fosr-ptsr	mms	11.2	8.1	6	11.4	0.02	12.9	0.21
L posterior middle cranial fossa	fosl-petal	mms	15.6	2.5	6	16.5	0.36	13.9	-0.68
R posterior middle cranial fossa	fosr-petar	mms	29.7	4.3	6	31.7	0.47	27.2	-0.58

Appendix 2 Measurements for the Experimental Standards and the Patients with Crouzon Syndrome:

Six Months of Age (continued):

			6 Month Standard			Patient RN		Patient SH	
Anatomical Unit	**Definition**	**unit**	**mean**	**sd**	**n**	**Value**	**Z**	**Value**	**Z**
SPHENOID (continued)									
Dimensions and Angles									
Posterior sphenoid width	fosl-fosr	mms	39.2	3.7	6	40.4	0.32	34.4	-1.30
L angle of greater wing splay	zfsl-gwml-ptsl	deg	132.5	13.7	6	123.0	-0.69	122.5	-0.73
R angle of greater wing splay	zfsr-gwmr-ptsr	deg	134.4	16.9	6	125.0	-0.56	114.5	-1.18
Total angle of protrusion	zfsl-gwml/gwmr-zfsr	deg	100.4	5.2	6	107.3	1.33	125.3	4.79
Inferior greater wing protrusion	gwll-gwml/gwmr-gwlr	deg	99.2	6.0	6	110.0	1.80	117.8	3.10
Posterior angle of greater wing	fosl-petal/petar-fosr	deg	96.5	12.4	6	79.0	-1.41	74.8	-1.75
Squamous Sphenoid									
L squamous spheno-frontal suture	zfsl-spcl	mms	14.4	4.0	6	6.8	-1.90	15.8	0.35
L squamous spheno-parietal suture	spcl-sptl	mms	8.2	1.5	6	14.4	4.13	11.9	2.47
L lateral spheno-temporal suture	fosl-sptl	mms	34.8	6.4	6	30.4	-0.69	31.0	-0.59
R squamous spheno-frontal suture	zfsr-spcr	mms	13.4	2.8	6	5.5	-2.82	16.2	1.00
R squamous spheno-parietal suture	spcr-sptr	mms	7.8	1.6	6	20.7	8.06	9.4	1.00
R lateral spheno-temporal suture	fosr-sptr	mms	32.8	8.5	6	29.2	-0.42	32.3	-0.06
Sphenoid Body									
Distances									
Lateral/Posterior Body									
L anterior inferior length	gwml-ptsl	mms	10.4	6.2	6	15.5	0.82	12.4	0.32
L spheno-occipital synchondrosis (lat)	ptsl-petal	mms	10.2	5.7	6	11.2	0.18	10.7	0.09
L posterior clinoid height	petal-pcl	mms	6.7	1.3	6	8.1	1.08	8.5	1.38
Posterior clinoid width	pcl-pcr	mms	6.8	1.1	6	6.6	-0.18	10.6	3.45
R anterior inferior length	gwmr-ptsr	mms	10.6	6.1	6	15.8	0.85	11.5	0.15
R spheno-occipital synchondrosis (lat)	ptsr-petar	mms	11.4	4.9	6	10.9	-0.10	11.5	0.02
R posterior clinoid height	petar-pcr	mms	7.2	2.0	6	8.7	0.75	10.9	1.85
Anterior Body									
L spheno-ethmoid suture	es-cppl	mms	4.6	1.5	6	5.2	0.40	6.3	1.13
L anterior lateral distance	cppl-ofaml	mms	8.4	2.5	6	3.0	-2.16	4.4	-1.60
L anterior superior length	ofaml-gwml	mms	7.6	1.7	6	4.0	-2.12	5.3	-1.35
R spheno-ethmoid suture	es-cppr	mms	4.4	1.6	6	7.0	1.62	5.2	0.50
R anterior lateral distance	cppr-ofamr	mms	8.2	2.5	6	2.9	-2.12	5.6	-1.04
R anterior superior length	ofamr-gwmr	mms	7.9	1.8	6	5.2	-1.50	6.1	-1.00
Sella									
L lateral anterior body	cppl-ofpml	mms	9.4	2.2	6	6.9	-1.14	8.2	-0.55
L lateral sella length	ofpml-petal	mms	15.9	3.8	6	15.8	-0.03	17.0	0.29
R lateral anterior body	cppr-ofpmr	mms	10.5	2.5	6	7.3	-1.28	8.7	-0.72
R lateral sella length	ofpmr-petar	mms	16.0	3.4	6	16.6	0.18	17.7	0.50
Base/Floor of Body									
Spheno-ethmoid medial plate junction	es-ves	mms	10.8	5.0	6	6.5	-0.86	12.0	0.24
Spheno-vomerine junction	h-ves	mms	10.4	5.1	6	4.5	-1.16	9.9	-0.10
L posterior width	h-ptsl	mms	11.3	1.1	6	15.6	3.91	8.8	-2.27
R posterior width	h-ptsr	mms	11.5	1.5	6	16.6	3.40	8.5	-2.00

Appendix 2 Measurements for the Experimental Standards and the Patients with Crouzon Syndrome:

Six Months of Age (continued):

			6 Month Standard			Patient RN		Patient SH	
Anatomical Unit	**Definition**	**unit**	**mean**	**sd**	**n**	**Value**	**Z**	**Value**	**Z**
SPHENOID (continued)									
Dimensions									
Anterior inferior body width	gwml-gwmr	mms	21.4	2.6	6	20.4	-0.38	19.3	-0.81
Spheno-occipital synchondrosis (inf)	ptsl-ptsr	mms	19.8	2.6	6	21.6	0.69	15.1	-1.81
Anterior superior body width	ofaml-ofamr	mms	15.6	3.1	6	14.3	-0.42	15.2	-0.13
Spheno-occipital synchondrosis (sup)	petal-petar	mms	16.0	2.6	6	19.0	1.15	16.9	0.35
L posterior body height	pcl-ptsl	mms	15.0	4.0	6	16.1	0.28	14.4	-0.15
R posterior body height	pcr-ptsr	mms	16.1	4.1	6	15.9	-0.05	17.2	0.27
L anterior body height	acl-gwml	mms	8.1	1.0	6	9.3	1.20	7.9	-0.20
L anterior body height	acr-gwmr	mms	8.8	0.4	6	8.7	-0.25	9.9	2.75
Angles									
Body floor angle	cs-ves-h	deg	108.1	27.7	6	148.8	1.47	105.7	-0.09
L lower body angle	s-n/gwml-ptsl	deg	43.7	10.7	6	34.5	-0.86	48.6	0.46
R lower body angle	s-n/gwmr-ptsr	deg	154.9	3.3	6	152.5	-0.73	156.4	0.45
L upper body angle	s-n/ofpml-petal	deg	21.3	4.9	6	27.3	1.22	29.0	1.57
R upper body angle	s-n/ofpmr-petar	deg	17.4	8.0	6	23.7	0.79	27.7	1.29
TEMPORAL									
Distances									
Squamous									
L lateral spheno-temporal suture	fosl-sptl	mms	34.8	6.4	6	30.4	-0.69	31.0	-0.59
L temporo-parietal suture	sptl-asl	mms	54.5	8.3	6	42.4	-1.46	46.6	-0.95
L occipital mastoid height	asl-mal	mms	30.0	5.1	6	26.5	-0.69	28.4	-0.31
L medial mastoid prominence	mal-smfl	mms	6.9	1.2	6			7.5	0.50
R lateral spheno-temporal suture	fosr-sptr	mms	32.8	8.5	6	29.2	-0.42	32.3	-0.06
R temporo-parietal suture	sptr-asr	mms	56.3	8.8	6	47.8	-0.97	48.1	-0.93
R occipital mastoid height	asr-mar	mms	32.9	3.1	6	23.9	-2.90	28.1	-1.55
R medial mastoid prominence	mar-smfr	mms	7.1	2.8	6			7.9	0.29
External Auditory Meatus (EAM)									
L lateral mastoid prominence	mal-eamil	mms	9.4	3.3	6	12.5	0.94	9.4	0.00
L inferior-posterior EAM rim	eamil-campl	mms	7.2	2.8	6	7.4	0.07	10.8	1.29
L posterior-superior EAM rim	eampl-pol	mms	3.8	1.2	6	9.7	4.92	6.5	2.25
L superior-anterior EAM rim	pol-eamal	mms	3.9	1.6	6	6.4	1.56	6.0	1.31
L anterior inferior EAM rim	eamal-eamil	mms	5.7	2.4	6	7.4	0.71	7.3	0.67
R lateral mastoid prominence	mar-camir	mms	8.8	3.7	6	12.2	0.92	8.3	-0.14
R inferior-posterior EAM rim	eamir-eampr	mms	7.2	3.1	6	7.3	0.03	9.2	0.65
R posterior-superior EAM rim	eampr-por	mms	4.1	0.6	6	8.2	6.83	5.9	3.00
R superior-anterior EAM rim	por-eamar	mms	3.7	2.3	6	9.2	2.39	5.4	0.74
R anterior-inferior EAM rim	eamar-eamir	mms	5.9	1.7	6	7.4	0.88	7.4	0.88

Appendix 2 Measurements for the Experimental Standards and the Patients with Crouzon Syndrome:

Six Months of Age (continued):

			6 Month Standard			Patient RN		Patient SH	
Anatomical Unit	**Definition**	**unit**	**mean**	**sd**	**n**	**Value**	**Z**	**Value**	**Z**
TEMPORAL (continued)									
Zygoma									
L EAM-articular fossa length	eamal-afl	mms	9.8	2.2	6	10.7	0.41	9.7	-0.05
L articular fossa height	afl-ael	mms	5.3	2.0	6	8.1	1.40	5.7	0.20
L inferior arch length	ael-parl	mms	5.7	2.7	6	5.8	0.04	4.0	-0.63
L zygomatico-temporal suture	parl-ztl	mms	12.6	3.2	6	10.8	-0.56	9.0	-1.13
L superior arch length	ztl-aul	mms	20.3	5.2	6	10.4	-1.90	10.5	-1.88
R EAM-articular fossa length	eamar-afr	mms	10.5	1.9	6	13.4	1.53	9.3	-0.63
R articular fossa height	afr-aer	mms	5.4	1.4	6	9.1	2.64	4.3	-0.79
R inferior arch length	aer-parr	mms	4.7	3.9	6	7.0	0.59	4.7	0.00
R zygomatico-temporal suture	parr-ztr	mms	11.7	4.8	6	12.6	0.19	10.4	-0.27
R superior arch length	ztr-aur	mms	19.8	5.4	6	13.4	-1.19	9.4	-1.93
Petrous									
L spheno-petrous temporal suture (sup)	fisl-petal	mms	14.4	2.4	6	13.9	-0.21	10.4	-1.67
L post-med temporo-occipital suture	petal-jfpl	mms	22.1	3.8	6	19.3	-0.74	19.4	-0.71
L lateral temporo-occipital suture	jfpl-asil	mms	28.3	5.7	6	28.7	0.07	30.0	0.30
L petrous superior margin	asil-petal	mms	44.8	6.8	6	41.2	-0.53	41.4	-0.50
R spheno-petrous temporal suture (sup)	fisr-petar	mms	15.3	0.9	6	14.5	-0.89	11.2	-4.56
R post-med temporo-occipital suture	petar-jfpr	mms	23.6	3.7	6	19.7	-1.05	21.5	-0.57
R lateral temporo-occipital suture	jfpr-asir	mms	31.2	6.2	6	28.6	-0.42	31.9	0.11
R petrous superior margin	asir-petar	mms	46.8	7.1	6	42.7	-0.58	44.3	-0.35
L occipital mastoid suture inferior	mal-jfll	mms	11.6	2.1	6	11.9	0.14	15.1	1.67
L jugular foramen width	jfll-jfml	mms	7.0	4.2	6	7.9	0.21	3.4	-0.86
L medial temporo-occipital suture (inf)	jfml-ptsl	mms	17.8	6.1	6	16.7	-0.18	25.1	1.20
L spheno-petrous temporal suture (inf)	fosl-ptsl	mms	10.5	8.7	6	8.9	-0.18	10.8	0.03
R occipital mastoid suture inferior	mar-jflr	mms	11.7	2.0	6	10.8	-0.45	15.1	1.70
R jugular foramen width	jflr-jfmr	mms	7.2	3.5	6	7.9	0.20	5.2	-0.57
R medial temporo-occipital suture (inf)	jfmr-ptsr	mms	21.3	5.2	6	16.8	-0.87	28.8	1.44
R spheno-petrous temporal suture (inf)	fosr-ptsr	mms	11.2	8.1	6	11.4	0.02	12.9	0.21
Dimensions									
L petrous ridge length	petal-petpl	mms	40.5	6.9	6	40.2	-0.04	39.9	-0.09
R petrous ridge length	petar-petpr	mms	43.9	8.5	6	41.6	-0.27	41.8	-0.25
Inter-internal aud meatus dimension	iamr-iaml	mms	30.3	6.6	6	33.4	0.47	29.0	-0.20
Inter-external aud meatus dimension	pol-por	mms	66.2	11.6	6	60.8	-0.47	60.4	-0.50
Inter-post jugular foramen dimension	jfpr-jfpl	mms	38.8	7.9	6	33.1	-0.72	33.5	-0.67
Inter-mastoid dimension	mal-mar	mms	56.8	13.7	6	56.2	-0.04	60.0	0.23
Angles									
Auditory canal angle	pol-iaml/iamr-por	deg	129.8	8.2	6	98.8	-3.78	135.4	0.68
Petrous ridge angle	petpl-petal/petar-petpr	deg	92.1	6.8	6	101.8	1.43	87.9	-0.62
L zygoma projection angle	petal-aul-ztl	deg	97.3	6.1	6	108.9	1.90	131.9	5.67
R zygoma projection angle	petar-aur-ztr	deg	98.8	4.8	6	104.8	1.25	130.0	6.50

Appendix 2 Measurements for the Experimental Standards and the Patients with Crouzon Syndrome:

Six Months of Age (continued):

			6 Month Standard			Patient RN		Patient SH	
Anatomical Unit	**Definition**	**unit**	**mean**	**sd**	**n**	**Value**	**Z**	**Value**	**Z**
PARIETAL									
Distances									
Sagittal suture	l-br	mms			0				
L parietal frontal (coronal) suture	br-spcl	mms			0				
L spheno-parietal suture	spcl-sptl	mms	8.2	1.5	6	14.4	4.13	11.9	2.47
L temporo-parietal suture	sptl-asl	mms	54.5	8.3	6	42.4	-1.46	46.6	-0.95
L occipito-parietal (lambdoid) suture	asl-l	mms	67.1	13.0	6	82.9	1.22	76.0	0.68
R parietal frontal (coronal) suture	br-spcr	mms			0				
R spheno-parietal suture	spcr-sptr	mms	7.8	1.6	6	20.7	8.06	9.4	1.00
R temporo-parietal suture	sptr-asr	mms	56.3	8.8	6	47.8	-0.97	48.1	-0.93
R occipito-parietal (lambdoid) suture	asr-l	mms	68.8	13.1	6	81.3	0.95	80.6	0.90
OCCIPITAL									
Distances									
Lambdoid and Cranial Base									
L occipito-parietal (lambdoid) suture	l-asl	mms	67.1	13.0	6	82.9	1.22	76.0	0.68
L lateral temporo-occipital suture (sup)	asl-jfll	mms	26.8	4.9	6	27.4	0.12	24.7	-0.43
L lateral jugular foramen	jfll-jfpl	mms	4.8	1.8	6	2.5	-1.28	7.7	1.61
L medial jugular foramen	jfpl-jfml	mms	5.2	4.2	6	6.0	0.19	6.5	0.31
L medial temporo-occipital suture (inf)	jfml-ptsl	mms	17.8	6.1	6	16.7	-0.18	25.1	1.20
R occipito-parietal (lambdoid) suture	l-asr	mms	68.8	13.1	6	81.3	0.95	80.6	0.90
R lateral temporo-occipital suture (sup)	asr-jflr	mms	29.5	4.3	6	27.2	-0.53	26.2	-0.77
R lateral jugular foramen	jflr-jfpr	mms	4.8	2.0	6	2.8	-1.00	7.9	1.55
R medial jugular foramen	jfpr-jfmr	mms	7.5	4.0	6	6.2	-0.33	9.2	0.42
R medial temporo-occipital suture (inf)	jfmr-ptsr	mms	21.3	5.2	6	16.8	-0.87	28.8	1.44
Inferior spheno-occipital synchondrosis	ptsr-ptsl	mms	19.8	2.6	6	21.6	0.69	15.1	-1.81
Foramen Magnum									
L anterior foramen magnum	ba-fmll	mms	14.1	2.4	6	14.6	0.21	14.6	0.21
L posterior foramen magnum	fmll-o	mms	19.9	3.6	6	19.1	-0.22	21.1	0.33
R anterior foramen magnum	ba-fmlr	mms	14.8	3.2	6	15.9	0.34	14.8	0.00
R posterior foramen magnum	fmlr-o	mms	19.6	3.4	6	19.7	0.03	21.0	0.41
Dimensions									
Foramen Magnum									
Foramen magnum length	ba-o	mms	27.2	4.8	6	29.3	0.44	28.9	0.35
Foramen magnum width	fmll-fmlr	mms	19.6	4.5	6	18.4	-0.27	19.5	-0.02
Posterior Cranial Fossa									
Posterior cranial fossa depth	o-iop	mms	25.5	2.8	6	15.3	-3.64	28.7	1.14
Posterior occipital height	iop-l	mms	50.5	9.3	6	62.2	1.26	56.6	0.66
L posterior fossa length	petpl-iop	mms	49.9	6.3	6	38.4	-1.83	44.1	-0.92
L posterior fossa length	petpr-iop	mms	47.0	6.1	6	53.7	1.10	46.9	-0.02

Appendix 2 Measurements for the Experimental Standards and the Patients with Crouzon Syndrome:

Six Months of Age (continued):

			6 Month Standard			Patient RN		Patient SH	
Anatomical Unit	**Definition**	**unit**	**mean**	**sd**	**n**	**Value**	**Z**	**Value**	**Z**
CRANIAL BASE SUTURES									
Anterior Cranial Fossa									
L spheno-ethmoid synchondrosis	es-cppl	mms	4.6	1.5	6	5.2	0.40	6.3	1.13
R spheno-ethmoid synchondrosis	es-cppr	mms	4.4	1.6	6	7.0	1.62	5.2	0.50
L spheno-frontal suture (ant fossa)	cppl-spal	mms	27.0	5.3	6	15.9	-2.09	22.4	-0.87
R spheno-frontal suture (ant fossa)	cppr-spar	mms	25.2	4.5	6	13.2	-2.67	25.1	-0.02
L spheno-frontal suture (orbital)	spal-zfsl	mms	12.1	3.8	6	15.6	0.92	12.3	0.05
R spheno-frontal suture (orbital)	spar-zfsr	mms	11.9	3.4	6	18.3	1.88	16.0	1.21
L spheno-zygomatic suture	zfsl-gwll	mms	10.6	1.5	6	16.2	3.73	8.9	-1.13
R spheno-zygomatic suture	zfsr-gwlr	mms	11.1	2.8	6	17.9	2.43	6.9	-1.50
Middle Cranial Fossa									
L spheno-squamous temporal suture	gwll-fisl	mms	23.3	4.6	6	20.2	-0.67	23.3	0.00
R spheno-squamous temporal suture	gwlr-fisr	mms	23.3	4.6	6	23.2	-0.02	24.0	0.15
L spheno-petrous temporal suture (sup)	fisl-petal	mms	14.4	2.4	6	13.9	-0.21	10.4	-1.67
R spheno-petrous temporal suture (sup)	fisr-petar	mms	15.3	0.9	6	14.5	-0.89	11.2	-4.56
L spheno-petrous temporal suture (inf)	fosl-ptsl	mms	10.5	8.7	6	8.9	-0.18	10.8	0.03
R spheno-petrous temporal suture (inf)	fosr-ptsr	mms	11.2	8.1	6	11.4	0.02	12.9	0.21
Posterior Cranial Fossa									
L medial temporo-occipital suture (sup)	petal-jfml	mms	16.1	3.4	6	13.5	-0.76	20.3	1.24
R medial temporo-occipital suture (sup)	petar-jfmr	mms	17.3	1.6	6	14.5	-1.75	23.4	3.81
L medial temporo-occipital suture (inf)	jfml-ptsl	mms	17.8	6.1	6	16.7	-0.18	25.1	1.20
R medial temporo-occipital suture (inf)	jfmr-ptsr	mms	21.3	5.2	6	16.8	-0.87	28.8	1.44
L occipital mastoid suture (superior)	jfll-petpl	mms	25.2	3.1	6	27.2	0.65	24.4	-0.26
R occipital mastoid suture (superior)	jflr-petpr	mms	26.3	4.6	6	28.6	0.50	27.7	0.30
Spheno-occipital synchondrosis (sup)	petal-petar	mms	16.0	2.6	6	19.0	1.15	16.9	0.35
Spheno-occipital synchondrosis (inf)	ptsl-ptsr	mms	19.8	2.6	6	21.6	0.69	15.1	-1.81
L spheno-occipital synchondrosis (lat)	ptsl-petal	mms	10.2	5.7	6	11.2	0.18	10.7	0.09
R spheno-occipital synchondrosis (lat)	ptsr-petar	mms	11.4	4.9	6	10.9	-0.10	11.5	0.02
CRANIAL BASE									
Facial Heights									
Anterior facial height	n-gn	mms	57.3	12.7	6	68.0	0.84	62.5	0.41
L posterior facial height	s-gol	mms	44.9	9.4	6	41.9	-0.32	40.7	-0.45
R posterior facial height	s-gor	mms	46.0	9.9	6	40.3	-0.58	42.8	-0.32
Facial Angles									
SNA	s-n-ss	deg	82.3	2.9	6	76.9	-1.86	77.4	-1.69
SNB	s-n-sm	deg	74.1	2.2	6	61.7	-5.64		
Cranial Base Angle									
Cranial base angle	ba-s-n	deg	140.9	4.1	6	141.8	0.22	124.4	-4.02
Cranial Base Dimensions									
Cranial base length	ba-n	mms	64.5	10.6	6	66.8	0.22	61.6	-0.27
Clivus length (posterior cranial base)	ba-s	mms	24.5	4.1	6	27.4	0.71	27.1	0.63
Anterior cranial base length	s-n	mms	43.8	7.2	6	43.0	-0.11	42.0	-0.25

Appendix 2 Measurements for the Experimental Standards and the Patients with Crouzon Syndrome:

Two Years of Age:

			2 Year Standard			Patient JS		Patient IP	
Anatomical Unit	**Definition**	**unit**	**mean**	**sd**	**n**	**Value**	**Z**	**Value**	**Z**
MANDIBLE									
Distances									
L anterior superior body	id-em1il	mms	18.5	0.7	5	19.8	1.86	20.6	3.00
L posterior superior body	em1il-cbl	mms	22.8	3.2	5	22.8	0.00	21.7	-0.34
L total superior body	id-cbl	mms	39.1	2.8	5	40.5	0.50	40.2	0.39
L anterior ramus	cbl-ctl	mms	16.9	2.2	5	21.5	2.09	21.2	1.95
L anterior mandibular notch	ctl-mnl	mms	10.8	1.1	5	8.3	-2.27	13.0	2.00
L posterior mandibular notch	mnl-cdl	mms	10.7	1.9	5	11.8	0.58	14.3	1.89
L posterior ramus	cdl-gol	mms	29.4	1.8	5	30.6	0.67	30.0	0.33
L inferior body	gol-gn	mms	47.8	4.6	5	50.2	0.52	50.9	0.67
R anterior superior body	id-em1ir	mms	19.9	1.3	5	18.6	-1.00	20.5	0.46
R posterior superior body	em1ir-cbr	mms	20.9	2.5	5	23.4	1.00	23.2	0.92
R total superior body	id-cbr	mms	37.6	1.5	5	39.7	1.40	41.5	2.60
R anterior ramus	cbr-ctr	mms	20.4	1.4	5	23.1	1.93	19.2	-0.86
R anterior mandibular notch	ctr-mnr	mms	11.1	1.3	5	8.6	-1.92	11.8	0.54
R posterior mandibular notch	mnr-cdr	mms	12.0	1.6	5	13.7	1.06	13.5	0.94
R posterior ramus	cdr-gor	mms	29.8	1.5	5	30.2	0.27	31.6	1.20
R inferior body	gor-gn	mms	46.9	3.4	5	51.6	1.38	49.8	0.85
Dimensions									
Intergonial dimension	gol-gor	mms	56.3	4.6	5	53.7	-0.57	59.0	0.59
Intercondylar dimension	cdl-cdr	mms	74.3	3.0	5	69.5	-1.60	85.2	3.63
Intercoronoid base dimension	cbl-cbr	mms	52.1	2.5	5	47.0	-2.04	56.4	1.72
Intermolar dimension	em1il-em1ir	mms	34.0	1.3	5	31.6	-1.85	36.5	1.92
L Superior ramus width	cdl-ctl	mms	18.9	2.0	5	17.7	-0.60	23.9	2.50
L inferior ramus width	gol-cbl	mms	21.2	3.3	5	24.7	1.06	27.0	1.76
R superior ramus width	cdr-ctr	mms	19.5	1.6	5	17.6	-1.19	22.9	2.12
R inferior ramus width	gor-cbr	mms	20.7	3.2	5	24.3	1.12	27.5	2.12
Anterior symphyseal height	gn-id	mms	19.4	4.0	5	24.5	1.28	23.6	1.05
L total mandibular length	gn-cdl	mms	68.9	4.3	5	73.8	1.14	75.0	1.42
R total mandibular length	gn-cdr	mms	69.7	3.0	5	75.2	1.83	74.5	1.60
Angles									
L mandibular notch angle	cdl-mnl-ctl	deg	116.0	7.6	5	122.5	0.86	121.8	0.76
R mandibular notch angle	cdr-mnr-ctr	deg	122.6	11.1	5	102.2	-1.84	128.9	0.57
L gonial angle	cdl-gol-gn	deg	129.4	5.2	5	130.3	0.17	134.2	0.92
R gonial angle	cdr-gor-gn	deg	132.7	4.6	5	131.9	-0.17	131.0	-0.37
L coronoid base angle	ctl-cbl-id	deg	131.8	7.8	5	139.3	0.96	136.5	0.60
R coronoid base angle	ctr-cbr-id	deg	132.1	6.6	5	139.3	1.09	136.2	0.62
L coronoid-dental base angle	ctl-cbl-em1il	deg	141.3	4.5	5	143.5	0.49	139.3	-0.44
R coronoid-dental base angle	ctr-cbr-em1ir	deg	139.5	6.0	5	146.3	1.13	140.3	0.13
L symphyseal angle	gol-gn-id	deg	91.9	2.8	5	92.8	0.32	96.2	1.54
R symphyseal angle	gor-gn-id	deg	91.7	3.6	5	90.0	-0.47	97.7	1.67
Anterior mandibular angle	gol-gn-gor	deg	75.9	6.2	5	63.7	-1.97	71.8	-0.66

Appendix 2 Measurements for the Experimental Standards and the Patients with Crouzon Syndrome:

Two Years of Age (continued):

			2 Year Standard			Patient JS		Patient IP	
Anatomical Unit	**Definition**	**unit**	**mean**	**sd**	**n**	**Value**	**Z**	**Value**	**Z**
MAXILLA									
Distances									
Orbital Region									
L fronto-maxillary suture	snml-morl	mms	6.8	1.3	6	5.9	-0.69	17.4	8.15
L frontal process orbital rim	nlil-morl	mms	12.1	1.5	6	11.7	-0.27	11.0	-0.73
L medial orbital floor	msl-nlil	mms	24.4	2.2	6	24.5	0.05	17.7	-3.05
L posterior lateral orbital floor	msl-iobfl	mms	16.8	1.2	6	17.3	0.42	14.1	-2.25
L anterior lateral orbital floor	orl-iobfl	mms	14.0	1.3	6	14.3	0.23	9.1	-3.77
L maxillary infra-orbital rim	orl-nlil	mms	11.9	2.1	6	13.7	0.86	14.3	1.14
R fronto-maxillary suture	snmr-morr	mms	5.8	0.7	6	5.3	-0.71	17.2	16.29
R frontal process orbital rim	nlir-morr	mms	12.0	0.9	6	11.3	-0.78	7.4	-5.11
R medial orbital floor	msr-nlir	mms	23.5	1.9	6	24.9	0.74	17.9	-2.95
R posterior lateral orbital floor	msr-iobfr	mms	16.0	1.2	6	17.0	0.83	17.0	0.83
R anterior lateral orbital floor	orr-iobfr	mms	13.9	1.3	6	14.2	0.23	7.5	-4.92
R maxillary infra-orbital rim	orr-nlir	mms	12.1	1.2	6	12.4	0.20	18.4	5.20
Anterior Wall									
L anterior zygo-maxillary suture	zmil-orl	mms	16.8	0.8	6	18.8	2.50	22.3	6.88
L lateral maxillary wall	zmil-em1sl	mms	17.3	1.9	6	21.2	2.05	23.6	3.32
L anterior alveolar margin	em1sl-pr	mms	21.3	1.7	6	23.2	1.12	24.4	1.82
L lower pyriform margin	ans-all	mms	10.1	0.9	6	10.9	0.89	13.7	4.00
L upper pyriform margin	all-inml	mms	13.5	1.6	6	11.4	-1.31	15.6	1.31
L naso-maxillary suture	inml-snml	mms	11.1	1.4	6	10.1	-0.71	17.6	4.64
R anterior zygo-maxillary suture	zmir-orr	mms	16.8	1.2	6	18.5	1.42	20.5	3.08
R lateral maxillary wall	zmir-em1sr	mms	18.0	1.9	6	19.0	0.53	26.3	4.37
R anterior alveolar margin	em1sr-pr	mms	21.6	1.5	6	24.0	1.60	22.9	0.87
R lower pyriform margin	ans-alr	mms	10.5	1.4	6	9.5	-0.71	12.5	1.43
R upper pyriform margin	alr-inmr	mms	12.5	1.2	6	11.3	-1.00	15.5	2.50
L naso-maxillary suture	inmr-snmr	mms	12.1	1.8	6	10.4	-0.94	17.1	2.78
Anterior alveolar height	pr-ans	mms	9.4	2.2	6	10.2	0.36	12.8	1.55
Lateral Wall									
L posterior alveolar margin	em1sl-mxtl	mms	19.1	4.1	6	23.5	1.07	17.0	-0.51
L posterior maxillary wall	mxtl-msl	mms	21.7	0.8	6	17.7	-5.00	28.8	8.87
L posterior lateral orbital floor	msl-iobfl	mms	16.8	1.2	6	17.3	0.42	14.1	-2.25
L posterior zygo-maxillary suture	iobfl-zmil	mms	13.6	0.6	6	14.3	1.17	24.7	18.50
R posterior alveolar margin	em1sr-mxtr	mms	18.4	4.0	6	24.7	1.58	16.6	-0.45
R posterior maxillary wall	mxtr-msr	mms	21.3	0.7	6	17.4	-5.57	29.1	11.14
R posterior lateral orbital floor	msr-iobfr	mms	16.0	1.2	6	17.0	0.83	17.0	0.83
R posterior zygo-maxillary suture	iobfr-zmir	mms	13.3	0.9	6	13.6	0.33	23.5	11.33
Palate									
L posterior palatal height	em1sl-gpfl	mms	21.0	2.8	6	22.9	0.68	18.6	-0.86
L posterior palatal width	gpfl-pns	mms	12.0	1.1	6	10.3	-1.55	11.9	-0.09
R posterior palatal height	em1sr-gpfr	mms	21.0	2.9	6	23.3	0.79	18.7	-0.79
R posterior palatal width	gpfr-pns	mms	11.4	1.1	6	11.6	0.18	12.8	1.27
Superior palatal length	ans-pns	mms	32.7	1.0	6	36.3	3.60	33.7	1.00

Appendix 2 Measurements for the Experimental Standards and the Patients with Crouzon Syndrome:

Two Years of Age (continued):

			2 Year Standard			Patient JS		Patient IP	
Anatomical Unit	**Definition**	**unit**	**mean**	**sd**	**n**	**Value**	**Z**	**Value**	**Z**
MAXILLA (continued)									
Dimensions									
Anterior midline height	n-pr	mms	38.0	2.7	6	39.5	0.56	57.1	7.07
L lateral height	morl-em1sl	mms	34.7	2.5	6	38.2	1.40	38.7	1.60
R lateral height	morr-em1sr	mms	34.7	2.4	6	38.7	1.67	38.2	1.46
L posterior height	gpfl-msl	mms	19.8	0.9	6	19.1	-0.78	25.2	6.00
R posterior height	gpfr-msr	mms	19.8	1.0	6	19.7	-0.10	23.3	3.50
L superior length	msl-inml	mms	33.5	1.9	6	34.2	0.37	28.1	-2.84
R superior length	msr-inmr	mms	33.8	1.5	6	34.1	0.20	30.0	-2.53
Posterior palatal width	gpfl-gpfr	mms	22.7	1.5	6	21.1	-1.07	23.3	0.40
Anterior inter-canine width	ecsl-ecsr	mms	27.8	3.5	6	31.2	0.97	30.1	0.66
Maximum maxillary width	zmil-zmir	mms	62.6	4.5	6	63.9	0.29	77.4	3.29
Superior (inter-orbital rim) width	orl-orr	mms	45.8	4.2	6	48.1	0.55	58.0	2.90
Nasal aperture height	na-ans	mms	17.0	1.7	6	15.4	-0.94	22.4	3.18
Nasal aperture width	all-alr	mms	17.1	1.9	6	15.8	-0.68	18.1	0.53
Angles									
L orbital floor angle	nlil-msl-iobfl	deg	55.5	5.1	6	54.5	-0.20	43.9	-2.27
R orbital floor angle	nlir-msr-iobfr	deg	57.8	6.1	6	53.3	-0.74	59.0	0.20
L posterior inferior angle	msl-gpfl-em1sl	deg	107.1	10.0	6	116.4	0.93	100.6	-0.65
R posterior inferior angle	msr-gpfr-em1sr	deg	105.7	5.7	6	116.6	1.91	107.2	0.26
Superior maxillary splay	iobfl-msl/msr-iobfr	deg	105.5	9.2	6	98.7	-0.74	94.8	-1.16
L superior /occlusal angle	snml-msl/em1sl-pr	deg	50.7	3.9	6	44.7	-1.54	57.0	1.62
R superior /occlusal angle	snmr-msr/em1sr-pr	deg	50.9	4.0	6	43.9	-1.75	52.9	0.50
L palatal/occlusal angle	ans-pns/em1sl-pr	deg	64.0	3.8	6	54.1	-2.61	60.4	-0.95
R palatal/occlusal angle	ans-pns/em1sr-pr	deg	58.2	4.0	6	55.0	-0.80	59.9	0.43
Anterior palatal angle	gpfl-ans-gpfr	deg	41.6	1.9	6	34.8	-3.58	41.0	-0.32
Maxillary arch angle	gpfl-pr-gpfr	deg	41.3	2.3	6	34.8	-2.83	44.7	1.48
NASAL BONES									
Distances									
Nasal length	na-n	mms	13.9	1.8	6	15.8	1.06	23.5	5.33
L inferior nasal width	na-inml	mms	5.2	1.1	6	8.8	3.27	8.6	3.09
L naso-maxillary suture	inml-snml	mms	11.1	1.4	6	10.1	-0.71	17.6	4.64
L fronto-nasal suture	n-snml	mms	5.9	1.3	6	8.6	2.08	8.9	2.31
R inferior nasal width	na-inmr	mms	4.8	1.0	6	8.8	4.00	8.0	3.20
R naso-maxillary suture	inmr-snmr	mms	12.1	1.8	6	10.4	-0.94	17.1	2.78
R fronto-nasal suture	n-snmr	mms	6.9	1.1	6	8.4	1.36	9.6	2.45
Dimensions									
Inferior width	inml-inmr	mms	8.3	1.6	6	12.9	2.87	12.3	2.50
Superior width	snml-snmr	mms	10.1	1.5	6	10.8	0.47	9.1	-0.67
Angles									
Nasal/anterior cranial base angle	s-n-na	deg	92.4	7.6	6	99.8	0.97	70.3	-2.91
Superior nasal bone angle	snml-n-snmr	deg	97.1	17.1	6	79.3	-1.04	58.8	-2.24
Inferior nasal bone angle	inml-na-inmr	deg	137.7	17.7	6	93.9	-2.47	94.8	-2.42
Splay of nasal bones	inml-snml/snmr-inmr	deg	9.5	6.8	6	12.3	0.41	11.3	0.26

Appendix 2 Measurements for the Experimental Standards and the Patients with Crouzon Syndrome:

Two Years of Age (continued):

			2 Year Standard			Patient JS		Patient IP	
Anatomical Unit	**Definition**	**unit**	**mean**	**sd**	**n**	**Value**	**Z**	**Value**	**Z**
FRONTAL									
Distances									
Supra-orbital									
L fronto-nasal suture	n-snml	mms	5.9	1.3	6	8.6	2.08	8.9	2.31
L fronto-maxillary suture	snml-morl	mms	6.8	1.3	6	5.9	-0.69	17.4	8.15
L superior medial orbital rim	morl-sorl	mms	17.8	0.9	6	17.4	-0.44	34.6	18.67
L superior lateral orbital rim	sorl-slorl	mms	23.1	1.8	6	26.8	2.06	27.0	2.17
L fronto-zygomatic suture (anterior)	slorl-zfl	mms	4.7	0.7	6	5.6	1.29	5.4	1.00
L fronto-zygomatic suture (lateral)	zfl-zfsl	mms	6.7	1.7	6	7.0	0.18	14.5	4.59
L fronto-zygomatic suture (medial)	zfsl-slorl	mms	9.5	1.5	6	9.6	0.07	16.4	4.60
R fronto-nasal suture	n-snmr	mms	6.9	1.1	6	8.4	1.36	9.6	2.45
R fronto-maxillary suture	snmr-morr	mms	5.8	0.7	6	5.3	-0.71	17.2	16.29
R superior medial orbital rim	morr-sorr	mms	16.8	0.6	6	16.7	-0.17	33.3	27.50
R superior lateral orbital rim	sorr-slorr	mms	23.2	1.3	6	26.0	2.15	28.1	3.77
R fronto-zygomatic suture (anterior)	slorr-zfr	mms	5.3	1.0	6	5.9	0.60	8.3	3.00
R fronto-zygomatic suture (lateral)	zfr-zfsr	mms	6.1	1.8	6	7.1	0.56	10.6	2.50
R fronto-zygomatic suture (medial)	zfsr-slorr	mms	8.9	1.7	6	9.2	0.18	13.5	2.71
Ethmoid									
Nasal root projection	n-fc	mms	7.9	1.5	6	9.2	0.87	4.4	-2.33
L fronto-ethmoid attachment (anterior)	fc-cpal	mms	6.3	1.3	6	6.5	0.15	20.6	11.00
L fronto-ethmoid attachment (cribriform)	cpal-cppl	mms	16.9	1.4	6	22.4	3.93	14.5	-1.71
L fronto-ethmoid attachment (posterior)	cppl-ofaml	mms	10.3	2.1	6	1.9	-4.00	8.0	-1.10
L fronto-ethmoid attachment (orbital)	morl-ofaml	mms	30.7	1.2	6	26.5	-3.50	21.3	-7.83
R fronto-ethmoid attachment (anterior)	fc-cpar	mms	5.9	1.1	6	6.9	0.91	20.5	13.27
R fronto-ethmoid attachment (cribriform)	cpar-cppr	mms	18.3	1.9	6	22.7	2.32	17.1	-0.63
R fronto-ethmoid attachment (posterior)	cppr-ofamr	mms	10.1	1.9	6	4.8	-2.79	8.2	-1.00
R fronto-ethmoid attachment (orbital)	morr-ofamr	mms	30.8	0.5	6	26.7	-8.20	22.3	-17.00
Sphenoid									
L superior orbital fissure	ofaml-sobfl	mms	13.1	3.2	6	12.0	-0.34	28.7	4.88
L fronto-sphenoid suture (orbital)	sobfl-zfsl	mms	17.5	4.2	6	18.7	0.29	15.1	-0.57
L lesser wing length	spal-cppl	mms	25.5	3.9	6	24.5	-0.26	31.0	1.41
R superior orbital fissure	ofamr-sobfr	mms	10.8	4.0	6	9.0	-0.45	30.5	4.93
R fronto-sphenoid suture (orbital)	sobfr-zfsr	mms	19.2	3.4	6	16.3	-0.85	11.7	-2.21
R lesser wing length	spar-cppr	mms	26.1	4.4	6	28.3	0.50	33.7	1.73
Dimensions									
Glabellar height	g-n	mms	8.5	1.3	6	7.6	-0.69	10.4	1.46
Glabellar prominence	s-g	mms	56.2	3.0	6	56.3	0.03	63.5	2.43
L anterior cranial fossa depth	sorl-spal	mms	32.8	2.5	6	34.9	0.84	28.5	-1.72
R anterior cranial fossa depth	sorr-spar	mms	33.9	2.1	6	34.7	0.38	26.1	-3.71
Anterior superior orbital width	sorl-sorr	mms	39.5	2.5	6	39.1	-0.16	62.0	9.00
Anterior supero-lateral orbital width	slorl-slorr	mms	70.9	4.0	6	76.2	1.32	90.9	5.00
Posterior width	spal-spar	mms	57.9	6.3	6	61.8	0.62	72.2	2.27

Appendix 2 Measurements for the Experimental Standards and the Patients with Crouzon Syndrome:

Two Years of Age (continued):

			2 Year Standard			Patient JS		Patient IP	
Anatomical Unit	Definition	unit	mean	sd	n	Value	Z	Value	Z
ZYGOMATIC BONE									
Distances									
L zygo-maxillary suture (orbital)	orl-iobfl	mms	14.0	1.3	6	14.3	0.23	9.1	-3.77
L inferior orbital fissure (ant height)	iobfl-gwll	mms	6.9	1.3	6	8.1	0.92	16.0	7.00
L spheno-zygomatic suture	zfsl-gwll	mms	13.2	1.2	6	12.9	-0.25	37.3	20.08
L fronto-zygomatic suture (medial)	zfsl-slorl	mms	9.5	1.5	6	9.6	0.07	16.4	4.60
L fronto-zygomatic suture (anterior)	slorl-zfl	mms	4.7	0.7	6	5.6	1.29	5.4	1.00
L fronto-zygomatic suture (lateral)	zfl-zfsl	mms	6.7	1.7	6	7.0	0.18	14.5	4.59
L infero-lateral orbital rim	orl-ilorl	mms	11.4	0.8	6	13.0	2.00	17.2	7.25
L infero-lateral orbital rim	ilorl-lorl	mms	10.9	1.4	6	10.1	-0.57	15.1	3.00
L lateral orbital rim	lorl-slorl	mms	3.9	1.9	6	4.2	0.16	0.0	-2.05
L lateral frontal process	zfl-ztl	mms	16.6	1.8	6	16.5	-0.06	27.0	5.78
L zygomatico-temporal suture	ztl-parl	mms	16.3	2.1	6	14.8	-0.71	17.7	0.67
L inferior arch	parl-zmil	mms	22.4	1.9	6	19.2	-1.68	18.6	-2.00
L zygo-maxillary suture	zmil-orl	mms	16.8	0.8	6	18.8	2.50	22.3	6.88
R zygo-maxillary suture (orbital)	orr-iobfr	mms	13.9	1.3	6	14.2	0.23	7.5	-4.92
R inferior orbital fissure (ant height)	iobfr-gwlr	mms	7.5	2.0	6	7.4	-0.05	14.6	3.55
R spheno-zygomatic suture	gwlr-zfsr	mms	12.8	2.2	6	14.9	0.95	31.3	8.41
R fronto-zygomatic suture (medial)	zfsr-slorr	mms	8.9	1.7	6	9.2	0.18	13.5	2.71
R fronto-zygomatic suture (anterior)	slorr-zfr	mms	5.3	1.0	6	5.9	0.60	8.3	3.00
R fronto-zygomatic suture (lateral)	zfr-zfsr	mms	6.1	1.8	6	7.1	0.56	10.6	2.50
R infero-lateral orbital rim	orr-ilorr	mms	9.9	1.3	6	12.0	1.62	14.4	3.46
R infero-lateral orbital rim	ilorr-lorr	mms	11.7	1.1	6	9.9	-1.64	15.0	3.00
R lateral orbital rim	lorr-slorr	mms	3.8	2.3	6	5.3	0.65	0.0	-1.65
R lateral frontal process	zfr-ztr	mms	16.9	2.0	6	17.5	0.30	26.5	4.80
R zygomatico-temporal suture	ztr-parr	mms	17.0	2.0	6	13.5	-1.75	20.7	1.85
R inferior arch	parr-zmir	mms	22.6	2.5	6	21.2	-0.56	16.8	-2.32
R zygo-maxillary suture	zmir-orr	mms	16.8	1.2	6	18.5	1.42	20.5	3.08
Dimensions									
L zygomatic height	slorl-zmil	mms	26.8	0.9	6	27.9	1.22	41.2	16.00
R zygomatic height	slorr-zmir	mms	71.7	4.3	6	75.3	0.84	91.1	4.51
L zygomatic length	parl-orl	mms	34.3	1.7	6	33.6	-0.41	36.4	1.24
R zygomatic length	parr-orr	mms	35.3	2.2	6	34.9	-0.18	34.4	-0.41
L zygomatic lateral depth	gwll-ilorl	mms	14.2	1.5	6	15.0	0.53	15.2	0.67
L zygomatic lateral depth	gwlr-ilorr	mms	15.3	2.2	6	16.3	0.45	11.0	-1.95
VOMER									
Distances									
Palatal length	ans-pns	mms	32.7	1.0	6	36.3	3.60	33.7	1.00
Posterior choanal height	pns-h	mms	15.2	1.8	6	14.7	-0.28	12.1	-1.72
Spheno-vomerine junction	h-ves	mms	10.9	3.0	6	11.4	0.17	16.6	1.90
Ethmoid-vomerine junction	ves-vei	mms	13.6	3.6	6	12.4	-0.33	7.7	-1.64
Septal attachment	vei-ans	mms	23.3	3.6	6	25.5	0.61	21.8	-0.42
Dimension and Angle									
Vomerine length	h-ans	mms	42.8	2.3	6	46.2	1.48	43.2	0.17
Vomerine angle	s-n/h-ans	deg	20.8	2.5	6	20.1	-0.28	36.0	6.08

Appendix 2 Measurements for the Experimental Standards and the Patients with Crouzon Syndrome:

Two Years of Age (continued):

			2 Year Standard			Patient JS		Patient IP	
Anatomical Unit	**Definition**	**unit**	**mean**	**sd**	**n**	**Value**	**Z**	**Value**	**Z**
ETHMOID									
Lateral Plate									
Distances									
L anterior border lateral plate	nlil-morl	mms	12.1	1.5	6	11.7	-0.27	11.0	-0.73
L frontal ethmoid attachment (orbital)	morl-ofaml	mms	30.7	1.2	6	26.5	-3.50	21.3	-7.83
L posterior border lateral plate	ofaml-msl	mms	9.9	1.1	6	8.1	-1.64	4.1	-5.27
L inferior border lateral plate	msl-nlil	mms	24.4	2.2	6	24.5	0.05	17.7	-3.05
R anterior border lateral plate	nlir-morr	mms	12.0	0.9	6	11.3	-0.78	7.4	-5.11
R frontal ethmoid attachment (orbital)	morr-ofamr	mms	30.8	0.5	6	26.7	-8.20	22.3	-17.00
R posterior border lateral plate	ofamr-msr	mms	10.5	1.1	6	7.3	-2.91	4.3	-5.64
R inferior border lateral plate	msr-nlir	mms	23.5	1.9	6	24.9	0.74	17.9	-2.95
L frontal ethmoid attachment (anterior)	morl-cpal	mms	6.8	1.2	6	4.4	-2.00	3.7	-2.58
L frontal ethmoid attachment (posterior)	cppl-ofaml	mms	10.3	2.1	6	1.9	-4.00	8.0	-1.10
R frontal ethmoid attachment (anterior)	morr-cpar	mms	6.0	1.3	6	7.5	1.15	4.9	-0.85
R frontal ethmoid attachment (posterior)	cppr-ofamr	mms	10.1	1.9	6	4.8	-2.79	8.2	-1.00
Dimensions									
Posterior inferior width	msl-msr	mms	23.3	2.4	6	22.1	-0.50	22.0	-0.54
Anterior inferior width	nlil-nlir	mms	24.0	2.1	6	22.9	-0.52	29.6	2.67
Anterior superior width	morl-morr	mms	16.9	1.7	6	16.9	0.00	25.7	5.18
Posterior superior width	ofaml-ofamr	mms	17.3	2.4	6	16.8	-0.21	18.5	0.50
Ant lateral projection of lateral plate	nlil-morl/morr-nlir	deg	34.8	4.9	6	31.2	-0.73	24.0	-2.20
Post lateral projection of lateral plate	msl-ofaml/ofamr-msr	deg	25.0	12.4	6	41.2	1.31	47.8	1.84
Cribriform Plate									
L anterior cribriform plate	fc-cpal	mms	6.3	1.3	6	6.5	0.15	20.6	11.00
L lateral cribriform plate	cpal-cppl	mms	16.9	1.4	6	22.4	3.93	14.5	-1.71
L posterior cribriform plate	es-cppl	mms	5.0	1.3	6	5.9	0.69	7.9	2.23
R anterior cribriform plate	fc-cpar	mms	5.9	1.1	6	6.9	0.91	20.5	13.27
R lateral cribriform plate	cpar-cppr	mms	18.3	1.9	6	22.7	2.32	17.1	-0.63
R posterior cribriform plate	es-cppr	mms	5.2	1.3	6	5.5	0.23	10.8	4.31
Angles									
L angle lateral cribriform plate cf SN	s-n/cpal-cppl	deg	7.5	2.6	6	3.8	-1.42	25.5	6.92
R angle lateral cribriform plate cf SN	s-n/cpar-cppr	deg	7.7	2.7	6	1.5	-2.30	23.5	5.85
Medial angle of plate cf SN	n-s/es-fc	deg	7.9	3.7	6	2.7	-1.41	7.7	-0.05
Medial Plate									
Distances									
Anterior height crista galli	fc-cg	mms	6.1	2.5	6	6.4	0.12	2.3	-1.52
Posterior height crista galli	cg-es	mms	18.7	2.6	6	21.4	1.04	28.6	3.81
Spheno-ethmoid medial plate junction	es-ves	mms	14.0	2.5	6	11.7	-0.92	16.6	1.04
Ethmoid-vomerine junction	ves-vei	mms	13.6	3.6	6	12.4	-0.33	7.7	-1.64
Septal attachment	vei-n	mms	28.5	1.7	6	29.0	0.29	41.7	7.76
Nasal projection	n-fc	mms	7.9	1.5	6	9.2	0.87	4.4	-2.33
Dimensions									
Maximum medial plate height	vei-cg	mms	25.2	4.5	6	20.7	-1.00	40.0	3.29
Maximum medial plate length	n-es	mms	30.3	1.5	6	35.9	3.73	32.3	1.33

Appendix 2 Measurements for the Experimental Standards and the Patients with Crouzon Syndrome:

Two Years of Age (continued):

			2 Year Standard			Patient JS		Patient IP	
Anatomical Unit	Definition	unit	mean	sd	n	Value	Z	Value	Z
SPHENOID									
Lesser Wing									
Distances									
L medial wing	ofaml-acl	mms	9.5	1.0	6	11.8	2.30	8.7	-0.80
L lateral wing (posterior)	acl-spal	mms	24.8	1.5	6	23.8	-0.67	32.2	4.93
L lateral wing (anterior)	spal-es	mms	29.8	3.6	6	29.4	-0.11	37.9	2.25
R medial wing	ofamr-acr	mms	10.4	1.9	6	12.9	1.32	8.8	-0.84
R lateral wing (posterior)	acr-spar	mms	25.0	3.0	6	27.6	0.87	35.3	3.43
R lateral wing (anterior)	spar-es	mms	30.6	4.0	6	33.4	0.70	43.4	3.20
Dimensions									
Maximum lesser wing width	spal-spar	mms	58.1	6.4	6	61.3	0.50	72.1	2.19
Lesser wing superior angle	spal-es -spar	deg	144.7	4.8	6	154.7	2.08	124.6	-4.19
L lateral projection (anterior angle)	n-s/acl-spal	deg	53.6	4.1	6	60.7	1.73	59.8	1.51
R lateral projection (anterior angle)	n-s/acr-spar	deg	56.6	4.5	6	65.5	1.98	61.3	1.04
Pterygoid Plate									
Distances									
L medial pterygoid plate	ptsl-hpl	mms	18.9	1.7	6	20.8	1.12	13.8	-3.00
L medial hamular notch	hpl-hnl	mms	3.5	1.5	6	4.0	0.33	3.7	0.13
L lateral hamular notch	hnl-ptll	mms	8.4	1.7	6	6.2	-1.29	5.9	-1.47
L lateral pterygoid plate	ptll-fool	mms	16.3	1.3	6	16.3	0.00	13.1	-2.46
R medial pterygoid plate	ptsr-hpr	mms	19.0	2.0	6	21.6	1.30	16.3	-1.35
R medial hamular notch	hpr-hnr	mms	4.1	2.1	6	3.9	-0.10	4.2	0.05
R lateral hamular notch	hnr-ptlr	mms	8.9	2.4	6	7.9	-0.42	6.8	-0.87
R lateral pterygoid plate	ptlr-foor	mms	16.0	1.0	6	15.9	-0.10	15.0	-1.00
Angles									
L pterygoid axis	n-s/ptsl-hpl	deg	55.0	7.3	6	64.2	1.26	94.1	5.36
R pterygoid axis	n-s/ptsr-hpr	deg	58.7	5.8	6	68.9	1.76	93.5	6.00
Greater Wing									
Distances									
Lateral									
L anterior middle cranial fossa	fosl-gwll	mms	29.8	1.4	6	32.1	1.64	33.7	2.79
L spheno-zygomatic suture	zfsl-gwll	mms	13.2	1.2	6	12.9	-0.25	37.3	20.08
R anterior middle cranial fossa	fosr-gwlr	mms	29.9	2.0	6	28.9	-0.50	31.3	0.70
R spheno-zygomatic suture	gwlr-zfsr	mms	12.8	2.2	6	14.9	0.95	31.3	8.41
Orbital									
L inferior lateral orbital length	gwll-gwml	mms	23.6	1.1	6	23.9	0.27	29.4	5.27
L superior orbital fissure height	gwml-sobfl	mms	17.6	4.5	6	15.2	-0.53	37.6	4.44
L spheno-frontal suture (orbital)	sobfl-zfsl	mms	17.5	4.2	6	18.7	0.29	15.1	-0.57
R inferior lateral orbital length	gwlr-gwmr	mms	23.1	1.9	6	19.3	-2.00	29.1	3.16
R superior orbital fissure height	gwmr-sobfr	mms	15.5	4.9	6	14.6	-0.18	38.1	4.61
R spheno-frontal suture (orbital)	sobfr-zfsr	mms	19.2	3.4	6	16.3	-0.85	11.7	-2.21
Posterior									
L spheno-petrous temporal suture (inf)	fosl-ptsl	mms	13.1	1.9	6	10.9	-1.16	15.3	1.16
R spheno-petrous temporal suture (inf)	fosr-ptsr	mms	14.1	1.8	6	11.5	-1.44	14.1	0.00
L posterior middle cranial fossa	fosl-petal	mms	16.9	1.4	6	18.1	0.86	21.5	3.29
R posterior middle cranial fossa	fosr-petar	mms	31.8	2.5	6	30.0	-0.72	33.9	0.84

Appendix 2 Measurements for the Experimental Standards and the Patients with Crouzon Syndrome:

Two Years of Age (continued):

			2 Year Standard			Patient JS		Patient IP	
Anatomical Unit	**Definition**	**unit**	**mean**	**sd**	**n**	**Value**	**Z**	**Value**	**Z**
SPHENOID (continued)									
Dimensions and Angles									
Posterior sphenoid width	fosl-fosr	mms	43.3	3.9	6	37.6	-1.46	39.7	-0.92
L angle of greater wing splay	zfsl-gwml-ptsl	deg	134.9	5.6	6	112.7	-3.96	128.5	-1.14
R angle of greater wing splay	zfsr-gwmr-ptsr	deg	132.8	6.7	6	112.8	-2.99	132.6	-0.03
Total angle of protrusion	zfsl-gwml/gwmr-zfsr	deg	95.8	4.1	6	119.0	5.66	89.7	-1.49
Inferior greater wing protrusion	gwll-gwml/gwmr-gwlr	deg	94.4	5.9	6	116.4	3.73	148.4	9.15
Posterior angle of greater wing	fosl-petal/petar-fosr	deg	95.2	8.7	6	80.0	-1.75	69.3	-2.98
Squamous Sphenoid									
L squamous spheno-frontal suture	zfsl-spcl	mms	18.5	3.0	6				
L squamous spheno-parietal suture	spcl-sptl	mms	10.9	1.9	6				
L lateral spheno-temporal suture	fosl-sptl	mms	40.1	1.9	6				
R squamous spheno-frontal suture	zfsr-spcr	mms	17.3	3.2	6				
R squamous spheno-parietal suture	spcr-sptr	mms	10.6	2.8	6				
R lateral spheno-temporal suture	fosr-sptr	mms	37.7	2.0	6				
Sphenoid Body									
Distances									
Lateral/Posterior Body									
L anterior inferior length	gwml-ptsl	mms	11.8	1.2	6	13.9	1.75	15.0	2.67
L spheno-occipital synchondrosis (lat)	ptsl-petal	mms	12.1	0.9	6	13.4	1.44	21.4	10.33
L posterior clinoid height	petal-pcl	mms	7.1	2.3	6	7.4	0.13	8.9	0.78
Posterior clinoid width	pcl-pcr	mms	8.4	1.8	6	8.9	0.28	11.2	1.56
R anterior inferior length	gwmr-ptsr	mms	12.1	1.2	6	13.4	1.08	14.4	1.92
R spheno-occipital synchondrosis (lat)	ptsr-petar	mms	13.0	0.9	6	13.1	0.11	19.0	6.67
R posterior clinoid height	petar-pcr	mms	7.9	2.1	6	8.9	0.48	8.1	0.10
Anterior Body									
L spheno-ethmoid suture	es-cppl	mms	5.0	1.3	6	5.9	0.69	7.9	2.23
L anterior lateral distance	cppl-ofaml	mms	10.3	2.1	6	1.9	-4.00	8.0	-1.10
L anterior superior length	ofaml-gwml	mms	8.4	0.9	6	8.1	-0.33	10.7	2.56
R spheno-ethmoid suture	es-cppr	mms	5.2	1.3	6	5.5	0.23	10.8	4.31
R anterior lateral distance	cppr-ofamr	mms	10.1	1.9	6	4.8	-2.79	8.2	-1.00
R anterior superior length	ofamr-gwmr	mms	9.2	0.7	6	9.0	-0.29	9.9	1.00
Sella									
L lateral anterior body	cppl-ofpml	mms	12.6	1.7	6	8.1	-2.65	8.4	-2.47
L lateral sella length	ofpml-petal	mms	17.6	1.4	6	17.6	0.00	25.2	5.43
R lateral anterior body	cppr-ofpmr	mms	12.5	1.9	6	7.2	-2.79	9.5	-1.58
R lateral sella length	ofpmr-petar	mms	18.0	1.5	6	18.5	0.33	23.5	3.67
Base/Floor Body									
Spheno-ethmoid medial plate junction	es-ves	mms	14.0	2.5	6	11.7	-0.92	16.6	1.04
Spheno-vomerine junction	ves-h	mms	10.9	3.0	6	11.4	0.17	16.6	1.90
L posterior width	h-ptsl	mms	11.6	1.8	6	11.9	0.17	11.6	0.00
R posterior width	h-ptsr	mms	11.5	1.2	6	11.4	-0.08	10.0	-1.25

Appendix 2 Measurements for the Experimental Standards and the Patients with Crouzon Syndrome:

Two Years of Age (continued):

			2 Year Standard			Patient JS		Patient IP	
Anatomical Unit	Definition	unit	mean	sd	n	Value	Z	Value	Z
SPHENOID (continued)									
Dimensions									
Anterior inferior body width	gwml-gwmr	mms	21.3	1.9	6	16.6	-2.47	16.2	-2.68
Spheno-occipital synchondrosis (inf)	ptsl-ptsr	mms	19.9	2.4	6	20.2	0.13	18.0	-0.79
Anterior superior body width	ofaml-ofamr	mms	17.3	2.4	6	16.8	-0.21	18.5	0.50
Spheno-occipital synchondrosis (sup)	petal-petar	mms	18.8	1.7	6	15.5	-1.94	17.6	-0.71
L posterior body height	pcl-ptsl	mms	15.0	2.3	6	18.4	1.48	24.9	4.30
R posterior body height	pcr-ptsr	mms	16.3	2.1	6	18.6	1.10	22.6	3.00
L anterior body height	acl-gwml	mms	9.6	1.1	6	8.8	-0.73	11.7	1.91
L anterior body height	acr-gwmr	mms	9.8	0.8	6	10.0	0.25	12.2	3.00
Angles									
Body floor angle	cs-ves-h	deg	131.8	27.8	6	111.7	-0.72	119.2	-0.45
L lower body angle	s-n/gwml-ptsl	deg	46.0	3.7	6	34.8	-3.03	33.5	-3.38
R lower body angle	s-n/gwmr-ptsr	deg	158.8	2.0	6	160.0	0.60	162.7	1.95
L upper body angle	s-n/ofpml-petal	deg	23.3	2.8	6	17.0	-2.25	9.8	-4.82
R upper body angle	s-n/ofpmr-petar	deg	21.5	3.3	6	20.7	-0.24	10.8	-3.24
TEMPORAL									
Distances									
Squamous									
L lateral spheno-temporal suture	fosl-sptl	mms	40.1	1.9	6				
L temporo-parietal suture	sptl-asl	mms	62.4	3.7	6				
L occipital mastoid height	asl-mal	mms	33.2	3.1	6				
L medial mastoid prominence	mal-smfl	mms	8.2	2.2	6	7.7	-0.23		
R lateral spheno-temporal suture	fosr-sptr	mms	37.7	2.0	6				
R temporo-parietal suture	sptr-asr	mms	61.7	6.6	6				
R occipital mastoid height	asr-mar	mms	31.0	4.3	6				
R medial mastoid prominence	mar-smfr	mms	9.9	2.2	6	10.5	0.27		
External Auditory Meatus (EAM)									
L lateral mastoid prominence	mal-camil	mms	14.2	1.5	6	14.6	0.27	13.9	-0.20
L inferior-posterior EAM rim	camil-campl	mms	7.3	1.9	6	7.5	0.11	11.1	2.00
L posterior-superior EAM rim	campl-pol	mms	4.9	0.3	6	4.5	-1.33	7.8	9.67
L superior-anterior EAM rim	pol-camal	mms	4.9	0.9	6	4.4	-0.56	10.3	6.00
L anterior-inferior EAM rim	camal-camil	mms	5.5	1.4	6	5.4	-0.07	6.0	0.36
R lateral mastoid prominence	mar-camir	mms	14.0	1.9	6	16.1	1.11	13.2	-0.42
R inferior-posterior EAM rim	camir-campr	mms	6.3	2.3	6	8.5	0.96	16.8	4.57
R posterior-superior EAM rim	campr-por	mms	4.8	0.6	6	4.7	-0.17	5.6	1.33
R superior-anterior EAM rim	por-camar	mms	4.6	1.6	6	3.0	-1.00	6.3	1.06
R anterior-inferior EAM rim	camar-camir	mms	5.4	0.6	6	6.2	1.33	13.7	13.83

Appendix 2 Measurements for the Experimental Standards and the Patients with Crouzon Syndrome:

Two Years of Age (continued):

Anatomical Unit	Definition	unit	2 Year Standard mean	sd	n	Patient JS Value	Z	Patient IP Value	Z
TEMPORAL (continued)									
Zygoma									
L EAM-articular fossa length	eamal-afl	mms	10.4	1.5	6	10.2	-0.13	14.0	2.40
L articular fossa height	afl-ael	mms	5.2	1.1	6	8.0	2.55	4.1	-1.00
L inferior arch length	ael-parl	mms	7.7	3.4	6	6.8	-0.26	12.2	1.32
L zygomatico-temporal suture	parl-ztl	mms	16.3	2.1	6	14.8	-0.71	17.7	0.67
L superior arch length	ztl-aul	mms	26.6	2.1	6	22.7	-1.86	16.3	-4.90
R EAM-articular fossa length	eamar-afr	mms	11.3	1.4	6	9.8	-1.07	8.7	-1.86
R articular fossa height	afr-acr	mms	4.8	1.2	6	7.7	2.42	3.2	-1.33
R inferior arch length	aer-parr	mms	8.7	3.8	6	7.6	-0.29	7.7	-0.26
R zygomatico-temporal suture	parr-ztr	mms	17.0	2.0	6	13.5	-1.75	20.7	1.85
R superior arch length	ztr-aur	mms	27.8	2.3	6	23.4	-1.91	13.3	-6.30
Petrous									
L spheno-petrous temporal suture (sup)	fisl-petal	mms	15.8	1.6	6	15.2	-0.38	18.8	1.87
L post-med temporo-occipital suture	petal-jfpl	mms	25.6	1.8	6	28.0	1.33	27.5	1.06
L lateral temporo-occipital suture	jfpl-asil	mms	36.8	4.8	6				
L petrous superior margin	asil-petal	mms	54.4	3.1	6				
R spheno-petrous temporal suture (sup)	fisr-petar	mms	15.8	1.2	6	15.1	-0.58	14.7	-0.92
R post-med temporo-occipital suture	petar-jfpr	mms	27.6	2.3	6	25.2	-1.04	26.8	-0.35
R lateral temporo-occipital suture	jfpr-asir	mms	37.3	4.4	6				
R petrous superior margin	asir-petar	mms	53.3	4.0	6				
L occipital mastoid suture inferior	mal-jfll	mms	14.3	2.9	6	16.4	0.72	24.1	3.38
L jugular foramen width	jfll-jfml	mms	8.5	1.8	6	7.5	-0.56	5.7	-1.56
L medial temporo-occipital suture (inf)	jfml-ptsl	mms	21.3	1.7	6	21.8	0.29	30.0	5.12
L spheno-petrous temporal suture (inf)	fosl-ptsl	mms	13.1	1.9	6	10.9	-1.16	15.3	1.16
R occipital mastoid suture inferior	mar-jflr	mms	13.6	1.8	6	18.0	2.44	22.8	5.11
R jugular foramen width	jflr-jfmr	mms	9.9	0.8	6	5.6	-5.37	7.3	-3.25
R medial temporo-occipital suture (inf)	jfmr-ptsr	mms	22.0	2.3	6	25.0	1.30	27.8	2.52
R spheno-petrous temporal suture (inf)	fosr-ptsr	mms	14.1	1.8	6	11.5	-1.44	14.1	0.00
Dimensions									
L petrous ridge length	petal-petpl	mms	46.7	4.1	6	52.6	1.44	64.6	4.37
R petrous ridge length	petar-petpr	mms	48.8	2.4	6	62.8	5.83	67.9	7.96
Inter-internal aud meatus dimension	iamr-iaml	mms	35.3	2.6	6	30.1	-2.00	38.6	1.27
Inter-external aud meatus dimension	pol-por	mms	73.9	4.4	6	71.0	-0.66	101.7	6.32
Inter-post jugular foramen dimension	jfpr-jfpl	mms	42.4	3.8	6	45.0	0.68	39.3	-0.82
Inter-mastoid dimension	mal-mar	mms	71.8	3.0	6	71.0	-0.27	76.1	1.43
Angles									
Auditory canal angle	pol-iaml/iamr-por	deg	140.7	6.2	6	149.8	1.47	147.1	1.03
Petrous ridge angle	petpl-petal/petar-petpr	deg	95.1	3.5	6	81.0	-4.03	90.8	-1.23
L zygoma projection angle	petal-aul-ztl	deg	97.4	5.7	6	111.8	2.53	89.0	-1.47
R zygoma projection angle	petar-aur-ztr	deg	93.7	7.4	6	98.6	0.66	92.9	-0.11

Appendix 2 Measurements for the Experimental Standards and the Patients with Crouzon Syndrome:

Two Years of Age (continued):

			2 Year Standard			Patient JS		Patient IP	
Anatomical Unit	**Definition**	**unit**	**mean**	**sd**	**n**	**Value**	**Z**	**Value**	**Z**
PARIETAL									
Distances									
Sagittal suture	l-br	mms	99.2	4.3	4				
L parietal frontal (coronal) suture	br-spcl	mms	80.6	3.6	4				
L spheno-parietal suture	spcl-sptl	mms	10.9	1.9	6				
L temporo-parietal suture	sptl-asl	mms	62.4	3.7	6				
L occipito-parietal (lambdoid) suture	asl-l	mms	72.9	2.0	6				
R parietal frontal (coronal) suture	br-spcr	mms	80.7	5.4	4				
R spheno-parietal suture	spcr-sptr	mms	10.6	2.8	6				
R temporo-parietal suture	sptr-asr	mms	61.7	6.6	6				
R occipito-parietal (lambdoid) suture	asr-l	mms	74.8	3.2	6				
OCCIPITAL									
Distances									
Lambdoid and Cranial Base									
L occipito-parietal (lambdoid) suture	l-asl	mms	72.9	2.0	6				
L lateral temporo-occipital suture (sup)	asl-jfll	mms	34.7	5.1	6				
L lateral jugular foramen	jfll-jfpl	mms	5.0	1.3	6	6.4	1.08	2.6	-1.85
L medial jugular foramen	jfpl-jfml	mms	7.1	1.9	6	6.5	-0.32	6.5	-0.32
L medial temporo-occipital suture (inf)	jfml-ptsl	mms	21.3	1.7	6	21.8	0.29	30.0	5.12
R occipito-parietal (lambdoid) suture	l-asr	mms	74.8	3.2	6				
R lateral temporo-occipital suture (sup)	asr-jflr	mms	32.4	4.4	6				
R lateral jugular foramen	jflr-jfpr	mms	5.8	1.6	6	5.5	-0.19	3.4	-1.50
R medial jugular foramen	jfpr-jfmr	mms	7.4	1.7	6	2.8	-2.71	6.1	-0.76
R medial temporo-occipital suture (inf)	jfmr-ptsr	mms	22.0	2.3	6	25.0	1.30	27.8	2.52
Inferior spheno-occipital synchondrosis	ptsr-ptsl	mms	19.9	2.4	6	20.2	0.13	18.0	-0.79
Foramen Magnum									
L anterior foramen magnum	ba-fmll	mms	17.4	1.0	6	18.6	1.20	19.5	2.10
L posterior foramen magnum	fmll-o	mms	21.9	1.4	6	17.2	-3.36	19.6	-1.64
R anterior foramen magnum	ba-fmlr	mms	17.1	0.4	6	19.0	4.75	16.6	-1.25
R posterior foramen magnum	fmlr-o	mms	22.3	1.5	6	20.0	-1.53	27.9	3.73
Dimensions									
Foramen Magnum									
Foramen magnum length	ba-o	mms	30.5	1.6	6	28.0	-1.56	31.0	0.31
Foramen magnum width	fmll-fmlr	mms	23.8	1.4	6	24.1	0.21	26.0	1.57
Posterior Cranial Fossa									
Posterior cranial fossa depth	o-iop	mms	34.5	3.9	6	37.7	0.82	39.3	1.23
Posterior occipital height	iop-l	mms	51.3	3.0	6				
L posterior fossa length	petpl-iop	mms	56.8	2.4	6	51.3	-2.29	58.2	0.58
L posterior fossa length	petpr-iop	mms	58.2	2.7	6	46.4	-4.37	58.2	0.00

Appendix 2 Measurements for the Experimental Standards and the Patients with Crouzon Syndrome:

Two Years of Age (continued):

			2 Year Standard			Patient JS		Patient IP	
Anatomical Unit	**Definition**	**unit**	**mean**	**sd**	**n**	**Value**	**Z**	**Value**	**Z**
CRANIAL BASE SUTURES									
Anterior Cranial Fossa									
L spheno-ethmoid synchondrosis	es-cppl	mms	5.0	1.3	6	5.9	0.69	7.9	2.23
R spheno-ethmoid synchondrosis	es-cppr	mms	5.2	1.3	6	5.5	0.23	10.8	4.31
L spheno-frontal suture (ant fossa)	cppl-spal	mms	25.5	3.9	6	24.5	-0.26	31.0	1.41
R spheno-frontal suture (ant fossa)	cppr-spar	mms	26.1	4.4	6	28.3	0.50	33.7	1.73
L spheno-frontal suture (orbital)	spal-zfsl	mms	15.5	1.6	6	12.8	-1.69	11.9	-2.25
R spheno-frontal suture (orbital)	spar-zfsr	mms	14.9	2.6	6	10.4	-1.73	9.9	-1.92
L spheno-zygomatic suture	zfsl-gwll	mms	13.2	1.2	6	12.9	-0.25	37.3	20.08
R spheno-zygomatic suture	zfsr-gwlr	mms	12.8	2.2	6	14.9	0.95	31.3	8.41
Middle Cranial Fossa									
L spheno-squamous temporal suture	gwll-fisl	mms	28.4	0.9	6	31.1	3.00	31.2	3.11
R spheno-squamous temporal suture	gwlr-fisr	mms	28.4	2.2	6	28.5	0.05	30.2	0.82
L spheno-petrous temporal suture (sup)	fisl-petal	mms	15.8	1.6	6	15.2	-0.38	18.8	1.87
R spheno-petrous temporal suture (sup)	fisr-petar	mms	15.8	1.2	6	15.1	-0.58	14.7	-0.92
L spheno-petrous temporal suture (inf)	fosl-ptsl	mms	13.1	1.9	6	10.9	-1.16	15.3	1.16
R spheno-petrous temporal suture (inf)	fosr-ptsr	mms	14.1	1.8	6	11.5	-1.44	14.1	0.00
Posterior Cranial Fossa									
L medial temporo-occipital suture (sup)	petal-jfml	mms	19.1	1.9	6	21.7	1.37	21.8	1.42
R medial temporo-occipital suture (sup)	petar-jfmr	mms	19.2	2.8	6	22.8	1.29	21.1	0.68
L medial temporo-occipital suture (inf)	jfml-ptsl	mms	21.3	1.7	6	21.8	0.29	30.0	5.12
R medial temporo-occipital suture (inf)	jfmr-ptsr	mms	22.0	2.3	6	25.0	1.30	27.8	2.52
L occipital mastoid suture (superior)	jfll-petpl	mms	30.4	5.1	6	35.3	0.96	46.7	3.20
R occipital mastoid suture (superior)	jflr-petpr	mms	29.3	4.2	6	45.5	3.86	51.9	5.38
Spheno-occipital synchondrosis (sup)	petal-petar	mms	18.8	1.7	6	15.5	-1.94	17.6	-0.71
Spheno-occipital synchondrosis (inf)	ptsl-ptsr	mms	19.9	2.4	6	20.2	0.13	18.0	-0.79
L spheno-occipital synchondrosis (lat)	ptsl-petal	mms	12.1	0.9	6	13.4	1.44	21.4	10.33
R spheno-occipital synchondrosis (lat)	ptsr-petar	mms	13.0	0.9	6	13.1	0.11	19.0	6.67
CRANIAL BASE									
Facial Heights									
Anterior facial height	n-gn	mms	68.9	7.1	5	86.8	2.52	102.8	4.77
L posterior facial height	s-gol	mms	50.0	3.4	5	52.6	0.76	55.9	1.74
R posterior facial height	s-gor	mms	51.3	4.2	5	51.3	0.00	56.9	1.33
Facial Angles									
SNA	s-n-ss	deg	78.9	2.6	6	78.6	-0.12	52.6	-10.12
SNB	s-n-sm	deg	72.6	2.4	5	68.3	-1.79	51.1	-8.96
Cranial Base Angle									
Cranial base angle	ba-s-n	deg	135.1	5.5	6	128.6	-1.18	162.7	5.02
Cranial Base Dimensions									
Cranial base length	ba-n	mms	72.1	2.2	6	71.8	-0.14	86.3	6.45
Clivus length (posterior cranial base)	ba-s	mms	26.6	2.1	6	27.3	0.33	30.2	1.71
Anterior cranial base length	s-n	mms	51.4	2.3	6	51.5	0.04	57.0	2.43

Appendix 2 Measurements for the Experimental Standards and the Patients with Crouzon Syndrome:

Six Years of Age:

			6 Year Standard			Patient LW		Patient AY	
Anatomical Unit	Definition	unit	mean	sd	n	Value	Z	Value	Z
MANDIBLE									
Distances									
L anterior superior body	id-em1il	mms	36.0	4.0	6	31.8	-1.05	17.9	-4.53
L posterior superior body	em1il-cbl	mms	12.9	4.5	6	22.5	2.13	32.7	4.40
L total superior body	id-cbl	mms	45.3	3.9	6	51.5	1.59	48.7	0.87
L anterior ramus	cbl-ctl	mms	26.3	1.3	6	27.9	1.23	23.6	-2.08
L anterior mandibular notch	ctl-mnl	mms	13.8	0.7	6	14.6	1.14	13.3	-0.71
L posterior mandibular notch	mnl-cdl	mms	14.8	1.4	6	18.1	2.36	16.1	0.93
L posterior ramus	cdl-gol	mms	35.8	3.0	6	40.8	1.67	30.6	-1.73
L inferior body	gol-gn	mms	60.7	5.0	6	65.3	0.92	62.8	0.42
R anterior superior body	id-em1ir	mms	35.8	4.2	6	28.7	-1.69	17.4	-4.38
R posterior superior body	em1ir-cbr	mms	10.2	4.5	6	25.5	3.40	30.7	4.56
R total superior body	id-cbr	mms	45.0	3.5	6	51.3	1.80	46.2	0.34
R anterior ramus	cbr-ctr	mms	27.8	1.4	6	27.4	-0.29	28.6	0.57
R anterior mandibular notch	ctr-mnr	mms	13.5	1.0	6	13.6	0.10	14.1	0.60
R posterior mandibular notch	mnr-cdr	mms	15.6	1.7	6	18.4	1.65	16.3	0.41
R posterior ramus	cdr-gor	mms	36.3	2.4	6	39.3	1.25	34.7	-0.67
R inferior body	gor-gn	mms	59.7	5.5	6	66.6	1.25	61.2	0.27
Dimensions									
Intergonial dimension	gol-gor	mms	70.3	6.5	6	71.0	0.11	66.6	-0.57
Intercondylar dimension	cdl-cdr	mms	91.1	6.1	6	91.9	0.13	92.8	0.28
Intercoronoid base dimension	cbl-cbr	mms	62.3	5.7	6	64.7	0.42	61.7	-0.11
Intermolar dimension	em1il-em1ir	mms	51.2	3.6	6	48.5	-0.75	31.2	-5.56
L Superior ramus width	cdl-ctl	mms	23.5	1.6	6	25.1	1.00	26.5	1.88
L inferior ramus width	gol-cbl	mms	25.0	2.4	6	29.4	1.83	30.1	2.12
R superior ramus width	cdr-ctr	mms	23.3	1.5	6	24.0	0.47	25.0	1.13
R inferior ramus width	gor-cbr	mms	25.8	2.1	6	27.7	0.90	29.0	1.52
Anterior symphyseal height	gn-id	mms	22.0	1.6	6	25.2	2.00	27.4	3.37
L total mandibular length	gn-cdl	mms	87.1	5.6	6	94.6	1.34	87.8	0.13
R total mandibular length	gn-cdr	mms	86.7	5.6	6	95.3	1.54	89.4	0.48
Angles									
L mandibular notch angle	cdl-mnl-ctl	deg	111.7	9.7	6	99.5	-1.26	128.2	1.70
R mandibular notch angle	cdr-mnr-ctr	deg	113.4	7.8	6	95.8	-2.26	110.1	-0.42
L gonial angle	cdl-gol-gn	deg	127.9	4.3	6	124.3	-0.84	137.4	2.21
R gonial angle	cdr-gor-gn	deg	126.2	4.3	6	126.3	0.02	136.0	2.28
L coronoid base angle	ctl-cbl-id	deg	126.0	7.7	6	126.5	0.06	139.3	1.73
R coronoid base angle	ctr-cbr-id	deg	126.2	5.9	6	127.9	0.29	134.1	1.34
L coronoid-dental base angle	ctl-cbl-em1il	deg	140.9	7.6	6	135.2	-0.75	138.8	-0.28
R coronoid-dental base angle	ctr-cbr-em1ir	deg	141.5	10.0	6	137.5	-0.40	137.4	-0.41
L symphyseal angle	gol-gn-id	deg	84.3	4.0	6	90.7	1.60	87.4	0.77
R symphyseal angle	gor-gn-id	deg	87.2	1.9	6	83.5	-1.95	85.6	-0.84
Anterior mandibular angle	gol-gn-gor	deg	70.1	3.3	6	65.1	-1.52	64.9	-1.58

Appendix 2 Measurements for the Experimental Standards and the Patients with Crouzon Syndrome:

Six Years of Age (continued):

			6 Year Standard			Patient LW		Patient AY	
Anatomical Unit	**Definition**	**unit**	**mean**	**sd**	**n**	**Value**	**Z**	**Value**	**Z**
MAXILLA									
Distances									
Orbital Region									
L fronto-maxillary suture	snml-morl	mms	6.7	1.1	6	15.7	8.18	10.6	3.55
L frontal process orbital rim	nlil-morl	mms	14.3	1.6	6	8.3	-3.75	9.7	-2.88
L medial orbital floor	msl-nlil	mms	28.0	1.5	6	31.0	2.00	27.1	-0.60
L posterior lateral orbital floor	msl-iobfl	mms	17.9	2.3	6	20.1	0.96	24.6	2.91
L anterior lateral orbital floor	orl-iobfl	mms	16.5	2.5	6	17.0	0.20	15.6	-0.36
L maxillary infra-orbital rim	orl-nlil	mms	12.9	2.4	6	21.5	3.58	20.5	3.17
R fronto-maxillary suture	snmr-morr	mms	7.3	1.5	6	13.3	4.00	7.8	0.33
R frontal process orbital rim	nlir-morr	mms	14.1	1.8	6	9.3	-2.67	9.5	-2.56
R medial orbital floor	msr-nlir	mms	27.5	2.4	6	31.0	1.46	27.9	0.17
R posterior lateral orbital floor	msr-iobfr	mms	18.3	3.1	6	22.7	1.42	25.5	2.32
R anterior lateral orbital floor	orr-iobfr	mms	16.2	2.7	6	17.9	0.63	13.9	-0.85
R maxillary infra-orbital rim	orr-nlirr	mms	12.4	2.8	6	21.0	3.10	21.0	3.10
Anterior Wall									
L anterior zygo-maxillary suture	zmil-orl	mms	21.9	1.5	6	17.3	-3.07	22.3	0.27
L lateral maxillary wall	zmil-em1sl	mms	14.8	1.4	6	20.6	4.14	28.0	9.43
L anterior alveolar margin	em1sl-pr	mms	36.4	3.3	6	32.3	-1.24	21.6	-4.48
L lower pyriform margin	ans-all	mms	12.6	1.5	6	16.3	2.47	11.6	-0.67
L upper pyriform margin	all-inml	mms	13.8	1.4	6	17.7	2.79	17.7	2.79
L naso-maxillary suture	inml-snml	mms	17.6	1.8	6	16.2	-0.78	15.6	-1.11
R anterior zygo-maxillary suture	zmir-orr	mms	20.9	1.9	6	17.7	-1.68	23.5	1.37
R lateral maxillary wall	zmir-em1sr	mms	14.9	1.2	6	21.4	5.42	28.2	11.08
R anterior alveolar margin	em1sr-pr	mms	35.0	3.7	6	31.4	-0.97	21.5	-3.65
R lower pyriform margin	ans-alr	mms	13.0	1.7	6	15.1	1.24	11.4	-0.94
R upper pyriform margin	alr-inmr	mms	14.2	2.2	6	25.2	5.00	13.9	-0.14
L naso-maxillary suture	inmr-snmr	mms	18.0	2.3	6	9.8	-3.57	15.4	-1.13
Anterior alveolar height	pr-ans	mms	13.5	9.3	6	14.5	0.11	14.0	0.05
Lateral Wall									
L posterior alveolar margin	em1sl-mxtl	mms	11.1	2.4	6	19.3	3.42	25.6	6.04
L posterior maxillary wall	mxtl-msl	mms	27.9	1.5	6	28.2	0.20	30.1	1.47
L posterior lateral orbital floor	msl-iobfl	mms	17.9	2.3	6	20.1	0.96	24.6	2.91
L posterior zygo-maxillary suture	iobfl-zmil	mms	17.6	1.1	6	18.4	0.73	18.4	0.73
R posterior alveolar margin	em1sr-mxtr	mms	12.0	1.2	6	19.3	6.08	23.3	9.42
R posterior maxillary wall	mxtr-msr	mms	28.1	1.2	6	32.3	3.50	32.9	4.00
R posterior lateral orbital floor	msr-iobfr	mms	18.3	3.1	6	22.7	1.42	25.5	2.32
R posterior zygo-maxillary suture	iobfr-zmir	mms	17.5	1.8	6	16.9	-0.33	19.7	1.22
Palate									
L posterior palatal height	em1sl-gpfl	mms	16.7	1.2	6	21.9	4.33	24.3	6.33
L posterior palatal width	gpfl-pns	mms	13.3	1.2	6	12.6	-0.58	13.2	-0.08
R posterior palatal height	em1sr-gpfr	mms	17.0	1.5	6	22.9	3.93	25.3	5.53
R posterior palatal width	gpfr-pns	mms	12.9	0.8	6	13.5	0.75	15.1	2.75
Superior palatal length	ans-pns	mms	36.9	1.6	6	44.1	4.50	39.8	1.81

Appendix 2 Measurements for the Experimental Standards and the Patients with Crouzon Syndrome:

Six Years of Age (continued):

			6 Year Standard			Patient LW		Patient AY	
Anatomical Unit	**Definition**	**unit**	**mean**	**sd**	**n**	**Value**	**Z**	**Value**	**Z**
MAXILLA (continued)									
Dimensions									
Anterior midline height	n-pr	mms	51.1	1.6	6	54.3	2.00	49.2	-1.19
L lateral height	morl-em1sl	mms	48.3	3.3	6	48.3	0.00	45.0	-1.00
R lateral height	morr-em1sr	mms	47.5	4.2	6	48.8	0.31	44.6	-0.69
L posterior height	gpfl-msl	mms	25.7	1.5	6	23.1	-1.73	28.2	1.67
R posterior height	gpfr-msr	mms	25.7	1.2	6	24.4	-1.08	30.1	3.67
L superior length	msl-inml	mms	38.6	1.9	6	45.6	3.68	47.2	4.53
R superior length	msr-inmr	mms	37.8	2.7	6	46.3	3.15	44.8	2.59
Posterior palatal width	gpfl-gpfr	mms	25.2	1.4	6	24.6	-0.43	26.4	0.86
Anterior inter-canine width	ccsl-ccsr	mms	31.8	2.3	6	33.8	0.87	29.6	-0.96
Maximum maxillary width	zmil-zmir	mms	75.8	4.1	6	75.3	-0.12	82.6	1.66
Superior (inter-orbital rim) width	orl-orr	mms	52.5	6.7	6	64.0	1.72	61.9	1.40
Nasal aperture height	na-ans	mms	23.0	2.6	6	23.6	0.23	19.5	-1.35
Nasal aperture width	all-alr	mms	20.8	2.7	6	23.3	0.93	17.6	-1.19
Angles									
L orbital floor angle	nlil-msl-iobfl	deg	56.2	2.4	6	68.4	5.08	61.2	2.08
R orbital floor angle	nlir-msr-iobfr	deg	54.3	7.4	6	65.2	1.47	56.1	0.24
L posterior inferior angle	msl-gpfl-em1sl	deg	102.7	4.2	6	129.1	6.29	121.1	4.38
R posterior inferior angle	msr-gpfr-em1sr	deg	104.8	7.5	6	136.5	4.23	116.7	1.59
Superior maxillary splay	iobfl-msl/msr-iobfr	deg	97.0	8.2	6	125.4	3.46	102.6	0.68
L superior /occlusal angle	snml-msl/em1sl-pr	deg	40.7	21.6	6	38.4	-0.11	50.4	0.45
R superior /occlusal angle	snmr-msr/em1sr-pr	deg	40.9	20.3	6	41.5	0.03	51.7	0.53
L palatal/occlusal angle	ans-pns/em1sl-pr	deg	47.7	26.5	6	47.1	-0.02	59.7	0.45
R palatal/occlusal angle	ans-pns/em1sr-pr	deg	47.4	25.4	6	50.8	0.13	63.2	0.62
Anterior palatal angle	gpfl-ans-gpfr	deg	40.7	2.2	6	34.2	-2.95	40.5	-0.09
Maxillary arch angle	gpfl-pr-gpfr	deg	40.6	46.1	6	36.6	-0.09	44.2	0.08
NASAL BONES									
Distances									
Nasal length	na-n	mms	16.5	2.2	6	20.9	2.00	18.4	0.86
L inferior nasal width	na-inml	mms	7.7	2.0	6	9.4	0.85	4.2	-1.75
L naso-maxillary suture	inml-snml	mms	17.6	1.8	6	16.2	-0.78	15.6	-1.11
L fronto-nasal suture	n-snml	mms	5.9	1.5	6	3.5	-1.60	7.6	1.13
R inferior nasal width	na-inmr	mms	8.2	2.5	6	10.9	1.08	8.6	0.16
R naso-maxillary suture	inmr-snmr	mms	18.0	2.3	6	9.8	-3.57	15.4	-1.13
R fronto-nasal suture	n-snmr	mms	5.9	0.7	6	3.7	-3.14	9.6	5.29
Dimensions									
Inferior width	inml-inmr	mms	11.8	1.0	6	12.0	0.20	11.8	0.00
Superior width	snml-snmr	mms	9.6	1.5	6	6.4	-2.13	11.3	1.13
Angles									
Nasal/anterior cranial base angle	s-n-na	deg	96.8	4.1	6	109.6	3.12	94.2	-0.63
Superior nasal bone angle	snml-n-snmr	deg	101.1	14.9	6	123.2	1.48	80.5	-1.38
Inferior nasal bone angle	inml-na-inmr	deg	103.0	20.8	6	71.7	-1.50	131.6	1.38
Splay of nasal bones	inml-snml/snmr-inmr	deg	8.6	3.5	6	21.6	3.71	9.3	0.20

Appendix 2 Measurements for the Experimental Standards and the Patients with Crouzon Syndrome:

Six Years of Age (continued):

			6 Year Standard			Patient LW		Patient AY	
Anatomical Unit	**Definition**	**unit**	**mean**	**sd**	**n**	**Value**	**Z**	**Value**	**Z**
FRONTAL									
Distances									
Supra-orbital									
L fronto-nasal suture	n-snml	mms	5.9	1.5	6	3.5	-1.60	7.6	1.13
L fronto-maxillary suture	snml-morl	mms	6.7	1.1	6	15.7	8.18	10.6	3.55
L superior medial orbital rim	morl-sorl	mms	16.3	1.3	6	19.5	2.46	16.3	0.00
L superior lateral orbital rim	sorl-slorl	mms	26.5	2.2	6	27.8	0.59	30.6	1.86
L fronto-zygomatic suture (anterior)	slorl-zfl	mms	7.3	0.9	6	10.7	3.78	10.8	3.89
L fronto-zygomatic suture (lateral)	zfl-zfsl	mms	7.9	1.9	6	7.7	-0.11	7.3	-0.32
L fronto-zygomatic suture (medial)	zfsl-slorl	mms	11.3	1.5	6	13.9	1.73	13.0	1.13
R fronto-nasal suture	n-snmr	mms	5.9	0.7	6	3.7	-3.14	9.6	5.29
R fronto-maxillary suture	snmr-morr	mms	7.3	1.5	6	13.3	4.00	7.8	0.33
R superior medial orbital rim	morr-sorr	mms	17.9	1.0	6	24.7	6.80	17.3	-0.60
R superior lateral orbital rim	sorr-slorr	mms	27.3	1.8	6	22.2	-2.83	29.3	1.11
R fronto-zygomatic suture (anterior)	slorr-zfr	mms	6.8	0.8	6	8.9	2.62	11.0	5.25
R fronto-zygomatic suture (lateral)	zfr-zfsr	mms	8.3	1.3	6	9.0	0.54	8.7	0.31
R fronto-zygomatic suture (medial)	zfsr-slorr	mms	11.3	1.4	6	13.9	1.86	13.0	1.21
Ethmoid									
Nasal root projection	n-fc	mms	11.6	1.5	6	8.2	-2.27	13.2	1.07
L fronto-ethmoid attachment (anterior)	fc-cpal	mms	7.2	1.4	6	6.5	-0.50	7.3	0.07
L fronto-ethmoid attachment (cribriform)	cpal-cppl	mms	21.0	3.0	6	27.0	2.00	26.0	1.67
L fronto-ethmoid attachment (posterior)	cppl-ofaml	mms	11.2	2.5	6	6.1	-2.04	6.9	-1.72
L fronto-ethmoid attachment (orbital)	morl-ofaml	mms	35.6	2.5	6	28.5	-2.84	33.2	-0.96
R fronto-ethmoid attachment (anterior)	fc-cpar	mms	7.0	1.3	6	6.2	-0.62	7.7	0.54
R fronto-ethmoid attachment (cribriform)	cpar-cppr	mms	22.3	2.5	6	27.8	2.20	25.8	1.40
R fronto-ethmoid attachment (posterior)	cppr-ofamr	mms	9.5	2.0	6	5.9	-1.80	7.0	-1.25
R fronto-ethmoid attachment (orbital)	morr-ofamr	mms	35.2	3.4	6	29.3	-1.74	35.3	0.03
Sphenoid									
L superior orbital fissure	ofaml-sobfl	mms	12.9	1.7	6	6.4	-3.82	7.6	-3.12
L fronto-sphenoid suture (orbital)	sobfl-zfsl	mms	19.5	4.6	6	24.9	1.17	26.0	1.41
L lesser wing length	spal-cppl	mms	28.3	2.5	6	33.1	1.92	21.3	-2.80
R superior orbital fissure	ofamr-sobfr	mms	11.8	3.6	6	6.0	-1.61	11.1	-0.19
R fronto-sphenoid suture (orbital)	sobfr-zfsr	mms	22.2	6.1	6	25.7	0.57	20.2	-0.33
R lesser wing length	spar-cppr		30.7	2.5	6	37.0	2.52	24.9	-2.32
Dimensions									
Glabellar height	g-n	mms	9.3	0.9	6	9.4	0.11	5.2	-4.56
Glabellar prominence	s-g	mms	62.5	4.6	6	64.8	0.50	64.1	0.35
L anterior cranial fossa depth	sorl-spal	mms	40.4	3.3	6	43.2	0.85	40.0	-0.12
R anterior cranial fossa depth	sorr-spar	mms	40.3	2.0	6	38.9	-0.70	40.1	-0.10
Anterior superior orbital width	sorl-sorr	mms	40.3	3.2	6	60.7	6.38	48.1	2.44
Anterior supero-lateral orbital width	slorl-slorr	mms	82.3	4.5	6	94.1	2.62	93.0	2.38
Posterior width	spal-spar	mms	66.6	4.4	6	77.6	2.50	63.4	-0.73

Appendix 2 Measurements for the Experimental Standards and the Patients with Crouzon Syndrome:

Six Years of Age (continued):

			6 Year Standard			Patient LW		Patient AY	
Anatomical Unit	**Definition**	**unit**	**mean**	**sd**	**n**	**Value**	**Z**	**Value**	**Z**
ZYGOMATIC BONE									
Distances									
L zygo-maxillary suture (orbital)	orl-iobfl	mms	16.5	2.5	6	17.0	0.20	15.6	-0.36
L inferior orbital fissure (ant height)	iobfl-gwll	mms	7.2	2.2	6	6.8	-0.18	5.8	-0.64
L spheno-zygomatic suture	zfsl-gwll	mms	15.6	2.1	6	11.3	-2.05	15.4	-0.10
L fronto-zygomatic suture (medial)	zfsl-slorl	mms	11.3	1.5	6	13.9	1.73	13.0	1.13
L fronto-zygomatic suture (anterior)	slorl-zfl	mms	7.3	0.9	6	10.7	3.78	10.8	3.89
L fronto-zygomatic suture (lateral)	zfl-zfsl	mms	7.9	1.9	6	7.7	-0.11	7.3	-0.32
L infero-lateral orbital rim	orl ilorl	mms	13.1	1.7	6	13.2	0.06	12.7	-0.24
L infero-lateral orbital rim	ilorl-lorl	mms	11.3	1.7	6	9.3	-1.18	8.9	-1.41
L lateral orbital rim	lorl-slorl	mms	4.8	1.5	6	10.8	4.00	4.7	-0.07
L lateral frontal process	zfl-ztl	mms	18.5	1.6	6	15.3	-2.00	17.0	-0.94
L zygomatico-temporal suture	ztl-parl	mms	19.4	2.6	6	18.9	-0.19	25.3	2.27
L inferior arch	parl-zmil	mms	28.0	3.5	6	26.2	-0.51	27.8	-0.06
L zygo-maxillary suture	zmil-orl	mms	21.9	1.5	6	17.3	-3.07	22.3	0.27
R zygo-maxillary suture (orbital)	orr-iobfr	mms	16.2	2.7	6	17.9	0.63	13.9	-0.85
R inferior orbital fissure (ant height)	iobfr-gwlr	mms	7.0	2.2	6	7.2	0.09	6.6	-0.18
R spheno-zygomatic suture	gwlr-zfsr	mms	14.9	2.3	6	10.9	-1.74	13.4	-0.65
R fronto-zygomatic suture (medial)	zfsr-slorr	mms	11.3	1.4	6	13.9	1.86	13.0	1.21
R fronto-zygomatic suture (anterior)	slorr-zfr	mms	6.8	0.8	6	8.9	2.62	11.0	5.25
R fronto-zygomatic suture (lateral)	zfr-zfsr	mms	8.3	1.3	6	9.0	0.54	8.7	0.31
R infero-lateral orbital rim	orr-ilorr	mms	11.6	0.8	6	10.0	-2.00	9.9	-2.13
R infero-lateral orbital rim	ilorr-lorr	mms	12.3	1.7	6	10.1	-1.29	10.7	-0.94
R lateral orbital rim	lorr-slorr	mms	4.6	1.7	6	10.6	3.53	4.1	-0.29
R lateral frontal process	zfr-ztr	mms	17.9	2.8	6	13.5	-1.57	16.6	-0.46
R zygomatico-temporal suture	ztr-parr	mms	20.5	4.2	6	20.3	-0.05	23.2	0.64
R inferior arch	parr-zmir	mms	29.1	5.0	6	28.5	-0.12	25.7	-0.68
R zygo-maxillary suture	zmir-orr	mms	20.9	1.9	6	17.7	-1.68	23.5	1.37
Dimensions									
L zygomatic height	slorl-zmil	mms	33.8	2.7	6	35.6	0.67	32.8	-0.37
R zygomatic height	slorr-zmir	mms	86.2	4.7	6	92.0	1.23	93.3	1.51
L zygomatic length	parl-orl	mms	40.7	2.8	6	39.1	-0.57	46.1	1.93
R zygomatic length	parr-orr	mms	41.4	4.5	6	40.8	-0.13	43.7	0.51
L zygomatic lateral depth	gwll-ilorl	mms	15.2	1.4	6	16.0	0.57	17.8	1.86
L zygomatic lateral depth	gwlr-ilorr	mms	16.3	1.4	6	18.1	1.29	18.1	1.29
VOMER									
Distances									
Palatal length	ans-pns	mms	36.9	1.6	6	44.1	4.50	39.8	1.81
Posterior choanal height	pns-h	mms	19.1	2.8	6	16.8	-0.82	14.0	-1.82
Spheno-vomerine junction	h-ves	mms	17.0	3.2	6	22.1	1.59	13.4	-1.13
Ethmoid-vomerine junction	ves-vet	mms	12.6	4.4	6	14.9	0.52	13.9	0.30
Septal attachment	vet-ans	mms	32.0	4.7	6	30.8	-0.26	25.0	-1.49
Dimension and Angle									
Vomerine length	h-ans	mms	51.9	5.2	6	58.3	1.23	47.9	-0.77
Vomerine angle	s-n/h-ans	deg	23.4	1.3	6	20.2	-2.46	20.2	-2.46

Appendix 2 Measurements for the Experimental Standards and the Patients with Crouzon Syndrome:

Six Years of Age (continued):

			6 Year Standard			Patient LW		Patient AY	
Anatomical Unit	**Definition**	**unit**	**mean**	**sd**	**n**	**Value**	**Z**	**Value**	**Z**
ETHMOID									
Lateral Plate									
Distances									
L anterior border lateral plate	nlil-morl	mms	14.3	1.6	6	8.3	-3.75	9.7	-2.88
L frontal ethmoid attachment (orbital)	morl-ofaml	mms	35.6	2.5	6	28.5	-2.84	33.2	-0.96
L posterior border lateral plate	ofaml-msl	mms	11.6	1.5	6	10.0	-1.07	4.8	-4.53
L inferior border lateral plate	msl-nlil	mms	28.0	1.5	6	31.0	2.00	27.1	-0.60
R anterior border lateral plate	nlir-morr	mms	14.1	1.8	6	9.3	-2.67	9.5	-2.56
R frontal ethmoid attachment (orbital)	morr-ofamr	mms	35.2	3.4	6	29.3	-1.74	35.3	0.03
R posterior border lateral plate	ofamr-msr	mms	12.9	1.7	6	6.8	-3.59	4.8	-4.76
R inferior border lateral plate	msr-nlir	mms	27.5	2.4	6	31.0	1.46	27.9	0.17
L frontal ethmoid attachment (anterior)	morl-cpal	mms	9.7	2.0	6	11.9	1.10	8.4	-0.65
L frontal ethmoid attachment (posterior)	cppl-ofaml	mms	11.2	2.5	6	6.1	-2.04	6.9	-1.72
R frontal ethmoid attachment (anterior)	morr-cpar	mms	9.0	1.3	6	11.5	1.92	11.1	1.62
R frontal ethmoid attachment (posterior)	cppr-ofamr	mms	9.5	2.0	6	5.9	-1.80	7.0	-1.25
Dimensions									
Posterior inferior width	msl-msr	mms	31.0	2.9	6	27.1	-1.34	25.7	-1.83
Anterior inferior width	nlil-nlir	mms	29.0	3.9	6	29.7	0.18	27.3	-0.44
Anterior superior width	morl-morr	mms	18.5	2.4	6	24.9	2.67	23.7	2.17
Posterior superior width	ofaml-ofamr	mms	20.6	1.5	6	28.2	5.07	26.5	3.93
Ant lateral projection of lateral plate	nlil-morl/morr-nlir	deg	39.6	8.1	6	31.3	-1.02	24.3	-1.89
Post lateral projection of lateral plate	msl-ofaml/ofamr-msr	deg	53.8	14.3	6	8.7	-3.15	9.7	-3.08
Cribriform Plate									
Distances									
L anterior cribriform plate	fc-cpal	mms	7.2	1.4	6	6.5	-0.50	7.3	0.07
L lateral cribriform plate	cpal-cppl	mms	21.0	3.0	6	27.0	2.00	26.0	1.67
L posterior cribriform plate	es-cppl	mms	6.2	0.9	6	9.3	3.44	10.7	5.00
R anterior cribriform plate	fc-cpar	mms	7.0	1.3	6	6.2	-0.62	7.7	0.54
R lateral cribriform plate	cpar-cppr	mms	22.3	2.5	6	27.8	2.20	25.8	1.40
R posterior cribriform plate	es-cppr	mms	6.1	1.1	6	8.7	2.36	8.2	1.91
Angles									
L angle lateral cribriform plate cf SN	s-n/cpal-cppl	deg	5.6	3.2	6	11.1	1.72	7.8	0.69
R angle lateral cribriform plate cf SN	s-n/cpar-cppr	deg	3.5	1.8	6	12.5	5.00	5.0	0.83
Medial angle of plate cf SN	n-s/es-fc	deg	9.5	3.7	6	2.7	-1.84	9.7	0.05
Medial Plate									
Distances									
Anterior height crista galli	fc-cg	mms	6.1	2.6	6	7.3	0.46	8.6	0.96
Posterior height crista galli	cg-es	mms	21.8	3.8	6	23.4	0.42	20.3	-0.39
Spheno-ethmoid medial plate junction	es-ves	mms	14.9	1.2	6	13.5	-1.17	14.4	-0.42
Ethmoid-vomerine junction	ves-vei	mms	12.6	4.4	6	14.9	0.52	13.9	0.30
Septal attachment	vei-n	mms	34.0	3.4	6	31.7	-0.68	34.8	0.24
Nasal projection	n-fc	mms	11.6	1.5	6	8.2	-2.27	13.2	1.07
Dimensions									
Maximum medial plate height	vei-cg	mms	30.8	2.7	6	27.2	-1.33	28.9	-0.70
Maximum medial plate length	n-es	mms	33.3	4.1	6	37.6	1.05	37.9	1.12

Appendix 2 Measurements for the Experimental Standards and the Patients with Crouzon Syndrome:

Six Years of Age (continued):

			6 Year Standard			Patient LW		Patient AY	
Anatomical Unit	Definition	unit	mean	sd	n	Value	Z	Value	Z
SPHENOID									
Lesser Wing									
Distances									
L medial wing	ofaml-acl	mms	11.8	0.9	6	18.1	7.00	13.7	2.11
L lateral wing (posterior)	acl-spal	mms	29.2	2.0	6	33.6	2.20	24.7	-2.25
L lateral wing (anterior)	spal-es	mms	34.6	2.7	6	41.3	2.48	31.9	-1.00
R medial wing	ofamr-acr	mms	11.7	1.2	6	16.4	3.92	13.2	1.25
R lateral wing (posterior)	acr-spar	mms	28.5	3.5	6	37.0	2.43	24.8	-1.06
R lateral wing (anterior)	spar-es	mms	36.3	3.1	6	44.1	2.52	32.4	-1.26
Dimensions									
Maximum lesser wing width	spal-spar	mms	65.8	4.7	6	79.2	2.85	62.3	-0.74
Lesser wing superior angle	spal-es -spar	deg	139.1	9.2	6	135.8	-0.36	150.9	1.28
L lateral projection (anterior angle)	n-s/acl-spal	deg	54.5	5.2	6	74.1	3.77	49.3	-1.00
R lateral projection (anterior angle)	n-s/acr-spar	deg	56.0	4.5	6	71.9	3.53	52.2	-0.84
Pterygoid Plate									
Distances									
L medial pterygoid plate	ptsl-hpl	mms	23.5	2.2	6	21.2	-1.05	27.9	2.00
L medial hamular notch	hpl-hnl	mms	3.6	0.9	6	4.4	0.89	5.3	1.89
L lateral hamular notch	hnl-ptll	mms	9.4	2.4	6	9.9	0.21	8.9	-0.21
L lateral pterygoid plate	ptll-fool	mms	19.3	0.8	6	18.6	-0.87	20.1	1.00
R medial pterygoid plate	ptsr-hpr	mms	23.1	1.1	6	21.7	-1.27	23.2	0.09
R medial hamular notch	hpr-hnr	mms	4.0	0.6	6	3.0	-1.67	4.0	0.00
R lateral hamular notch	hnr-ptlr	mms	9.2	1.6	6	9.4	0.12	9.9	0.44
R lateral pterygoid plate	ptlr-foor	mms	20.1	2.0	6	17.8	-1.15	19.3	-0.40
Angles									
L pterygoid axis	n-s/ptsl-hpl	deg	60.3	4.1	6	52.4	-1.93	57.2	-0.76
R pterygoid axis	n-s/ptsr-hpr	deg	59.1	2.9	6	47.5	-4.00	60.1	0.34
Greater Wing									
Distances									
Lateral									
L anterior middle cranial fossa	fosl-gwll	mms	36.0	2.9	6	36.4	0.14	39.8	1.31
L spheno-zygomatic suture	zfsl-gwll	mms	15.6	2.1	6	11.3	-2.05	15.4	-0.10
R anterior middle cranial fossa	fosr-gwlr	mms	34.3	4.2	6	37.7	0.81	37.4	0.74
R spheno-zygomatic suture	gwlr-zfsr	mms	14.9	2.3	6	10.9	-1.74	13.4	-0.65
Orbital									
L inferior lateral orbital length	gwll-gwml	mms	26.4	3.0	6	23.5	-0.97	25.2	-0.40
L superior orbital fissure height	gwml-sobfl	mms	17.5	2.2	6	12.0	-2.50	13.4	-1.86
L spheno-frontal suture (orbital)	sobfl-zfsl	mms	19.5	4.6	6	24.9	1.17	26.0	1.41
R inferior lateral orbital length	gwlr-gwmr	mms	26.1	1.8	6	23.9	-1.22	25.4	-0.39
R superior orbital fissure height	gwmr-sobfr	mms	15.9	3.2	6	10.1	-1.81	15.7	-0.06
R spheno-frontal suture (orbital)	sobfr-zfsr	mms	22.2	6.1	6	25.7	0.57	20.2	-0.33
Posterior									
L spheno-petrous temporal suture (inf)	fosl-ptsl	mms	14.0	0.7	6	14.9	1.29	13.2	-1.14
R spheno-petrous temporal suture (inf)	fosr-ptsr	mms	14.0	1.2	6	16.0	1.67	17.0	2.50
L posterior middle cranial fossa	fosl-petal	mms	18.9	1.1	6	24.4	5.00	24.6	5.18
R posterior middle cranial fossa	fosr-petar	mms	37.0	2.3	6	40.2	1.39	41.1	1.78

Appendix 2 Measurements for the Experimental Standards and the Patients with Crouzon Syndrome:

Six Years of Age (continued):

			6 Year Standard			Patient LW		Patient AY	
Anatomical Unit	**Definition**	**unit**	**mean**	**sd**	**n**	**Value**	**Z**	**Value**	**Z**
SPHENOID (continued)									
Dimensions and Angles									
Posterior sphenoid width	fosl-fosr	mms	49.8	3.3	6	51.2	0.42	53.8	1.21
L angle of greater wing splay	zfsl-gwml-ptsl	deg	134.6	6.9	6	115.6	-2.75	110.3	-3.52
R angle of greater wing splay	zfsr-gwmr-ptsr	deg	132.9	6.4	6	115.7	-2.69	113.6	-3.02
Total angle of protrusion	zfsl-gwml/gwmr-zfsr	deg	90.8	4.7	6	129.7	8.28	120.3	6.28
Inferior greater wing protrusion	gwll-gwml/gwmr-gwlr	deg	94.2	4.5	6	131.8	8.36	112.1	3.98
Posterior angle of greater wing	fosl-petal/petar-fosr	deg	95.6	10.7	6	80.7	-1.39	86.8	-0.82
Squamous Sphenoid									
L squamous spheno-frontal suture	zfsl-spcl	mms	24.1	7.0	6				
L squamous spheno-parietal suture	spcl-sptl	mms	10.1	2.5	6				
L lateral spheno-temporal suture	fosl-sptl	mms	49.8	2.2	6				
R squamous spheno-frontal suture	zfsr-spcr	mms	20.3	6.6	6				
R squamous spheno-parietal suture	spcr-sptr	mms	8.4	3.0	6				
R lateral spheno-temporal suture	fosr-sptr	mms	47.3	3.7	6				
Sphenoid Body									
Distances									
Lateral/Posterior Body									
L anterior inferior length	gwml-ptsl	mms	15.9	1.7	6	20.4	2.65	21.1	3.06
L spheno-occipital synchondrosis (lat)	ptsl-petal	mms	12.8	1.4	6	18.5	4.07	17.5	3.36
L posterior clinoid height	petal-pcl	mms	9.5	1.9	6	12.8	1.74	12.3	1.47
Posterior clinoid width	pcl-pcr	mms	14.2	2.9	6	15.0	0.28	12.4	-0.62
R anterior inferior length	gwmr-ptsr	mms	16.9	2.0	6	21.3	2.20	20.3	1.70
R spheno-occipital synchondrosis (lat)	ptsr-petar	mms	13.3	1.5	6	18.0	3.13	16.5	2.13
R posterior clinoid height	petar-pcr	mms	9.1	3.1	6	13.0	1.26	10.9	0.58
Anterior Body									
L spheno-ethmoid suture	es-cppl	mms	6.2	0.9	6	9.3	3.44	10.7	5.00
L anterior lateral distance	cppl-ofaml	mms	11.2	2.5	6	6.1	-2.04	6.9	-1.72
L anterior superior length	ofaml-gwml	mms	8.8	1.3	6	12.6	2.92	8.8	0.00
R spheno-ethmoid suture	es-cppr	mms	6.1	1.1	6	8.7	2.36	8.2	1.91
R anterior lateral distance	cppr-ofamr	mms	9.5	2.0	6	5.9	-1.80	7.0	-1.25
R anterior superior length	ofamr-gwmr	mms	9.2	1.3	6	10.9	1.31	7.6	-1.23
Sella									
L lateral anterior body	cppl-ofpml	mms	13.6	1.5	6	15.5	1.27	8.9	-3.13
L lateral sella length	ofpml-petal	mms	20.3	1.4	6	21.7	1.00	25.1	3.43
R lateral anterior body	cppr-ofpmr	mms	12.8	2.2	6	11.7	-0.50	7.4	-2.45
R lateral sella length	ofpmr-petar	mms	21.4	2.7	6	23.6	0.81	25.1	1.37
Base/Floor Body									
Spheno-ethmoid medial plate junction	es-ves	mms	14.9	1.2	6	13.5	-1.17	14.4	-0.42
Spheno-vomerine junction	ves-h	mms	17.0	3.2	6	22.1	1.59	13.4	-1.13
L posterior width	h-ptsl	mms	14.8	2.4	6	15.0	0.08	22.5	3.21
R posterior width	h-ptsr	mms	13.6	3.3	6	13.9	0.09	16.1	0.76

Appendix 2 Measurements for the Experimental Standards and the Patients with Crouzon Syndrome:

Six Years of Age (continued):

			6 Year Standard			Patient LW		Patient AY	
Anatomical Unit	**Definition**	**unit**	**mean**	**sd**	**n**	**Value**	**Z**	**Value**	**Z**
SPHENOID (continued)									
Dimensions									
Anterior inferior body width	gwml-gwmr	mms	25.0	1.7	6	25.7	0.41	26.6	0.94
Spheno-occipital synchondrosis (inf)	ptsl-ptsr	mms	24.4	1.9	6	24.5	0.05	30.1	3.00
Anterior superior body width	ofaml-ofamr	mms	20.6	1.5	6	28.2	5.07	26.5	3.93
Spheno-occipital synchondrosis (sup)	petal-petar	mms	21.3	1.8	6	20.3	-0.56	20.9	-0.22
L posterior body height	pcl-ptsl	mms	18.1	3.6	6	28.0	2.75	25.9	2.17
R posterior body height	pcr-ptsr	mms	20.1	4.4	6	27.8	1.75	23.3	0.73
L anterior body height	acl-gwml	mms	10.8	1.1	6	12.6	1.64	10.7	-0.09
L anterior body height	acr-gwmr	mms	11.5	1.0	6	11.2	-0.30	10.9	-0.60
Angles									
Body floor angle	es-ves-h	deg	127.6	6.0	6	114.8	-2.13	129.4	0.30
L lower body angle	s-n/gwml-ptsl	deg	37.2	4.6	6	39.5	0.50	31.2	-1.30
R lower body angle	s-n/gwmr-ptsr	deg	157.9	2.3	6	160.5	1.13	158.1	0.09
L upper body angle	s-n/ofpml-petal	deg	24.3	5.6	6	23.7	-0.11	8.2	-2.87
R upper body angle	s-n/ofpmr-petar	deg	22.9	2.3	6	23.3	0.17	14.0	-3.87
TEMPORAL									
Distances									
Squamous									
L lateral spheno-temporal suture	fosl-sptl	mms	49.8	2.2	6				
L temporo-parietal suture	sptl-asl	mms	76.9	7.0	6				
L occipital mastoid height	asl-mal	mms	37.7	3.5	6				
L medial mastoid prominence	mal-smfl	mms	11.5	1.3	6	15.7	3.23	16.2	3.62
R lateral spheno-temporal suture	fosr-sptr	mms	47.3	3.7	6				
R temporo-parietal suture	sptr-asr	mms	76.6	4.6	6				
R occipital mastoid height	asr-mar	mms	38.6	2.8	6				
R medial mastoid prominence	mar-smfr	mms	11.6	0.8	6	11.4	-0.25	13.0	1.75
External Auditory Meatus (EAM)									
L lateral mastoid prominence	mal-eamil	mms	16.0	3.1	6	23.2	2.32	18.1	0.68
L inferior-posterior EAM rim	eamil-eampl	mms	6.6	2.6	6	7.8	0.46	10.8	1.62
L posterior-superior EAM rim	eampl-pol	mms	6.2	1.8	6	5.5	-0.39	10.0	2.11
L superior-anterior EAM rim	pol-eamal	mms	5.6	1.0	6	4.1	-1.50	9.8	4.20
L anterior-inferior EAM rim	eamal-eamil	mms	6.2	1.4	6	8.1	1.36	7.4	0.86
R lateral mastoid prominence	mar-eamir	mms	15.0	1.1	6	21.5	5.91	18.8	3.45
R inferior-posterior EAM rim	eamir-eampr	mms	8.0	2.5	6	8.0	0.00	11.0	1.20
R posterior-superior EAM rim	eampr-por	mms	7.4	1.8	6	5.7	-0.94	7.6	0.11
R superior-anterior EAM rim	por-eamar	mms	6.3	1.1	6	4.1	-2.00	11.2	4.45
R anterior-inferior EAM rim	eamar-eamir	mms	6.4	1.6	6	7.3	0.56	7.3	0.56

Appendix 2 Measurements for the Experimental Standards and the Patients with Crouzon Syndrome:

Six Years of Age (continued):

			6 Year Standard			Patient LW		Patient AY	
Anatomical Unit	**Definition**	**unit**	**mean**	**sd**	**n**	**Value**	**Z**	**Value**	**Z**
TEMPORAL (continued)									
Zygoma									
L EAM-articular fossa length	eamal-afl	mms	10.5	2.9	6	13.0	0.86	13.7	1.10
L articular fossa height	afl-ael	mms	7.2	1.3	6	8.4	0.92	8.3	0.85
L inferior arch length	ael-parl	mms	13.8	3.3	6	9.7	-1.24	8.4	-1.64
L zygomatico-temporal suture	parl-ztl	mms	19.4	2.6	6	18.9	-0.19	25.3	2.27
L superior arch length	ztl-aul	mms	34.6	3.4	6	25.6	-2.65	34.7	0.03
R EAM-articular fossa length	eamar-afr	mms	11.5	2.2	6	14.8	1.50	14.0	1.14
R articular fossa height	afr-aer	mms	6.7	1.7	6	6.9	0.12	6.4	-0.18
R inferior arch length	aer-parr	mms	12.5	4.6	6	8.4	-0.89	7.2	-1.15
R zygomatico-temporal suture	parr-ztr	mms	20.5	4.2	6	20.3	-0.05	23.2	0.64
R superior arch length	ztr-aur	mms	32.8	3.9	6	27.5	-1.36	30.4	-0.62
Petrous									
L spheno-petrous temporal suture (sup)	fisl-petal	mms	16.8	1.5	6	19.5	1.80	21.1	2.87
L post-med temporo-occipital suture	petal-jfpl	mms	29.3	2.6	6	30.3	0.38	34.1	1.85
L lateral temporo-occipital suture	jfpl-asil	mms	44.1	4.8	6				
L petrous superior margin	asil-petal	mms	61.1	4.3	6				
R spheno-petrous temporal suture (sup)	fisr-petar	mms	18.1	0.9	6	20.2	2.33	19.7	1.78
R post-med temporo-occipital suture	petar-jfpr	mms	31.7	2.2	6	28.8	-1.32	33.3	0.73
R lateral temporo-occipital suture	jfpr-asir	mms	42.7	3.7	6				
R petrous superior margin	asir-petar	mms	61.6	2.0	6				
L occipital mastoid suture inferior	mal-jfll	mms	18.0	2.5	6	25.8	3.12	26.2	3.28
L jugular foramen width	jfll-jfml	mms	13.7	3.0	6	11.2	-0.83	8.4	-1.77
L medial temporo-occipital suture (inf)	jfml-ptsl	mms	19.4	1.8	6	25.2	3.22	24.0	2.56
L spheno-petrous temporal suture (inf)	fosl-ptsl	mms	14.0	0.7	6	14.9	1.29	13.2	-1.14
R occipital mastoid suture inferior	mar-jflr	mms	16.0	1.5	6	28.6	8.40	23.2	4.80
R jugular foramen width	jflr-jfmr	mms	14.1	2.9	6	3.4	-3.69	8.5	-1.93
R medial temporo-occipital suture (inf)	jfmr-ptsr	mms	20.6	3.3	6	25.9	1.61	25.6	1.52
R spheno-petrous temporal suture (inf)	fosr-ptsr	mms	14.0	1.2	6	16.0	1.67	17.0	2.50
Dimensions									
L petrous ridge length	petal-petpl	mms	53.7	2.7	6	64.9	4.15	60.8	2.63
R petrous ridge length	petar-petpr	mms	53.4	2.8	6	59.4	2.14	62.5	3.25
Inter-internal aud meatus dimension	iamr-iaml	mms	41.1	4.8	6	42.3	0.25	45.6	0.94
Inter-external aud meatus dimension	pol-por	mms	93.2	6.6	6	87.8	-0.82	108.1	2.26
Inter-post jugular foramen dimension	jfpr-jfpl	mms	48.4	6.2	6	51.2	0.45	47.6	-0.13
Inter-mastoid dimension	mal-mar	mms	86.0	6.7	6	85.6	-0.06	89.6	0.54
Angles									
Auditory canal angle	pol-iaml/iamr-por	deg	151.3	4.9	6	151.7	0.08	144.9	-1.31
Petrous ridge angle	petpl-petal/petar-petpr	deg	97.8	8.8	6	85.2	-1.43	88.7	-1.03
L zygoma projection angle	petal-aul-ztl	deg	88.9	4.5	6	91.7	0.62	84.9	-0.89
R zygoma projection angle	petar-aur-ztr	deg	90.4	3.1	6	96.0	1.81	88.9	-0.48

Appendix 2 Measurements for the Experimental Standards and the Patients with Crouzon Syndrome:

Six Years of Age (continued):

			6 Year Standard			Patient LW		Patient AY	
Anatomical Unit	Definition	unit	mean	sd	n	Value	Z	Value	Z
PARIETAL									
Distances									
Sagittal suture	l-br	mms	104.2	6.6	6				
L parietal frontal (coronal) suture	br-spcl	mms	89.3	5.0	6				
L spheno-parietal suture	spcl-sptl	mms	10.1	2.5	6				
L temporo-parietal suture	sptl-asl	mms	76.9	7.0	6				
L occipito-parietal (lambdoid) suture	asl-l	mms	82.4	5.8	6				
R parietal frontal (coronal) suture	br-spcr	mms	94.1	4.0	6				
R spheno-parietal suture	spcr-sptr	mms	8.4	3.0	6				
R temporo-parietal suture	sptr-asr	mms	76.6	4.6	6				
R occipito-parietal (lambdoid) suture	asr-l	mms	84.8	3.0	6				
OCCIPITAL									
Distances									
Lambdoid and Cranial Base									
L occipito-parietal (lambdoid) suture	l-asl	mms	82.4	5.8	6				
L lateral temporo-occipital suture (sup)	asl-jfll	mms	39.8	3.1	6				
L lateral jugular foramen	jfll-jfpl	mms	7.2	1.3	6	6.3	-0.69	2.6	-3.54
L medial jugular foramen	jfpl-jfml	mms	9.9	2.3	6	7.4	-1.09	6.0	-1.70
L medial temporo-occipital suture (inf)	jfml-ptsl	mms	19.4	1.8	6	25.2	3.22	24.0	2.56
R occipito-parietal (lambdoid) suture	l-asr	mms	84.8	3.0	6				
R lateral temporo-occipital suture (sup)	asr-jflr	mms	39.8	1.6	6				
R lateral jugular foramen	jflr-jfpr	mms	7.9	2.4	6	3.8	-1.71	4.2	-1.54
R medial jugular foramen	jfpr-jfmr	mms	10.9	2.7	6	6.5	-1.63	6.4	-1.67
R medial temporo-occipital suture (inf)	jfmr-ptsr	mms	20.6	3.3	6	25.9	1.61	25.6	1.52
Inferior spheno-occipital synchondrosis	ptsr-ptsl	mms	24.4	1.9	6	24.5	0.05	30.1	3.00
Foramen Magnum									
L anterior foramen magnum	ba-fmll	mms	20.0	2.1	6	20.4	0.19	22.5	1.19
L posterior foramen magnum	fmll-o	mms	24.0	4.5	6	27.5	0.78	24.5	0.11
R anterior foramen magnum	ba-fmlr	mms	20.6	2.3	6	22.5	0.83	22.0	0.61
R posterior foramen magnum	fmlr-o	mms	24.9	2.8	6	24.5	-0.14	24.1	-0.29
Dimensions									
Foramen Magnum									
Foramen magnum length	ba-o	mms	35.0	3.9	6	35.4	0.10	37.7	0.69
Foramen magnum width	fmll-fmlr	mms	27.0	3.6	6	30.2	0.89	25.8	-0.33
Posterior Cranial Fossa									
Posterior cranial fossa depth	o-iop	mms	42.3	5.4	6	36.0	-1.17	50.0	1.43
Posterior occipital height	iop-l	mms	58.2	10.0	6				
L posterior fossa length	petpl-iop	mms	68.2	7.9	6	57.9	-1.30	69.0	0.10
L posterior fossa length	petpr-iop	mms	60.6	4.7	6	60.0	-0.13	68.2	1.62

Appendix 2 Measurements for the Experimental Standards and the Patients with Crouzon Syndrome:

Six Years of Age (continued):

			6 Year Standard			Patient LW		Patient AY	
Anatomical Unit	**Definition**	**unit**	**mean**	**sd**	**n**	**Value**	**Z**	**Value**	**Z**
CRANIAL BASE SUTURES									
Anterior Cranial Fossa									
L spheno-ethmoid synchondrosis	es-cppl	mms	6.2	0.9	6	9.3	3.44	10.7	5.00
R spheno-ethmoid synchondrosis	es-cppr	mms	6.1	1.1	6	8.7	2.36	8.2	1.91
L spheno-frontal suture (ant fossa)	cppl-spal	mms	28.3	2.5	6	33.1	1.92	21.3	-2.80
R spheno-frontal suture (ant fossa)	cppr-spar	mms	30.7	2.5	6	37.0	2.52	24.9	-2.32
L spheno-frontal suture (orbital)	spal-zfsl	mms	16.7	3.0	6	20.5	1.27	17.4	0.23
R spheno-frontal suture (orbital)	spar-zfsr	mms	18.0	3.1	6	21.3	1.06	17.4	-0.19
L spheno-zygomatic suture	zfsl-gwll	mms	15.6	2.1	6	11.3	-2.05	15.4	-0.10
R spheno-zygomatic suture	zfsr-gwlr	mms	14.9	2.3	6	10.9	-1.74	13.4	-0.65
Middle Cranial Fossa									
L spheno-squamous temporal suture	gwll-fisl	mms	35.3	2.2	6	34.5	-0.36	37.9	1.18
R spheno-squamous temporal suture	gwlr-fisr	mms	34.7	2.7	6	35.4	0.26	36.4	0.63
L spheno-petrous temporal suture (sup)	fisl-petal	mms	16.8	1.5	6	19.5	1.80	21.1	2.87
R spheno-petrous temporal suture (sup)	fisr-petar	mms	18.1	0.9	6	20.2	2.33	19.7	1.78
L spheno-petrous temporal suture (inf)	fosl-ptsl	mms	14.0	0.7	6	14.9	1.29	13.2	-1.14
R spheno-petrous temporal suture (inf)	fosr-ptsr	mms	14.0	1.2	6	16.0	1.67	17.0	2.50
Posterior Cranial Fossa									
L medial temporo-occipital suture (sup)	petal-jfml	mms	20.1	2.4	6	24.3	1.75	29.3	3.83
R medial temporo-occipital suture (sup)	petar-jfmr	mms	20.5	2.9	6	23.7	1.10	27.4	2.38
L medial temporo-occipital suture (inf)	jfml-ptsl	mms	19.4	1.8	6	25.2	3.22	24.0	2.56
R medial temporo-occipital suture (inf)	jfmr-ptsr	mms	20.6	3.3	6	25.9	1.61	25.6	1.52
L occipital mastoid suture (superior)	jfll-petpl	mms	32.7	2.0	6	43.0	5.15	34.8	1.05
R occipital mastoid suture (superior)	jflr-petpr	mms	31.8	2.1	6	44.1	5.86	40.8	4.29
Spheno-occipital synchondrosis (sup)	petal-petar	mms	21.3	1.8	6	20.3	-0.56	20.9	-0.22
Spheno-occipital synchondrosis (inf)	ptsl-ptsr	mms	24.4	1.9	6	24.5	0.05	30.1	3.00
L spheno-occipital synchondrosis (lat)	ptsl-petal	mms	12.8	1.4	6	18.5	4.07	17.5	3.36
R spheno-occipital synchondrosis (lat)	ptsr-petar	mms	13.3	1.5	6	18.0	3.13	16.5	2.13
CRANIAL BASE									
Facial Heights									
Anterior facial height	n-gn	mms	85.8	5.7	6	106.0	3.54	104.7	3.32
L posterior facial height	s-gol	mms	59.8	4.3	6	73.2	3.12	64.5	1.09
R posterior facial height	s-gor	mms	62.2	4.4	6	71.5	2.11	65.9	0.84
Facial Angles									
SNA	s-n-ss	deg	81.0	3.9	6	78.9	-0.54	69.1	-3.05
SNB	s-n-sm	deg	75.1	4.2	6	72.4	-0.64	68.7	-1.52
Cranial Base Angle									
Cranial base angle	ba-s-n	deg	133.1	4.5	6	118.0	-3.36	124.3	-1.96
Cranial Base Dimensions									
Cranial base length	ba-n	mms	82.9	5.7	6	86.0	0.54	85.6	0.47
Clivus length (posterior cranial base)	ba-s	mms	30.6	4.0	6	38.6	2.00	34.8	1.05
Anterior cranial base length	s-n	mms	57.2	4.1	6	60.8	0.88	61.1	0.95

Appendix 2 Measurements for the Experimental Standards and the Patients with Crouzon Syndrome:

Adult:

			Adult Standard			Patient HC		Patient TS	
Anatomical Unit	Definition	unit	mean	sd	n	Value	Z	Value	Z
MANDIBLE									
Distances									
L anterior superior body	id-em1il	mms	34.7	1.8	6	38.5	2.11	36.7	1.11
L posterior superior body	em1il-cbl	mms	27.0	2.2	6	24.1	-1.32	28.5	0.68
L total superior body	id-cbl	mms	60.2	2.0	6	62.0	0.90	64.5	2.15
L anterior ramus	cbl-ctl	mms	36.8	4.1	6	29.2	-1.85	45.7	2.17
L anterior mandibular notch	ctl-mnl	mms	17.9	4.7	6	15.4	-0.53	21.1	0.68
L posterior mandibular notch	mnl-cdl	mms	19.4	2.8	6	16.0	-1.21	21.6	0.79
L posterior ramus	cdl-gol	mms	51.7	4.9	6	41.3	-2.12	61.0	1.90
L inferior body	gol-gn	mms	80.2	4.0	6	72.7	-1.88	88.6	2.10
R anterior superior body	id-em1ir	mms	34.8	2.0	6	37.9	1.55	34.8	0.00
R posterior superior body	em1ir-cbr	mms	25.4	2.9	6	23.8	-0.55	28.0	0.90
R total superior body	id-cbr	mms	58.1	2.3	6	60.1	0.87	61.8	1.61
R anterior ramus	cbr-ctr	mms	37.8	5.5	6	31.2	-1.20	41.8	0.73
R anterior mandibular notch	ctr-mnr	mms	19.0	4.7	6	14.4	-0.98	19.3	0.06
R posterior mandibular notch	mnr-cdr	mms	19.3	2.9	6	16.0	-1.14	18.3	-0.34
R posterior ramus	cdr-gor	mms	52.4	4.4	6	46.2	-1.41	60.4	1.82
R inferior body	gor-gn	mms	80.4	4.9	6	74.0	-1.31	85.5	1.04
Dimensions									
Intergonial dimension	gol-gor	mms	87.0	7.0	6	74.6	-1.77	105.4	2.63
Intercondylar dimension	cdl-cdr	mms	114.3	7.3	6	95.3	-2.60	110.7	-0.49
Intercoronoid base dimension	cbl-cbr	mms	77.3	1.8	6	72.5	-2.67	84.1	3.78
Intermolar dimension	em1il-em1ir	mms	53.7	1.8	6	53.4	-0.17	53.4	-0.17
L Superior ramus width	cdl-ctl	mms	30.6	2.6	6	25.9	-1.81	32.3	0.65
L inferior ramus width	gol-cbl	mms	31.3	3.5	6	30.8	-0.14	37.1	1.66
R superior ramus width	cdr-ctr	mms	30.8	2.8	6	26.3	-1.61	32.1	0.46
R inferior ramus width	gor-cbr	mms	31.9	3.1	6	31.0	-0.29	37.3	1.74
Anterior symphyseal height	gn-id	mms	27.0	2.5	6	33.0	2.40	41.5	5.80
L total mandibular length	gn-cdl	mms	116.4	6.2	6	105.5	-1.76	129.0	2.03
R total mandibular length	gn-cdr	mms	115.6	6.3	6	110.6	-0.79	121.3	0.90
Angles									
L mandibular notch angle	cdl-mnl-ctl	deg	103.3	7.5	6	110.7	0.99	98.5	-0.64
R mandibular notch angle	cdr-mnr-ctr	deg	109.3	7.7	6	120.1	1.40	117.2	1.03
L gonial angle	cdl-gol-gn	deg	117.8	4.3	6	133.5	3.65	118.0	0.05
R gonial angle	cdr-gor-gn	deg	117.1	4.5	6	132.7	3.47	111.3	-1.29
L coronoid base angle	ctl-cbl-id	deg	112.2	1.5	6	133.2	14.00	111.4	-0.53
R coronoid base angle	ctr-cbr-id	deg	114.1	3.7	6	131.8	4.78	106.8	-1.97
L coronoid-dental base angle	ctl-cbl-em1il	deg	118.3	5.4	6	136.2	3.31	119.4	0.20
R coronoid-dental base angle	ctr-cbr-em1ir	deg	116.7	5.5	6	137.7	3.82	108.9	-1.42
L symphyseal angle	gol-gn-id	deg	86.1	4.1	6	85.2	-0.22	81.8	-1.05
R symphyseal angle	gor-gn-id	deg	84.9	3.4	6	81.4	-1.03	84.1	-0.24
Anterior mandibular angle	gol-gn-gor	deg	65.7	2.8	6	61.1	-1.64	74.5	3.14

Appendix 2 Measurements for the Experimental Standards and the Patients with Crouzon Syndrome:

Adult (continued):

			Adult Standard			Patient HC		Patient TS	
Anatomical Unit	**Definition**	**unit**	**mean**	**sd**	**n**	**Value**	**Z**	**Value**	**Z**
MAXILLA									
Distances									
Orbital Region									
L fronto-maxillary suture	snml-morl	mms	12.1	3.0	6	14.6	0.83	13.6	0.50
L frontal process orbital rim	nlil-morl	mms	15.7	2.6	6	10.4	-2.04	14.3	-0.54
L medial orbital floor	msl-nlil	mms	30.6	3.7	6	30.8	0.05	31.7	0.30
L posterior lateral orbital floor	msl-iobfl	mms	22.2	4.8	6	28.5	1.31	26.7	0.94
L anterior lateral orbital floor	orl-iobfl	mms	19.8	1.9	6	6.0	-7.26	15.0	-2.53
L maxillary infra-orbital rim	orl-nlil	mms	13.1	2.5	6	23.7	4.24	24.8	4.68
R fronto-maxillary suture	snmr-morr	mms	11.4	1.7	6	9.7	-1.00	12.1	0.41
R frontal process orbital rim	nlir-morr	mms	16.6	2.1	6	15.2	-0.67	11.0	-2.67
R medial orbital floor	msr-nlir	mms	32.4	3.6	6	30.4	-0.56	29.1	-0.92
R posterior lateral orbital floor	msr-iobfr	mms	21.9	3.4	6	31.0	2.68	25.2	0.97
R anterior lateral orbital floor	orr-iobfr	mms	18.9	2.0	6	2.6	-8.15	14.0	-2.45
R maxillary infra-orbital rim	orr-nlir	mms	13.5	3.2	6	20.3	2.10	28.8	4.80
Anterior Wall									
L anterior zygo-maxillary suture	zmil-orl	mms	25.5	4.5	6	20.9	-1.02	22.7	-0.62
L lateral maxillary wall	zmil-cm1sl	mms	25.0	5.1	6	22.3	-0.53	35.4	2.04
L anterior alveolar margin	cm1sl-pr	mms	39.0	2.0	6	32.2	-3.40	32.8	-3.10
L lower pyriform margin	ans-all	mms	17.0	1.5	6	16.0	-0.67	17.3	0.20
L upper pyriform margin	all-inml	mms	17.1	2.5	6	21.7	1.84	18.4	0.52
L naso-maxillary suture	inml-snml	mms	20.8	2.8	6	20.6	-0.07	26.8	2.14
R anterior zygo-maxillary suture	zmir-orr	mms	27.9	3.9	6	22.6	-1.36	22.4	-1.41
R lateral maxillary wall	zmir-em1sr	mms	25.4	5.4	6	24.9	-0.09	30.3	0.91
R anterior alveolar margin	cm1sr-pr	mms	37.7	1.8	6	30.5	-4.00	38.0	0.17
R lower pyriform margin	ans-alr	mms	16.5	1.1	6	15.7	-0.73	17.3	0.73
R upper pyriform margin	alr-inmr	mms	15.8	2.6	6	22.4	2.54	17.1	0.50
L naso-maxillary suture	inmr-snmr	mms	21.0	2.9	6	21.8	0.28	27.7	2.31
Anterior alveolar height	pr-ans	mms	14.2	2.8	6	19.3	1.82	23.6	3.36
Lateral Wall									
L posterior alveolar margin	cm1sl-mxtl	mms	23.0	2.0	6	20.9	-1.05	27.7	2.35
L posterior maxillary wall	mxtl-msl	mms	41.8	4.2	6	43.6	0.43	60.5	4.45
L posterior lateral orbital floor	msl-iobfl	mms	22.2	4.8	6	28.5	1.31	26.7	0.94
L posterior zygo-maxillary suture	iobfl-zmil	mms	23.0	2.3	6	22.7	-0.13	24.1	0.48
R posterior alveolar margin	cm1sr-mxtr	mms	23.9	2.5	6	18.5	-2.16	23.4	-0.20
R posterior maxillary wall	mxtr-msr	mms	42.6	3.3	6	47.3	1.42	62.1	5.91
R posterior lateral orbital floor	msr-iobfr	mms	21.9	3.4	6	31.0	2.68	25.2	0.97
R posterior zygo-maxillary suture	iobfr-zmir	mms	23.8	2.4	6	20.9	-1.21	25.0	0.50
Palate									
L posterior palatal height	cm1sl-gpfl	mms	25.3	1.4	6	21.3	-2.86	24.2	-0.79
L posterior palatal width	gpfl-pns	mms	16.5	1.7	6	15.9	-0.35	17.1	0.35
R posterior palatal height	cm1sr-gpfr	mms	27.1	1.4	6	20.9	-4.43	25.0	-1.50
R posterior palatal width	gpfr-pns	mms	16.8	1.8	6	15.9	-0.50	17.0	0.11
Superior palatal length	ans-pns	mms	46.9	4.6	6	43.0	-0.85	51.3	0.96

Appendix 2 Measurements for the Experimental Standards and the Patients with Crouzon Syndrome:

Adult (continued):

			Adult Standard			Patient HC		Patient TS	
Anatomical Unit	Definition	unit	mean	sd	n	Value	Z	Value	Z
MAXILLA (continued)									
Dimensions									
Anterior midline height	n-pr	mms	59.5	3.9	6	66.1	1.69	74.9	3.95
L lateral height	morl-em1sl	mms	54.5	3.2	6	59.2	1.47	69.0	4.53
R lateral height	morr-em1sr	mms	56.2	2.9	6	63.6	2.55	69.5	4.59
L posterior height	gpfl-msl	mms	33.4	3.3	6	35.3	0.58	45.8	3.76
R posterior height	gpfr-msr	mms	33.5	2.6	6	40.2	2.58	45.1	4.46
L superior length	msl-inml	mms	47.6	3.8	6	52.1	1.18	53.0	1.42
R superior length	msr-inmr	mms	47.3	3.3	6	49.5	0.67	50.1	0.85
Posterior palatal width	gpfl-gpfr	mms	31.2	2.7	6	30.2	-0.37	33.1	0.70
Anterior inter-canine width	ecsl-ecsr	mms	35.7	1.9	6	35.9	0.11	34.6	-0.58
Maximum maxillary width	zmil-zmir	mms	95.1	9.6	6	79.1	-1.67	99.0	0.41
Superior (inter-orbital rim) width	orl-orr	mms	65.8	2.8	6	64.8	-0.36	79.7	4.96
Nasal aperture height	na-ans	mms	30.8	2.7	6	29.5	-0.48	22.6	-3.04
Nasal aperture width	all-alr	mms	26.3	1.5	6	22.9	-2.27	24.4	-1.27
Angles									
L orbital floor angle	nlil-msl-iobfl	deg	53.0	10.4	6	43.3	-0.93	62.4	0.90
R orbital floor angle	nlir-msr-iobfr	deg	52.9	12.0	6	39.7	-1.10	72.9	1.67
L posterior inferior angle	msl-gpfl-em1sl	deg	117.5	6.8	6	127.8	1.51	118.9	0.21
R posterior inferior angle	msr-gpfr-em1sr	deg	116.7	8.1	6	115.8	-0.11	113.6	-0.38
Superior maxillary splay	iobfl-msl/msr-iobfr	deg	91.1	10.0	6	72.4	-1.87	103.5	1.24
L superior /occlusal angle	snml-msl/em1sl-pr	deg	33.8	4.1	6	46.8	3.17	29.3	-1.10
R superior /occlusal angle	snmr-msr/em1sr-pr	deg	34.4	3.3	6	37.0	0.79	35.2	0.24
L palatal/occlusal angle	ans-pns/em1sl-pr	deg	48.8	2.1	6	54.1	2.52	46.3	-1.19
R palatal/occlusal angle	ans-pns/em1sr-pr	deg	50.0	2.6	6	51.1	0.42	52.5	0.96
Anterior palatal angle	gpfl-ans-gpfr	deg	41.3	2.6	6	42.6	0.50	37.5	-1.46
Maxillary arch angle	gpfl-pr-gpfr	deg	37.9	2.2	6	44.8	3.14	41.9	1.82
NASAL BONES									
Distances									
Nasal length	na-n	mms	16.7	2.3	6	22.6	2.57	32.7	6.96
L inferior nasal width	na-inml	mms	11.1	2.2	6	6.9	-1.91	8.3	-1.27
L naso-maxillary suture	inml-snml	mms	20.8	2.8	6	20.6	-0.07	26.8	2.14
L fronto-nasal suture	n-snml	mms	6.8	1.8	6	6.2	-0.33	8.0	0.67
R inferior nasal width	na-inmr	mms	11.4	2.1	6	9.5	-0.90	8.6	-1.33
R naso-maxillary suture	inmr-snmr	mms	21.0	2.9	6	21.8	0.28	27.7	2.31
R fronto-nasal suture	n-snmr	mms	7.7	1.9	6	7.7	0.00	8.4	0.37
Dimensions									
Inferior width	inml-inmr	mms	16.3	2.5	6	11.7	-1.84	12.8	-1.40
Superior width	snml-snmr	mms	10.7	3.0	6	9.2	-0.50	11.0	0.10
Angles									
Nasal/anterior cranial base angle	s-n-na	deg	108.9	5.9	6	97.3	-1.97	87.9	-3.56
Superior nasal bone angle	snml-n-snmr	deg	101.6	20.5	6	81.5	-0.98	84.1	-0.85
Inferior nasal bone angle	inml-na-inmr	deg	88.4	8.9	6	89.8	0.16	98.5	1.13
Splay of nasal bones	inml-snml/snmr-inmr	deg	16.0	7.2	6	7.5	-1.18	4.0	-1.67

Appendix 2 Measurements for the Experimental Standards and the Patients with Crouzon Syndrome:

Adult (continued):

			Adult Standard			Patient HC		Patient TS	
Anatomical Unit	**Definition**	**unit**	**mean**	**sd**	**n**	**Value**	**Z**	**Value**	**Z**
FRONTAL									
Distances									
Supra-orbital									
L fronto-nasal suture	n-snml	mms	6.8	1.8	6	6.2	-0.33	8.0	0.67
L fronto-maxillary suture	snml-morl	mms	12.1	3.0	6	14.6	0.83	13.6	0.50
L superior medial orbital rim	morl-sorl	mms	19.4	2.7	6	24.3	1.81	18.1	-0.48
L superior lateral orbital rim	sorl-slorl	mms	29.8	1.5	6	31.8	1.33	41.4	7.73
L fronto-zygomatic suture (anterior)	slorl-zfl	mms	8.5	1.4	6	8.8	0.21	9.2	0.50
L fronto-zygomatic suture (lateral)	zfl-zfsl	mms	11.1	2.3	6	6.4	-2.04	8.0	-1.35
L fronto-zygomatic suture (medial)	zfsl-slorl	mms	12.5	3.8	6	6.5	-1.58	8.1	-1.16
R fronto-nasal suture	n-snmr	mms	7.7	1.9	6	7.7	0.00	8.4	0.37
R fronto-maxillary suture	snmr-morr	mms	11.4	1.7	6	9.7	-1.00	12.1	0.41
R superior medial orbital rim	morr-sorr	mms	20.3	2.0	6	24.7	2.20	22.7	1.20
R superior lateral orbital rim	sorr-slorr	mms	30.5	1.5	6	30.8	0.20	37.8	4.87
R fronto-zygomatic suture (anterior)	slorr-zfr	mms	8.3	1.1	6	9.7	1.27	9.3	0.91
R fronto-zygomatic suture (lateral)	zfr-zfsr	mms	10.8	2.7	6	8.3	-0.93	8.8	-0.74
R fronto-zygomatic suture (medial)	zfsr-slorr	mms	11.5	2.8	6	9.8	-0.61	9.0	-0.89
Ethmoid									
Nasal root projection	n-fc	mms	16.0	2.0	5	9.8	-3.10	18.7	1.35
L fronto-ethmoid attachment (anterior)	fc-cpal	mms	9.2	2.0	5	7.6	-0.80	16.1	3.45
L fronto-ethmoid attachment (cribriform)	cpal-cppl	mms	18.7	1.9	6	26.6	4.16	11.8	-3.63
L fronto-ethmoid attachment (posterior)	cppl-ofaml	mms	13.9	1.9	6	7.3	-3.47	19.9	3.16
L fronto-ethmoid attachment (orbital)	morl-ofaml	mms	37.9	0.9	6	29.0	-9.89	38.1	0.22
R fronto-ethmoid attachment (anterior)	fc-cpar	mms	8.9	1.3	5	6.3	-2.00	15.5	5.08
R fronto-ethmoid attachment (cribriform)	cpar-cppr	mms	16.5	2.9	6	25.9	3.24	10.3	-2.14
R fronto-ethmoid attachment (posterior)	cppr-ofamr	mms	14.9	1.7	6	8.3	-3.88	19.1	2.47
R fronto-ethmoid attachment (orbital)	morr-ofamr	mms	36.8	1.8	6	30.9	-3.28	35.3	-0.83
Sphenoid									
L superior orbital fissure	ofaml-sobfl	mms	12.1	3.3	6	6.1	-1.82	16.6	1.36
L fronto-sphenoid suture (orbital)	sobfl-zfsl	mms	26.2	3.3	6	31.3	1.55	25.6	-0.18
L lesser wing length	spal-cppl	mms	32.0	4.5	6	28.3	-0.82	36.3	0.96
R superior orbital fissure	ofamr-sobfr	mms	10.2	2.3	6	7.5	-1.17	14.4	1.83
R fronto-sphenoid suture (orbital)	sobfr-zfsr	mms	28.3	4.0	6	25.4	-0.72	25.5	-0.70
R lesser wing length	spar-cppr	mms	33.2	2.4	6	30.6	-1.08	38.7	2.29
Dimensions									
Glabellar height	g-n	mms	8.5	2.6	6	11.9	1.31	6.6	-0.73
Glabellar prominence	s-g	mms	71.0	3.9	6	68.8	-0.56	68.6	-0.62
L anterior cranial fossa depth	sorl-spal	mms	44.2	3.9	6	36.8	-1.90	43.7	-0.13
R anterior cranial fossa depth	sorr-spar	mms	45.3	2.8	6	34.5	-3.86	43.2	-0.75
Anterior superior orbital width	sorl-sorr	mms	47.8	2.3	6	58.0	4.43	48.9	0.48
Anterior supero-lateral orbital width	slorl-slorr	mms	96.2	2.3	6	98.2	0.87	113.3	7.43
Posterior width	spal-spar	mms	69.0	3.9	6	81.5	3.21	86.8	4.56

Appendix 2 Measurements for the Experimental Standards and the Patients with Crouzon Syndrome:

Adult (continued):

			Adult Standard			Patient HC		Patient TS	
Anatomical Unit	**Definition**	**unit**	**mean**	**sd**	**n**	**Value**	**Z**	**Value**	**Z**
ZYGOMATIC BONE									
Distances									
L zygo-maxillary suture (orbital)	orl-iobfl	mms	19.8	1.9	6	6.0	-7.26	15.0	-2.53
L inferior orbital fissure (ant height)	iobfl-gwll	mms	10.0	1.8	3	12.2	1.22	5.3	-2.61
L spheno-zygomatic suture	zfsl-gwll	mms	12.4	0.9	3	22.0	10.67	20.9	9.44
L fronto-zygomatic suture (medial)	zfsl-slorl	mms	12.5	3.8	6	6.5	-1.58	8.1	-1.16
L fronto-zygomatic suture (anterior)	slorl-zfl	mms	8.5	1.4	6	8.8	0.21	9.2	0.50
L fronto-zygomatic suture (lateral)	zfl-zfsl	mms	11.1	2.3	6	6.4	-2.04	8.0	-1.35
L infero-lateral orbital rim	orl-ilorl	mms	13.4	2.0	6	11.4	-1.00	11.3	-1.05
L infero-lateral orbital rim	ilorl-lorl	mms	13.5	2.6	6	10.9	-1.00	15.9	0.92
L lateral orbital rim	lorl-slorl	mms	7.8	3.3	6	5.8	-0.61	6.7	-0.33
L lateral frontal process	zfl-ztl	mms	23.9	1.9	6	21.1	-1.47	20.9	-1.58
L zygomatico-temporal suture	ztl-parl	mms	23.3	1.4	6	23.8	0.36	26.4	2.21
L inferior arch	parl-zmil	mms	37.2	1.5	6	29.6	-5.07	30.6	-4.40
L zygo-maxillary suture	zmil-orl	mms	25.5	4.5	6	20.9	-1.02	22.7	-0.62
R zygo-maxillary suture (orbital)	orr-iobfr	mms	18.9	2.0	6	2.6	-8.15	14.0	-2.45
R inferior orbital fissure (ant height)	iobfr-gwlr	mms	10.0	2.6	3	16.1	2.35	5.1	-1.88
R spheno-zygomatic suture	gwlr-zfsr	mms	14.5	1.5	3	19.3	3.20	19.7	3.47
R fronto-zygomatic suture (medial)	zfsr-slorr	mms	11.5	2.8	6	9.8	-0.61	9.0	-0.89
R fronto-zygomatic suture (anterior)	slorr-zfr	mms	8.3	1.1	6	9.7	1.27	9.3	0.91
R fronto-zygomatic suture (lateral)	zfr-zfsr	mms	10.8	2.7	6	8.3	-0.93	8.8	-0.74
R infero-lateral orbital rim	orr-ilorr	mms	11.5	2.5	6	10.9	-0.24	10.9	-0.24
R infero-lateral orbital rim	ilorr-lorr	mms	12.5	2.6	6	14.0	0.58	16.0	1.35
R lateral orbital rim	lorr-slorr	mms	6.9	3.3	6	7.2	0.09	5.8	-0.33
R lateral frontal process	zfr-ztr	mms	24.3	1.8	6	18.2	-3.39	20.3	-2.22
R zygomatico-temporal suture	ztr-parr	mms	22.7	2.5	6	26.4	1.48	27.0	1.72
R inferior arch	parr-zmir	mms	35.3	2.1	6	30.5	-2.29	31.5	-1.81
R zygo-maxillary suture	zmir-orr	mms	27.9	3.9	6	22.6	-1.36	22.4	-1.41
Dimensions									
L zygomatic height	slorl-zmil	mms	40.8	2.1	6	40.5	-0.14	44.0	1.52
R zygomatic height	slorr-zmir	mms	101.8	6.0	6	97.2	-0.77	114.9	2.18
L zygomatic length	parl-orl	mms	50.9	4.2	6	41.1	-2.33	43.0	-1.88
R zygomatic length	parr-orr	mms	49.2	3.3	6	45.4	-1.15	43.1	-1.85
L zygomatic lateral depth	gwll-ilorl	mms	16.4	1.6	3	10.6	-3.62	15.4	-0.62
L zygomatic lateral depth	gwlr-ilorr	mms	17.6	1.1	3	12.3	-4.82	17.4	-0.18
VOMER									
Distances									
Palatal length	ans-pns	mms	46.9	4.6	6	43.0	-0.85	51.3	0.96
Posterior choanal height	pns-h	mms	22.8	2.2	6	20.5	-1.05	20.2	-1.18
Spheno-vomerine junction	h-ves	mms	18.8	2.2	6	18.4	-0.18	13.8	-2.27
Ethmoid-vomerine junction	ves-vei	mms	20.9	6.4	6	5.6	-2.39	18.1	-0.44
Septal attachment	vei-ans	mms	33.3	6.6	6	34.7	0.21	34.2	0.14
Dimension and Angle									
Vomerine length	h-ans	mms	64.7	4.2	6	53.3	-2.71	60.8	-0.93
Vomerine angle	s-n/h-ans	deg	20.4	3.2	6	27.4	2.19	29.3	2.78

Appendix 2 Measurements for the Experimental Standards and the Patients with Crouzon Syndrome:

Adult (continued):

			Adult Standard			Patient HC		Patient TS	
Anatomical Unit	**Definition**	**unit**	**mean**	**sd**	**n**	**Value**	**Z**	**Value**	**Z**
ETHMOID									
Lateral Plate									
Distances									
L anterior border lateral plate	nlil-morl	mms	15.7	2.6	6	10.4	-2.04	14.3	-0.54
L frontal ethmoid attachment (orbital)	morl-ofaml	mms	37.9	0.9	6	29.0	-9.89	38.1	0.22
L posterior border lateral plate	ofaml-msl	mms	14.7	3.7	6	7.6	-1.92	5.7	-2.43
L inferior border lateral plate	msl-nlil	mms	30.6	3.7	6	30.8	0.05	31.7	0.30
R anterior border lateral plate	nlir-morr	mms	16.6	2.1	6	15.2	-0.67	11.0	-2.67
R frontal ethmoid attachment (orbital)	morr-ofamr	mms	36.8	1.8	6	30.9	-3.28	35.3	-0.83
R posterior border lateral plate	ofamr-msr	mms	12.6	2.9	6	6.0	-2.28	5.4	-2.48
R inferior border lateral plate	msr-nlir	mms	32.4	3.6	6	30.4	-0.56	29.1	-0.92
L frontal ethmoid attachment (anterior)	morl-cpal	mms	13.3	1.6	6	9.1	-2.62	12.9	-0.25
L frontal ethmoid attachment (posterior)	cppl-ofaml	mms	13.9	1.9	6	7.3	-3.47	19.9	3.16
R frontal ethmoid attachment (anterior)	morr-cpar	mms	12.7	2.0	6	8.5	-2.10	15.8	1.55
R frontal ethmoid attachment (posterior)	cppr-ofamr	mms	14.9	1.7	6	8.3	-3.88	19.1	2.47
Dimensions									
Posterior inferior width	msl-msr	mms	40.9	4.6	6	28.3	-2.74	40.7	-0.04
Anterior inferior width	nlil-nlir	mms	39.4	3.5	6	30.3	-2.60	36.3	-0.89
Anterior superior width	morl-morr	mms	23.5	1.3	6	24.2	0.54	28.9	4.15
Posterior superior width	ofaml-ofamr	mms	26.7	2.2	6	29.1	1.09	33.7	3.18
Ant lateral projection of lateral plate	nlil-morl/morr-nlir	deg	57.4	9.2	6	27.1	-3.29	33.9	-2.55
Post lateral projection of lateral plate	msl-ofaml/ofamr-msr	deg	53.6	11.8	6	15.5	-3.23	83.9	2.57
Cribriform Plate									
Distances									
L anterior cribriform plate	fc-cpal	mms	9.2	2.0	5	7.6	-0.80	16.1	3.45
L lateral cribriform plate	cpal-cppl	mms	18.7	1.9	6	26.6	4.16	11.8	-3.63
L posterior cribriform plate	es-cppl	mms	6.4	1.7	6	13.1	3.94	8.4	1.18
R anterior cribriform plate	fc-cpar	mms	8.9	1.3	5	6.3	-2.00	15.5	5.08
R lateral cribriform plate	cpar-cppr	mms	16.5	2.9	6	25.9	3.24	10.3	-2.14
R posterior cribriform plate	es-cppr	mms	7.1	1.8	6	12.8	3.17	8.3	0.67
Angles									
L angle lateral cribriform plate cf SN	s-n/cpal-cppl	deg	8.1	5.4	6	11.9	0.70	28.9	3.85
R angle lateral cribriform plate cf SN	s-n/cpar-cppr	deg	5.4	4.8	6	21.1	3.27	34.8	6.12
Medial angle of plate cf SN	n-s/es-fc	deg	19.2	3.3	5	3.6	-4.73	23.6	1.33
Medial Plate									
Distances									
Anterior height crista galli	fc-cg	mms	4.2	2.2	5	8.4	1.91	2.0	-1.00
Posterior height crista galli	cg-es	mms	21.8	2.0	6	20.1	-0.85	21.9	0.05
Spheno-ethmoid medial plate junction	es-ves	mms	21.8	1.6	6	21.7	-0.06	26.6	3.00
Ethmoid-vomerine junction	ves-vei	mms	20.9	6.4	6	5.6	-2.39	18.1	-0.44
Septal attachment	vei-n	mms	39.6	4.0	6	46.2	1.65	58.2	4.65
Nasal projection	n-fc	mms	16.0	2.0	5	9.8	-3.10	18.7	1.35
Dimensions									
Maximum medial plate height	vei-cg	mms	39.6	3.1	6	35.7	-1.26	53.7	4.55
Maximum medial plate length	n-es	mms	35.8	3.9	6	36.6	0.21	36.9	0.28

Appendix 2 Measurements for the Experimental Standards and the Patients with Crouzon Syndrome:

Adult (continued):

			Adult Standard			Patient HC		Patient TS	
Anatomical Unit	**Definition**	**unit**	**mean**	**sd**	**n**	**Value**	**Z**	**Value**	**Z**
SPHENOID									
Lesser Wing									
Distances									
L medial wing	ofaml-acl	mms	15.1	1.4	6	14.3	-0.57	9.7	-3.86
L lateral wing (posterior)	acl-spal	mms	28.5	2.6	6	34.3	2.23	39.3	4.15
L lateral wing (anterior)	spal-es	mms	36.5	3.9	6	40.8	1.10	44.0	1.92
R medial wing	ofamr-acr	mms	15.6	1.3	6	15.2	-0.31	11.7	-3.00
R lateral wing (posterior)	acr-spar	mms	29.0	2.0	6	37.9	4.45	30.1	0.55
R lateral wing (anterior)	spar-es	mms	38.8	2.2	6	43.3	2.05	44.7	2.68
Dimensions									
Maximum lesser wing width	spal-spar	mms	69.1	3.3	6	81.3	3.70	86.3	5.21
Lesser wing superior angle	spal-es -spar	deg	129.0	7.4	6	150.1	2.85	153.3	3.28
L lateral projection (anterior angle)	n-s/acl-spal	deg	54.1	8.3	6	59.2	0.61	51.7	-0.29
R lateral projection (anterior angle)	n-s/acr-spar	deg	56.8	5.6	6	56.2	-0.11	57.8	0.18
Pterygoid Plate									
Distances									
L medial pterygoid plate	ptsl-hpl	mms	30.6	3.3	6	26.1	-1.36	37.6	2.12
L medial hamular notch	hpl-hnl	mms	5.2	1.8	6	4.3	-0.50	6.4	0.67
L lateral hamular notch	hnl-ptll	mms	10.0	1.6	6	9.6	-0.25	13.2	2.00
L lateral pterygoid plate	ptll-fool	mms	26.0	2.3	6	20.0	-2.61	27.3	0.57
R medial pterygoid plate	ptsr-hpr	mms	30.4	2.2	6	26.3	-1.86	33.3	1.32
R medial hamular notch	hpr-hnr	mms	5.8	2.5	6	4.6	-0.48	4.6	-0.48
R lateral hamular notch	hnr-ptlr	mms	10.4	2.5	6	11.1	0.28	13.4	1.20
R lateral pterygoid plate	ptlr-foor	mms	24.3	2.4	6	20.6	-1.54	27.0	1.13
Angles									
L pterygoid axis	n-s/ptsl-hpl	deg	61.7	3.4	6	83.4	6.38	79.5	5.24
R pterygoid axis	n-s/ptsr-hpr	deg	60.6	3.1	6	86.5	8.03	79.9	6.23
Greater Wing									
Distances									
Lateral									
L anterior middle cranial fossa	fosl-gwll	mms	42.1	2.9	3	38.6	-1.21	45.4	1.14
L spheno-zygomatic suture	zfsl-gwll	mms	12.4	0.9	3	22.0	10.67	20.9	9.44
R anterior middle cranial fossa	fosr-gwlr	mms	39.6	2.1	3	38.1	-0.71	43.8	2.00
R spheno-zygomatic suture	gwlr-zfsr	mms	14.5	1.5	3	19.3	3.20	19.7	3.47
Orbital									
L inferior lateral orbital length	gwll-gwml	mms	30.5	2.7	3	28.3	-0.81	24.6	-2.19
L superior orbital fissure height	gwml-sobfl	mms	15.5	4.2	6	14.0	-0.36	15.7	0.05
L spheno-frontal suture (orbital)	sobfl-zfsl	mms	26.2	3.3	6	31.3	1.55	25.6	-0.18
R inferior lateral orbital length	gwlr-gwmr	mms	29.0	2.8	3	23.8	-1.86	25.0	-1.43
R superior orbital fissure height	gwmr-sobfr	mms	13.4	4.4	6	12.2	-0.27	18.8	1.23
R spheno-frontal suture (orbital)	sobfr-zfsr	mms	28.3	4.0	6	25.4	-0.72	25.5	-0.70
Posterior									
L spheno-petrous temporal suture (inf)	fosl-ptsl	mms	14.4	1.8	6	15.3	0.50	14.6	0.11
R spheno-petrous temporal suture (inf)	fosr-ptsr	mms	15.0	2.1	6	17.0	0.95	15.2	0.10
L posterior middle cranial fossa	fosl-petal	mms	22.5	1.0	6	25.9	3.40	26.3	3.80
R posterior middle cranial fossa	fosr-petar	mms	43.8	1.6	6	42.5	-0.81	41.9	-1.19

Appendix 2 Measurements for the Experimental Standards and the Patients with Crouzon Syndrome:

Adult (continued):

Anatomical Unit	Definition	unit	Adult Standard			Patient HC		Patient TS	
			mean	sd	n	Value	Z	Value	Z
SPHENOID (continued)									
Dimensions and Angles									
Posterior sphenoid width	fosl-fosr	mms	58.3	2.3	6	52.3	-2.61	57.1	-0.52
L angle of greater wing splay	zfsl-gwml-ptsl	deg	135.1	5.1	6	130.1	-0.98	140.3	1.02
R angle of greater wing splay	zfsr-gwmr-ptsr	deg	136.7	6.0	6	140.2	0.58	136.1	-0.10
Total angle of protrusion	zfsl-gwml/gwmr-zfsr	deg	89.1	5.5	6	105.5	3.16	106.5	3.35
Inferior greater wing protrusion	gwll-gwml/gwmr-gwlr	deg	87.6	3.4	3	121.0	9.82	122.5	10.26
Posterior angle of greater wing	fosl-petal/petar-fosr	deg	92.9	7.1	6	79.7	-1.86	94.1	0.28
Squamous Sphenoid									
L squamous spheno-frontal suture	zfsl-spcl	mms	27.6	6.4	5				
L squamous spheno-parietal suture	spcl-sptl	mms	11.5	2.3	5				
L lateral spheno-temporal suture	fosl-sptl	mms	52.2	2.6	5				
R squamous spheno-frontal suture	zfsr-spcr	mms	26.8	4.8	5				
R squamous spheno-parietal suture	spcr-sptr	mms	10.3	2.7	5				
R lateral spheno-temporal suture	fosr-sptr	mms	51.8	3.3	5				
Sphenoid Body									
Distances									
Lateral/Posterior Body									
L anterior inferior length	gwml-ptsl	mms	21.1	2.8	6	21.1	0.00	31.5	3.71
L spheno-occipital synchondrosis (lat)	ptsl-petal	mms	16.2	1.9	6	17.7	0.79	15.8	-0.21
L posterior clinoid height	petal-pcl	mms	12.0	3.2	6	12.9	0.28	10.8	-0.37
Posterior clinoid width	pcl-pcr	mms	15.9	1.7	6	14.8	-0.65	16.5	0.35
R anterior inferior length	gwmr-ptsr	mms	19.5	2.5	6	21.6	0.84	29.9	4.16
R spheno-occipital synchondrosis (lat)	ptsr-petar	mms	15.9	2.1	6	17.2	0.62	15.8	-0.05
R posterior clinoid height	petar-pcr	mms	12.0	3.0	6	14.4	0.80	12.6	0.20
Anterior Body									
L spheno-ethmoid suture	es-cppl	mms	6.4	1.7	6	13.1	3.94	8.4	1.18
L anterior lateral distance	cppl-ofaml	mms	13.9	1.9	6	7.3	-3.47	19.9	3.16
L anterior superior length	ofaml-gwml	mms	9.5	2.2	6	12.8	1.50	7.5	-0.91
R spheno-ethmoid suture	es-cppr	mms	7.1	1.8	6	12.8	3.17	8.3	0.67
R anterior lateral distance	cppr-ofamr	mms	14.9	1.7	6	8.3	-3.88	19.1	2.47
R anterior superior length	ofamr-gwmr	mms	11.7	1.4	6	14.0	1.64	8.3	-2.43
Sella									
L lateral anterior body	cppl-ofpml	mms	17.1	2.1	6	12.3	-2.29	19.8	1.29
L lateral sella length	ofpml-petal	mms	23.3	1.7	6	24.7	0.82	23.1	-0.12
R lateral anterior body	cppr-ofpmr	mms	19.2	2.2	6	12.0	-3.27	19.9	0.32
R lateral sella length	ofpmr-petar	mms	24.5	2.0	6	28.9	2.20	27.6	1.55
Base/Floor Body									
Spheno-ethmoid medial plate junction	es-ves	mms	21.8	1.6	6	21.7	-0.06	26.6	3.00
Spheno-vomerine junction	ves-h	mms	18.8	2.2	6	18.4	-0.18	13.8	-2.27
L posterior width	h-ptsl	mms	16.7	1.4	6	13.5	-2.29	20.5	2.71
R posterior width	h-ptsr	mms	17.1	1.4	6	13.5	-2.57	17.1	0.00

Appendix 2 Measurements for the Experimental Standards and the Patients with Crouzon Syndrome:

Adult (continued):

			Adult Standard			Patient HC		Patient TS	
Anatomical Unit	Definition	unit	mean	sd	n	Value	Z	Value	Z
SPHENOID (continued)									
Dimensions									
Anterior inferior body width	gwml-gwmr	mms	33.7	2.7	6	30.6	-1.15	42.0	3.07
Spheno-occipital synchondrosis (inf)	ptsl-ptsr	mms	29.8	2.1	6	23.9	-2.81	29.1	-0.33
Anterior superior body width	ofaml-ofamr	mms	26.7	2.2	6	29.1	1.09	33.7	3.18
Spheno-occipital synchondrosis (sup)	petal-petar	mms	24.5	1.2	6	20.7	-3.17	19.6	-4.08
L posterior body height	pcl-ptsl	mms	26.6	3.5	6	28.1	0.43	26.2	-0.11
R posterior body height	pcr-ptsr	mms	25.2	3.3	6	26.6	0.42	27.6	0.73
L anterior body height	acl-gwml	mms	14.1	1.9	6	11.8	-1.21	13.6	-0.26
L anterior body height	acr-gwmr	mms	14.9	0.8	6	10.9	-5.00	9.5	-6.75
Angles									
Body floor angle	es-ves-h	deg	129.8	14.7	6	128.9	-0.06	141.0	0.76
L lower body angle	s-n/gwml-ptsl	deg	40.2	9.3	6	36.2	-0.43	20.6	-2.11
R lower body angle	s-n/gwmr-ptsr	deg	155.9	3.0	6	158.4	0.83	152.0	-1.30
L upper body angle	s-n/ofpml-petal	deg	26.7	5.8	6	22.3	-0.76	8.6	-3.12
R upper body angle	s-n/ofpmr-petar	deg	27.4	4.9	6	17.6	-2.00	14.9	-2.55
TEMPORAL									
Distances									
Squamous									
L lateral spheno-temporal suture	fosl-sptl	mms	52.2	2.6	5				
L temporo-parietal suture	sptl-asl	mms	80.2	7.8	5				
L occipital mastoid height	asl-mal	mms	48.6	9.3	6				
L medial mastoid prominence	mal-smfl	mms	15.8	2.7	6	12.4	-1.26	22.6	2.52
R lateral spheno-temporal suture	fosr-sptr	mms	51.8	3.3	5				
R temporo-parietal suture	sptr-asr	mms	83.6	4.4	5				
R occipital mastoid height	asr-mar	mms	50.5	6.2	6				
R medial mastoid prominence	mar-smfr	mms	15.6	4.0	6	14.1	-0.38	24.8	2.30
External Auditory Meatus (EAM)									
L lateral mastoid prominence	mal-camil	mms	20.9	2.1	6			28.6	3.67
L inferior-posterior EAM rim	eamil-eampl	mms	8.8	1.9	6			9.7	0.47
L posterior-superior EAM rim	campl-pol	mms	6.8	0.9	6			7.0	0.22
L superior-anterior EAM rim	pol-eamal	mms	6.4	1.0	6			6.2	-0.20
L anterior-inferior EAM rim	eamal-eamil	mms	6.3	0.7	6			4.9	-2.00
R lateral mastoid prominence	mar-camir	mms	20.4	2.4	6	23.4	1.25	26.8	2.67
R inferior-posterior EAM rim	eamir-eampr	mms	11.7	1.6	6	8.9	-1.75	8.3	-2.12
R posterior-superior EAM rim	campr-por	mms	7.5	0.7	6	6.8	-1.00	6.9	-0.86
R superior-anterior EAM rim	por-eamar	mms	6.5	0.7	6	4.6	-2.71	7.0	0.71
R anterior-inferior EAM rim	eamar-eamir	mms	6.8	1.1	6	7.0	0.18	4.3	-2.27

Appendix 2 Measurements for the Experimental Standards and the Patients with Crouzon Syndrome:

Adult (continued):

			Adult Standard			Patient HC		Patient TS	
Anatomical Unit	**Definition**	**unit**	**mean**	**sd**	**n**	**Value**	**Z**	**Value**	**Z**
TEMPORAL (continued)									
Zygoma									
L EAM-articular fossa length	eamal-afl	mms	12.5	1.4	6			14.2	1.21
L articular fossa height	afl-ael	mms	9.0	2.1	6	7.6	-0.67	8.4	-0.29
L inferior arch length	ael-parl	mms	14.8	2.3	6	17.4	1.13	12.5	-1.00
L zygomatico-temporal suture	parl-ztl	mms	23.3	1.4	6	23.8	0.36	26.4	2.21
L superior arch length	ztl-aul	mms	44.5	2.8	6	36.3	-2.93	41.3	-1.14
R EAM-articular fossa length	eamar-afr	mms	12.0	1.2	6	12.5	0.42	13.7	1.42
R articular fossa height	afr-aer	mms	8.9	2.3	6	8.0	-0.39	9.3	0.17
R inferior arch length	aer-parr	mms	14.1	3.0	6	14.2	0.03	10.8	-1.10
R zygomatico-temporal suture	parr-ztr	mms	22.7	2.5	6	26.4	1.48	27.0	1.72
R superior arch length	ztr-aur	mms	41.4	1.5	6	40.7	-0.47	40.8	-0.40
Petrous									
L spheno-petrous temporal suture (sup)	fisl-petal	mms	19.8	1.9	6	19.8	0.00	22.1	1.21
L post-med temporo-occipital suture	petal-jfpl	mms	33.5	1.3	6	31.8	-1.31	30.8	-2.08
L lateral temporo-occipital suture	jfpl-asil	mms	47.1	5.7	6				
L petrous superior margin	asil-petal	mms	64.8	5.9	6				
R spheno-petrous temporal suture (sup)	fisr-petar	mms	20.2	0.5	6	16.8	-6.80	21.6	2.80
R post-med temporo-occipital suture	petar-jfpr	mms	36.0	1.5	6	34.5	-1.00	35.4	-0.40
R lateral temporo-occipital suture	jfpr-asir	mms	47.3	2.9	6				
R petrous superior margin	asir-petar	mms	66.0	4.7	6				
L occipital mastoid suture inferior	mal-jfll	mms	26.0	2.7	6	32.6	2.44	36.8	4.00
L jugular foramen width	jfll-jfml	mms	13.4	4.8	6	4.6	-1.83	10.2	-0.67
L medial temporo-occipital suture (inf)	jfml-ptsl	mms	21.5	5.1	6	32.6	2.18	17.5	-0.78
L spheno-petrous temporal suture (inf)	fosl-ptsl	mms	14.4	1.8	6	15.3	0.50	14.6	0.11
R occipital mastoid suture inferior	mar-jflr	mms	23.1	3.5	6	25.8	0.77	26.3	0.91
R jugular foramen width	jflr-jfmr	mms	12.3	2.3	6	8.1	-1.83	13.7	0.61
R medial temporo-occipital suture (inf)	jfmr-ptsr	mms	25.3	5.4	6	31.8	1.20	25.1	-0.04
R spheno-petrous temporal suture (inf)	fosr-ptsr	mms	15.0	2.1	6	17.0	0.95	15.2	0.10
Dimensions									
L petrous ridge length	petal-petpl	mms	54.9	6.0	6	64.9	1.67	78.1	3.87
R petrous ridge length	petar-petpr	mms	57.0	3.9	6	57.7	0.18	74.6	4.51
Inter-internal aud meatus dimension	iamr-iaml	mms	43.8	3.6	6	35.6	-2.28	45.3	0.42
Inter-external aud meatus dimension	pol-por	mms	103.1	2.0	6	101.4	-0.85	110.7	3.80
Inter-post jugular foramen dimension	jfpr-jfpl	mms	55.1	2.4	6	51.5	-1.50	57.8	1.13
Inter-mastoid dimension	mal-mar	mms	99.1	5.1	6	86.5	-2.47	106.7	1.49
Angles									
Auditory canal angle	pol-iaml/iamr-por	deg	152.3	5.7	6	133.8	-3.25	145.6	-1.18
Petrous ridge angle	petpl-petal/petar-petpr	deg	86.7	3.8	6	85.1	-0.42	84.8	-0.50
L zygoma projection angle	petal-aul-ztl	deg	88.7	4.6	6	79.5	-2.00	83.7	-1.09
R zygoma projection angle	petar-aur-ztr	deg	90.2	4.6	6	79.1	-2.41	87.4	-0.61

Appendix 2 Measurements for the Experimental Standards and the Patients with Crouzon Syndrome:

Adult (continued):

			Adult Standard			Patient HC		Patient TS	
Anatomical Unit	**Definition**	**unit**	**mean**	**sd**	**n**	**Value**	**Z**	**Value**	**Z**
PARIETAL									
Distances									
Sagittal suture	l-br	mms	108.8	4.0	6				
L parietal frontal (coronal) suture	br-spcl	mms	86.4	7.6	5				
L spheno-parietal suture	spcl-sptl	mms	11.5	2.3	5				
L temporo-parietal suture	sptl-asl	mms	80.2	7.8	5				
L occipito-parietal (lambdoid) suture	asl-l	mms	74.7	3.3	6				
R parietal frontal (coronal) suture	br-spcr	mms	91.5	6.0	5				
R spheno-parietal suture	spcr-sptr	mms	10.3	2.7	5				
R temporo-parietal suture	sptr-asr	mms	83.6	4.4	5				
R occipito-parietal (lambdoid) suture	asr-l	mms	76.4	4.8	6				
OCCIPITAL									
Distances									
Lambdoid and Cranial Base									
L occipito-parietal (lambdoid) suture	l-asl	mms	74.7	3.3	6				
L lateral temporo-occipital suture (sup)	asl-jfll	mms	45.9	6.4	6				
L lateral jugular foramen	jfll-jfpl	mms	7.7	2.9	6	6.8	-0.31	5.8	-0.66
L medial jugular foramen	jfpl-jfml	mms	10.1	4.7	6	5.1	-1.06	5.2	-1.04
L medial temporo-occipital suture (inf)	jfml-ptsl	mms	21.5	5.1	6	32.6	2.18	17.5	-0.78
R occipito-parietal (lambdoid) suture	l-asr	mms	76.4	4.8	6				
R lateral temporo-occipital suture (sup)	asr-jflr	mms	44.0	3.4	6				
R lateral jugular foramen	jflr-jfpr	mms	8.5	1.4	6	8.7	0.14	8.8	0.21
R medial jugular foramen	jfpr-jfmr	mms	10.0	3.4	6	8.8	-0.35	5.8	-1.24
R medial temporo-occipital suture (inf)	jfmr-ptsr	mms	25.3	5.4	6	31.8	1.20	25.1	-0.04
Inferior spheno-occipital synchondrosis	ptsr-ptsl	mms	29.8	2.1	6	23.9	-2.81	29.1	-0.33
Foramen Magnum									
L anterior foramen magnum	ba-fmll	mms	19.8	2.8	6	21.3	0.54	26.0	2.21
L posterior foramen magnum	fmll-o	mms	23.3	1.5	6	21.1	-1.47	27.5	2.80
R anterior foramen magnum	ba-fmlr	mms	20.8	1.8	6	19.5	-0.72	24.0	1.78
R posterior foramen magnum	fmlr-o	mms	23.5	3.3	6	25.5	0.61	26.1	0.79
Dimensions									
Foramen Magnum									
Foramen magnum length	ba-o	mms	32.8	4.2	6	33.9	0.26	39.8	1.67
Foramen magnum width	fmll-fmlr	mms	28.3	1.8	6	25.9	-1.33	33.0	2.61
Posterior Cranial Fossa									
Posterior cranial fossa depth	o-iop	mms	42.8	2.9	6	37.5	-1.83	49.7	2.38
Posterior occipital height	iop-l	mms	50.2	4.0	6				
L posterior fossa length	petpl-iop	mms	59.7	5.4	6	57.7	-0.37	72.3	2.33
L posterior fossa length	petpr-iop	mms	64.3	5.1	6	57.1	-1.41	63.6	-0.14

Appendix 2 Measurements for the Experimental Standards and the Patients with Crouzon Syndrome:

Adult (continued):

			Adult Standard			Patient HC		Patient TS	
Anatomical Unit	**Definition**	**unit**	**mean**	**sd**	**n**	**Value**	**Z**	**Value**	**Z**
CRANIAL BASE SUTURES									
Anterior Cranial Fossa									
L spheno-ethmoid synchondrosis	es-cppl	mms	6.4	1.7	6	13.1	3.94	8.4	1.18
R spheno-ethmoid synchondrosis	es-cppr	mms	7.1	1.8	6	12.8	3.17	8.3	0.67
L spheno-frontal suture (ant fossa)	cppl-spal	mms	32.0	4.5	6	28.3	-0.82	36.3	0.96
R spheno-frontal suture (ant fossa)	cppr-spar	mms	33.2	2.4	6	30.6	-1.08	38.7	2.29
L spheno-frontal suture (orbital)	spal-zfsl	mms	22.9	4.7	6	20.0	-0.62	14.0	-1.89
R spheno-frontal suture (orbital)	spar-zfsr	mms	22.4	4.0	6	13.1	-2.32	21.1	-0.32
L spheno-zygomatic suture	zfsl-gwll	mms	12.4	0.9	3	22.0	10.67	20.9	9.44
R spheno-zygomatic suture	zfsr-gwlr	mms	14.5	1.5	3	19.3	3.20	19.7	3.47
Middle Cranial Fossa									
L spheno-squamous temporal suture	gwll-fisl	mms	40.5	3.1	3	36.2	-1.39	42.5	0.65
R spheno-squamous temporal suture	gwlr-fisr	mms	38.6	2.2	3	35.6	-1.36	40.5	0.86
L spheno-petrous temporal suture (sup)	fisl-petal	mms	19.8	1.9	6	19.8	0.00	22.1	1.21
R spheno-petrous temporal suture (sup)	fisr-petar	mms	20.2	0.5	6	16.8	-6.80	21.6	2.80
L spheno-petrous temporal suture (inf)	fosl-ptsl	mms	14.4	1.8	6	15.3	0.50	14.6	0.11
R spheno-petrous temporal suture (inf)	fosr-ptsr	mms	15.0	2.1	6	17.0	0.95	15.2	0.10
Posterior Cranial Fossa									
L medial temporo-occipital suture (sup)	petal-jfml	mms	24.3	4.6	6	29.3	1.09	26.2	0.41
R medial temporo-occipital suture (sup)	petar-jfmr	mms	25.8	3.9	6	27.0	0.31	30.5	1.21
L medial temporo-occipital suture (inf)	jfml-ptsl	mms	21.5	5.1	6	32.6	2.18	17.5	-0.78
R medial temporo-occipital suture (inf)	jfmr-ptsr	mms	25.3	5.4	6	31.8	1.20	25.1	-0.04
L occipital mastoid suture (superior)	jfll-petpl	mms	34.7	5.8	6	39.1	0.76	50.1	2.66
R occipital mastoid suture (superior)	jflr-petpr	mms	37.1	3.1	6	32.6	-1.45	47.7	3.42
Spheno-occipital synchondrosis (sup)	petal-petar	mms	24.5	1.2	6	20.7	-3.17	19.6	-4.08
Spheno-occipital synchondrosis (inf)	ptsl-ptsr	mms	29.8	2.1	6	23.9	-2.81	29.1	-0.33
L spheno-occipital synchondrosis (lat)	ptsl-petal	mms	16.2	1.9	6	17.7	0.79	15.8	-0.21
R spheno-occipital synchondrosis (lat)	ptsr-petar	mms	15.9	2.1	6	17.2	0.62	15.8	-0.05
CRANIAL BASE									
Facial Heights									
Anterior facial height	n-gn	mms	104.8	6.8	6	125.9	3.10	139.0	5.03
L posterior facial height	s-gol	mms	84.5	7.0	6	80.8	-0.53	93.8	1.33
R posterior facial height	s-gor	mms	87.4	6.9	6	78.9	-1.23	98.7	1.64
Facial Angles									
SNA	s-n-ss	deg	85.8	5.1	6	63.4	-4.39	64.6	-4.16
SNB	s-n-sm	deg	80.3	3.9	6	67.7	-3.23	65.8	-3.72
Cranial Base Angle									
Cranial base angle	ba-s-n	deg	126.6	5.2	6	139.8	2.54	140.9	2.75
Cranial Base Dimensions									
Cranial base length	ba-n	mms	100.1	7.4	6	95.6	-0.61	98.7	-0.19
Clivus length (posterior cranial base)	ba-s	mms	43.0	2.7	6	39.9	-1.15	38.8	-1.56
Anterior cranial base length	s-n	mms	67.6	3.7	6	61.6	-1.62	65.5	-0.57

Appendix 3

Measurements for Three Dimensional Quantitative Analysis of the Surgical Morphology in Crouzon Syndrome

---

The surgery of five patients was analysed and included:

1.	Patient SH	Fronto-orbital Advance
2.	Patient JS	Fronto-orbital Advance
3.	Patient IP	Fronto-orbital Advance
4.	Patient LW	Extended Fronto-orbital Advance
5.	Patient HC	Fronto-orbital Advance

Three comparisons of the surgery were undertaken:

a) Pre-operative Surgical Unit vs Standard Surgical Unit

b) Pre-operative Surgical Unit vs Post-operative Surgical Unit

c) Post-operative Surgical Unit vs Standard Surgical Unit

Appendix 3 Results of Three Dimensional Quantitative Analysis of Surgical Morphology:

Patient SH Fronto-orbital Advance:

a. Pre-operative Surgical Unit vs Standard Surgical Unit

Landmarks	Landmark Differences (mm)			
	x (right)	y (anterior)	z (superior)	Magnitude
glabella	-3.0	2.7	-11.5	12.2
superior orbitale left	-2.4	2.8	-11.0	11.6
superior orbitale right	-5.6	-0.2	-13.6	14.7
supero-lateral orbitale superius left	-4.2	0.7	-12.0	12.7
supero-lateral orbitale superius right	1.0	-0.1	-10.1	10.2
supero-medial orbitale left	-2.3	0.3	-13.3	13.5
supero-medial orbitale right	-2.8	-2.1	-14.7	15.1
zygo-frontale superius left	-5.3	-1.0	-9.5	11.0
zygo-frontale superius right	2.8	-0.8	-8.0	8.5

Translation of Pre-operative Surgical Unit from the Standard Surgical Unit	Displacement (mm)			
	x (right)	y (anterior)	z (superior)	Magnitude
	-2.9	0.3	-11.4	11.8 mm

b. Pre-operative Surgical Unit vs Post-operative Surgical Unit

Landmarks	Landmark Differences (mm)			
	x (right)	y (anterior)	z (superior)	Magnitude
glabella	0.6	4.1	7.0	8.2
superior orbitale left	-0.8	0.7	4.7	4.8
superior orbitale right	3.9	4.1	8.1	9.9
supero-lateral orbitale superius left	4.6	4.5	12.1	13.7
supero-lateral orbitale superius right	2.8	4.7	11.1	12.3
supero-medial orbitale left	-1.4	-0.5	6.9	7.1
supero-medial orbitale right	1.7	1.9	8.9	9.3
zygo-frontale superius left	1.4	7.9	11.2	13.8
zygo-frontale superius right	2.1	5.9	9.0	11.0

Translation of Pre-operative Surgical Unit to Post-operative position	Displacement (mm)			
	x (right)	y (anterior)	z (superior)	Magnitude
	1.5	3.3	7.6	8.5 mm

c. Post-operative Surgical Unit vs Standard Surgical Unit

Landmarks	Landmark Differences (mm)			
	x (right)	y (anterior)	z (superior)	Magnitude
glabella	-4.6	11.3	-1.2	12.3
superior orbitale left	-5.3	7.6	-3.6	10.0
superior orbitale right	-4.0	9.8	-2.6	10.9
supero-lateral orbitale superius left	-1.5	9.7	1.9	10.0
supero-lateral orbitale superius right	2.3	9.4	3.3	10.2
supero-medial orbitale left	-5.9	5.2	-4.2	8.9
supero-medial orbitale right	-3.5	6.3	-4.0	8.2
zygo-frontale superius left	-5.6	10.5	2.5	12.2
zygo-frontale superius right	3.6	9.1	2.8	10.1

Translation of Post-operative Surgical Unit from the Standard Surgical Unit	Displacement (mm)			
	x (right)	y (anterior)	z (superior)	Magnitude
	-3.7	9.3	0.1	10.0 mm

Appendix 3 Results of Three Dimensional Quantitative Analysis of Surgical Morphology (continued):

Patient JS Fronto-orbital Advance:

a. Pre-operative Surgical Unit vs Standard Surgical Unit

Landmarks	Landmark Differences (mm)			
	x (right)	y (anterior)	z (superior)	Magnitude
glabella	-1.1	-2.3	5.1	5.7
superior orbitale left	-0.1	-4.3	3.4	5.5
superior orbitale right	0.0	-4.1	3.1	5.1
supero-lateral orbitale superius left	-2.7	-6.2	1.9	7.0
supero-lateral orbitale superius right	1.1	-4.9	0.1	5.0
supero-medial orbitale left	-1.6	-2.0	5.5	6.1
supero-medial orbitale right	1.0	-1.8	4.4	4.9
zygo-frontale superius left	-3.1	-6.7	0.9	7.4
zygo-frontale superius right	1.7	-4.8	0.1	5.1

Translation of Pre-operative Surgical Unit from the Standard Surgical Unit	Displacement (mm)			
	x (right)	y (anterior)	z (superior)	Magnitude
	-0.2	-4.3	2.7	5.1 mm

b. Pre-operative Surgical Unit vs Post-operative Surgical Unit

Landmarks	Landmark Differences (mm)			
	x (right)	y (anterior)	z (superior)	Magnitude
glabella	1.7	6.5	2.2	7.1
superior orbitale left	3.0	10.5	3.7	11.5
superior orbitale right	0.7	6.6	2.5	7.1
supero-lateral orbitale superius left	3.2	16.0	5.2	17.1
supero-lateral orbitale superius right	0.0	9.7	-1.8	9.9
supero-medial orbitale left	0.7	7.2	4.9	8.7
supero-medial orbitale right	1.4	7.7	5.6	9.6
zygo-frontale superius left	-0.7	17.6	6.1	18.6
zygo-frontale superius right	0.1	10.6	0.0	10.6

Translation of Pre-operative Surgical Unit to Post-operative position	Displacement (mm)			
	x (right)	y (anterior)	z (superior)	Magnitude
	0.7	10.0	3.0	10.5 mm

c. Post-operative Surgical Unit vs Standard Surgical Unit

Landmarks	Landmark Differences (mm)			
	x (right)	y (anterior)	z (superior)	Magnitude
glabella	0.3	4.9	5.6	7.4
superior orbitale left	2.6	6.7	5.7	9.2
superior orbitale right	0.4	3.1	3.6	4.8
supero-lateral orbitale superius left	0.1	10.0	6.0	11.7
supero-lateral orbitale superius right	0.8	5.2	-3.4	6.3
supero-medial orbitale left	-1.2	5.6	8.8	10.5
supero-medial orbitale right	2.1	6.3	8.3	10.6
zygo-frontale superius left	-4.1	11.1	6.0	13.3
zygo-frontale superius right	1.5	6.1	-1.7	6.5

Translation of Post-operative Surgical Unit from the Standard Surgical Unit	Displacement (mm)			
	x (right)	y (anterior)	z (superior)	Magnitude
	0.7	6.5	4.2	7.8 mm

Appendix 3 Results of Three Dimensional Quantitative Analysis of Surgical Morphology (continued):

Patient IP Fronto-orbital Advance:

a. Pre-operative Surgical Unit vs Standard Surgical Unit

Landmarks	Landmark Differences (mm)			
	x (right)	y (anterior)	z (superior)	Magnitude
glabella	3.5	-14.9	28.0	31.9
superior orbitale left	-6.8	-18.6	25.4	32.2
superior orbitale right	16.2	-19.3	23.5	34.5
supero-lateral orbitale superius left	-5.7	-7.3	15.4	18.0
supero-lateral orbitale superius right	13.1	-12.8	12.5	22.2
supero-medial orbitale left	-0.5	-10.3	18.4	21.1
supero-medial orbitale right	8.9	-10.6	19.1	23.6
zygo-frontale superius left	-8.0	-6.8	16.9	19.9
zygo-frontale superius right	15.4	-12.3	19.7	27.9

Translation of Pre-operative Surgical Unit from the Standard Surgical Unit	Displacement (mm)			
	x (right)	y (anterior)	z (superior)	Magnitude
	2.9	-12.2	21.0	24.5 mm

b. Pre-operative Surgical Unit vs Post-operative Surgical Unit

Landmarks	Landmark Differences (mm)			
	x (right)	y (anterior)	z (superior)	Magnitude
glabella	-5.1	20.8	1.2	21.4
superior orbitale left	-5.8	19.5	4.4	20.8
superior orbitale right	-2.0	24.1	4.5	24.6
supero-lateral orbitale superius left	-4.5	13.2	15.4	20.8
supero-lateral orbitale superius right	0.0	19.0	19.3	27.0
supero-medial orbitale left	-3.7	19.9	11.5	23.3
supero-medial orbitale right	-11.3	20.6	14.1	27.4
zygo-frontale superius left	-4.3	11.1	15.7	19.7
zygo-frontale superius right	-1.3	16.4	12.3	20.5

Translation of Pre-operative Surgical Unit to Post-operative position	Displacement (mm)			
	x (right)	y (anterior)	z (superior)	Magnitude
	-3.8	18.1	13.0	22.6 mm

c. Post-operative Surgical Unit vs Standard Surgical Unit

Landmarks	Landmark Differences (mm)			
	x (right)	y (anterior)	z (superior)	Magnitude
glabella	0.7	9.2	31.7	33.0
superior orbitale left	-10.7	4.7	33.2	35.2
superior orbitale right	15.9	6.6	30.3	34.9
supero-lateral orbitale superius left	-8.7	8.7	32.7	34.9
supero-lateral orbitale superius right	14.2	6.6	33.5	37.0
supero-medial orbitale left	-2.5	12.1	32.1	34.4
supero-medial orbitale right	-0.6	11.8	34.9	36.9
zygo-frontale superius left	-10.9	7.5	34.4	36.9
zygo-frontale superius right	15.6	5.3	33.4	37.3

Translation of Post-operative Surgical Unit from the Standard Surgical Unit	Displacement (mm)			
	x (right)	y (anterior)	z (superior)	Magnitude
	-0.6	7.5	32.8	33.6 mm

Appendix 3 Results of Three Dimensional Quantitative Analysis of Surgical Morphology (continued):

Patient LW Extended Fronto-orbital Advance:

a. Pre-operative Surgical Unit vs Standard Surgical Unit

Landmarks	Landmark Differences (mm)			
	x (right)	y (anterior)	z (superior)	Magnitude
glabella	2.2	7.8	-1.5	8.2
infero-lateral orbitale left	-3.8	-4.5	-2.1	6.2
infero-lateral orbitale right	4.8	-2.6	-4.6	7.1
orbitale zygomatic left	-4.8	-4.4	-3.6	7.5
orbitale zygomatic right	8.6	-3.2	-3.0	9.6
pre-articulare left	-1.5	-2.3	-2.3	3.6
pre-articulare right	2.7	-4.7	-3.4	6.4
superior orbitale left	-5.5	4.5	-2.3	7.5
superior orbitale right	15.9	1.2	-2.8	16.2
supero-lateral orbitale left	-5.3	-0.9	1.0	5.5
supero-lateral orbitale right	8.4	-1.1	-1.0	8.5
supero-medial orbitale left	-1.3	5.4	-3.5	6.6
supero-medial orbitale right	3.6	5.9	-4.1	8.0
zygo-frontale left	-4.5	-4.6	0.1	6.4
zygo-frontale right	8.2	-4.6	-2.9	9.9
zygo-maxillare inferius laterale left	-0.1	-3.7	0.0	3.7
zygo-maxillare inferius laterale right	-0.3	-2.4	0.0	2.4
zygo-temporale left	-2.6	-6.0	4.6	8.0
zygo-temporale right	6.2	-5.4	1.7	8.4

Translation of Pre-operative Surgical Unit from the Standard Surgical Unit	Displacement (mm)			
	x (right)	y (anterior)	z (superior)	Magnitude
	0.5	-1.3	-0.7	1.6 mm

b. Pre-operative Surgical Unit vs Post-operative Surgical Unit

Landmarks	Landmark Differences (mm)			
	x (right)	y (anterior)	z (superior)	Magnitude
glabella	-0.4	-0.8	1.4	1.6
infero-lateral orbitale left	-1.2	5.1	0.3	5.2
infero-lateral orbitale right	4.5	5.4	7.2	10.1
orbitale zygomatic left	-2.3	-1.2	2.1	3.4
orbitale zygomatic right	3.2	2.0	2.9	4.8
pre-articulare left	-4.8	11.0	-0.5	12.1
pre-articulare right	2.1	20.4	-0.1	20.5
superior orbitale left	0.3	5.6	2.8	6.3
superior orbitale right	-1.7	5.7	4.9	7.7
supero-lateral orbitale left	-1.3	6.3	-2.9	7.0
supero-lateral orbitale right	3.0	4.8	2.9	6.4
supero-medial orbitale left	-0.2	1.5	6.1	6.2
supero-medial orbitale right	2.7	2.5	7.3	8.2
zygo-frontale left	-2.6	8.2	-1.4	8.7
zygo-frontale right	3.6	7.0	5.6	9.7
zygo-maxillare inferius laterale left	-6.1	1.3	1.7	6.5
zygo-maxillare inferius laterale right	10.1	1.8	2.2	10.5
zygo-temporale left	-2.8	9.6	2.2	10.3
zygo-temporale right	3.8	9.4	5.7	11.6

Translation of Pre-operative Surgical Unit to Post-operative position	Displacement (mm)			
	x (right)	y (anterior)	z (superior)	Magnitude
	0.8	5.3	3.0	6.1 mm

Appendix 3 Results of Three Dimensional Quantitative Analysis of Surgical Morphology (continued):

Patient LW Extended Fronto-orbital Advance (continued):

c. Post-operative Surgical Unit vs Standard Surgical Unit

Landmarks	Landmark Differences (mm)			
	x (right)	y (anterior)	z (superior)	Magnitude
glabella	1.2	6.5	-0.4	6.6
infero-lateral orbitale left	-4.9	-0.2	-2.2	5.4
infero-lateral orbitale right	9.4	2.2	3.4	10.2
orbitale zygomatic left	-6.9	-6.6	-1.9	9.7
orbitale zygomatic right	11.9	-1.7	0.8	12.0
pre-articulare left	-6.2	7.9	-3.2	10.6
pre-articulare right	5.0	15.1	-2.4	16.1
superior orbitale left	-5.6	9.4	-0.2	11.0
superior orbitale right	13.8	6.7	3.1	15.7
supero-lateral orbitale left	-6.9	4.7	-2.6	8.7
supero-lateral orbitale right	11.1	3.4	2.9	12.0
supero-medial orbitale left	-1.8	6.2	2.1	6.8
supero-medial orbitale right	6.0	7.8	3.2	10.3
zygo-frontale left	-7.3	2.9	-1.8	8.1
zygo-frontale right	11.7	2.0	3.9	12.5
zygo-maxillare inferius laterale left	-6.1	-3.1	1.5	7.1
zygo-maxillare inferius laterale right	9.9	-1.2	2.7	10.3
zygo-temporale left	-5.6	3.1	6.4	9.1
zygo-temporale right	9.8	3.7	8.6	13.6

Translation of Post-operative Surgical Unit from the Standard Surgical Unit	Displacement (mm)			
	x (right)	y (anterior)	z (superior)	Magnitude
	1.8	3.5	1.4	4.2 mm

Appendix 3 Results of Three Dimensional Quantitative Analysis of Surgical Morphology (continued):

Patient HC Fronto-orbital Advance:

a. Pre-operative Surgical Unit vs Standard Surgical Unit

Landmarks	Landmark Differences (mm)			
	x (right)	y (anterior)	z (superior)	Magnitude
glabella	-3.5	-13.0	23.2	26.8
superior orbitale left	-8.3	-18.8	18.9	27.9
superior orbitale right	2.7	-11.8	22.4	25.4
supero-lateral orbitale superius left	-3.9	-17.9	7.7	19.9
supero-lateral orbitale superius right	-2.7	-11.1	13.6	17.8
supero-medial orbitale left	-6.8	-11.6	19.7	23.8
supero-medial orbitale right	-4.9	-9.8	17.7	20.8
alare left	-0.4	-13.4	18.5	22.8
alare right	-3.7	-16.0	15.0	22.2
anterior nasal spine	-2.5	-12.7	17.2	21.5
ecto-canine superius left	-1.2	-15.3	16.9	22.8
ecto-canine superius right	-1.4	-15.2	16.6	22.6
ecto-incision central superius left	-1.5	-15.1	13.9	20.5
ecto-incision central superius right	-1.1	-15.3	15.2	21.6
ectomolare 1st superius left	2.6	-7.5	10.2	12.9
ectomolare 1st superius right	-7.1	-8.1	11.0	15.4
greater palatine foramen left	-1.6	-6.1	5.6	8.4
greater palatine foramen right	-2.7	-6.1	4.6	8.1
infero-lateral orbitale left	-0.6	-19.1	10.2	21.7
infero-lateral orbitale right	-6.4	-15.2	11.2	20.0
lateral orbitale left	-2.1	-17.0	8.1	18.9
lateral orbitale right	-2.3	-11.7	11.6	16.6
maxillary tuberosity left	-2.4	-6.3	6.7	9.5
maxillary tuberosity right	0.1	-3.4	6.8	7.6
medial orbitale left	-3.1	-12.7	15.3	20.1
medial orbitale right	-3.0	-10.5	20.3	23.0
nasale	-2.8	-7.4	15.9	17.8
nasion	-3.4	-12.1	18.2	22.1
naso-lacrimal inferius left	2.7	-14 4	18.8	23.9
naso-lacrimal inferius right	-5.6	-13.3	17.3	22.5
orbitale left	-4.5	-18.6	9.6	21.5
orbitale right	-6.1	-15.4	12.8	21.0
posterior nasal spine	-2.7	-6.6	4.4	8.4
prosthion	-1.8	-13.9	12.8	18.9
subspinale	-2.6	-16.0	10.6	19.4
superior naso-maxillare left	-1.4	-11.6	17.3	20.9
superior naso-maxillare right	-3.4	-11.9	18.3	22.0
supero-lateral orbitale left	-3.9	-17.9	7.7	19.9
supero-lateral orbitale right	-1.9	-11.5	12.7	17.2
zygo-frontale left (± superius)	-3.9	-18.8	6.2	20.2
zygo-frontale right (± superius)	-0.4	-13.9	7.8	15.9
zygo-maxillare inferius left	6.2	-13.7	8.0	17.0
zygo-maxillare inferius right	-10.2	-12.3	11.8	19.8
zygo-temporale left	2.2	-13.6	7.7	15.8
zygo-temporale right	-5.5	-10.0	11.6	16.2
canine superius left	-2.2	-11.5	15.4	19.3
canine superius right	-3.3	-9.9	16.0	19.1
disto-molare superius left	2.6	-7.6	9.2	12.2
disto-molare superius right	-6.3	-5.4	9.8	12.8
incision superius left	-1.9	-14.2	14.5	20.4
incision superius right	-1.4	-13.7	14.5	19.9
medio-molare 1st superius left	1.8	-6.2	11.3	13.1
medio-molare 1st superius right	-7.8	-7.2	11.8	15.9

Translation of Pre-operative Surgical Unit from the Standard Surgical Unit	Displacement (mm)			
	x (right)	y (anterior)	z (superior)	Magnitude
	-2.1	-12.4	11.9	17.3 mm

Appendix 3 Results of Three Dimensional Quantitative Analysis of Surgical Morphology (continued):

Patient HC Fronto-orbital Advance (continued):

b. Pre-operative Surgical Unit vs Post-operative Surgical Unit

Landmarks	Landmark Differences (mm)			
	x (right)	y (anterior)	z (superior)	Magnitude
glabella	-6.4	16.5	4.8	18.4
superior orbitale left	-3.1	13.4	8.9	16.4
superior orbitale right	-6.3	9.9	4.5	12.6
supero-lateral orbitale superius left	-1.5	10.9	6.8	12.9
supero-lateral orbitale superius right	-0.5	21.2	3.3	21.4
supero-medial orbitale left	-3.1	11.0	3.6	12.0
supero-medial orbitale right	-4.6	11.4	4.8	13.2
alare left	-3.3	15.7	5.7	17.1
alare right	-3.7	17.4	6.5	18.9
anterior nasal spine	-3.3	17.0	4.1	17.8
ecto-canine superius left	-2.8	17.4	2.4	17.8
ecto-canine superius right	2.8	19.4	4.2	20.1
ecto-incision central superius left	-3.0	18.0	3.5	18.5
ecto-incision central superius right	-2.7	17.6	3.0	18.0
ectomolare 1st superius left	-1.1	15.7	2.3	15.9
ectomolare 1st superius right	-2.0	18.2	1.5	18.4
greater palatine foramen left	-9.2	14.6	-5.0	17.9
greater palatine foramen right	4.3	14.9	-3.2	15.9
infero-lateral orbitale left	-1.2	15.4	2.0	15.6
infero-lateral orbitale right	-0.6	20.0	4.8	20.5
lateral orbitale left	-3.1	11.5	12.2	17.1
lateral orbitale right	-2.7	16.7	11.4	20.4
maxillary tuberosity left	-1.4	15.7	4.1	16.2
maxillary tuberosity right	0.7	17.4	4.1	17.8
medial orbitale left	-1.9	18.1	10.8	21.2
medial orbitale right	-5.9	19.5	5.6	21.1
nasale	-5.8	15.4	5.9	17.5
nasion	-4.5	15.5	4.1	16.6
naso-lacrimal inferius left	-5.8	15.5	2.0	16.7
naso-lacrimal inferius right	-2.3	16.7	5.2	17.7
orbitale left	-3.8	11.8	4.6	13.2
orbitale right	2.5	17.4	3.0	17.8
posterior nasal spine	0.9	15.5	5.3	16.4
prosthion	-2.5	15.0	6.1	16.4
subspinale	-2.2	16.7	8.5	18.9
superior naso-maxillare left	-4.7	16.3	6.7	18.2
superior naso-maxillare right	-5.1	16.1	6.3	18.0
supero-lateral orbitale left	-1.5	10.9	6.8	12.9
supero-lateral orbitale right	-1.2	21.7	4.3	22.1
zygo-frontale left (± superius)	-4.6	13.2	5.6	15.1
zygo-frontale right (± superius)	-0.8	20.4	4.3	20.9
zygo-maxillare inferius left	-1.8	12.5	3.7	13.1
zygo-maxillare inferius right	-3.6	19.4	2.7	19.9
zygo-temporale left	-2.7	12.8	1.1	13.1
zygo-temporale right	-2.3	19.8	3.7	20.3
canine superius left	-2.2	13.6	1.1	13.9
canine superius right	-1.4	15.7	-0.9	15.8
disto-molare superius left	-1.5	13.9	1.2	14.0
disto-molare superius right	-3.1	14.6	4.4	15.6
incision superius left	-1.8	14.1	0.4	14.3
incision superius right	-3.7	14.9	3.5	15.8
medio-molare 1st superius left	0.0	12.6	-2.3	12.8
medio-molare 1st superius right	-3.1	17.3	1.6	17.6

Translation of Pre-operative Surgical Unit to Post-operative position	Displacement (mm)			
	x (right)	y (anterior)	z (superior)	Magnitude
	-2.3	15.9	4.0	16.5 mm

Appendix 3 Results of Three Dimensional Quantitative Analysis of Surgical Morphology (continued):

Patient HC Fronto-orbital Advance (continued):

c. Post-operative Surgical Unit vs Standard Surgical Unit

Landmarks	Landmark Differences (mm)			
	x (right)	y (anterior)	z (superior)	Magnitude
glabella	-12.3	4.2	27.9	30.7
superior orbitale left	-14.6	-3.9	27.2	31.1
superior orbitale right	-5.9	-2.3	27.3	28.0
supero-lateral orbitale superius left	-8.1	-6.4	13.8	17.2
supero-lateral orbitale superius right	-5.0	10.3	17.6	21.0
supero-medial orbitale left	-11.9	0.5	22.8	25.7
supero-medial orbitale right	-11.2	2.3	22.5	25.2
alare left	-5.6	2.1	23.9	24.7
alare right	-9.5	1.7	21.6	23.6
anterior nasal spine	-7.3	4.3	21.1	22.7
ecto-canine superius left	-5.8	1.8	19.0	19.9
ecto-canine superius right	-5.9	4.0	21.0	22.2
ecto-incision central superius left	-6.1	2.7	17.1	18.4
ecto-incision central superius right	-5.5	2.0	18.1	19.0
ectomolare 1st superius left	1.0	7.2	12.1	14.2
ectomolare 1st superius right	-9.6	10.5	12.7	19.1
greater palatine foramen left	-11.1	8.2	0.6	13.8
greater palatine foramen right	1.3	8.6	1.7	8.9
infero-lateral orbitale left	-4.6	-3.7	11.6	13.0
infero-lateral orbitale right	-9.2	5.5	16.5	19.6
lateral orbitale left	-7.7	-5.1	19.6	21.7
lateral orbitale right	-6.7	5.1	23.6	25.1
maxillary tuberosity left	-4.0	9.2	10.5	14.5
maxillary tuberosity right	1.0	13.3	11.4	17.5
medial orbitale left	-7.0	5.8	25.8	27.4
medial orbitale right	-10.7	9.4	25.9	29.6
nasale	-9.7	8.2	21.6	25.1
nasion	-9.9	3.9	22.2	24.6
naso-lacrimal inferius left	-5.3	0.6	20.7	21.3
naso-lacrimal inferius right	-9.8	4.1	22.6	25.0
orbitale left	-10.9	-6.3	13.7	18.6
orbitale right	-5.7	2.7	16.2	17.4
posterior nasal spine	-2.2	8.8	9.8	13.3
prosthion	-5.7	0.9	18.7	19.6
subspinale	-6.6	0.7	19.0	20.1
superior naso-maxillare left	-8.1	4.9	23.9	25.7
superior naso-maxillare right	-10.5	4.7	24.5	27.0
supero-lateral orbitale left	-8.1	-6.4	13.8	17.2
supero-lateral orbitale right	-5.0	10.3	17.6	21.0
zygo-frontale left (± superius)	-11.3	-4.9	11.2	16.6
zygo-frontale right (± superius)	-3.4	6.4	12.9	14.8
zygo-maxillare inferius left	2.8	-2.5	11.2	11.9
zygo-maxillare inferius right	-15.1	8.2	15.0	22.8
zygo-temporale left	-2.5	-1.2	8.2	8.7
zygo-temporale right	-9.1	10.3	16.0	21.1
canine superius left	-5.4	1.9	16.1	17.1
canine superius right	-5.4	5.6	15.1	17.0
disto-molare superius left	0.7	5.2	10.1	11.4
disto-molare superius right	-9.4	9.4	14.5	19.6
incision superius left	-5.1	-0.3	14.7	15.6
incision superius right	-6.4	0.9	17.9	19.0
medio-molare 1st superius left	1.6	5.5	8.7	10.4
medio-molare 1st superius right	-11.2	10.5	13.6	20.5

Translation of Post-operative Surgical Unit from the Standard Surgical Unit	Displacement (mm)			
	x (right)	y (anterior)	z (superior)	Magnitude
	-6.4	3.2	15.7	17.2 mm